Mathematical and Experimental Modelling of the Dynamic Response of the Transfemoral Bone Implant System and Bone Anchored Hearing Aids and its Potential Application to the Non-invasive Evaluation of Implant Stability

by

Mostafa Mohamed

A thesis submitted in partial fulfillment of the requirements for the degree of

Doctor of Philosophy

Department of Mechanical Engineering

University of Alberta

Abstract

Osseointegrated implants rely on the direct structural and functional attachment of an implant to the surrounding bone tissues. These implants are used in various fields including dentistry, bone conduction hearing and lower-limb amputations. Determining the quality of the bond between the implant and the surrounding bone (implant stability) is important in evaluating the surgical outcomes, early failure-detection and optimising rehabilitation. Vibration analysis can non-invasively quantify the bone-implant-interface (BII) properties. The Advanced System for Implant Stability Testing (ASIST) is a vibration-based stability measurement system that has been used with Bone Anchored Hearing Aids (BAHA). It evaluates the BII stiffness by matching the measured acceleration to the prediction of a mathematical model. This work focuses on the mathematical and experimental analysis of the dynamic behavior of the implant for Transfemoral lower-limb Amputations (TFA) and BAHA systems. The analysis extends the ASIST approach to TFA systems and builds on the existing knowledge of BAHA systems using novel modelling approaches.

The TFA bone-implant system was first analysed using 3D Finite Element (FE) modal analysis and benchtop experiments under different BII, loading, boundary and implant-adapter conditions. The analysis indicated that a measurement system based on the axial modes is: 1) more sensitive to the BII condition, 2) more immune to the femoral boundary condition and 3) more characterizable for different implant-adapter configurations compared to the transverse modes. Therefore, a 1D FE model of the TFA system was developed using axial bar elements. The model was validated by: 1) testing the 1D FE formulation using a uniform cylinder, 2) comparing the 1D FE modal behavior with a 3D FE model for the actual implant geometry and 3) using the 1D FE model to analyse signals generated from 3D FE implicit and benchtop models. The 1D FE

formulation converged to the analytical and 3D FE solutions for the uniform cylinder. The 1D model was representative of the TFA system and predicted similar axial modes (maximum frequency difference of 2.07%) compared to the 3D FE model. The 1D FE model was then incorporated into a custom-built MATLAB® application that extracts the BII stiffness by matching the input signal to the model's prediction using an optimization routine. The approach was highly sensitive to the BII condition and predicted interface stiffness values of 4.75×10^6, 1.43×10^8 and 2.21×10^9 N/m for the experimental LOW, INTERMEDIATE and HIGH conditions respectively. The model also predicted similar damping ratios compared to the 3D FE simulations. The optimization routine successfully matched the signals, with frequency domain similarity scores of 94-100%.

1D and 3D FE models of the BAHA systems were developed. Although the previous work involved modelling BAHA implants using an analytical 4 Degree of Freedom (DOF) and benchtop setups, the developed FE models tested the implant system under a wider range of conditions. The 3D FE signals were analysed with the ASIST utility, the ASIST Stability Coefficient (ASC; directly computed from the BII stiffness) was more sensitive to the BII condition and less sensitive to the abutment geometry compared to the natural frequencies. The 3D models were also validated with benchtop and clinical signals that represented extreme BII cases and were then used to study the nature of the BII and its influencing parameters. Finally, a 1D FE model was developed for BAHA systems using Timoshenko beam elements. The 1D FE model behaved similarly to the previously developed 4 DOF model, where they both predicted similar natural frequencies with differences of -0.77 to 4.40% and -1.07 to -2.76% for the 1st and 2nd modes respectively. The consistently lower 2nd mode frequencies of the 1D FE model (due the larger number of DOF) resulted in lower ASC scores but the trends between both models were preserved.

The mathematical analysis performed in this work offers a comprehensive understanding of the dynamic behavior of both implant systems. This is the first attempt to model the Osseointegrated Prosthetic Limb (OPL) TFA system and the first one to propose a vibration-based implant stability measurement method for it. The 1D FE models for both bone-implant systems (TFA and BAHA) show high promise in modelling them and evaluating the BII stiffness. This approach paves the way for the non-invasive evaluation of the BII properties in clinical settings.

Preface

This thesis is the original work of Mostafa Mohamed. The research project received research ethics approval from the University of Alberta Research Ethics board, Project name "Evaluation of the mechanical properties of the bone-implant interface in lower limb amputees", No. Pro00091955, Completed April 25, 2022 and Project name "An innovative approach for non-invasive evaluation of stability at the implant-bone interface for transfemoral Osseointegrated implants, No. Pro00109990, Currently Active.

This research was supported and funded by MITACS, NSERC, Suncor Energy Inc and the Office of the Assistant Secretary of Defense for Health Affairs through the FY20 Peer Reviewed Orthopaedic Research Program, endorsed by the Department of Defense under Award No. W81XWH-21-1-0857. Opinions, interpretations, conclusions, and recommendations are those of the author and are not necessarily endorsed by the Department of Defense.

This research is part of an ongoing collaborative investigation that aims at designing a vibration-based measurement system for the bone anchored implant for transfemoral amputations. The project focuses on the mathematical and experimental modelling aspect of the project. The first author's role in the publications involved developing the 1D and 3D finite element simulations and the design and data collection for the experimental setup.

Complete list of publications that came out of this research:

The role of M. Mohamed as a first author involved developing the mathematical and experimental models, results generation and analysis in the following publications.

> **M. Mohamed**, E. Beaudry, A.W. Shehata, D. Raboud, J.S. Hebert, and L. Westover, "Determining the Bone Implant Interface Properties of Transfemoral Implants using Vibration Analysis (TO BE SUBMITTED)," *Ann Biomed Eng*.
>
> **M. Mohamed** and L. Westover, "Evaluating the dynamic behavior of bone anchored hearing aids using a finite element model and its applications to implant stability assessment.," *Med Biol Eng Comput*, vol. 60, pp. 2779–2795, 2022, doi: https://doi.org/10.1007/s11517-022-02607-y.

M. Mohamed, H. Pisavadia, and L. Westover, "A finite element model for evaluating the effectiveness of the Advanced System for Implant Stability Testing (ASIST)," *J Biomech*, vol. 124, 2021, doi: https://doi.org/10.1016/j.jbiomech.2021.110570.

M. Mohamed, D. Raboud, J. S. Hebert, and L. Westover, "Stability Assessment of Osseointegrated Transfemoral Bone-Implant Systems using Finite Element Modal Analysis," in *Proceedings of the Canadian Society for Mechanical Engineering International Congress 2022*, Edmonton, 2022. doi: http://dx.doi.org/10.7939/r3-s23c-as14.

The role of M. Mohamed as a second author involved sharing the mathematical model with the first author of the following publications and assisting them with the analysis.

E. Beaudry, **M. Mohamed**, J. Hebert, and L. Westover, "Design of a Handheld Impactor for Transfemoral Osseointegrated Implant Stability Assessment," in *FEGRS*, Edmonton: University of Alberta, 2023.

A. Lau, **M. Mohamed**, and L. Westover, "Application of the Effects Model for Evaluating Interaction of Impact Properties on Impact Response," in *UofA Dean's Research Award*, Edmonton: University of Alberta, 2021.

Acknowledgements

I would like to thank and acknowledge:

My supervisor Dr. Lindsey Westover for her constant and unwavering guidance and support throughout the duration of this project. I appreciate the opportunity of working on this project and being a member of your research group.

Dr. Jacqueline Hebert and Dr. Donald Raboud for serving on my supervisory committee and for their continuous and thorough feedback over the course of this project.

Dr. Ben Jar and Dr. Heidi Ploeg for taking the time to be part of my examination committee.

Dr. Andrew Martin for chairing the exam.

Dr. Gary Faulkner and Dr. Samer Adeeb for their interest in this project and their willingness to provide advice and support.

I would also like to thank the BLINC lab members (Ahmed and Rory) for their input and support throughout the duration of this project.

My parents (Amany and Omar), my sister (Mariam), my friend since high school (Mohab), all my other friends and lab members (Annette, Ashreen, Boyu, Cass, Chester, Dylan, Eric, Jonelle, Maha, Mostafa, Nada and Tod) for their love and support.

Table of Contents

List of Tables

List of Figures

Chapter 1 Introduction

1.1 Background

In the 1950s PI-Brånemark reported that titanium structures can be permanently and directly adhered to the bone tissues without having to use bone cement and he introduced the term osseointegration to describe this bonding process [1]. This gave rise to the field of osseointegrated implants with the first human application reported in dentistry in 1965 [2]. Since then, the field of bone anchored implants rapidly evolved to include Bone Anchored Hearing Aids (BAHA), facial prostheses, finger-joint prostheses, cementless hip arthroplasty and implants for lower limb Transfemoral Amputations (TFA) [1], [3]. The longitudinal survival of osseointegrated implants (which can be denoted as implant stability) is directly related to the quality of the bone-implant interface (BII) [4], [5]. Therefore, assessing the properties of the BII is critical in early-failure detection, assessing surgical outcomes and optimizing the rehabilitation protocols [4]–[6]. Rehabilitation protocols for TFA implants for example, currently rely on periodic radiographic assessments to determine the quality of the BII and physiotherapists have to use standardized schedules and their judgement (among other qualitative tools such as an analogue visual scale to assess pain) to determine the suitable loads for the patients [7]–[9]. A quantitative and non-invasive implant stability measurement system could reduce the patient's exposure to harmful ionizing radiation and help in making better informed decisions (such as appropriate load bearing) during the rehabilitation process. Furthermore, it could help in better understanding the biomechanics of osseointegration and the parameters that can influence it. It is believed that there exists an optimal relationship between the timely application of loads and the quality of the bond since excessive early loading can lead to implant failure while acceptable loading levels can promote bone in-growth and remodeling, however this relationship is not well understood yet [6].

Vibration methods can be used to assess the quality of the BII non-invasively and quantitatively [4], [5], [10], [11]. Vibration methods rely on exciting the bone-implant system and analyzing the signal for the system's natural frequencies and/or its damping properties which are indicative of the interface condition [4], [5]. A stable implant experiences a limited degree of micromotion at the BII upon loading and thus retains a high BII stiffness. Since a higher BII stiffness leads to higher natural frequencies, the natural frequencies can be used as an implant stability metric [4], [5], [10]. The main limitation of relying on the natural frequency is its dependency on other

parameters such as the implant system's geometry and thus the natural frequency (as a metric) cannot be used in an absolute sense but rather can only be used for longitudinal evaluation of the BII condition for the same patient [12]–[15]. The Advanced System for Implant Stability Testing (ASIST) is a vibration-based measurement system that attempts to overcome the limitation of frequency-based measurements by utilizing a mathematical model of the bone-implant system [14]. The measured acceleration response is matched with a mathematical model's prediction using optimization to solve for the BII stiffness, which is treated as an unknown in the optimization routine [14]. Computing the interface stiffness in this manner and using it as the primary measure for implant stability has shown better potential in characterizing the BII condition compared to other frequency-based metrics, as the stiffness-based metric was more sensitive to the BII condition and less influenced by the system's geometry [14], [15].

The ASIST has been developed and used for BAHA implants [14]–[16]. This project aims at building on the existing knowledge of the ASIST interface evaluation approach by extending the measurement system to a more complex and relatively newer TFA implant system and further studying the dynamic behavior of BAHA implants using novel modelling approaches. This will be achieved by conducting extensive mathematical and experimental analysis of the dynamic behavior of the bone-implant systems. The mathematical analysis involves utilizing 3D FE simulations which offer higher fidelity than the analytical models previously used by Westover et al. [14] and will allow for testing the implant systems in conditions that could not be mimicked experimentally for BAHA systems. This is also the first (to the authors best knowledge) investigation to attempt studying the dynamic behavior of the Osseointegrated Prosthetic Limb (OPL, Permedica, Italy) TFA system and the first one that proposes a vibration-based measurement system for evaluating the interface properties for this system.

1.2 Motivation and Significance of this Work

The previous modelling attempts for the TFA and BAHA systems are discussed in more details in the literature review, however this subsection will briefly discuss the motivation of this work and the main differences between it and those investigations. The previous modelling attempts for the TFA system primarily focused on the experimental analysis of the Osseointegrated Prosthesis for the Rehabilitation of Amputees (OPRA Integrum, Sweden) [17]–[20], while this investigation focuses on analyzing the response of the OPL system. The OPL system has a longer length

(L =120-160 mm) compared to shorter OPRA (L =80 mm) system, and it achieves primary stability through press-fitting the implant into the femoral canal while the OPRA system achieves it through threading the implant into the canal. Thus, the dynamic response of the OPL system is expected to be different and this investigation is the first one to document it. In addition to this, the previous work was primarily experimentally driven (with some basic validation using 3D FE modal analysis) and primarily focused on correlating the natural frequencies to the BII condition [17]–[20]. However, this work aims at constructing 1D and 3D mathematical models that can perform both eigenvalue (modal) analysis and time domain analysis which provides a more holistic understanding of the system's response and helps in evaluating the stiffness of the BII directly for the TFA systems.

Although mathematically modelling osseointegrated implants has been implemented for BAHA systems, extending the analysis to the TFA OPL system is expected to have additional levels of complexity due to the major differences in the systems' geometries. BAHA systems are significantly smaller (implant-abutment assembly $L \approx$ 10 - 20 mm with an approximate length to diameter ratio of 3.5) and modelling them using an analytical model with 4 degree of freedom, DOF, (and treating the implant and abutment as rigid bodies) may be appropriate since the stiffness of the BAHA implant system is expected to be much larger than the BII stiffness. However, the larger length of the TFA system (implant-adapter assembly $L \approx$200 mm with an approximate length to diameter ratio of over 12.5) is expected to reduce the stiffness of the implant system and can make it comparable to the BII stiffness. Accordingly, treating the system as a rigid body may not capture its response accurately. Introducing the 1D and 3D FE models allows for abandoning the rigid body assumption approach and better represent the system's dynamic properties.

As was mentioned before, the BAHA implant systems were analyzed experimentally and analytically. The adoption of the 1D and 3D FE models for TFA systems is expected to provide a better understanding of the system's dynamic properties. Therefore, it is of interest to also consider the adoption of these models to the BAHA systems. The previous experimental/analytical studies provide a baseline for the dynamic behavior of the system [14]–[16] and incorporating the FE method to the BAHA system is useful in assessing the power of the proposed modelling approach. Having a validated FE model reduces time and increases parameter control compared to conducting experiments. It also provides a full field view of the system's response which can help in better understanding the response. Finally, the incremental validation approach of the 1D FE

model (by comparing its eigenvalues/eigenmodes and its time domain signals with 3D FE and experimental signals) increases the confidence and the physical relevance of the modelling approach for both systems. Therefore, developing the 1D and 3D FE mathematical models is expected to help in understanding the dynamic response of the TFA system and its potential applicability to implant stability assessment. Furthermore, developing 1D and 3D FE BAHA models will build on the existing knowledge acquired from the previous analytical and experimental investigations.

1.3 Thesis Objective

This project aims at formulating a comprehensive understanding of the dynamic behavior of the TFA and BAHA bone-implant systems using mathematical and experimental models. The primary objective of this study is to develop the mathematical models that can predict the vibration response of both implant systems and use them to evaluate the properties of the BII. Therefore, this investigation attempts to answer the following research questions: 1) Are the mathematical models physically representative of the implant systems? 2) Can the models detect changes in the BII condition and become part of a vibration-based implant stability measurement system?

To address these questions, the TFA OPL system is modelled experimentally and mathematically using 1D FE and 3D FE simulations. The 1D FE model is the model intended for clinical use. However, the experimental and 3D FE models are used for building and validating the 1D FE application. As for the BAHA systems, the experimental and analytical models were developed by Westover et al. [14]. Accordingly, this investigation will focus on the development of the 3D FE model of the system to test the capabilities and limitations of the current ASIST approach for BAHA systems. The BAHA system will also be modelled using a 1D FE model to see if this novel approach will yield similar results to the previously developed 4 DOF analytical model and explore the opportunities associated with its higher fidelity.

1.4 Thesis Organization

This thesis is organized into 9 chapters and an appendix. Each chapter starts and ends with a summary and consists of subsections. Chapters 4, 6 and 7 are written in publication format since they are either prepared for submission or have been published. The formatting of those three chapters was adjusted from the submission format to preserve the uniformity of this document's formatting style.

- Chapter 1 is the introduction, and it briefly tackles the topic of the research, its objectives and significance.
- Chapter 2 is the literature review; it primarily focusses on the field of osseointegration, the implant systems used in this investigation and the different implant stability measurement techniques.
- Chapter 3 involves conducting a preliminary mathematical and experimental analysis of the TFA implant system, the primary purpose of the analysis is to determine the most appropriate testing conditions for the proposed measurement system.
- Chapter 4 utilizes the conclusions of Chapter 3 and is allocated to the development of a 1D FE axial model of the TFA implant system. The 1D FE model undergoes a series of validations with 3D FE simulations and physical models.
- Chapter 5 is allotted to addressing some of the challenges that faced the 1D model in extracting the experimental LOW BII condition in Chapter 4. It also discusses the damping model and tests the particle assumption of the impactor. The chapter concludes with the evaluation of the experimental LOW conditions and summarizes the achievements and limitations of the work done for TFA systems in this research.
- Chapter 6 discusses the development of a 3D FE model for BAHA implants and is dedicated to assessing the performance of the ASIST 4 DOF model in evaluating the BII properties over a wide range of conditions.
- Chapter 7 involves validating the 3D BAHA FE model with previously collected benchtop and clinical signals. The model is then used to better understand the system in terms of the: 1) interface influencing parameters and 2) relationship between the impact instigated in the rod and the stress wave travelling through the bone implant system.
- Chapter 8 shows the development and testing of the 1D FE model for BAHA implants and compares its performance to the previously developed 4 DOF model.
- Chapter 9 is the last chapter and serves as the conclusion; it summarizes the work, its limitations and the recommendations for future work.

Chapter 2 Literature Review

2.1 Osseointegrated Bone-Implant Systems

2.1.1 Historical Overview of Osseointegration

P-I Brånemark was investigating the blood flow in a rabbit's ear chamber and introduced a threaded titanium implant to the rabbit's ear canal in the 1950s [1]. The growth of a stable and functional osseous layer between the implant and the surrounding bone tissues led the investigators to consider its potential use for other applications. In 1965, P-I Brånemark commenced the clinical trials of using osseointegrated implants to replace missing teeth [2]. Owing to its superior performance compared to conventional prosthodontics, more than 800,000 patients have been treated with osseointegrated dental implants from the period between 1965-2001 [1]. More recent estimates indicate that the size of the dental implants market was valued at 4.6 billion USD in 2022 with nearly 5 million implants in the US alone [21]. In addition to replacing single missing teeth, osseointegrated implants have been successfully used in the partial and complete restoration of edentulous segments [1]. The success of osseointegration in dentistry gave rise to the use of osseointegrated implants in other fields such as bone conduction hearing, facial prosthetics, cementless hip arthroplasty and transfemoral implants for lower limb amputations [1]. Bone conduction hearing devices rely on surgically installing a percutaneous or transcutaneous (depending on the implant design) implant to the mastoid region of the temporal bone, the implant is connected to an external hearing aid which converts the sound waves into mechanical waves that are transmitted directly though the bone to the cochlea [1], [22]. The first bone conduction hearing aid device was designed by P-I Brånemark and Kuikka in 1977 [1]. In 1990, Rickard Brånemark reported the first successful implantation of a percutaneous osseointegrated transfemoral implant [7]. The implant is surgically inserted into the intramedullary canal and allows for direct load bearing between the prosthesis and the residual bone which could not be previously achieved using a socket prosthesis [6], [7], [23].

2.1.2 Biomechanics of Osseointegration and the Formation of the Bone-Implant-Interface

The definition of osseointegration has underwent several changes since the introduction of the term in the 1950s. The first definition described it as "the direct structural and functional attachment" between the implant and the surrounding bone tissues [1], [2]. Later, the definition changed to indicate that a successfully osseointegrated implant is viewed as an implant that does

not experience “progressive relative movement between the implant and the bone” [1]. The aforementioned definitions evolved from a biomechanical perspective of osseointegration; there are, however, other definitions from other fields. For example from a histologic perspective, osseointegration can be viewed as the direct contact between the bone and implant [1]. Regardless of the definition in use, there is strong emphasis on the relationship between the implant and the surrounding bone and its effect on the short- and long-term survival of the implant, which can be denoted as implant stability. Implant stability is classified into primary and secondary stability where primary stability refers to the quality of the mechanical fixation achieved during surgical implantation while secondary stability refers to the biological integration of the implant with the surrounding tissues [4], [24].

Both primary and secondary stability play an instrumental role in the survival of the implant [4], [24]. The formation of a healthy bone-implant interface (BII) governs the secondary stability of the implant system, where the BII has been described as a “transition zone” between the implant surface and the surrounding bone [24]. The development of the BII is the byproduct of complex (and dynamic) biological and mechanical interactions that occur between the bone tissues and the implant immediately after implantation [24]. Biologically, the successful development of the BII occurs in a series of stages. The first stage involves the formation of a hematoma at the implantation site, where the implant becomes surrounded by blood and the blood provides the required cellar materials needed for bone resorption, growth, and remodeling [24]. The inflammatory response triggers the formation of a provisional bone matrix through fibroblasts (second stage of osseointegration), over time and through the continuous combined action of osteoclasts (for bone resorption) and osteoblasts (for bone growth and remodeling) the bone matrix acquires the composition of the surrounding “native” bone [4], [24].

There are biomechanical determinants that govern implant stability. Primary (mechanical) stability is highly dependent on the surgical implantation conditions while secondary (biological) stability and the formation of the BII depend on a number of factors including the nature and quality of the surrounding bone and the design of the implant [3], [24]. Low quality of the surrounding bone, which can be due to radiation therapy or systemic diseases, can negatively affect the osseointegration process [24]. As for implant related stability determinants, the implants’ geometric attributes, surface topography and material play a critical role in implant stability [3], [24]. Increasing the implant’s surface roughness and adding a porous coating of bioactive material

can positively influence the implant's osteoinductive (implant's ability to stimulate cell's growth) and osteoconductive (implant's ability to host bone deposition) properties [3], [4], [24]. The choice of the material can influence the stability of the implant, where highly stiff materials (in comparison to the surrounding bone) can lead to stress shielding since the implant becomes the primary load bearing component and reduces the loads on the bone. Over time (and according to Wolff's law) the bone gets weaker and experiences reduction in its density [3], [4], [24].

2.1.3 Transfemoral Bone-Implant Systems for Lower Limb Amputations

Trauma, tumor resection, diabetes and peripheral vascular disease can lead to the loss of a limb [6], [23]. While the exact global prevalence of above the knee amputations is not known, in 2005, estimates indicated that there were 1.6 million transfemoral amputees who suffered an above the knee lower limb amputation in the United States [23]. The age adjusted incidence rate in Canada stood at 22.9 lower limb amputations per 100,000 individuals based on the data collected between 2006 to 2011 [25]. Traditional rehabilitation involves the use of a prosthesis that is attached to the residual limb through a custom-made socket over the residual limb (Figure 2-1) [6], [23], [26]. Ideally, the socket must securely fit to allow for the proper load transfer between the residual limb and the prosthesis. However, socket fitting problems, poor suspension, rotation and slippage can occur and lead to intolerable perspiration, skin irritation (sores and ulcers), biomechanical gait deviations and limited hip range of motion [6], [23], [26]. In 1990, Rickard Brånemark performed the first transfemoral implant surgery in Sweden and this development gave rise to the field of bone anchored implants for Transfemoral Amputations (TFA) [7], [23]. Bone anchored TFA implants achieve direct load bearing between the bone and the prosthesis (Figure 2-1), accordingly they eliminate the need for using a socket prosthesis and the problems associated with it.

Figure 2-1 Traditional rehabilitation for lower limb amputations is achieved using socket prosthesis (Left). Alternatively bone anchored implants for lower limb amputation can be used to achieve direct load bearing between the implant and the prosthesis (Right) [27] .

The Osseointegrated Prosthesis for the Rehabilitation of Amputees or the OPRA system (Integrum, Sweden) is the earliest implant system used for the treatment of TFA patients (Figure 2-2) [6], [7], [23]. The implantation process involves installing a threaded titanium implant into the intramedullary canal and approximately 6 months later the patient would undergo a second surgery that involves installing a percutaneous adapter that serves as a connector between the prosthesis and the implant and thus allows for direct load bearing between the prosthesis and the residual bone [6], [7], [23], [26]. The threaded design of the OPRA system allows it to achieve primary stability efficiently and allows the implant to be 80 mm in length which is relatively shorter than the other TFA implant systems [6], [23]. A standardized rehabilitation protocol was established 9 years after the first OPRA surgery in 1999 [7]. The protocol is offered at two paces depending on the patient's skeletal condition. The normal speed protocol is a 12-month program that starts from the first surgery to complete and unrestricted use of the prosthesis while the half speed protocol is an 18-month program [7]. Between 1990 and 2008 one hundred patients underwent treatment using an OPRA implant system by Brånemark's team. It was observed that the implant failure rate and removal was substantially higher (10/15) for the group treated before establishing the

rehabilitation protocol compared to the patients treated with the protocol (5/41) [7]. Although implant failure (and removal) is a risk associated with the OPRA TFA implant systems, the majority of the failures occurred before the establishment of the standardized protocol and the most common complication are superficial infections (66%) which can be treated using oral antibiotics [7], [26]. In addition to this, significantly higher scores for the four categories (Prosthetic Use, Mobility, Problem and Global) of the Questionnaire for Persons with a Transfemoral Amputation (Q-TFA) before the operation (using a socket prosthesis) and at different follow up years after the operation indicated a significant improvement in the quality of life of the patients after the introduction of the implant system [26].

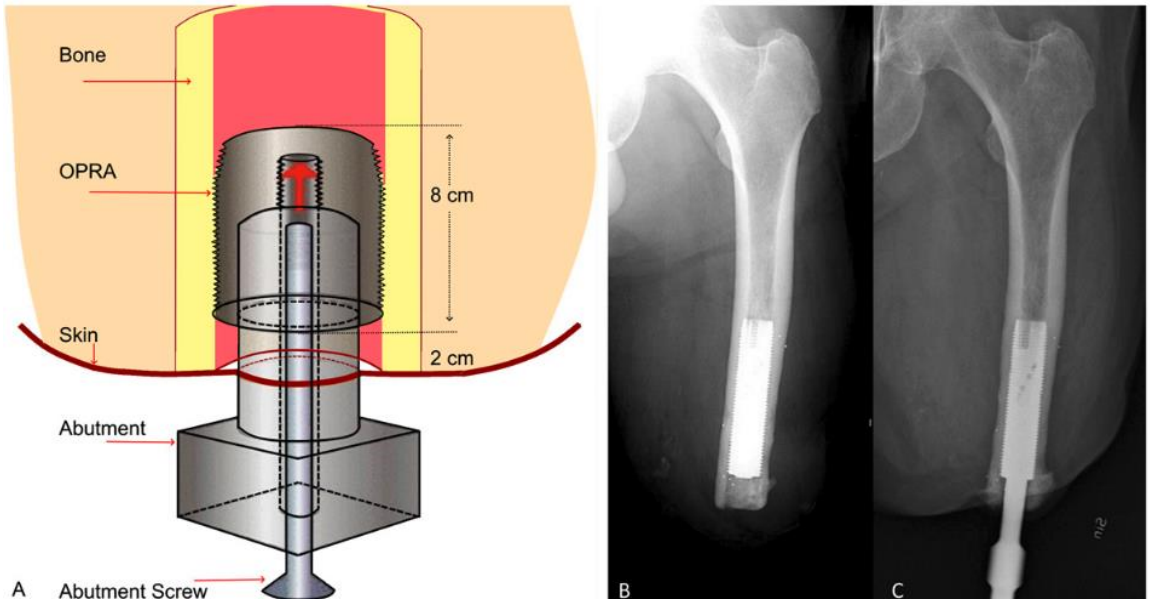

Figure 2-2 The OPRA TFA implant system and its main components (Left). The intramedullary stem achieves primary stability through its threaded design (Right) [23], [28].

The Integral Leg Prosthesis or the ILP (Orthodynamics, Germany) and the Osseointegrated Prosthetic limb, OPL, (Permedica, Italy) are two common TFA implant systems [6], [23], [26]. They both achieve primary stability through press fitting the implant system directly in the intramedullary canal [6], [23]. The ILP system went through different iterations that changed some of its design features (Figure 2-3), however all iterations were manufactured from a cobalt chromium molybdenum alloy and the surface was roughened by introducing Czech hedgehog texture to promote osteoconduction (bone in-growth) [23]. The OPL system is manufactured from a titanium alloy and the surface is plasma sprayed to promote osteoconduction (Figure 2-4) [6], [23]. Radiographic evaluation of patients treated with the ILP and OPL systems indicated that the

OPL system is associated with lower reductions in the surrounding bone density from stress shielding since titanium alloys have lower tensile modulus (and in turn stiffness) compared to cobalt chromium molybdenum [29]. However, both systems benefited from shorter rehabilitation protocols compared to the OPRA system owing to their higher osteoconductive properties and surface features [23]. Munjed el Muderis et al. introduced the Osseointegration Group of Australia Accelerated protocols, OGAAP-1 and OGAAP-2 [8], [9]. OGAAP-1 is a two-stage surgery protocol and has been used for the ILP and OPL systems while the OGAAP-2 protocol is a single stage surgery protocol (where the implant and the percutaneous adapter are both installed in the same surgical procedure) and has been used for the OPL system [8], [9]. Similar to the OPRA systems, the reported outcomes for the ILP and OPL systems indicated significant improvements in the patient's quality of life using a number of metrics such as the Q-TFA or the 6-minute walk test [8], [9], [23], [26]. Superficial infections have also been the most prevalent complication (36%) and the implant infection rates have been reported to be less frequent for the press-fit ILP and OPL systems in comparison to the screw fixated OPRA system [26], [30].

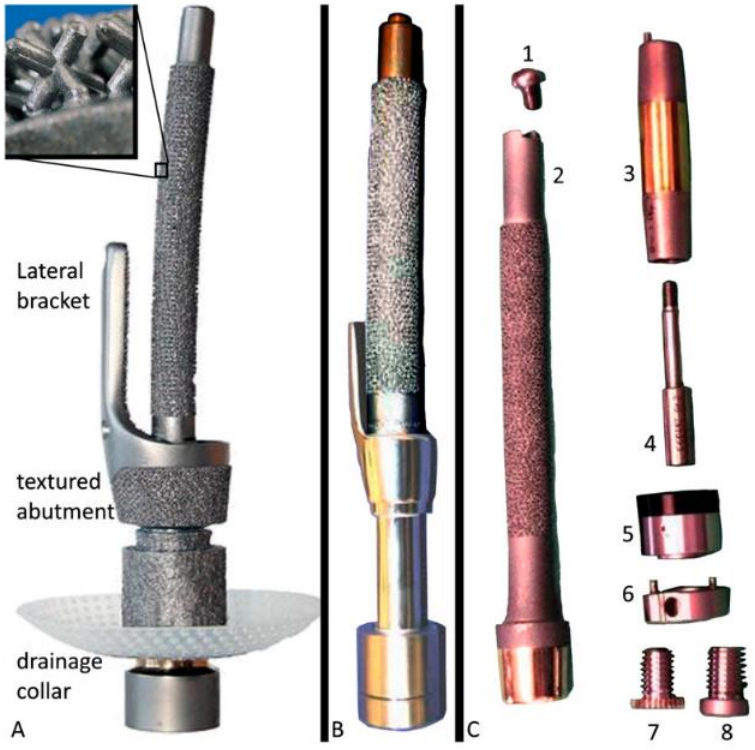

Figure 2-3 The different iterations of the ILP implant system, the leftmost figure shows the earliest design of the implant system while the rightmost figure shows the latest design of the implant system [23].

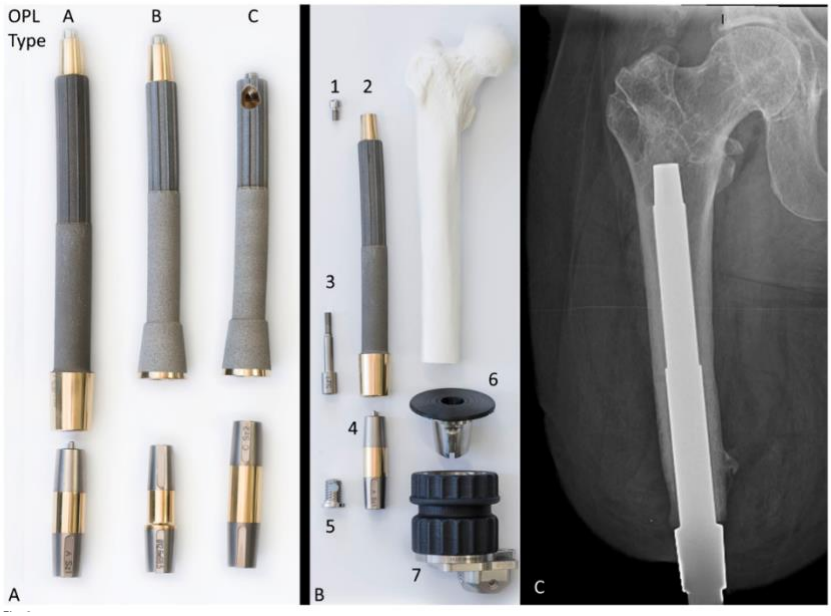

Figure 2-4 The OPL system is available in three different designs to accommodate for the different needs of the patients depending on their residual femur condition. All designs are made from titanium alloy with a plasma sprayed coating that aims at promoting bone growth and deposition (Left). OPL system achieve primary stability by press fitting the implant into the intramedullary canal (Right) [23].

2.1.4 The Bone Anchored Hearing Aid

Patients experiencing unilateral or bilateral conductive hearing losses and single sided deafness have benefited from the use of bone conduction hearing aid devices [22], [31]. Traditional treatment is achieved by air conduction auditory devices; however, their use can be challenging for patients experiencing recurring infections or experiencing congenital anomalies such as missing ear canals or constricted canals (stenosis), or for patients who cannot tolerate wearing headbands for lengthy durations such as in the case of having a benign tumor [22], [31]. In bone conduction hearing an implant is directly installed to the temporal bone, the implant is connected to an external sound processor which converts the sound wave to mechanical waves that can travel through the bone to the cochlea [22], [31]. Bone conduction devices can be classified into two main categories: 1) Percutaneous devices where a skin penetrating adapter (which is also referred to as an abutment) is responsible for connecting the osseointegrated implant to the sound processor (Figure 2-5) and 2) Transcutaneous devices that involve installing the implant directly on the bone along with a magnet and, after the skin is closed (over the implant and the magnet), the sound

processor is connected to the implant magnetically [22]. This research only focuses on percutaneous auditory devices.

The surgical procedure can occur as either a two-stage surgical procedure (where the implant is installed and then the abutment is installed 3 - 6 months afterwards) or as a single-stage surgical procedure (where both the implant and the abutment are installed within the same operation) [31]. The two-stage surgical procedures is primarily reserved for patients with poorer bone conditions (cranial bone thickness $<$ 3 mm) and children [31]. There are two main implant systems that are commercially available in the market: the Oticon Ponto System (Oticon, Sweden) and the Cochlear bone anchored hearing aid connect system (Cochlear Bone-Anchored Solutions, Sweden) [22]. Both systems consist of a threaded implant and a percutaneous abutment. The typical diameter of the implant ranges between 3-4.5 mm and the abutment length can significantly vary between 6-14 mm [22]. Treatments using bone-anchored hearing aid (BAHA) devices have shown significant improvements in functional outcomes such as pure tone average or speech perception compared to the unaided performance [31]. The most prevalent complications of BAHA implants are skin complications such as soft tissue overgrowth and skin infections (ranges from 9.4 to 84%), while there are also cases of dislodgment which require corrective surgeries [31], [32].

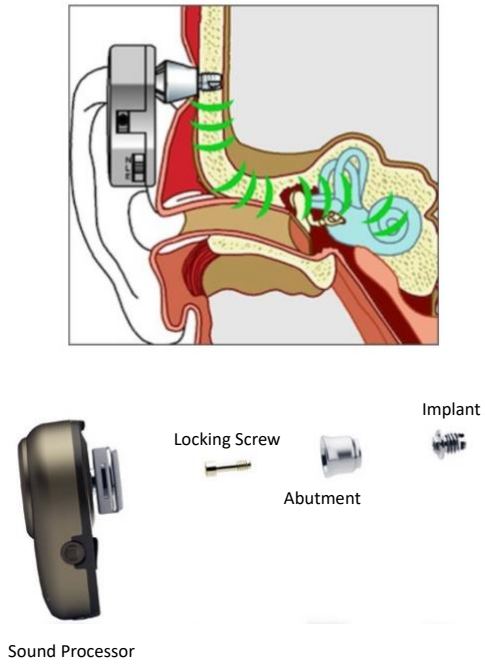

Figure 2-5 A schematic of a bone conduction hearing aid system (Top) and an exploded view of the systems' components (Bottom) [33], [34].

2.2 Implant Stability Assessment

2.2.1 Overview of Implant Stability Assessment Methods

Studying the properties of the bone-implant interface (BII) and in turn implant stability can be achieved through destructive or non-destructive techniques [4], [5], [35]. Histologic analysis can reveal the tissues' structure and composition of the BII through the use of dyes and microscopy; however due to the highly invasive or destructive nature of the analysis procedure these methods are reserved for animal models and non-clinical investigations [4], [5], [35]. Mechanical tests such as tensile, push-out/pull-out and removal torque tests can be used to characterize the tensile, shear and torsional resistance of the BII to these failure modes and assess the quality of the BII in a non-clinical setting [4], [35]. Although these methods have limited clinical applicability, they are useful in cross-validating the non-destructive techniques employed clinically.

Non-destructive testing of the BII condition can be broadly classified into: 1) Imaging and 2) Mechanical techniques. Traditional imaging methods (X-rays and magnetic resonance imaging) rely on the qualitative assessment of the bond between the bone and the implant. Radiolucency at the zones between the implant and the adjacent bones can be indicative of septic or aseptic loosening while a well-integrated implant would appear radiopaque [5], [35]. However, there are several limitations to these methods. X-ray scans (and its derivatives like CT) contain hazardous ionizing radiation and the longitudinal exposure to this radiation could lead to an increased risk of developing cancer [5]. Magnetic resonance imaging does not contain radiation but is highly sensitive to metal artifacts which can distort the quality of the image [5]. Imaging techniques can also be subjective in terms of how the test is conducted and how the results are interpreted and can thus be viewed as qualitative assessments of the BII condition [5], [35]. Finally, traditional imaging techniques are not highly sensitive to the BII condition; it can take up to 40% reduction in the bone density to observe detectable changes in the interface condition using X-ray imaging [5], [35]. To overcome these limitations, X-ray micro-CT can be used to construct a 3D model of the bone-implant system [4]. The model is not only useful in visualizing the quality of the BII but can also be incorporated in FE analysis for studying the behavior of the system under different loading scenarios [4]. Furthermore, Radiosterometric Analysis (RSA) can be used to quantify X-ray radiographs. In RSA, tantalum beads are surgically inserted in the vicinity of the bone-implant system [36], [37]. Through the use of digital image correlation, the migration of the implant can be accurately (with an approximate precision of 50 μm) recorded and quantified [36]. The use of

RSA analysis has been investigated for the OPRA implant systems. Nebergall et al. investigated implant migration for 51 patients over a period of 10 years [36]. They concluded that the median implant migrations were in the order of 0.01-0.02 mm in the period between year 1 to year 7 and that there were no statistically significant migration patterns to indicate loosening which shows that the implant is stable [36]. The main limitation of this conclusion is that it assumes that implant migration patterns of OPRA systems is indicative of potential loosening. While implant migration patterns have the predictive power to predict loosening for hip arthroplasty [38], the OPRA bone-implant system is a completely different system with different boundary conditions and thus the predictive power of RSA analysis should be first assessed. In another study conducted on the OPRA system 7 years later, RSA demonstrated its predictive power to implant failure by showing statistically significant higher implant migration patterns between the patients who had their implants removed (mean migration of 0.55 ± 0.75 mm) and the patients that preserved their implants (mean migration of 0.31 ± 0.51 mm) [37]. Despite of the higher quality of information obtained from 3D X-ray (micro-CT) or the quantitative nature RSA radiography, both tests are highly influenced by the testing procedure and expose the patients to ionizing radiations.

The other class of methods can be broadly labelled as mechanical methods. These methods include: 1) vibration analysis, 2) reverse torque and 3) wave guided methods (like quantitative ultrasound) [4], [5], [10], [35]. Reverse torque methods have been investigated for osseointegrated dental implants where the test involves loading the abutment and checking if it can withstand a certain torque threshold (20 Ncm for dental implants) [5], [35]. The simplicity of this test is its primary advantage; the prosthetists would already have the implant tightening kit which includes all the necessary tools needed to perform the test and would also have the expertise to perform it [5]. However, this test is usually viewed in binary terms (success/failure) and cannot be used for the quantitative assessment of the BII condition [5], [35]. More importantly, applying torsional loads can be risky and can potentially damage the BII and lead to loosening [5], [35]. Wave guided methods or quantitative ultrasound are a more recent development in the field of implant stability assessment. The method relies on transmitting a high-band frequency (10 MHz) pressure wave throughout the bone implant system by attaching a transducer on the implant system and analyzing the radiofrequency signal [4], [5], [39]. Animal studies indicated that averaging the amplitude of the radiofrequency signal (which can be viewed as acoustical power) can be sensitive to BII changes [4], [5], [39]. Despite the promising prospects of quantitative ultrasound due to its non-

invasiveness and quantitative nature, more analysis needs to be conducted to better understand the physical relevance of any metric produced from it since wave-propagation throughout the bone-implant system is a complex phenomenon and is not only influenced by the BII but the entire system and its boundary conditions [4].

2.2.2 Vibration Methods

Vibration analysis (sometimes referred to as resonant frequency analysis) is an appealing method for the non-invasive and quantitative assessment of the BII condition [4], [5], [10], [11]. Vibration analysis relies on analyzing the dynamic response of the bone-implant system upon excitation [5], [10], [11]. The bone-implant system can be mechanically excited under a steady-state load (forced vibration) or a transient (impact) load (free vibration). In both cases the system's response (which is typically an acceleration signal recorded by an accelerometer) can be analyzed for some load-independent (assuming linear vibrations) characteristics namely: the natural frequencies, damping ratios and mode shapes [10], [35]. Those characteristics have proven to be sensitive to the BII condition. The BII stiffness influences at least one of the natural frequencies of the bone-implant system and since there is a direct (but not linear) relationship between the stiffness and the frequency, the measured frequency can be indicative of the BII condition [4], [5], [10], [35]. Damping ratios can also be indicative of the interface condition (albeit commonly used as a secondary metric), since it is expected that softer tissues (in the case of developing fibrous tissues) are expected to exhibit higher damping characteristics [5].

As was mentioned earlier, the bone-implant system can either undergo forced or free vibration and both methods should yield the same signal characteristics since the natural frequencies, damping ratios and mode shapes are invariant to the applied loads according to linear vibration theory [40], [41]. However, there are practical considerations in choosing one method over the other. Impact (transient) tests are simpler to apply and they excite a wide range of frequencies at once, while shaker tests involve exciting one frequency at a time and performs a sweep over the measurement range of interest [41]. Therefore, shaker tests use more complex equipment but typically end up with higher signal to noise ratio than impact tests [18], [41]. The use of vibration analysis has been popular in the fields of dentistry. The Osstell ISQ (Osstell AB, Sweden) is one of the most commonly used systems within dentistry. The testing involves installing a transducer (Smartpeg^{TM}) on the abutment, the bone-implant-transducer system is then excited using a sine wave that ranges from 5 to 15 kHz with a step size of 25 Hz [5], [10], [11], [35]. The response of

the system is analyzed and the Implant Stability Quotient (ISQ) is computed from the resonant frequencies [5], [11], [35]. Since the transducers are part of the bone-implant system during the testing, calibration needs to be implemented for the different transducer geometries designed for different implant systems [11]. Several clinical studies validated the sensitivity of the ISQ to implant stability however some studies indicated that the ISQ values are more sensitive to the early phases of osseointegration and cases of rapid failure and are less sensitive to incremental changes to the interface condition [5]. The Periotest® (Siemens, Germany) is another vibration-based measurement instrument original developed to measure the quality of the periodontal ligament of natural teeth. It consists of a small electromagnetic rod that is attached to an accelerometer [5], [35]. The rod impacts the system and the contact time is used to compute the Periotest Value (PTV). A large contact time would yield a high PTV (high mobility) and low implant stability while a small contact time indicates lower mobility and a more stable configuration [5], [35]. When the impact rod is in direct contact with the system, it becomes (temporarily) part of the system and thus its retraction is viewed as the dynamic response of the bone-implant-rod system and thus the contact time is a function of the bone-implant-rod system's natural frequency and is therefore indicative of the BII stiffness [5]. It should be noted that some studies compared the performance of both devices, and it was found that the PTV and ISQ values are strongly correlated for a given set of interface conditions, which suggests that both metrics measure the same outcome [42], [43]. The primary limitation of relying on the natural frequency as an implant stability metric is its dependence on other factors (such as the implant-abutment geometry) besides the BII condition [14]. Pattijn et al. and Zanetti et al. both conducted numerical (finite element) simulations and analyzed the modal behavior of dental implant and observed that the geometry of the implant-abutment system has a significant influence on the resonant frequencies of the system [12], [13]. Therefore, they both concluded that relying on the natural frequency is only useful for the longitudinal evaluation of a single patient's implant condition but a universal metric that is solely computed from the system's natural frequency would be hard to establish due to this limitation [12], [13].

Due to its relative novelty, there are no vibration-based commercial devices for TFA systems. However, there were four primary investigations that evaluated the potential use of vibration methods for the TFA OPRA system. The first study was conducted by Shao et al. who studied the bending response of the OPRA system under an impact condition (generated by a small oscillating

pendulum) [17]. In their in-vitro experiment (Figure 2-6), Shao. et al. simulated different interface conditions by installing the replica OPRA implants (manufactured from stainless steel instead of Titanium) in a composite femur (SAWBONES Pacific, USA) with similar biomechanical properties to human femurs using three different silicon rubber elastomers (with different tensile moduli) [17]. The fundamental bending frequency was shown to increase over the elastomers curing time and between the three different elastomers [17]. Both observations confirm the sensitivity of the fundamental bending mode to the tensile modulus of the BII, which is a factor that governs the interface stiffness [17]. In their in-vitro study, Shao et al. showed statistically significant longitudinal variations in the fundamental bending mode and was also able to attribute those variations to the patient's load bearing capacity [17]. Cairns et al. conducted a series of studies on the OPRA system as well [18]–[20]. In their studies, experimental modal analysis was conducted on the bone-implant system under various conditions. In their first study, they compared the behavior of the bone-implant system under two interface condition which were :1) secure (with an insertion torque of 4 Nm) and 2) loose (with an insertion torque of 0.5 Nm) [18]. The bone-implant system was transversely excited at 17 different locations (and the response was also measured at those locations) using an impact hammer and an electromagnetic shaker to test the effectiveness of both excitation methods [18]. Since they were measuring both the input and output signals over different locations, they were able to construct the Frequency Response Functions (FRF) and not only estimate the natural frequencies of the system but also its mode shapes and the coherence of the measurement, which is a signal quality metric [18]. The investigation showed that the shaker performed better since the coherence was higher than the impact hammer and they also reported higher natural frequencies [18]. The other two investigations focused on further assessing the behavior of the bone-implant system under different interface and femoral boundary conditions using the same modal analysis procedure performed in their first study. In their second study, Cairns et al. modelled the behavior of the bone-implant system under two femoral conditions (free-end and cantilever). They concluded that the bending natural frequencies were sensitive to the interface condition (secure/loose) for both femoral conditions [20]. However, they concluded that the values of the natural frequencies changed between each femoral condition and deduced that the transverse modes are sensitive to how the femoral head is constrained [20]. In their last study, they attempted to model the physiological interface changes which is based on Brånemark's observation on osseointegration, and they concluded that the bending modes are sensitive in

detecting interface changes however the higher order bending modes tend to be more sensitive to the physiological changes in the BII [19].

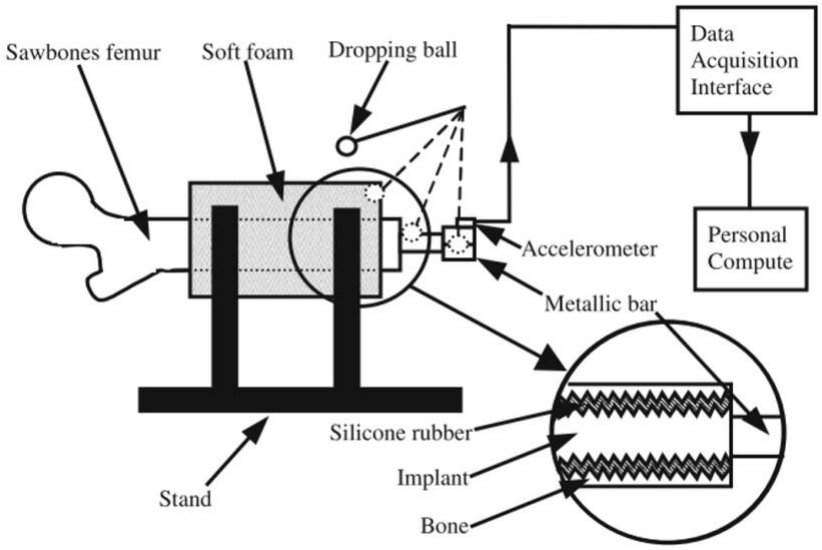

Figure 2-6 A schematic of the experimental setup used by Shao et al. [17].

2.2.3 Advanced System of Implant Stability Testing (ASIST)

As it was mentioned in the previous section, a primary limitation of relying on a stability metric that is defined from the natural frequency is that the natural frequencies depend on other factors such as the implant system's geometry. Westover et al. developed the Advanced System for Implant Stability Testing (ASIST) to overcome this limitation [14]. The ASIST is a vibration-based implant stability measurement system developed for BAHA implants. It relies on a modified Periotest® for exciting the system and measuring the impact rod's response [14]. Instead of just relying on the contact time and PTV scores (which are solely frequency-based metrics), the ASIST matches the input signal to a mathematical model's prediction [14]. The mathematical model aims to properly represent the stiffness, inertial and damping properties of the bone-implant system since an accurate mathematical representation would allow for the direct computation of the BII stiffness [14]. By definition, the BII stiffness is a more direct measure (compared to the natural frequency) of implant stability, since the BII stiffness is defined as the resistance of BII to the applied loads on the bone-implant system. The BII stiffness is also invariant to the implant geometry since it is a property of the BII [14]. Therefore, Westover et al. constructed a 4 DOF representation of an osseointegrated BAHA implant system using the method of influence coefficients [14]. The

interface stiffness is treated as the model's only unknown and can be solved for numerically using an optimization routine that minimizes the least square distance between the input signal and the mathematical model's prediction [14]. In-vitro investigations of the ASIST, showed that the ASIST Stability Coefficients (ASC), which are directly computed from the BII stiffness, are sensitive to the interface condition and less sensitive to the length of the abutment [14]. Furthermore, the ASIST ASC scores outperformed the Osstell's ISQ scores since the ASC scores were more sensitive to the interface condition and were minimally influenced by the abutment length [15], [16]. Longitudinal evaluation of the BAHA patients using the ASIST, showed that the ASIST was able to detect variations (scores ranging from 11.9 to 137) throughout different stages of healing. Results showed that patients would typically have high ASC scores due to high primary stability that gradually decrease for a period of 3 months and then an increase for up to 1 year [38].

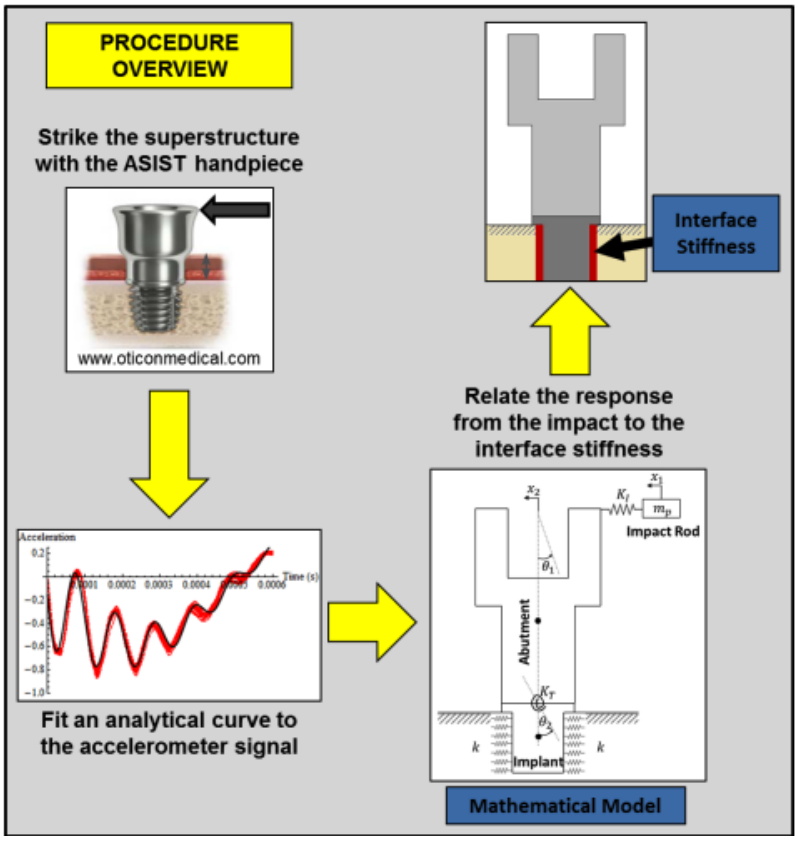

Figure 2-7 Overview of the implant stability assessment method using the ASIST approach [44].

Chapter 3 Preliminary Mathematical and Experimental Modelling of the TFA System

In this chapter, preliminary mathematical and experimental analysis of the TFA system is conducted. The purpose of this chapter is to establish a better understanding of the main parameters that influence the vibration response of the system and narrow down the scope of the mathematical analysis to specific behaviors of interest, that are most relevant to the clinical situation, in the proceeding chapters. The chapter commences by analyzing the system using a 3D FE model on ABAQUS®. The model performs modal analysis and extracts the bending (transverse) and axial frequencies and mode shapes of interest. The modes extracted from the 3D FE model provide a baseline for the expected behavior of the system and can help in assessing the experimental results. The experiment entails installing the implant system into a residual femur in a similar manner to the clinical scenario. Two levels of secondary stability are mimicked by bonding the implant using silicone rubber and cyanoacrylate (superglue) adhesives which represent a soft (LOW) and a stiff (HIGH) configuration respectively. The primary objective of the experimental setup is to assess the sensitivity of the vibration response to different BII conditions. Additionally, the experiment, coupled with the results of the 3D FE modal simulations, can help in determining the effect of influencing parameters on the response namely the: 1) striking condition, 2) boundary condition, 3) adapter geometry, 4) presence of an additional connector (GV connector) and 5) accelerometer mounting method. Some of these parameters are unavoidable in a clinical setting and therefore studying their effect is critical in selecting the ideal testing conditions and developing the clinical mathematical model accordingly. The chapter concludes by summarizing the primary points of the mathematical and experimental analysis and highlights the key features of the subsequent model development and analysis in the coming chapters.

3.1 3D FE Modal Analysis of the Transfemoral Implant System

In linear vibration theory, the dynamic response of a system is the linear combination of its modes of vibration [40], [45]. A mode of vibration is a deformed configuration that indicates the relative position of each DOF with respect to its undeformed (undisturbed) state at a particular frequency (natural frequency). Evaluating the structure's modes of vibrations is essential in 1) understanding the dynamic behavior of the system and its possible sets of solutions and 2) constructing the time domain solution of a structure under specific loading conditions [40], [45]. The latter will be the

subject of the coming chapters however, this section focusses on obtaining the mode shapes and natural frequencies of the TFA system.

Simple structures can be approximately modeled using a discrete set of DOF (like in single and multi-degree of freedom analysis). The number of modes will be equal to the number of independent DOF in the system and they can be extracted by performing eigenvalue analysis of the mass and stiffness matrices of the system. However, the approximation can, in some cases, lead to gross inaccuracies in estimating the mode shapes and natural frequencies and modelling the structure as a continuous system becomes more appropriate. Continuous systems have infinite DOF and the solution (which is obtained by solving a partial differential equation) for the mode shapes and natural frequencies is expressed in terms of a transcendental equation. However, the complexity of the analyses increases substantially for problems with complex geometries and boundary conditions, therefore numerical analysis becomes the more appropriate solution method [40], [45].

The TFA bone-implant system is a complex structure and extracting its modes of vibration is implemented with the FE method on ABAQUS® (Dassault Systèmes, France). Figure 3-1 shows a schematic of the TFA bone-implant system. The system is composed of the stem, dual cone adapter, internal locking screw (connects the dual cone to the stem), distal screw, BII and the bone. Although modal analysis reveals the possible solutions of the system without considering the excitation conditions, it is important to highlight the experimental accelerometer location and excitation locations on the schematic as it will be used in analyzing the results and evaluating whether a mode can be experimentally observed or not based on these locations and the mode shape of the structure. The material properties are summarized in Table 3-1. The linear elastic isotropic model (with two-independent material constants) is used to define the elastic behavior of the components. The material model is suitable for all the metal components and, although the bone is orthotropic (transversely isotropic), the linear elastic model can be used as a good approximation for long cortical bones under small deformation [46]. The mass density is also defined to account for the component's inertial properties. The BII is modelled as a thin uniform layer that connects the implant to the bone at the interface region on the stem (distal region from the femoral head). Although the quality of the BII is the by-product of many factors such as its material properties, density and its distribution [4], the quality of the interface is mainly controlled by a single parameter in these simulations, which is the elastic modulus. Two interface conditions

are simulated with values of 0.45 and 1000 MPa which correspond to LOW and HIGH interface conditions. The choice of these conditions is explained in more detail in the experimental sub-section. The components are assembled and tied constraints are applied between the different components to inhibit relative motion at the nodes of the intersecting surfaces of the different components. The outer walls of the cortical shaft were fixed in all directions. The eigenvalue Lancsoz solver was set to extract all the modes up to 24 kHz (accelerometer's bandwidth) or up to the first 8 modes (since no more than 5 peaks in the frequency domain were ever observed experimentally). The components were meshed (Figure 3-1) using full integration linear hexahedral elements (C3D8). Reduced integration elements were avoided since they can give rise to spurious modes due to reduced stiffness (hour-glass elements). Mesh independence was carried out by doubling the total number of elements until no observable changes (that exceed 1%) are recorded in any of the natural frequencies. Although the mode shapes can be visualized using the solver's GUI (Figure 3-2), it is useful to create a path along the implant system's length and extract the deformed configurations along this path in the directions of interest which are U_1 (x-direction) for the bending modes and U_3 (z-direction) for the axial modes (Figure 3-3). It should be noted that the bone and BII were graphically suppressed to make the visualization of the mode shapes easier.

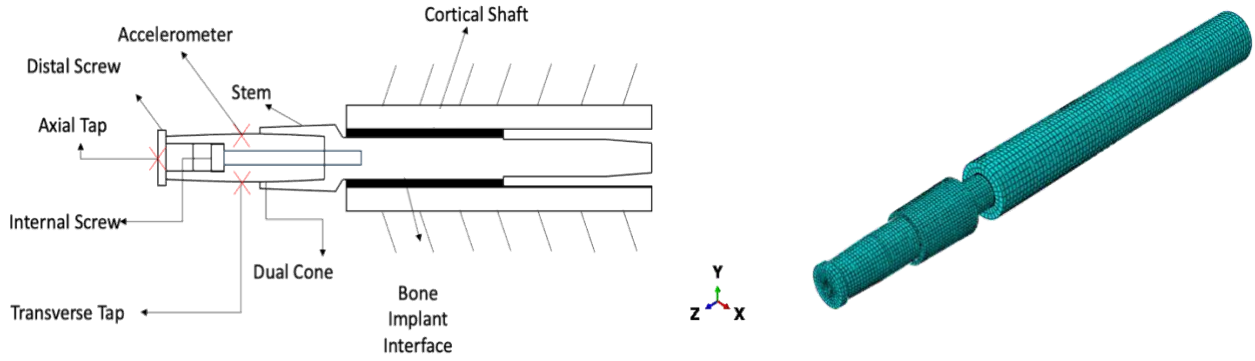

Figure 3-1. Schematic of the TFA bone-implant system (Left) and the corresponding 3D FE model constructed on ABAQUS® using linear full integration (C3D8) hexahedral elements (Right).

Table 3-1. Summary of the material properties of the different components of the system [47]–[49].

Component	**Material**	**Elastic Modulus (MPa)**	**Poisson's Ratio**	**Density (g/cm^3)**
Distal Screw	Titanium	100000	0.31	4.40
Dual Cone	Titanium	100000	0.31	4.40
Stem	Titanium	100000	0.31	4.40
Internal Locking Screw	Titanium	100000	0.31	4.40
BII	Variable	{0.45, 1000}	0.30	1.24
Cortical Shaft (SKU 3403, SAWBONES)	Short Fiber Epoxy	16000	0.30	1.90

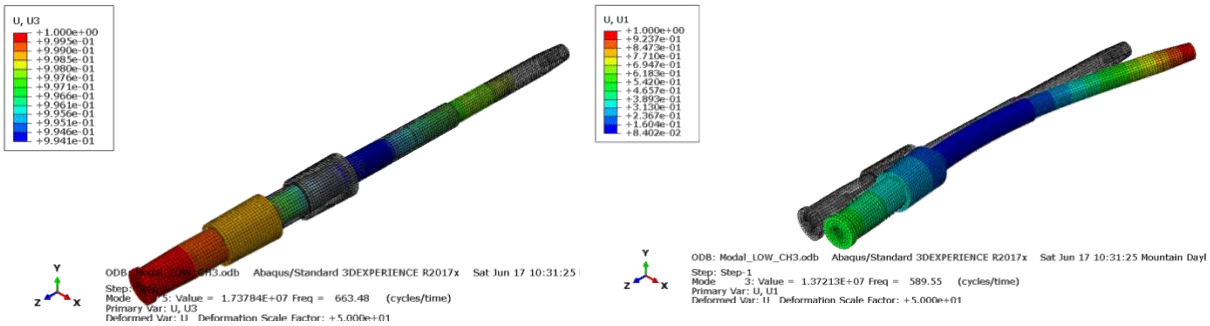

Figure 3-2. The mode shapes can be visualised using the GUI of ABAQUS (R) by plotting the deformed (Colored) and undeformed (Gray) configurations. The figure shows an axial (Left) and a bending (Right) modes and the corresponding frequencies.

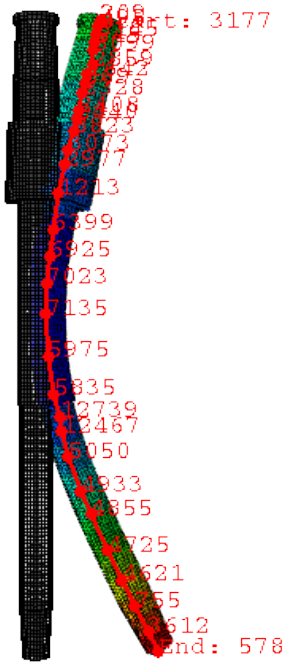

Figure 3-3. A path is defined along the implant system's length and used to extract the mode shapes.

Table 3-2 and Table 3-3 summarize the natural frequencies and the nature of the mode shapes for the two interface conditions. It should be noted that this analysis only focused on the bending and axial responses of the system and excluded other modes (such as torsional modes). Figure 3-4 shows the six bending modes of the LOW interface condition. The blue dashed vertical lines indicate the experimental accelerometer locations (A_1 and A_2) which are discussed in the experimental section. The transverse excitation location (Figure 3-1) is near A_1. From the tapping and measurement locations, it can be inferred that there is potential to identify bending modes 1, 2, and 6 experimentally, while modes 3, 4 and 5 will be harder to identify because the striking/measuring location is very close to a node (a location where there is no deformation in the mode shape). The actual modes that are triggered would depend on the modal contributions due to the excitation conditions, but from the mode shapes it can at least be inferred which modes are more likely to appear in the experimental response. Figure 3-5 shows the axial modes of vibration for the low condition. The 1st axial mode appears to be a mode of relative sliding between the implant and the BII with negligible regions of axial (tension or compression) along the implant length while the 2nd mode appears to have regions of tension and compression along its length. Over the same frequency extraction range, it is expected to observe fewer modes of vibrations for

a stiffer configuration as it is more expensive (energy wise) for the structure to deform. Figure 3-6 and Figure 3-7 illustrate the bending and axial behavior of the system respectively under a stiffer configuration. From the bending mode shapes, it is expected to only observe the second bending mode and maybe weakly observe the fourth bending mode. The results presented here in this section will be compared and further discussed with the experimental results (3.3.1).

Table 3-2. Summary of the 3D FE modal analysis results for the LOW BII condition.

LOW Interface Condition		
Mode	Frequency (Hz)	Nature
1	262	1st Bending
2	590	2nd Bending
3	663	1st Axial
4	1700	3rd Bending
5	2790	4th Bending
6	5420	5th Bending
7	8370	6th Bending
8	9380	2nd Axial

Table 3-3 Summary of the 3D FE modal analysis results for the HIGH BII condition.

HIGH Interface Condition		
1	890	1st Bending
2	1070	2nd Bending
3	4960	3rd Bending
4	6480	4th Bending
5	9770	1st Axial

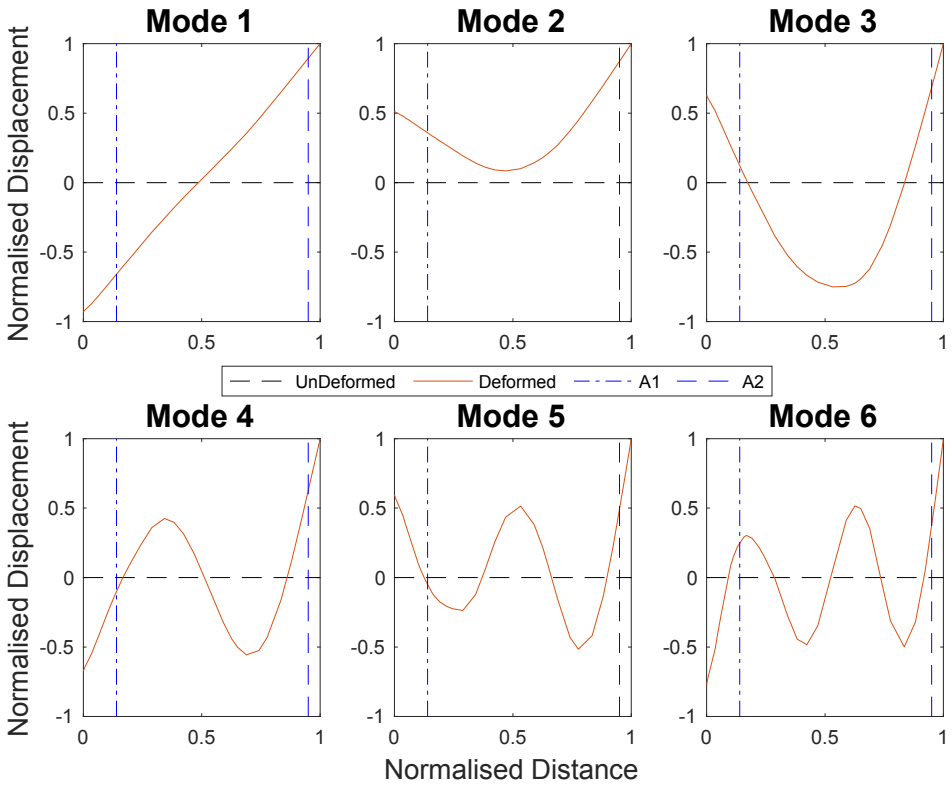

Figure 3-4. The six bending mode shapes for the LOW interface condition. The x-axis represents the normalized distance along the implant length where 0 indicates the tip of the distal screw and 1 indicates the end of the stem and the region of the implant interacting with the BII is between 0.35 to 0.60 . The y-axis represents the normalized transverse displacement of each location along the system. The external and internal accelerometer locations are indicated by A_1 and A_2 respectively.

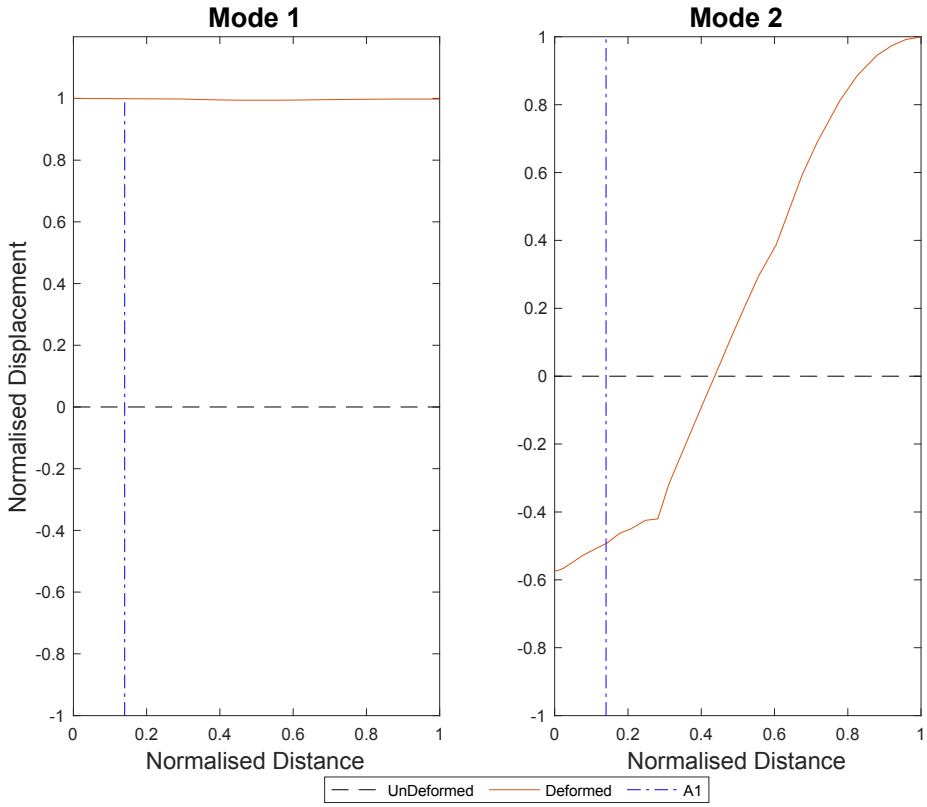

Figure 3-5. The axial modes for the LOW interface condition. The x-axis represents the normalized distance along the implant length where 0 indicates the tip of the distal screw and 1 indicates the end of the stem and the region of the implant interacting with the BII is between 0.35 to 0.60. The y-axis represents the normalized axial displacement of each location along the system. The external accelerometer location is indicated by A_1.

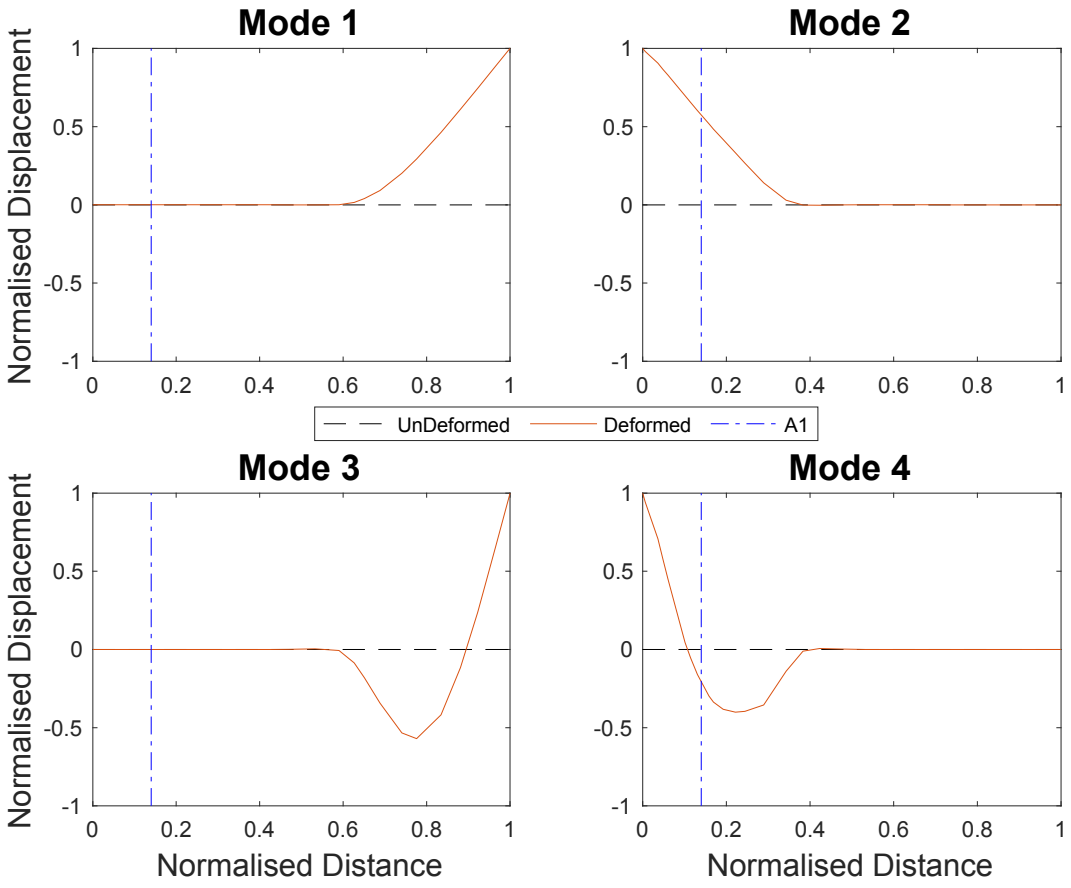

Figure 3-6. The bending mode shapes for the HIGH interface condition. The x-axis represents the normalized distance along the implant length where 0 indicates the tip of the distal screw and 1 indicates the end of the stem and the region of the implant interacting with the BII is between 0.35 to 0.60. The y-axis represents the normalized transverse displacement of each location along the system. The external accelerometer location is indicated by A_1.

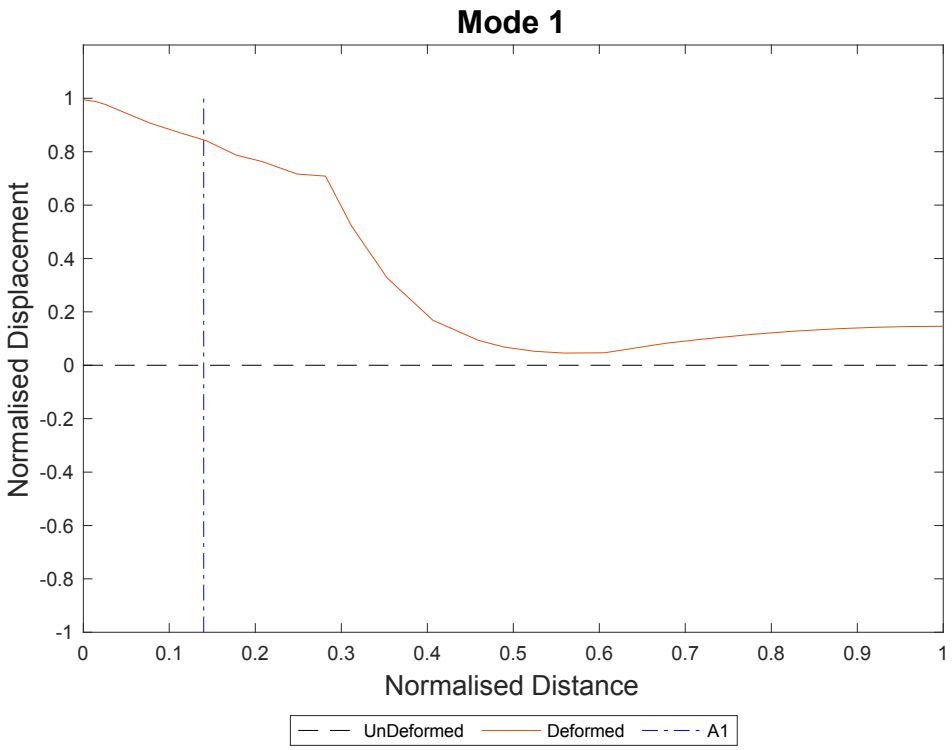

Figure 3-7. The axial mode for the HIGH interface condition. The x-axis represents the normalized distance along the implant length where 0 indicates the tip of the distal screw and 1 indicates the end of the stem and the region of the interacting with the BII is between 0.35 to 0.60. The y-axis represents the normalized axial displacement of each location along the system. The external accelerometer location is indicated by A_1.

3.2 Experimental Setup

A benchtop (in-vitro) experimental setup of the TFA is shown in Figure 3-8. The experimental setup is composed of a type A (Diameter $D = 14$ mm and Length $L = 160$ mm) OPL stem (Permedica, Italy) installed in a composite femur (Pacific Research group, USA). The bone is drilled to a slightly larger diameter (0.2 mm larger than the stem) and the BII is applied uniformly to the distal region (from femoral head) of the stem. To mimic different secondary stability conditions, the interface was generated using DOWSIL 7091^{TM} silicone rubber adhesive (DOW, USA) and using LePage Ultra Gel superglue (LePage, Canada) to represent LOW and HIGH interface configurations respectively. The silicone rubber adhesive was chosen to mimic the behavior of fibrous tissue which is orders of magnitude lower in stiffness compared to immature and mature healthy bone [4]. Silicone rubber adhesives have been used by Waide et al. in modelling the behavior of fibrous tissues in hip arthroplasty and was used by Cairns et al. in modelling fibrous tissue formation for the OPRA TFA system [19], [50]. The tensile modulus of Silicone was found

to be around 0.45 MPa after conducting tensile tests on Electroforce© 3200 UTM (TA Instruments, USA) according to ISO 527 standard. Superglue was chosen to mimic a HIGH stiffness configuration where there is a strong and healthy cortical bone. The average elastic modulus of cyanoacrylates is around 1260 MPa [48]. The technical datasheet does not provide the elastic modulus of the gel-based superglue but it provides its shear and bonding strength which were found to be close to the average values in the web-based database [48], [51]. Therefore, a value of 1000 MPa (which is close to the average) was chosen to represent the elastic behavior of the HIGH interface condition. Although knowledge of the exact material properties is important for cross-validation purposes, those interface conditions were chosen to set two extreme behaviors with orders of magnitude differences in stiffness and are thus viewed as LOW and HIGH conditions. It was more critical to exactly determine the properties of silicone since the dynamic behavior has additional axial and bending modes while the response after a specific elastic modulus threshold of around 5 MPa becomes dominated by fewer modes of vibration. For the LOW interface configuration (where it is expected to observe additional bending modes from 3.1), a secondary internal accelerometer is installed at the stem's tip. Type A dual cone adapter ($L =$ 68.5 mm) is connected to the stem using the internal locking screw which is tightened to 10 Nm similar to the clinical procedure. The distal locking screw serves as a connector between the dual cone adapter and another connector (GV connector discussed in more detail in 3.3.3).

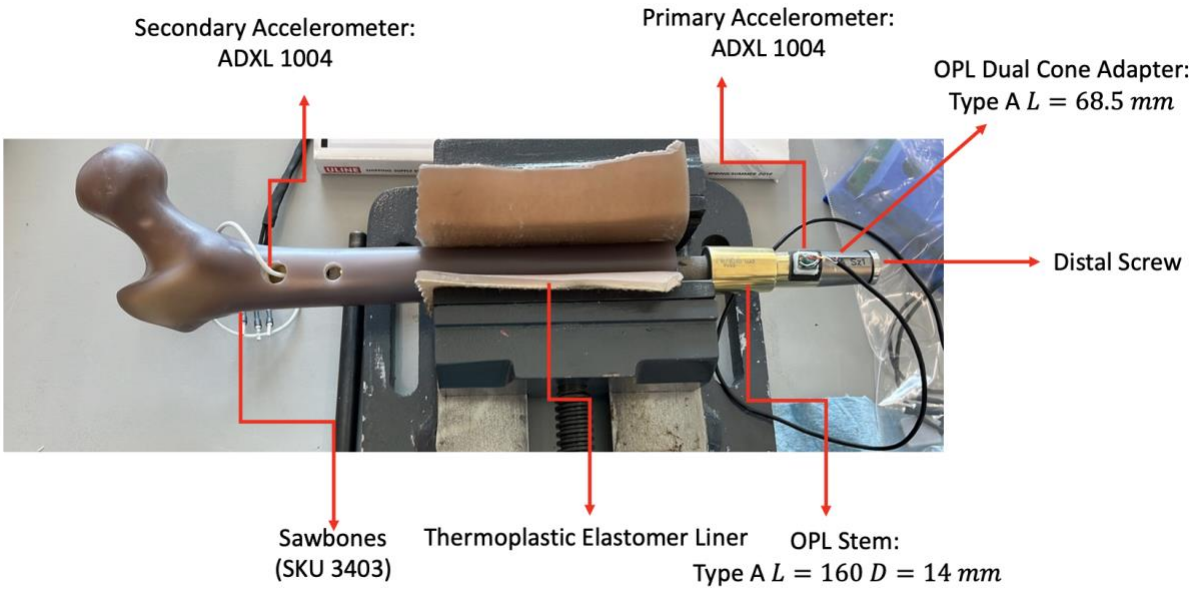

Figure 3-8. The benchtop experimental setup of the TFA system.

ADXL 1004 (Analog Devices, USA) single axis accelerometers are used in measuring the acceleration response of the system. To measure the axial and the bending responses, the accelerometer's sensitivity axis was oriented along the longitudinal direction for axial measurements and then re-oriented along the lateral direction for transverse measurements. The accelerometers have a measurement range of $\pm$ 500 g and a measurement bandwidth of 0-24 kHz where 24 kHz is the 3dB point of the sensor [52]. The accelerometer is mounted using superglue adhesives and the effect of changing the mounting technique is later discussed in 3.3.6. The accelerometer is connected to NI 9205™ data acquisition system (National Instruments, USA) and the acquisition is controlled using Labview™ (National Instruments, USA). The sampling rate is set to 250 kHz which is chosen to be more than ten times the accelerometer's bandwidth to avoid aliasing from higher frequencies and to fulfill Nyquist-Shannon criterion of at least sampling at twice the rate of the highest expected frequency in the signal [41]. Therefore, aliasing is considered to be a minor risk and the need for an anti-aliasing filter is not critical due to the sensor's bandwidth and the oversampling performed by the data acquisition system.

The testing procedure involves clamping the bone with the support (Figure 3-8) five times for each testing condition (except for the BII condition, which was only installed once for each BII condition, since re-installing the BII material required destroying the bone), and for each repetition the Periotest® strikes the implant system 16 times. The first strike is used for triggering the data acquisition and the remaining 15 strikes are recorded, aligned (same starting point) and then averaged. The primary outcome of the test is the dominant peaks (natural frequencies) of the system from the external accelerometers placed on the system. To avoid spectral leakage (a numerical error that occurs when the periodicity assumption is not satisfied in the FFT), for the lightly damped signals (that do not decay to 2% of the initial amplitude within the measurement time) an exponential window is applied to bring down the response close to zero as shown in Figure 3-9 [41]. The frequencies are extracted by identifying the location of the peaks (using MATLAB® (findpeaks) function) and locally interpolating a parabola around the peak (Figure 3-9). Quadratic (parabola) interpolation is a common technique for improving the frequency resolution in the frequency spectrum and improving the estimate for the location of the peak [53].

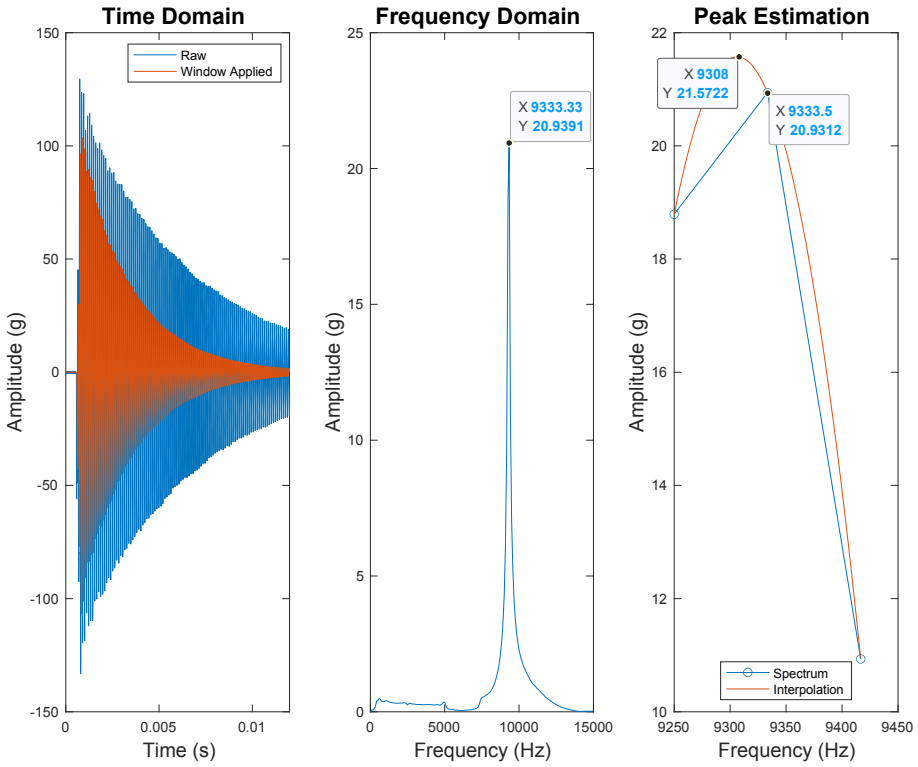

Figure 3-9. Only for the lightly damped signals, an exponential window is applied to reduce the risk of spectral leakage (Left). Applying a small exponential window does not affect the estimation of the frequency but can add artificial damping to the response. In this section, frequency is the primary outcome of the analysis. To improve the resolution of the frequency spectrum (Middle), quadratic interpolation is applied in the vicinity of the peak and the natural frequency is estimated from the maximum point of the interpolated curve (Right).

3.3 Axial and Bending Response of the TFA System

3.3.1 Comparison Between the Experimental and 3D FE Modes

In this subsection, the experimental results are analyzed and compared with the 3D FE model's predictions presented earlier in 3.1. The bending modes of the implant system under LOW and HIGH interface conditions are summarized in Table 3-4. For the LOW BII condition, the response measured using the primary accelerometer (A_1) is dominated by the 2nd bending mode (Figure 3-10). The 4th bending mode seems to be also present in the signal since its amplitude is 60% of the dominant 2nd mode. Those two modes were the only two peaks sharp (and well separated) enough to be detected using A_1. The secondary internal accelerometer (A_2) also captured those two modes, but the peak picking function managed to detect the 5th mode of vibration and, in some strikes, managed to record the 1st mode (where "_" indicates that the mode was not detectable).

Although, there is an agreement between the measurements of A_1 and A_2 with respect to the 2nd bending mode (an absolute difference of 4.5 Hz between the average of A_1 and A_2), there is a wider discrepancy (90 Hz) between the averages for the 4th bending mode. The natural frequency is a system characteristic and should be independent of the excitation and measurement locations [33]. However, there can be (in practice) sources of experimental errors (such as differences in instrumentation or maintaining the proper alignment for A_2 during insertion) that can lead to systematic experimental differences between A_1 and A_2. Considering, however, that the frequency resolution (before applying the quadratic peak estimation technique) is around 60 Hz, this difference can be viewed as a minor difference between those two measurement locations. As for the change in the dominant frequency between A_1 and A_2 and the presence of more modes in A_2, this behavior is expected since the modal contributions to the signal depend on the excitation conditions and the mode shape. For example, the mode shape of the 5th bending mode (Figure 3-4), shows that there is greater deflection at A_2 than A_1 and this indicates that there is a greater chance of observing this mode from A_2 which was reflected in the experimental results.

Table 3-4. Summary of the bending modes acquired experimentally for the LOW condition (using the primary and secondary accelerometers) and the HIGH condition. f, f_{Ri}, f_μ and f_σ correspond to the natural frequencies of the 3D FE model, the frequency of each experimental repetition, the average experimental frequency, and the standard deviation respectively.

Bending Modes for the LOW Interface Condition Acquired Using the Primary Accelerometer (A_1)									
3D FE		Experiment							Difference
Bending Mode	$f\ (Hz)$	$f_{R1}\ (Hz)$	$f_{R2}\ (Hz)$	$f_{R3}\ (Hz)$	$f_{R4}(Hz)$	$f_{R5}(Hz)$	$f_\mu(Hz)$	$f_\sigma(Hz)$	$\frac{\lvert f_\mu - f\rvert}{f}$ (%)
2	590	582	579	578	581	580	580	1.7	1.73%
4	2790	2680	2610	2600	2600	2620	2620	34.6	6.02%
Bending Modes for the LOW Interface Condition Acquired Using the Secondary Accelerometer (A_2)									
1	262	_	262	274	261	263	265	6.0	1.20%
2	590	572	575	575	577	578	575	2.4	2.50%
4	2790	2600	2510	2500	2510	2530	2530	39.6	9.40%
5	5420	4730	4760	4650	4750	_	4720	51.3	12.90%
Bending Modes for the HIGH Interface Condition Acquired using Primary Accelerometer (A_1)									
2	1060	930	940	931	932	929	932	3.8	12.10%

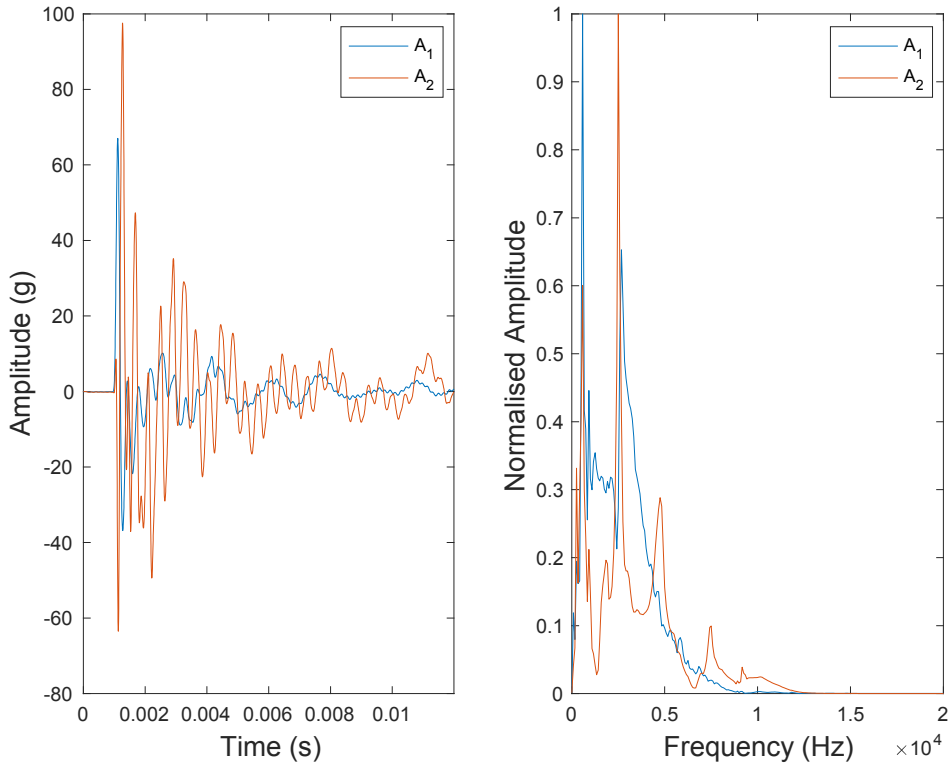

Figure 3-10. Comparison between the time (Left) and frequency (Right) responses obtained using the primary and secondary accelerometers for the LOW interface condition. The response measured by A_1 is dominated by the 2nd and then the 4th bending modes. Due to the nature of the modes shapes (presented in Figure 3-4), the signal from A_2 appears to be carrying more information on the bending behavior of the system.

As for the bending response of the HIGH interface condition, the response is dominated by a single peak in the frequency spectrum at around $f_u = 932$ Hz. Based on the measurement location and the mode shapes (Figure 3-6), this frequency seems to correspond to the 2nd bending mode. This corresponds to an increase of 62% in the 2nd bending mode between the two interface conditions and indicates that the mode is sensitive to interface changes (Figure 3-11 and Table 3-4). Since Cyanoacrylate provides a stiffer configuration, it was expected that fewer modes would be present in the signal. As for the variance between measurements, the standard deviation is significantly lower for the low bending frequencies and seems to be getting higher for the higher frequencies. The maximum standard deviation was reported for the 5th bending mode of the LOW BII condition and stood at 51.3 Hz. Overall, the difference between the model's prediction seems to be minor (1.20-6.02%) for the 1st, 2nd and 3rd bending modes for the LOW stiffness configuration. The error is higher (in the order of 12%) for the 5th LOW BII mode and for 2nd HIGH bending mode. A

possible interpretation for the nature of the error is that for the LOW BII, the lower bending modes (1st, 2nd and 4th) are mainly governed by the BII stiffness since it is the softest region in the implant system. While the higher order modes (like the 5th mode for the LOW BII or the 2nd mode for the HIGH condition) have complex mode shapes that involve more deformation in the implant geometry compared to the BII region (Figure 3-4 and Figure 3-6). This means that for these modes, any errors in the geometry or in conducting the experiment can magnify the difference between the 3D model's prediction and the experimental results and also increases the variance between the measurements.

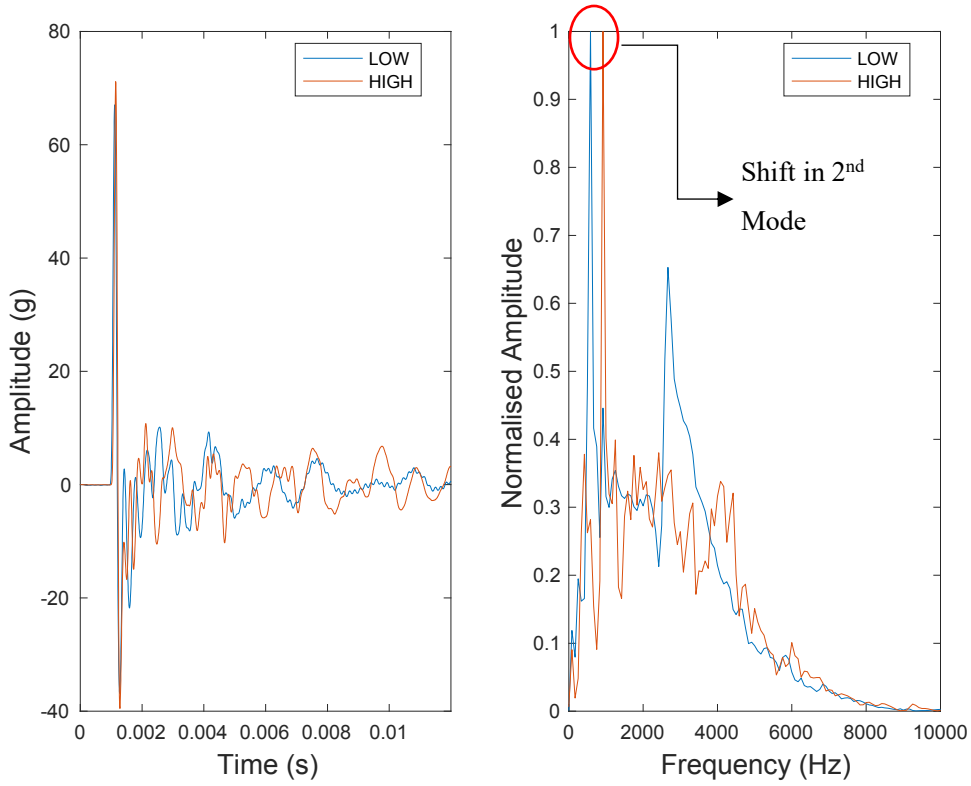

Figure 3-11. Comparison between the time (Left) and frequency (Right) domains for the LOW and HIGH interface condition. There is an increase in the dominant frequency between the two conditions. This indicates that this mode of vibration is sensitive to the interface quality.

The experimental results for the axial responses of the implant were obtained by changing the orientation of the external accelerometer (A_1) to be aligned with the implant's longitudinal axis and using the Periotest® to strike the system along the longitudinal direction at the distal locking screw. The experimental results are summarized in Table 3-5 below. For the LOW interface condition, the 2nd axial mode highly dominated the response and there was a very faint (and

dispersed) presence of another frequency at around 667 Hz by visually inspecting the power spectrum in Figure 3-12. Due to the minor contribution of this mode to the response (the peak is not well characterised), the peak estimation algorithm estimated to be around 599 Hz (Table 3-5). From the mode shape of the 1st axial mode of the LOW BII condition, it appears that there is little to no resistance coming from the BII or within the implant (Figure 3-5). This mode of vibration invokes relative sliding between the entire system and the BII which means that it would require a significant amount of inertia to trigger it. The current impactor has a mass of around 9.4 g [54] and it was mainly designed for dental implants and hearing aids (with a total mass of a few grams), while the mass of the stem-dual cone assembly is around 200 g. Therefore, it is highly plausible that the current impactor does not provide the needed amount of kinetic energy to trigger the 1st axial mode and triggers the 2nd mode (which can be viewed as stress-wave propagating through the system) instead. The 1st axial mode for the HIGH interface situation had an average value of 9540 Hz. There also seems to be a non-negligible presence of another peak in the frequency spectrum at around 2900 Hz. This frequency appears to be a systematic source of noise in the measurement. Stiffer configurations tend to be sensitive to other sources of noise in the system [55]. In this specific cases it is believed that striking asymmetry and/or the bone clamp (since the peak disappeared for the cantilever condition) are causing this peak. In the next section, the main limitations of relying on transverse and axial modes will be discussed and this will involve further analysis of the benefits and limitations of each loading condition. However, it seems that the 3D modal analysis was able to predict the behavior of the system under those experimental conditions and a decision will be made on the most suitable loading condition in a clinical setting based on the additional experiments in the next three sections.

Table 3-5. Summary of the Axial modes for the LOW and HIGH BII conditions.

Axial Modes for the LOW Interface Condition Acquired Using Primary Accelerometer (A_1)									
3D FE		Experiment							Difference
Axial Mode	$f\ (Hz)$	$f_{R1}\ (Hz)$	$f_{R2}\ (Hz)$	$f_{R3}\ (Hz)$	$f_{R4}(Hz)$	$f_{R5}(Hz)$	$f_{\mu}(Hz)$	$f_{\sigma}(Hz)$	$\frac{\lvert f_{\mu} - f \rvert}{f}$ (%)
1	663	596	583	612	597	610	599	11.8	9.59%
2	9380	9310	9310	9310	9310	9310	9310	0.4	0.79%
Axial Modes for the HIGH Interface condition Acquired using Primary Accelerometer (A_1)									
1	9770	9480	9540	9600	9460	9630	9540	72.3	2.33%

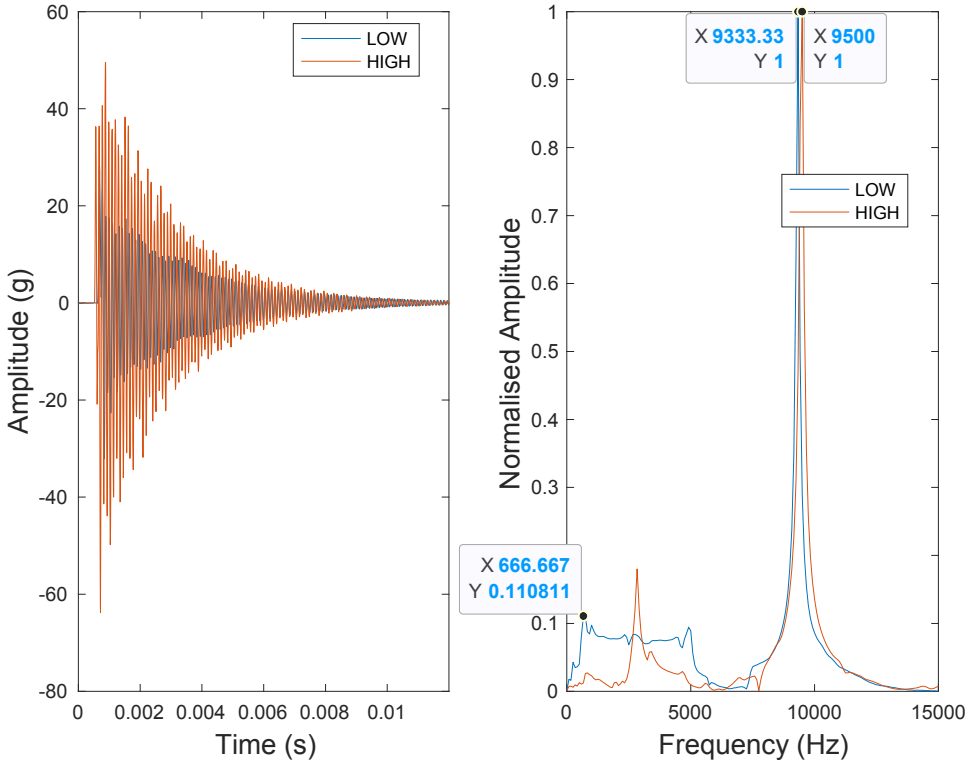

Figure 3-12. The time (Left) and frequency (Right) domain responses of the experimental LOW and HIGH interface conditions.

3.3.2 Effect of changing the Femur's Boundary Conditions on the Axial and Transverse Responses

The experimental results (presented in 3.3.1) were, overall, in agreement with the 3D model's prediction for the bending and axial modes. The experimental results were acquired under the assumption that the femoral head is free. Under this assumption, there are no displacement constraints applied at the femoral head (and thus no corresponding reaction forces) and this allows the model to ignore the geometry of the proximal (relative to the hip joint) femur (head, neck greater and lower trochanter) and focuses on the localized interactions between the intramedullary stem, the BII and the cortical shaft. Shao et al. also experimentally (in-vitro) modelled with an unconstrained femoral head and managed to show the sensitivity to BII under these conditions [17]. Furthermore, they showed statistically significant changes to the fundamental bending frequency and the load bearing capacity of a patient in their in-vivo study [17]. Cairns et al. tested the bending response of the implant system under two femoral boundary conditions: a free end and a cantilever [20]. The cantilever boundary condition involved installing the femoral head, neck and greater trochanter (while stopping before the lesser trochanter) in a resin block [20]. Their findings indicated fundamental changes to the bending behavior of the implant depending on the femoral boundary condition [20].

In this section, the axial and bending behavior is compared between two different femoral boundary conditions. Physiologically, the femur is connected to the pelvis at the hip joint, which can be viewed as a ball-socket joint, where the femoral head acts as the ball connected to the acetabulum (the socket). Therefore, to simulate this experimentally, the femoral head (excluding neck and greater trochanter) is installed in a rigid dental resin block as shown in Figure 3-13 and the axial and bending responses are collected in a similar manner to the previously collected free-end measurements. Although the femoral head is not (physiologically) fully constrained like in this installation, this simplified change to the boundary condition is meant to test two extreme configurations (one where the reaction forces at the femoral head are non-existent, like in the free-end case, and the other one with a full set of reaction loads) and their effect on the bending and axial response of the system.

Figure 3-13. The boundary condition was changed from a free end (Figure 3-8) to a cantilever. The femoral head (excluding the neck and the trochanter) is fixed in a resin block to simulate a cantilever boundary condition.

The bending behavior of the system changed considerably under different femoral boundary conditions. For the LOW BII configuration, the response was dominated by two frequencies located at 580 and 2630 Hz under the free-end condition, while under the cantilever condition the dominant peak is around 2550 Hz (Figure 3-14). Furthermore, other peaks are present in the cantilever response and they were not observed using the model or the experimental results under a free-end condition. For the HIGH BII configuration, the free-end and cantilever responses shared the same dominant peak at around 940 Hz. However, the response for the cantilever condition had an additional peak at around 2550 Hz. This peak is common between the LOW and HIGH BII conditions under a cantilever boundary condition.

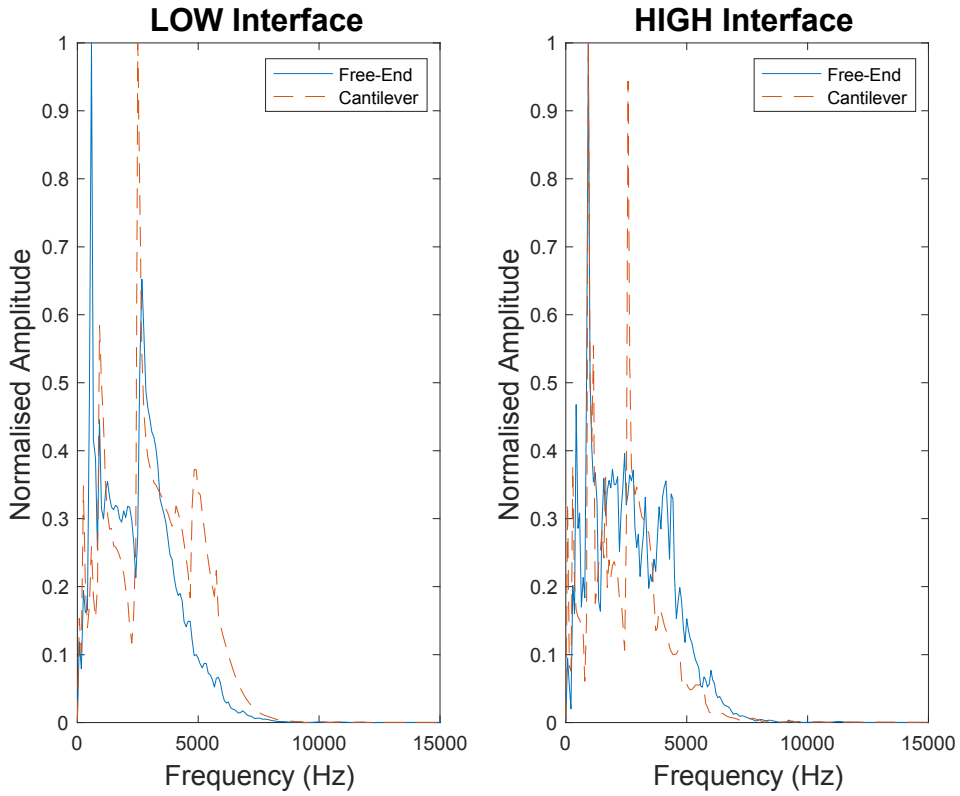

Figure 3-14. Changing the boundary condition from a free end to a cantilever significantly alters the bending response. For the LOW BII condition (Left), the dominant mode changes from around 580 Hz to 2500 Hz. For the HIGH BII (Right) condition, the dominant peak is still around 940 Hz for both boundary conditions but there is an additional peak 2550 Hz for the Cantilever boundary condition.

The dominant frequency under axial loading conditions appears to be less influenced by the boundary condition of the femur (Figure 3-15 and Table 3-6). This indicates that the axial response of the system is insensitive to how the femur is constrained. The axial modes for both boundary conditions, seem to be governed by the local interaction between the BII and the cortical shaft and does not seem to be influenced by the reactions at the femoral head. This is going to be a critical point in 3.3.4. when deciding on the most promising testing conditions for the TFA system.

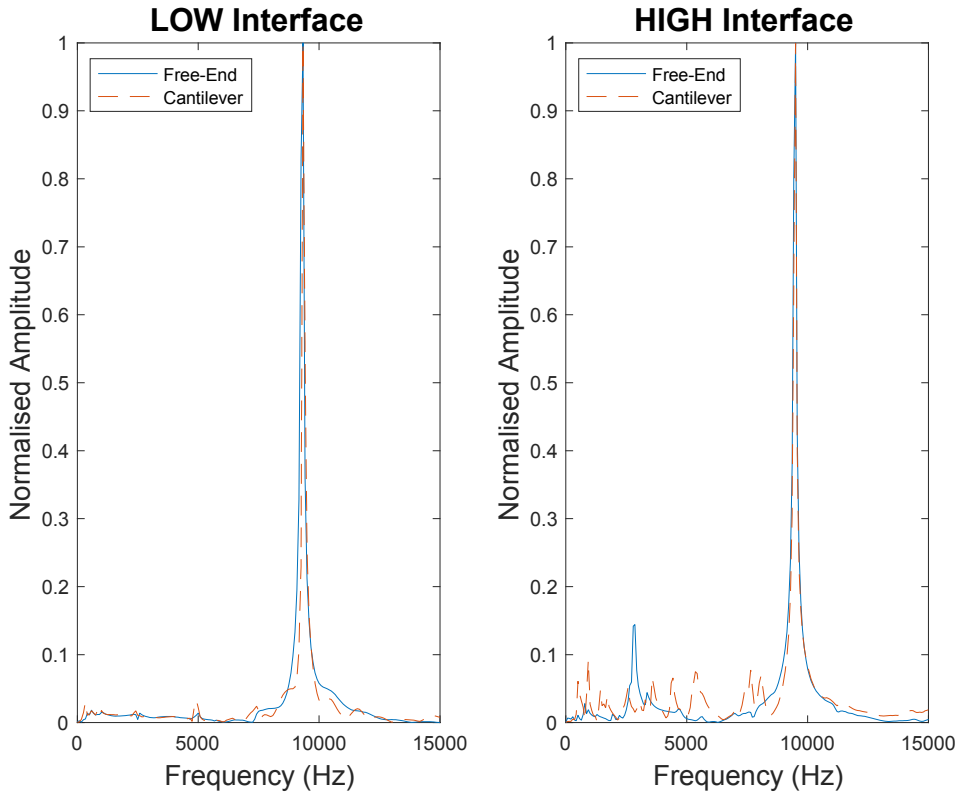

Figure 3-15. The dominant frequency of the axial response is more immune to the femoral boundary condition for the LOW (Left) and HIGH (Right) interface conditions.

Table 3-6. Effect of changing the femur's boundary condition on the dominant frequency of the response.

Axial Response for the LOW Interface Condition		
Boundary Condition	$f_\mu\ (Hz)$	$f_\sigma\ (Hz)$
Free	9310	0.40
Cantilever	9350	0.33
Axial Response for the HIGH Interface Condition		
Free	9540	72.9
Cantilever	9490	0.30

3.3.3 Effect of Adding the GV Connector on the Axial and Transverse Responses

The GV connector is one of the components of the OPL system. It aims to provide a "quick connect" between the implant system (intramedullary stem and dual cone adapter) and the external prosthesis (Figure 3-16). The GV connector is a relatively bulky component (compared to the more slender stem and dual cone adapter) with an approximate mass of 70 g. It is attached to the dual-cone adapter through the distal screw and tightened to 10 Nm. Clinically, frequent installation and removal of the GV connector can be stressful for the patients and must be performed by a prosthetist, therefore it would be challenging to remove the connector before each measurement session. In this subsection, the effect of adding this additional component is briefly investigated experimentally.

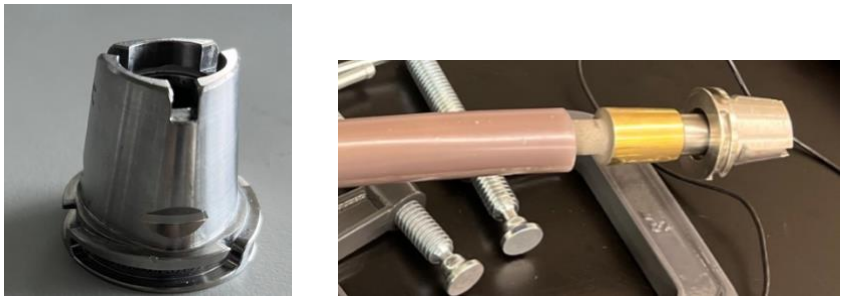

Figure 3-16. The GV Connector (Left) and the stem-dual cone and GV assembly (Right).

The bending and axial responses of the implant system with and without the GV connector are shown in Figure 3-17 and Figure 3-18 respectively. The presence of the GV connector changes the entire nature of the bending response and makes the peaks indistinguishable from each other. This is expected as the GV connector introduces major changes to the stiffness matrix (through the second moment of area) and the mass matrix (through the changes introduced by its larger mass and mass moment of inertia) which highly complicates the mathematical modelling and analysis of the system's response. Introducing the GV connector shifted the dominant peak of the axial mode to the left and decreased the natural frequency of the system. This change is analogous to increasing the mass of a SDOF which in turn decreases the natural frequency of the system if the stiffness is held constant through $f = \sqrt{\left(\frac{k}{m}\right)}$. Therefore, it seems that modelling the GV connector using an axial model is more straightforward as bar (axial) elements are not affected by changes to the second moment of area or the mass moment of inertia.

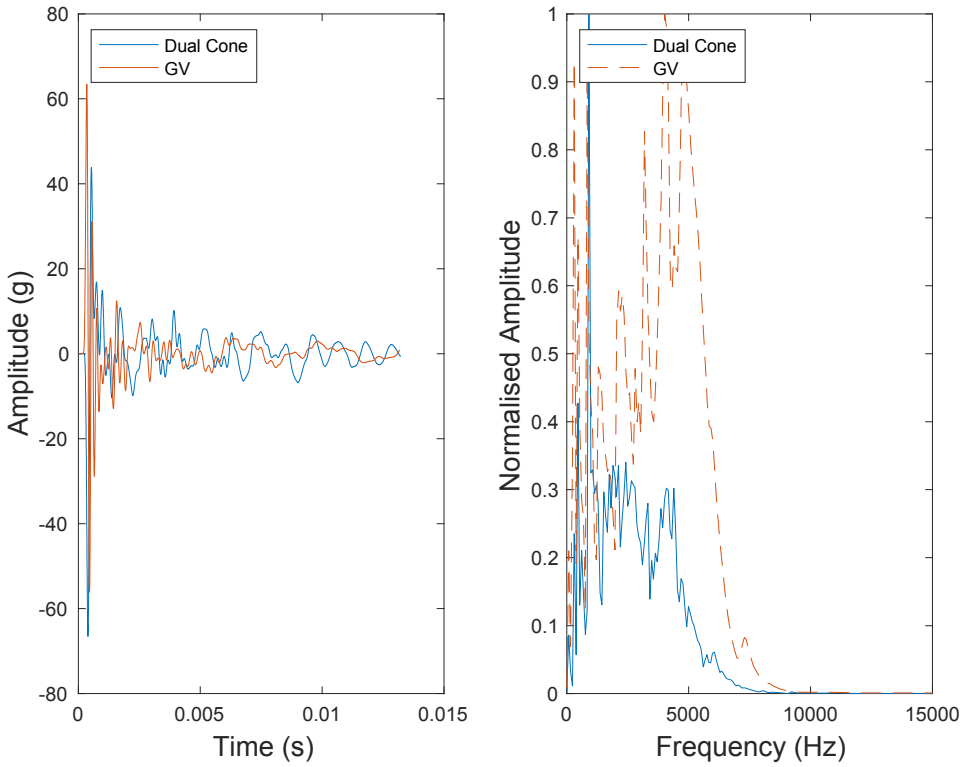

Figure 3-17. Adding the GV connector makes the peaks of the bending response less distinguishable.

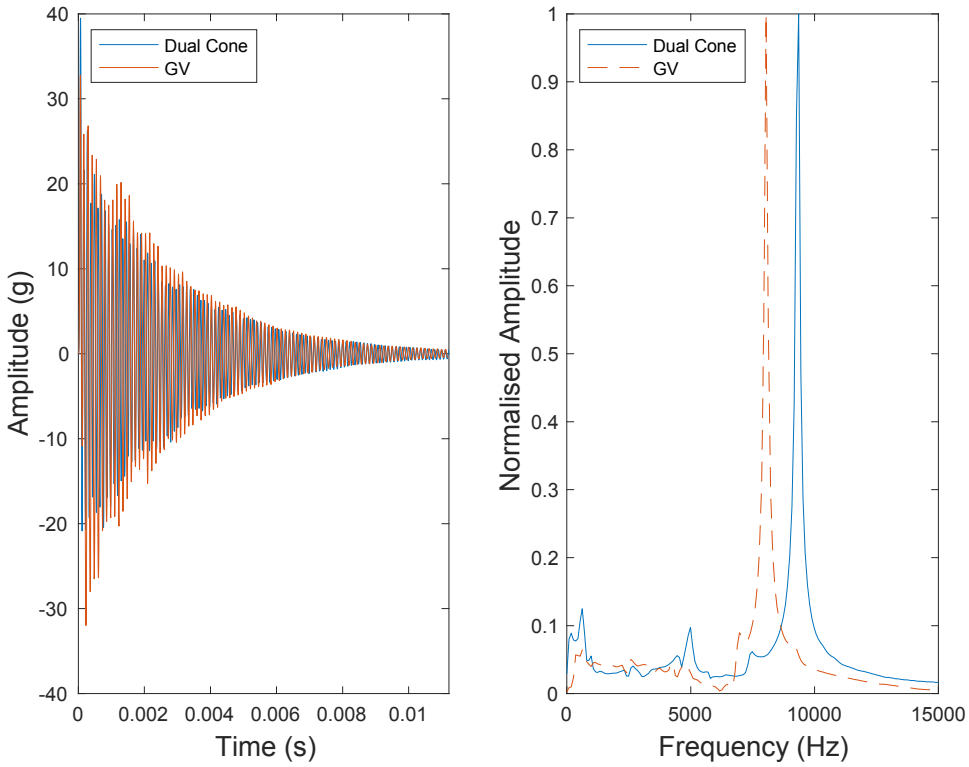

Figure 3-18. Adding the GV connector shifts the dominant peak (from around 9,300 Hz to 8,000 Hz) of the axial response to the left.

3.3.4 Benefits and Limitations of Axial and Transverse Loading Conditions

Based on the analysis presented in the previous three subsections, the following key points can be deduced regarding loading and analyzing the system in the bending and axial directions. With the current instrumentation, the system can be used in both loading conditions however there is more potential (in terms of measurement sensitivity and specificity) to rely on the axial model for the measurement system. The transverse direction is highly sensitive to the femoral boundary condition. If the clinical situation is closer to the cantilever boundary condition, mathematically modelling the entire residual bone (cortical shaft, femoral head, neck, and trochanters) is going to be necessary for comparing the clinical results with the mathematical analysis. In addition to the geometric complexity of reconstructing the patient's femur (which is patient specific) in the model, modelling the bone involves increasing the unknowns in the model from the inertial and stiffness parameters of the BII as the only unknown in the system to having the inertial and stiffness parameters of the BII and the residual femur (cortical shaft and proximal femoral end which has both cancellous and cortical zones) in the model. It should be noted that the actual boundary

condition is neither a cantilever nor a free-end, and knowledge of the most representative boundary condition should be inferred from clinical experimentation and collecting and analyzing a significant data set of transverse measurements and comparing them to mathematical predictions. Since the primary scope of the overall TFA project is the development of an implant stability measurement that is clinically usable, relying on the bending response is risky without the full knowledge of the most appropriate femoral boundary condition. Furthermore, it may be unavoidable to have the GV connector on while taking measurements and as was mentioned earlier, the GV connector changes the entire nature of the bending response of the system and makes the analysis more complex due to the bulkiness of the part and its severe changes to the inertial and stiffness (and in turn damping) attributes of the system.

The axial behavior of the system appears to be more immune to changes to the femoral boundary condition and more predictable with the introduction of the GV connector. The main limitation of relying on the axial response is the low contribution of the 1st mode to the response. The 1st axial mode appears to be potentially sensitive to the interface condition since the frequency changed from 660 Hz to 9,770 Hz for the LOW and HIGH condition respectively. However, it has only a minor contribution to the experimental LOW signal and is hard to identify and distinguish from potential noise in the signal. The current dominant mode for the LOW condition is the 2nd axial mode ($f_\mu = 9310$ Hz) and the dominant mode for the HIGH condition is the 1st axial mode ($f_\mu = 9540$ Hz). Therefore, determining the interface quality would be challenging unless the contribution of the 1st axial mode is amplified for the lower interface configurations.

This brings up two questions: 1) Why is the contribution of the 1st axial mode for the LOW interface condition minor? and 2) How can it be amplified in the signal? The first question can be addressed by observing the changes in the mode shape of the 1st axial mode for different BII stiffness values obtained using the 3D FE model (Figure 3-19). For the LOW stiffness configuration, there is little to no resistance from the BII to the implant motion. As the BII increases in stiffness, the BII introduces more resistance (experiences less deformation) to the implant's motion. The current impactor (Periotest®) is unable to provide the required kinetic energy to excite this mode of vibration which entails sliding the entire implant for the measurement duration and it becomes easier for the system to trigger the 2nd axial mode as mentioned in 3.3.1. The movable part of the Periotest® weighs approximately 9.4 g [54] and in order for it to trigger the relative

sliding nature of the 1st axial mode of the LOW interface condition, it needs to introduce considerable kinetic energy to the 200 g implant system. Thus it becomes easier (under the current excitation conditions) to excite the 2nd axial mode which can be viewed as a stress wave in comparison to the relative sliding nature of mode 1 (Figure 3-5). Accordingly, it is believed that the axial response of the system has more potential compared to the transverse modes. However, two important investigations must be conducted to verify its potential. The first investigation is to introduce an INTEREMEDIATE BII condition (which according to Figure 3-19 should have $E > 5$ MPa) where it is expected to have a higher contribution of the 1st mode, yet the frequency of the 1st mode is expected to be away from the HIGH condition which is around 9600 Hz. Therefore, testing the system under an INTEREMEDIATE BII condition is expected to reveal more information on the sensitivity of the axial response to the BII condition. The other investigation involves redesigning the impactor to amplify the presence of the 1st axial mode for low interface configurations which is a separate in-house parallel project.

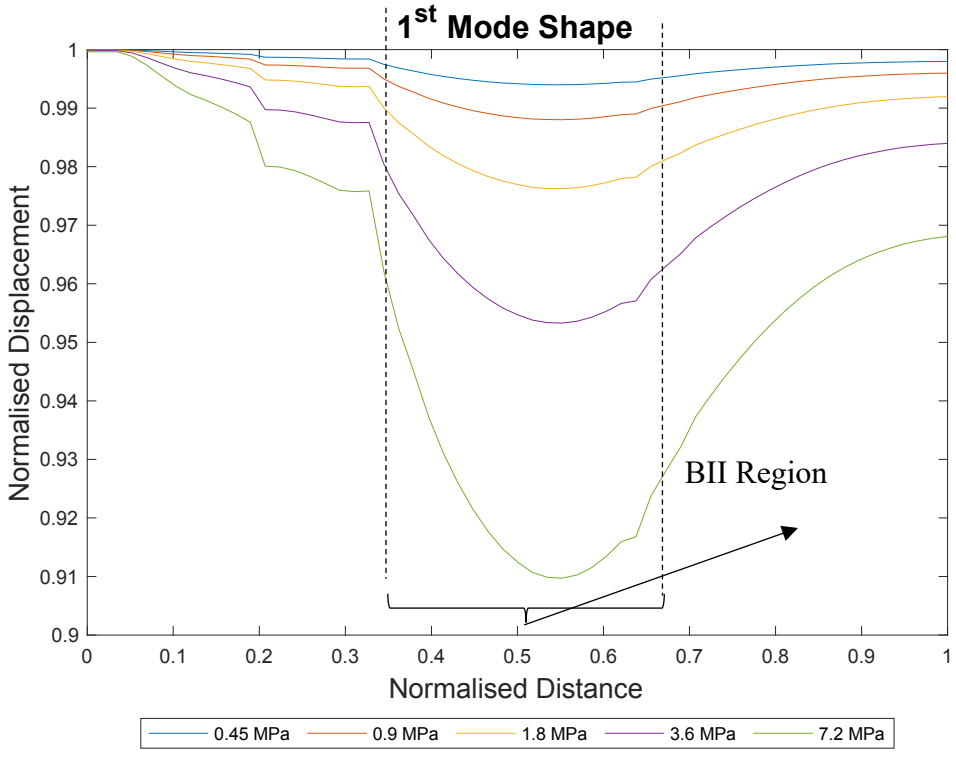

Figure 3-19. Changes to the nature of the 1st axial mode for different interface conditions. As the interface stiffness increases, the BII experiences more deformation and introduces more resistance to the implant's motion. The degree of relative sliding decreases as the stiffness of the BII increases and in turn the 1st mode of vibration becomes more observable.

3.3.5 Effect of Changing the Adapter's Geometry on the Axial Response

Before developing the axial model, there are two additional experiments that are of interest. The first one is the effect of changing the dual cone adapter geometry and the second one is the effect of the accelerometer mounting method. The dual cone adapter for the OPL system comes in a range of lengths (68.5-108.5 mm) depending on the patient's requirements. The length of the dual cone adapter is increased from 68.5 to 108.5 mm and the axial response is collected for both cases. Increasing the length of the adapter shifts the dominant frequency to the left (Figure 3-20). This behavior is expected as increasing the length (while holding the mass density, cross sectional area and tensile modulus constant) decreases the stiffness and increases mass of a bar element which in turn decreases the natural frequencies of the system. The shift in the dominant frequency is observed for both the LOW and HIGH interface conditions (Table 3-7). Similarly to the dual cone results (3.3.1), the dominant mode for the LOW condition is the 2nd axial mode while the dominant mode for the HIGH interface condition is the 1st axial mode.

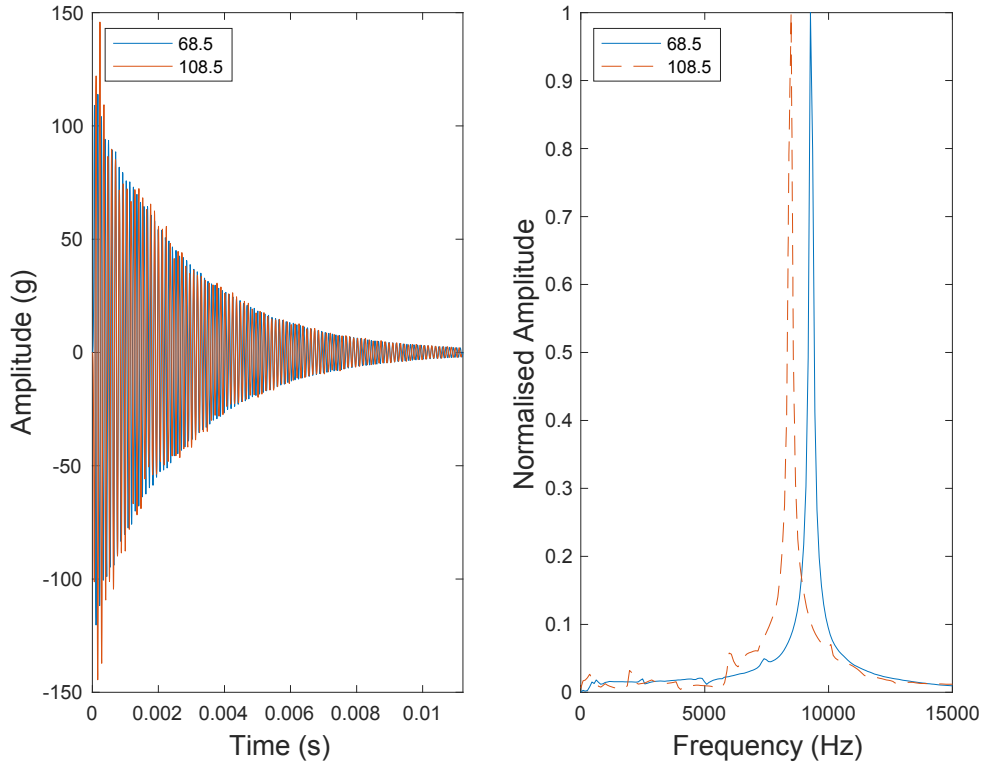

Figure 3-20. The longer adapter has a lower dominant frequency due to its added mass and lower stiffness.

Table 3-7. Increasing the length of the adapter shifts the dominant response by almost 800 Hz for the LOW and HIGH conditions.

Axial Response for the LOW Interface condition		
Dual Cone Length	$f_\mu\ (Hz)$	$f_\sigma\ (Hz)$
68.5	9310	0.40
108.5	8460	0.84
Axial Response for the HIGH Interface condition		
68.5	9540	72.9
108.5	8680	52.9

3.3.6 Effect of Changing the Accelerometer's Mounting Method on the Axial Response

Mounting the accelerometer to the implant system using superglue is not clinically attainable, alternatively double-sided tape can be used for mounting. Attaching the accelerometer using double sided tape decreases the amplitude of the time domain signal considerably, however there is minimal change to the location of the dominant peak (estimate of the natural frequency) and the spread of the peak (estimate of damping) between superglue and double-sided tape mounts (Figure 3-21). The natural frequencies and damping ratios are system characteristics and using double sided tape appears to preserve them. The amplitude of the response can depend on many factors such as the excitation method and changes to the amplitude using double sided mounts can potentially be accounted for by a constant correction factor on the initial velocity in the model. It is interesting to note that using the double-sided tape gave closer predictions to the model compared to the superglue mount (Table 3-8). Attaching and reattaching the superglue mount carried a potential risk for damaging the accelerometer and therefore the accelerometer was installed and fixed once for the 5 repetitions. For the double-sided tape, the accelerometer was attached and re-attached for each repetition and thus it is believed that the average is more immune

to systematic errors (due to accelerometer installation) in this case and brought the double sided tape results closer to the predictions of the 3D FE models predictions.

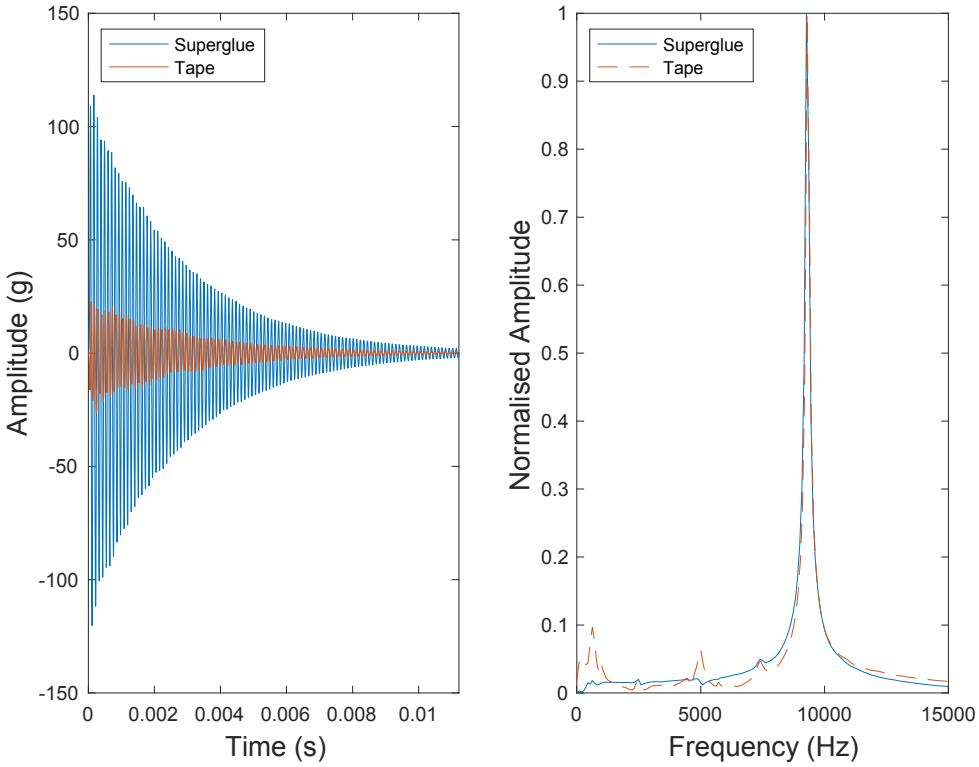

Figure 3-21. Using a double sided tape mount preserves the two main signal characteristics (natural frequency and damping) but lowers the amplitude of the time domain signal.

Table 3-8. The dominant frequencies estimated using both mounting methods yielded similar results. The double sided tape had closer predictions to the 3D FE model due to higher immunity of the average to systematic errors since the tape was applied and re-applied for each repitition.

Axial Response for the LOW Interface Condition 3D FE Model $f = 9380$ Hz		
Mounting Method	$f_\mu\ (Hz)$	$f_\sigma\ (Hz)$
Superglue	9310	0.40
Double Sided Tape	9330	0.13
Axial Response for the HIGH Interface Condition 3D FE Model $f = 9770$ Hz		
Superglue	9540	72.9
Double Sided Tape	9650	31.8

3.4 Summary and Concluding Remarks on the Preliminary Experimental Investigation and the Important Points of Consideration for the Upcoming Sections

In this chapter, preliminary experimental and mathematical analysis is conducted to formulate a better understanding of the system's behavior. The primary objective from this preliminary investigation is to choose the more promising testing conditions and develop the mathematical model in the proceeding chapters. Although there was an agreement between the 3D FE model's predications and the experimental findings for both the bending and axial modes (3.3.1), the bending modes responses were found to be more sensitive to the femur's boundary condition compared to the axial modes (3.3.2). Furthermore, the nature of the bending response completely changed with the presence of the GV connector, and this complicates the mathematical modelling of the system (3.3.3). Accordingly, exciting the axial modes appears to have more potential compared to the bending response. The main limitation of relying on the axial modes is the minor

modal contribution of the 1st mode to the response for the LOW interface condition which makes it more challenging to distinguish between the LOW and HIGH interface condition. To further investigate this: 1) an INTERMEDIATE (where it is expected to observe a dominant 1st axial mode that is far from 9300-9500 Hz) will be experimentally investigated to check whether the 1st axial mode is a reliable indicator for implant stability measurement and 2) mathematical and experimental investigations will try to address amplifying the 1st axial for the LOW interface condition. Those two investigations will be further discussed in chapters 4 and 5. Although chapters 4 and 5 primarily focus on the axial behavior of TFA implants, the 1D FE bending behavior was also modelled and documented in Appendix A.

Chapter 4 Developing a 1D FE Axial Model for Evaluating the BII Properties of TFA Systems

This chapter focuses on the development and validation of 1D FE axial model of the TFA implant system. The development of the model involved expressing the inertial and stiffness properties of the implant system using axial (bar) elements. The stiffness and mass matrices were generated and assembled using a custom-built MATLAB® program. To check the 1D FE formulation and the matrices generation and assembly process, the 1D FE modal solution is compared with the analytical and 3D FE solution of a uniform cylinder. Afterwards, the 1D FE modal solution of the actual implant geometry is compared with the 3D FE modal solution. After performing these two checks, modal superposition is implemented to generate the time domain responses of the system. To evaluate the interface properties, the 1D FE model is incorporated in a simple MATLAB® GUI that matches between an input signal and the model's prediction using an optimization routine. The application is tested for different interface conditions generated using a 3D FE time-integration model and experimental signals. As it was mentioned in the concluding remarks of Chapter 3, an additional intermediate condition is added to better understand the axial behavior of the implant system. The chapter is intended for submission at Annals of Biomedical Engineering.

4.1 Abstract

A 1D FE axial model of the Osseointegrated Prosthetic Limb (OPL) transfemoral system was developed and used to evaluate the bone-implant interface properties. The 1D FE formulation was validated with the analytical and 3D FE solution of a cylinder. Afterwards, the implant was modelled and the modes were compared to a 3D model. The 1D model was then extended to perform modal superposition in a custom-built MATLAB® application that uses optimization to match between the input signal and the 1D model's prediction and reports the interface properties. The application was tested with signals generated from 3D FE implicit simulations and in-vitro experiments. The application was able to evaluate the interface properties for the different interface conditions (LOW, INTERMEDIATE and HIGH) generated using the 3D simulations and the experimental INTERMEDIATE and HIGH signals. The model distinguished between the interface conditions using the interface stiffness and 1st mode frequency, however the stiffness was more sensitive to the interface condition. The model also determined the interface damping properties. The primary limitation of the approach is the inability of the Periotest® (impactor) to trigger the

1st mode for the LOW condition. Redesigning the impactor is expected to amplify the presence of this mode. This work is part of an ongoing project that aims at developing a complete stability measurement system for the OPL TFA system and this includes redesigning the impactor. However, this investigation focussed on the modelling aspect of the project and demonstrated the sensitivity and reliability of the proposed approach using numerical and physical models.

4.2 Introduction

The first bone anchored (Osseointegrated) implant for transfemoral amputation (TFA) was introduced by Rickard Brånemark in 1990 in Sweden after the successful implementation of bone-anchored implants in dentistry, hearing aids, facial prosthesis, hip arthroplasty and finger joint prosthesis [1], [7]. This treatment aimed at replacing the conventional socket prosthesis which is associated with skin complications (such as ulcers), limited hip joint range of motion, improper socket suspension and biomechanical gait deviations [6], [7], [23]. There have been, since then, considerable advances in implant designs and perioperative protocols [6]–[9], [23].

The majority of bone-anchored prostheses involved using one of the following implant systems: (1) the Osseointegrated Prosthesis for the Rehabilitation of Amputees or the OPRA system (Integrum, Sweden), (2) the Integral Leg Prosthesis or the ILP system (Orthodynamics, Germany) and (3) the Osseointegrated Prosthetic Limb or the OPL system (Permedica, Italy) [6], [23]. The OPRA system relies on a screw fixated titanium stem to achieve primary (mechanical) stability with the intramedullary canal [6], [23]. The ILP and OPL systems both achieve primary stability through press fitting the stem into the canal. The implants utilize a porous coating that promotes the osseous growth and deposition between the implant and the surrounding bone [6], [23]. The threaded design of the OPRA allows it to be mechanically efficient and achieve high stability using a relatively shorter implant length of 80 mm compared to the ILP and OPL system where the implant length can range from 120-160 mm [6], [23]. Nevertheless, it is more prone to loosening due to torsional loads [6]. The porous design of the ILP and OPL is credited for promoting osseointegration and reducing rehabilitation programs to 6-8 weeks [6], [8], [9], [23]. Although the ILP and OPL share similar design principles, the OPL system is manufactured from titanium alloys which has lower stiffness compared to the cobalt chromium ILP system and reduces stress shielding [29]. The most recent development is introducing the single stage OGAAP-2 protocol

which unlike the OPRA and the OGAAP-1 protocol involves installing the OPL stem and percutaneous dual cone adapter in a single surgical procedure instead of two [7]–[9].

Despite of all these advancements in implant designs and the surgical and rehabilitation protocols, assessing implant stability remains a key challenge. The stability of an Osseointegrated implant is a function of the biomechanical properties of the bone implant interface (BII) [4], [5]. Evaluating the condition of the BII is critical for early failure detection and prevention, evaluating the surgical outcomes and designing patient specific rehabilitation protocols since it is believed that there exists an optimal relationship between the timely application of loads (and promoting osseointegration) and excessive early loading (which can cause loosening), however this relationship is not well understood [4]–[6]. Imaging techniques are currently used to evaluate the BII condition. Translucency in the areas surrounding the bone and the implant can be indicative of potential implant septic or aseptic loosening [4]–[6], [56]. Imaging techniques however are susceptible to noise from metal artefacts, generally lack quantitative metrics, can expose the patient to excessive radiation and usually lack the sensitivity for early failure detection; it can take up to 40% reduction in bone density before detecting it with traditional X-ray imaging [5]. There have been attempts to improve imaging methods by introducing tantalum beads during the surgery and using digital image correlation to track implant migration using Radiosterometric X-ray analysis (RSA) [36], [37]. In a clinical study conducted on OPRA implants, longitudinal RSA evaluation of distal implants migration patterns was indicative of implant loosening since the removed implants had statistically significant higher migration values compared to the non-removed implants group and that there was a 22.5% odds ratio of implant removal associated with implant migration [37].

Vibration methods have been an appealing choice for assessing implant stability due to the non-invasive and quantitative nature of the test [4], [5]. The bone-implant system is mechanically stimulated, and the response is analysed for some signal characteristics such as the natural frequencies which can be directly correlated to the BII stiffness [4], [5]. The main limitation of relying on the natural frequency as a metric is its dependency on other system parameters such as the implant geometry and thus inhibits using it as an absolute stability metric [12]–[15]. The Advanced System for Implant Stability Testing (ASIST) was developed to overcome this limitation, instead of solely relying on the measured frequencies, the ASIST compares the measured acceleration response with the prediction of a mathematical model [14]. The mathematical model is a representation of the physical bone-implant system and is derived using

the discrete form of Newton's second law of motion. In the model, the BII stiffness (k) is treated as the primary unknown that is evaluated by matching the measured response with the model's prediction using an optimization routine [14]. Evaluating the BII condition of bone anchored hearing aid implants using the ASIST has shown that the evaluated k and ASIST stability scores (ASC values) are more sensitive to the interface condition and are minimally affected by the implant geometry compared to the system's natural frequencies [14], [15], [57].

Although the majority of vibration assessment investigations focussed on dental applications and bone-anchored hearing aids, there have been some investigations for TFA systems. Shao et al. investigated the sensitivity of the fundamental bending mode of the OPRA system to the interface condition upon an impact excitation, initiated using a small pendulum, and measuring the response using an accelerometer attached to the abutment [17]. Their in-vitro findings supported the strong correlation between the natural frequency and the material of the interface, where softer material (with lower elastic modulus) had lower natural frequencies than stiffer materials [17]. Furthermore, they showed statistically significant longitudinal variations in the natural frequencies for one patient and reported that these changes reflect on the patient's load bearing ability [17]. Cairns et al. conducted a series of benchtop experimental modal analysis investigations on the OPRA system. In their investigations, the response was collected using 17 measuring locations which allowed for evaluating the Frequency Response Function (FRF) and estimating the mode shape [19], [20]. In one study, two extreme interface conditions were simulated using an implant insertion torque of 0.5 and 4 Nm to mimic LOW and HIGH interface conditions respectively while the other investigation attempted to vary the interface condition based on Brånemark's physiological model [19], [20]. In both studies, they concluded that the natural frequencies and mode shapes are sensitive to the BII condition and warrants further investigation of the technique for TFA implant systems [19], [20].

In our previous work, a numerical investigation of the OPL TFA systems entailed constructing a 1D finite element model (FE) of the system using different beam formulations and cross validating the bending modes with a 3D FE model of the system on ABAQUS® (Dassault Systèmes, France) [58]. It was concluded that a 1D FE model based on Timoshenko beam theory had enough power to capture the bending modes of interest (Appendix A) [58]. The goal of this investigation (and the previous one) is to extend the ASIST stability assessment approach (which has been in use for hearing aids) to the TFA OPL system. Therefore, a representative TFA mathematical model is

needed for evaluating the BII condition clinically. Although the previous work focussed on the bending modes of the system, preliminary experimental findings indicated more complex bending responses for different implant-adapter configurations and femoral boundary conditions in comparison to the axial response which is easier to mathematically predict for different conditions. Thus, it was deemed appropriate that the analysis of the axial vibration of the system should be the primary focus of this project.

The primary objective of this work is to construct a representative 1D FE axial model (using bar elements) of the TFA OPL system. This investigation involves testing the model through a series of steps: 1) cross validating the axials modes of the 1D FE formulation with an analytical solution and 3D modal FE simulation for a simpler uniform cylinder, 2) cross validating the modes of the actual TFA geometry (without modelling the BII) with a 3D FE modal simulation 3) cross validating the time domain response of the 1D model with a 3D FE implicit simulation for different BII conditions and 4) testing the 1D FE model with benchtop (in-vitro) signals. This work expands on the previous work and extends the analysis to time domain signals instead of solely relying on frequency extraction. To the authors best knowledge, this work is the first one to investigate the potential use of the axial modes of vibration for the stability assessment of the OPL system using numerical and physical models. Previous work primarily focussed on the bending response of the OPRA system and focussed on extracting the natural frequencies and mode shapes while in this work the focus is to evaluate the actual stiffness of the BII which is believed to be a more direct measure of the BII condition. Finally, the previous work was primarily experimentally driven, it is believed that coupling the experimental analysis with mathematical (1D and 3D FE) analysis increases the confidence in the results.

4.3 Methods

4.3.1 1D FE Model

A bar is a solid structure that undergoes axial deformation along its longitudinal axis. The free vibration axial displacement response $u(x,t)$ can be defined for any position along the bar x and at any instant t using EQ 4-1 given that the density ρ, cross-sectional area A and elastic modulus E are known [59]. EQ 4-1 can be solved analytically for bar problems with simple boundary conditions and geometries using separation of variables [45]. More complex problems are solved numerically. The FE method is a numerical technique in which the problem's continuous domain

(with an infinite number of DOF) is discretized using a specific set of elements [59]. This transforms the governing PDE to a simpler discrete form where the rules of linear algebra can be employed [59]. EQ 4-2 shows the discretized form of the governing equation; the product between the mass matrix $[M]$ and the acceleration vector $\{\ddot{u}\}$ represents the system's inertial forces while the product between stiffness matrix $[K]$ and displacement vector $\{u\}$ represents the system's elastic forces. A bar can be discretized using line (1D) elements, a linear 1D element has two DOFs (one at each end) and the element-wise mass $[M_e]$ and stiffness matrices $[K_e]$ can be defined for each element according to its material and geometric properties using EQ 4-3. Deriving $[M_e]$ and $[K_e]$ can be achieved by several techniques, variational methods employ minimising the system's energy (principle of least work) while the Bubnov-Galerikin formulation utilizes deriving the weak form and assigning an appropriate function that satisfies the problem's requirements (Appendix A) [45], [59].

$$\rho A \frac{\partial^2 u}{\partial t^2} - \frac{\partial}{\partial x}\left(EA \frac{\partial u}{\partial x}\right) = 0 \qquad \text{(EQ 4-1)}$$

$$[\mathrm{M}]\{\ddot{\mathrm{u}}\} + [\mathrm{K}]\{\mathrm{u}\} = 0 \qquad \text{(EQ 4-2)}$$

$$[K_e] = \frac{EA}{L}\begin{bmatrix} 1 & -1 \\ -1 & 1 \end{bmatrix} \text{ and } [M_e] = \frac{\rho AL}{3}\begin{bmatrix} 2 & 1 \\ 1 & 2 \end{bmatrix} \qquad \text{(EQ 4-3)}$$

To model the TFA implant system using the 1D bar formulation, a simplified representation of the system is used to discretize the system into 9 regions (Figure 4-1). The tapered regions are assumed to have a diameter that is equal to the average diameter between the two ends of any given region. The distal screw is used to connect the dual cone adapter to the GV connector which is responsible for connecting the implant to the prosthesis. The GV connector was not modelled in this investigation however the distal screw was used in the model since it provides an ideal axial impact location. Furthermore, there is an internal screw (not shown on the diagram) that connects the dual cone adapter with the stem.

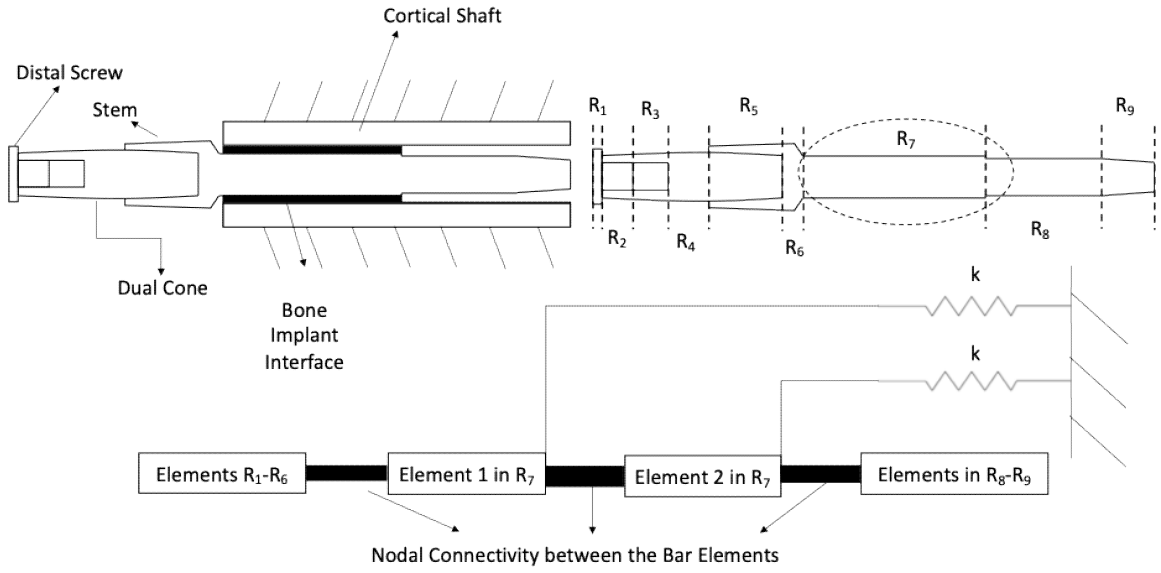

Figure 4-1. A simplified representation of the TFA bone implant system. The system consists of: the distal screw (used to connect the dual cone to additional connectors which are not modelled in this investigation), dual cone adapter, the stem, a uniform BII and cortical shaft (Left). The stem and dual cone are discretized into 9 regions with varying L and A and the BII is represented as a series of linear grounded springs distributed uniformly over R_7 (Right). To illustrate the application of the interface stiffness (k) into the 1D model, a simplified schematic demonstrates the discretization of the system (Bottom). Elements from R_1 to R_6 and R_8-R_9 are inherently connected to each other using nodal connectivity. Elements in the interface region (R_7) are connected to each other using nodal connectivity, however they are also connected to linear axial grounded springs which represent the BII stiffness. It should be noted that the two bar elements used in discretizing R_7 in this schematic are for illustration only and that the number of elements used in the discretization is significantly higher.

Each region is divided into a set of 1D elements and for each element $[M_e]$ and $[K_e]$ are defined. $[M_e]$ and $[K_e]$ can then be assembled into the global mass and stiffness matrices according to the elements' nodal connectivity. The problem's boundary conditions are then imposed. For the TFA system, grounded linear axial springs (representing the BII) are added to R_7. The first step in evaluating the system's response is performing modal analysis. In modal analysis, the system's natural frequencies ω_n (eigenvalues) and mode shapes ϕ_n (eigenvectors) are evaluated for each n mode present in the system (EQ 4-4), the mode shapes can be rearranged into the modal matrix where each mode shape would occupy a column resulting in a square matrix $[\phi]$ [40]. A MATLAB® (MathWorks, USA) code was developed to discretize the system, compute $[M_e]$ and $[K_e]$ matrices, assemble them into the global $[M]$ and $[K]$ matrices, impose the boundary conditions to R_7 and evaluate ω_n and ϕ_n using MATLAB®'s eigenvalue solver (eig) function. Once ω_n and ϕ_n are extracted modal superposition can be performed to analyse the system's time domain response for a specific set of initial conditions. It is expected that the acquired (physical)

signal to exhibit significant energy losses over time, therefore damping must be introduced to account for this behavior (EQ 4-5). Stiffness proportional damping model is a convenient way of accounting for energy losses without overly complicating the analysis procedure since the damping matrix $[C]$ is directly derived from $[K]$, as shown in EQ 4-6, and thus preserves the system's orthogonality properties [40]. The constant β is defined using one of the systems natural frequencies for any chosen damping ratio value (ζ_j) and is usually chosen as the last frequency that is expected to be physically observed since the damping ratios increase significantly for the remaining modes [40]. In this case, j is set to the second mode since experimental observations showed that the axial response is dominated by two modes at most.

$$[\,[K] - \omega_n^2[M]\,]\{\phi\}_n = 0 \qquad \text{(EQ 4-4)}$$

$$[M]\{\ddot{u}\} + [C]\{\dot{u}\} + [K]\{u\} = 0 \qquad \text{(EQ 4-5)}$$

$$C = \beta[K] \text{ and } \beta = \frac{2\zeta_j}{\omega_j} \qquad \text{(EQ 4-6)}$$

The time domain response can be evaluated by modal superposition in which the system of equations shown earlier in EQ 4-5 can be uncoupled by expressing the system in terms of the natural coordinates $\{q(t)\}$ and converting $[M]$, $[C]$ and $[K]$ into diagonal matrices with diagonal elements M_n, C_n and K_n respectively using the modal matrix $[\phi]$ (EQ 4-7) [40]. The n uncoupled equations are expressed individually in terms of the natural coordinates $q_n(t)$ (EQ 4-8) which can be solved using the solution form of a single DOF system (EQ 4-9) and (EQ 4-10), the solution can then be converted back to the original coordinate system ($u(t)$) using EQ 4-11 [40]. The vibration response of the TFA system under consideration can be viewed as the superposition of two problems (Figure 4-2). The first problem is the response of the system under the impact generated by the Periotest®, the movable, impacting, part of the Periotest® is around 9.4 g which is relatively much smaller in size compared to the implant system which exceeds 200 g. Therefore, it is modelled as a particle m_p that imposes an initial velocity condition on the implant system. The impact stiffness K_I is treated as a linear spring that connects m_p with the corresponding impact location on the implant system. The first problem is treated as a free vibration problem, where the entire system is initially at rest and the vibration is triggered by the initial velocity of m_p. Preliminary testing indicated that the acceleration of m_p is dominated by a single frequency and

that the rod experiences half a cycle where the x-intercept physically represents the rod's contact time t_{2o}. The second part of the response (Figure 4-2) is the free vibration of the implant system after the rod loses contact with the system, the initial conditions can be determined using the displacement and velocity vectors at t_{2o} or $u_2(t_{2o})$ and $\dot{u_2}(t_{2o})$ respectively.

$$[\phi]^T[M][\phi]\{\ddot{q}\} + [\phi]^T[C][\phi]\{\dot{q}\} + [\phi]^T[K][\phi]\{q\} = 0 \quad \text{(EQ 4-7)}$$

$$M_n\ddot{q}_n + C_n\dot{q}_n + K_n q_n = 0 \quad \text{(EQ 4-8)}$$

$$q_n(t) = e^{-\zeta_n\omega_n t}\left(q_n(0)\cos(\omega_n D t) + \frac{\dot{q}_n(0)+\zeta_n\omega_n q_n(0)}{\omega_n D}\sin(\omega_n D t)\right) \quad \text{(EQ 4-9)}$$

$$\zeta_n = \frac{\beta\omega_n}{2},\ \omega_n D = \omega_n\sqrt{1-\zeta_n^2}\ ,\ q_n(0) = \frac{\{\phi\}_n^T[M]\{u(0)\}}{\{\phi\}_n^T[M]\{\phi\}_n} \text{ and } \dot{q_n}(0) = \frac{\{\phi\}_n^T[M]\{\dot{u}(0)\}}{\{\phi\}_n^T[M]\{\phi\}_n} \quad \text{(EQ 4-10)}$$

$$\{u(t)\} = \sum_1^N \{\phi\}_n q_n(t) \quad \text{(EQ 4-11)}$$

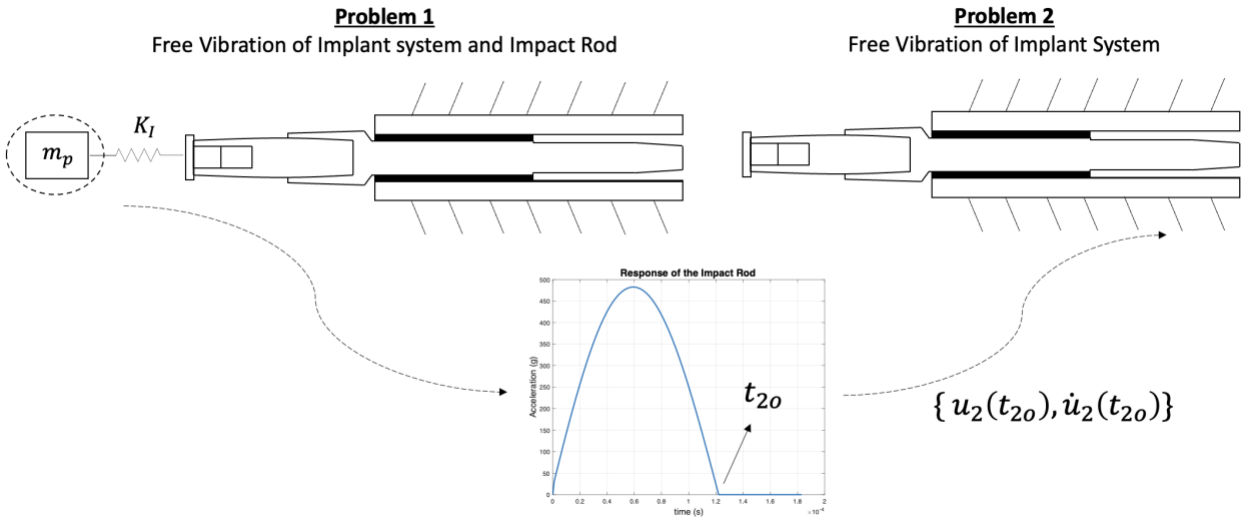

Figure 4-2. The vibration response of the TFA system under consideration can be viewed as the linear superposition of two problems. The first problem is the free vibration of the implant system under the Periotest®'s excitation. The acceleration response of m_p can be used to determine the contact time of the rod and then determine the initial conditions $\{u_2(t_{2o})\ ,\ \dot{u}_2(t_{2o})\}$ for the second problem, namely the free vibration of the implant system alone (without the impact rod).

4.3.2 3D FE Model

A 3D FE model was also developed on ABAQUS® for cross validation with the 1D FE model. The implant system (OPL type A length $L = 160$ mm and Diameter $D = 14$ mm) was obtained from the manufacturer (Permedica, Italy) and its main components were reconstructed on Solidworks®

(Dassault Systèmes, France) after taking its physical measurements with a digital vernier caliper and 3D scanning it (MetraScan 3D, Canada). The CAD models of the parts were assembled in Solidworks® and then imported to ABAQUS® for analysis. Table 4-1 shows the material properties of the parts, all the components are assumed to be linear elastic and isotropic. This isotropic material model is suitable for metals and can be used as a good approximation to the material behavior of the bone and the BII (which are actually orthotropic) for small deformations. The density should also be defined for all the parts to account for the component's inertial effects. It should be noted that for computational purposes, the Periotest® is modelled as a uniform cylinder ($D = 2$ mm and $L = 15$ mm) in the 3D FE simulation. This reduction in size can be accounted for by adjusting the density to 200 g/cm^3 to end up with a total of 9.4 g for the mass of the rod. Tied interactions, where the nodes of the two interacting surfaces are inhibited from moving with respect to each other, are introduced between all the connections in the system. The parts were meshed using the C3D8 linear full integration hexahedral elements. The geometric boundary condition of this problem involved fixing the outer walls of the cortical shaft.

Two types of analysis were conducted using the 3D FE model, the first one was modal analysis where the Lancsoz (a numerical algorithm for eigenvalue analysis) solver was set to extract all the natural frequencies and mode shapes up to 24 kHz of the implant system without modeling the impact rod or the BII or the bone (Figure 4-3). The second type of analysis involved introducing the bone, BII and the impact rod. It was performed using ABAQUS® implicit solver, in this analysis the impact rod was given an axial (in the negative z-direction) initial velocity of 200 mm/s which is an estimated value of the experimental velocity (Figure 4-3). The solver was set to record the solution every 4 μs like the experimental time step, the time step was chosen to create a sampling rate that exceeds Nyquist criteria by at least a factor of 10. Furthermore, stability analysis was conducted by varying the time step from 8 to 0.5 μs and it was found that the solution was stable for the entire range. Frictionless surface to surface contact defined the behavior between the impact rod and the distal screw (impact location), the linear contact (impact) stiffness was set to 1×10^7 N/m. The actual contact stiffness is not known but experimental analysis indicate that the contact stiffness can be inferred from the rod's contact time and that a contact stiffness of 1×10^7 N/m falls in the experimental contact time range of 100 μs. The implicit simulations were conducted for three interface conditions: LOW, INTERMEDIATE and HIGH which correspond to a tensile moduli of 0.45, 40 and 1000 MPa respectively. These values were chosen to be in range

with their experimental counterparts which were found using mechanical testing or from the literature [48], [60]. Although damping is physically expected to vary between the three conditions, it was set to a damping ratio of 1% (for the second mode) to only have a single interface variable at a time for validation purposes. The primary analysis output is the average nodal axial acceleration on the accelerometer's measurement location on the dual cone adapter (Figure 4-3). Furthermore, since the physical impact cannot be conducted at the exact centre of the distal screw, the analysis was also conducted for skewed strikes where the impact rod strikes the outer side of the screw which is the physical striking location to see the effect of this asymmetry on the measurement.

Table 4-1. Material properties of the components used in the simulations [47]–[49], [60].

Component	**Material**	**Elastic Modulus (MPa)**	**Poisson's Ratio**	**Density (g/cm^3)**
Distal Screw	Titanium	100000	0.310	4.40
Dual Cone	Titanium	100000	0.310	4.40
Stem	Titanium	100000	0.310	4.40
BII	Variable	{0.45,40,1000}	0.300	1.24
Cortical Shaft	Short Fiber Epoxy	16000	0.300	1.90
Periotest®	Stainless Steel	190000	0.265	Modified to 200 to account for size reduction

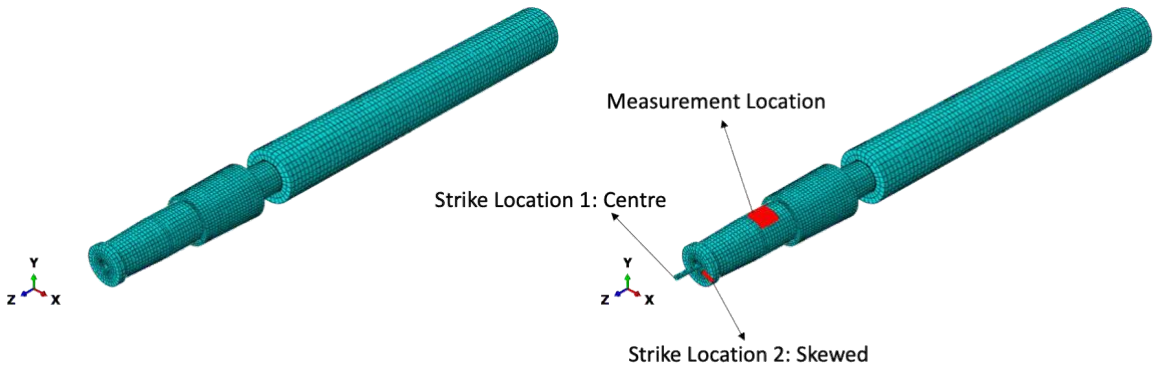

Figure 4-3. The 3D FE model was used to conduct: 1) Modal analysis of the bone-implant system to extract the mode shapes and natural frequencies of the system (Left) and 2) Implicit dynamic analysis to extract the axial acceleration response after simulating accounting for the rod and simulating impact.

4.3.3 Experimental Model

A benchtop experimental model of the bone implant system was also used to study the dynamic behavior of the system (Figure 4-4). Composite femurs (SKU 3403) were acquired from SAWBONES (Pacific Research group, USA), those femurs, anatomically and biomechanically, mimic the behavior of healthy femurs. The bone was uniformly drilled to have a diameter of 15 mm which is slightly larger than the diameter of the implant's distal end (from the hip joint) of 14.8 mm, the entire gap between the two surfaces was filled using: 1) DOWSIL 7091™ silicone rubber adhesive (Dow, USA), 2) paraffin wax and 3) Lepage ultra-gel superglue™ to simulate the behavior of LOW, INTERMEDIATE and HIGH BII conditions respectively. The three materials were chosen to create three extreme conditions with a wide range of tensile moduli. Silicone rubber can be used to simulate the behavior of fibrous tissue where the BII has negligible stiffness (in the sub-megapascal range) that is orders of magnitude smaller than both the INTERMEDIATE and HIGH conditions [4]. Although the changes in the interface condition are the by-product of several parameters (material properties, density, surface parameters, contact area and interface distribution) and their potential interactions [4], in this investigation interface changes were modelled by varying the material of the interface while holding the other parameters constant. ADXL 1004 single axis accelerometers (Analog Devices, USA) were used to measure the acceleration response of the system, the primary accelerometer was placed on the dual cone adapter. NI 9205^{TM} data acquisition system (National Instruments, USA) was used to store the acceleration response at a sampling rate 250 kHz. The Periotest® impact rod was used to excite the system axially at the distal screw. Each measurement consisted of 16 strikes, 15 of which were

fully recorded while the first strike was used for triggering the acquisition, the 15 acceleration responses were then aligned and averaged. For each interface condition the test was repeated 5 times, each repetition involved reinstalling the femur in the support and reorienting the Periotest®.

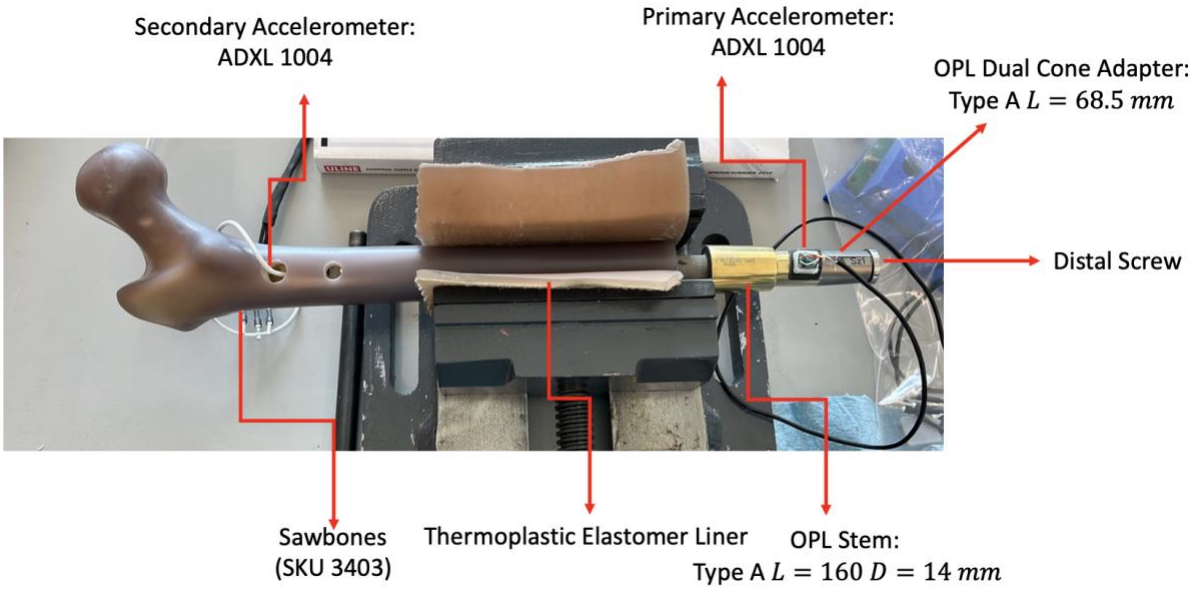

Figure 4-4. The benchtop setup used for cross validating the 1D and 3D FE models.

4.3.4 Application

The 1D FE model mentioned earlier in 4.3.1. was incorporated in a simple custom-made GUI interface created using MATLAB®'s app builder. The GUI is a prototype version of the GUI intended for clinical application. The user is prompted to load the acceleration response collected using the primary accelerometer. The user can change the system and loading parameters such as the initial velocity of the rod V_o or the impact stiffness K_I. Afterwards, the initial estimate of the interface stiffness k and second mode damping ratio are specified to initially approximate the input acceleration response. The final values can be estimated upon initiating the optimization routine which minimises the L_4 norm between the power spectral density of the input acceleration $a_{input}(f)$ and the model's prediction $a_{model}(f)$ (EQ 4-12) using MATLAB®'s built-in unconstrained search function (fminsearch).

$$L_4 = \sum \sqrt[4]{(a_{input}(f)^4 - a_{model}(f)^4)} \qquad \text{(EQ 4-12)}$$

4.3.5 Cross Validation Stages

The 1D FE model underwent several validation stages: 1) validating the natural frequencies f_n^N and mode shapes U^N for $N = 1$, 2 modes of a free-free uniform bar (L =100 mm, D = 10 mm, ρ = 4.4 g/cm^3 and E =100 GPa) with the analytical solution (EQ 4-13) [45] and a 3D FE model. This step ensures that the developed code properly generates and assembles the stiffness and mass matrices properly. The second stage of validation involves cross validating the natural frequencies and mode shapes 1D FE model of the stem and dual cone assembly (without modelling the BII or the bone) in order to evaluate the ability of 1D elements to represent the implant system. The third step of validation involves using the application to evaluate the interface properties for LOW, INTERMEDIATE and HIGH interface conditions for: 1) 3D FE signals under symmetric loading conditions, 2) 3D FE signals under skewed loading conditions and 3) experimental signals.

$$f_n^N = \frac{N}{2L}\sqrt{\frac{E}{\rho}} \text{ and } U^N(x) = \cos\left(\frac{N\pi}{L}x\right) \quad \text{(EQ 4-13)}$$

4.4 Results

4.4.1 Modal analysis of a Uniform Bar using the 1D FE

The 1D FE code was first used to compute the 1st and 2nd natural frequencies and mode shapes for a uniform cylinder. The analytical solution was 23840 and 47670 Hz for the 1st and 2nd modes respectively. The 1D FE solution converged to the analytical solution using 32 uniformly distributed bar elements and the corresponding values for the 1st and 2nd mode were 23850 and 47750 Hz respectively. The 3D FE simulation yielded similar results of 23830 and 47650 Hz. Furthermore, plotting the normalised axial displacement for different points over the bar's length indicates that the three solutions predicted nearly identical mode shapes (Figure 4-5).

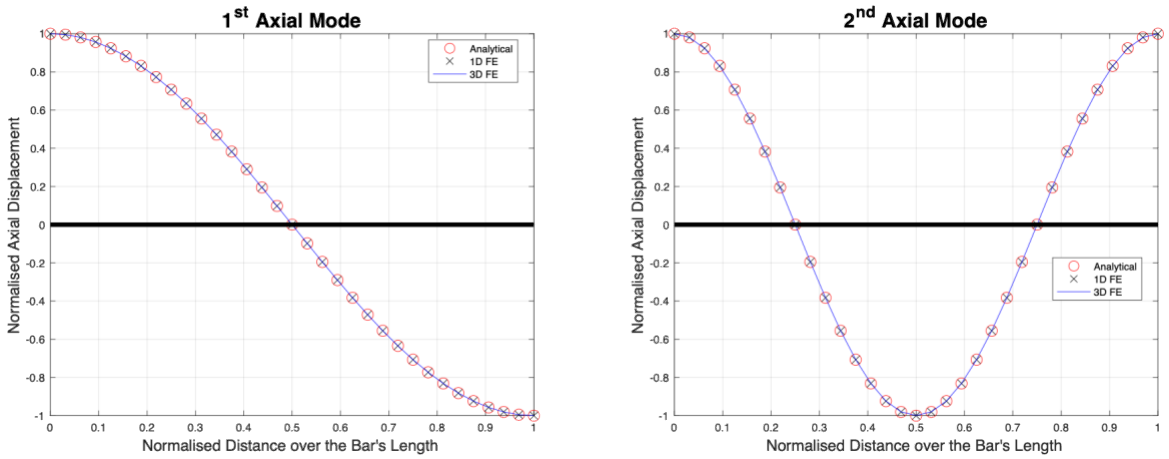

Figure 4-5. 1st (Left) and 2nd (Right) mode shapes predicted using the analytical, 1D FE and 3D FE models. The x-axis represents the normalized location of points along the cylinder's length (where 0 marks the beginning of the cylinder and 1 indicates its end at L=100 mm) and the y-axis represents the normalized axial displacement with respect to the original (undeformed) configuration (where 1 marks maximum displacement and -1 marks maximum displacement but in the opposite direction and 0 marks no displacement).

4.4.2 Modal Analysis of TFA Implant System using the 1D FE model

The second stage of validation involved comparing the natural frequencies and mode shapes of the free-free TFA implant system (without modelling the bone, BII and the rod) between the 1D and 3D FE models. The 1D FE model predicted a 1st mode frequency of 9550 Hz which is 1.17% higher than the 9440 Hz predicted using the 3D FE model. The 2nd mode frequency predicted with the 1D FE model was 20250 Hz while the 3D FE model predicted 19850 Hz which indicates that the 1D FE model overestimates this mode by 2.02%. Figure 4-6 shows the mode shapes of the 1st and 2nd axial modes predicted using both models, there is a good similarity between the predictions of both models and the distal screw/dual cone region seems to be the area of the largest deviations between the predictions of both models. It should be noted that the 1st and 2nd axial modes of a freely supported TFA implant system do not correspond to the axial modes of vibration of the TFA system connected to the BII and the bone. The nature of the modes change with the introduction of BII and the bone. The analysis of the freely supported TFA system is meant to test the power of the 1D FE model in representing the TFA implant geometry in comparison with the higher fidelity 3D FE model.

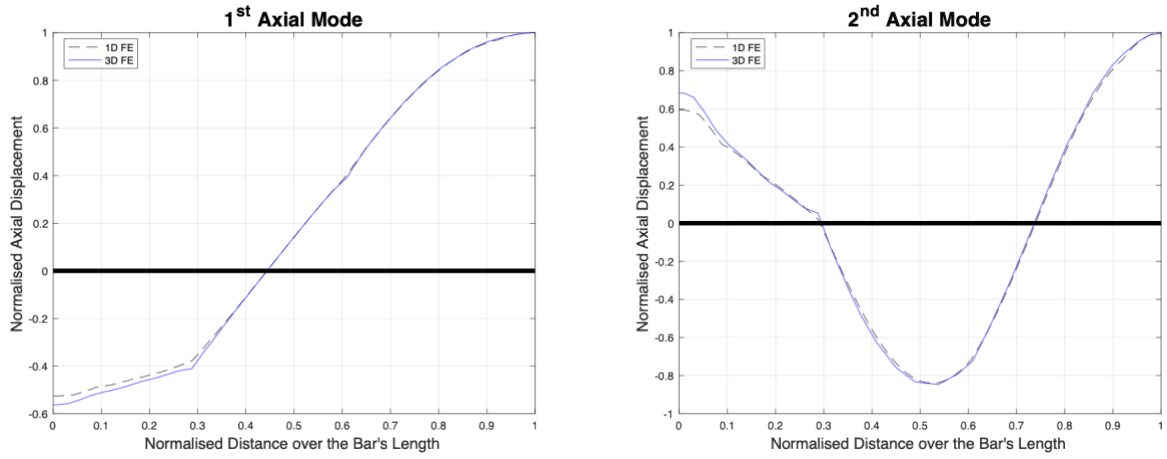

Figure 4-6. A comparison between the 1st (Left) and 2nd (Right) mode shapes predicted using the 1D and 3D models. There is a good agreement between both models and the area of the largest deviation (located between 0-0.1) is the distal screw dual cone region.

4.4.3 Evaluating the Interface Properties of the 3D FE Implicit Signals using the 1D FE Application

The third stage of validation involved using the model to evaluate the interface properties for: 1) Ideal (with a symmetric impact condition) signals and 2) Asymmetric signals generated using the 3D FE implicit simulations for the three interface conditions. Figure 4-7 illustrates the matching process using an ideal INTERMEDIATE condition signal, the user sets the system's parameters (like implant model and the rod size) and sets the initial estimate for the interface condition (k and ζ). After the optimization process, the user can determine the final interface condition and the goodness of fit (assessed using cosine similarity) between the input signal and the model's prediction in the frequency domain. The results of the interface properties evaluation are summarised in Table 4-2 below. As it can be observed the 1D model was able to associate the changes in the elastic modulus of the BII (E) to significant (orders of magnitude) changes in the interface stiffness (k) ranging from 3.77×10^6 to 2.58×10^9 N/m . Additionally, the model was able to identify changes (from 665 to 9710 Hz) in the 1st mode frequency (f_1) to the interface condition. f_2 appears to be less sensitive (9340 to 10730 Hz) to interface changes compared to both k and f_1. The interface condition in the 3D FE simulation was only controlled by varying the E and the second mode damping ratio (ζ_2) was fixed to 1% for the three simulations. As it can be observed, the 1D model predicted that the 2nd mode damping is close 1% with a maximum absolute difference of 0.20% for the ideal strikes.

The asymmetric loading condition yielded minor changes to the predictions for the k and f_1, yet those changes are not large enough to cause issues distinguishing between the different interface conditions. The largest difference in k was in the order of 1.86% (between the ideal and asymmetric striking conditions) for the LOW interface condition while the change in k between the LOW and INTERMEDIATE conditions were in the order of 8120%. There were virtually no changes in the prediction of the model for f_2 between both striking conditions. Nevertheless, the asymmetric loading condition seems to be amplifying the absolute error in the predictions of ζ_2 from 0.20% to almost two folds (0.5%). For both (Ideal and Asymmetric) cases, the developed application managed to find a good fit between the input signals which is showcased by the high cosine similarity (analysed signals are shown in Appendix B) between the model and the signals in the frequency domain.

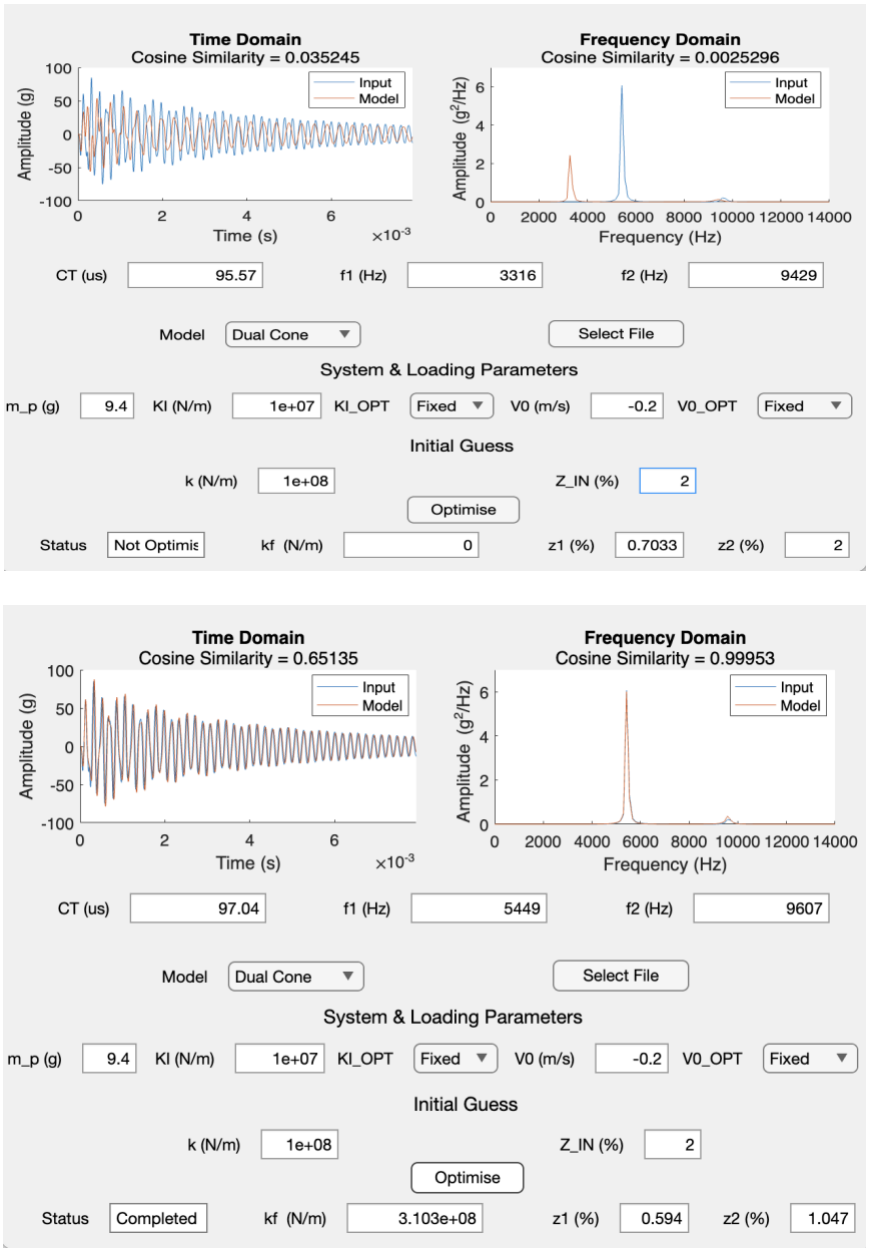

Figure 4-7. The user sets the system's parameters and sets an initial estimate for the interface stiffness (k) and 2nd mode damping ratio (Top), the user then initiates the optimization process to find the best fit between the 1D FE model and the final interface values (Bottom). The matching process was illustrated using an ideal INTERMEDIATE signal.

Table 4-2. Summary of the interface properties and signal characteristics extracts for LOW, INTERMEDIATE and HIGH conditions for Ideal and Asymmetric signals.

Ideal Strikes with $\zeta_2 = 1\%$						
Interface Condition	k (N/m)	f_1 (Hz)	ζ_1 (%)	f_2 (Hz)	ζ_2 (%)	Cosine Similarity (%)
LOW ($E = 0.45$ MPa)	3.77×10^6	665	0.0858	9340	1.17	99.4
INTERMEDIATE ($E = 40$ MPa)	3.10×10^8	5450	0.590	9610	1.05	99.9
HIGH ($E = 1000$ MPa)	2.58×10^9	9710	1.09	10700	1.20	99.3
Asymmetric Strikes with $\zeta_2 = 1\%$						
LOW ($E = 0.45$ MPa)	3.84×10^6	671	0.0960	9340	1.34	97.6
INTERMEDIATE ($E = 40$ MPa)	3.10×10^8	5450	0.680	9610	1.20	99.9
HIGH ($E = 1000$ MPa)	2.59×10^9	9720	1.340	10700	1.48	98.9

4.4.4 Evaluating the Interface Properties of the Experimental Signals using the 1D FE Application

Figure 4-8 summarises the time and frequency domain experimental responses for the three interface conditions. The LOW interface condition is overwhelmingly dominated by f_2 while the INTERMEDIATE and HIGH interface conditions are dominated by f_1. The LOW response was digitally filtered using a lowpass filter set at 6000 Hz. The attenuated response demonstrates the presence of another frequency in the 600 Hz range (Figure 4-9). The signals generated from the 3D FE model also predicted similar trends in the modal contributions, however f_1 (despite having smaller contribution to the response compared to f_2) was still large enough to objectively perform the matching process on it using the application without having to digitally attenuate the response.

Therefore, the 1D application was used to analyse the INTERMEDIATE and HIGH experimental signals. The discussion will involve a section on the possible reasons for not sufficiently triggering f_1 for the LOW condition experimentally and potential solutions for amplifying it. Table 4-3 summarises the interface properties and signal characteristics of the experimental INTERMEDIATE and HIGH interface conditions. Similarly, to the 3D FE analysis, the 1D application managed to distinguish between the two interface conditions. The Wilcoxon rank sum test indicates that there is statistical significance between the medians (η) of the two groups for all the model's outputs (k,$\zeta_1, \zeta_2, f_1, f_2$), Results also indicate the consistency and repeatability of the measurements and the analysis procedure which is evident by the small Interquartile Range (IQR). The medians of the k (for example) were 1.43×10^8 and 2.21×10^9 N/m for the INTERMEDIATE and HIGH conditions respectively while the IQR was 4×10^5 and 9.3×10^7 N/m respectively, the IQR (which is an expression of the variations between the measurements for a given condition) is at least two orders of magnitude lower than the medians.

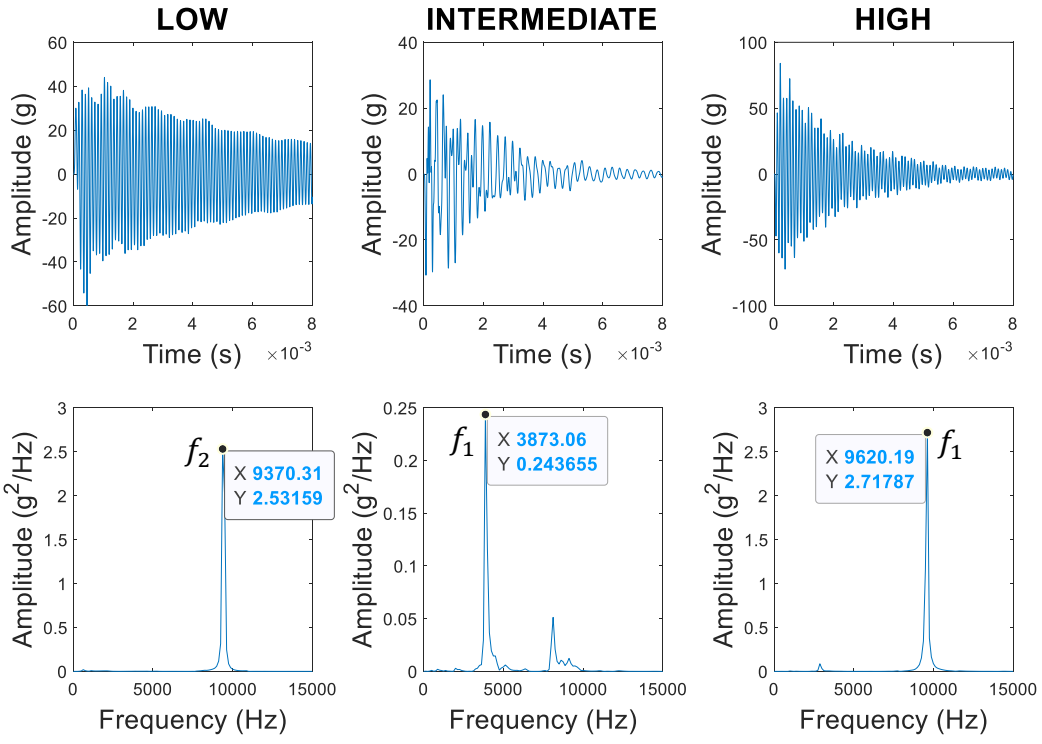

Figure 4-8. The time and frequency domain responses for the three interface conditions collected experimentally. The LOW condition appears to be dominated by the 2nd axial mode (f_2) while the INTERMEDIATE and HIGH conditions appear to be dominated by the 1st axial mode.

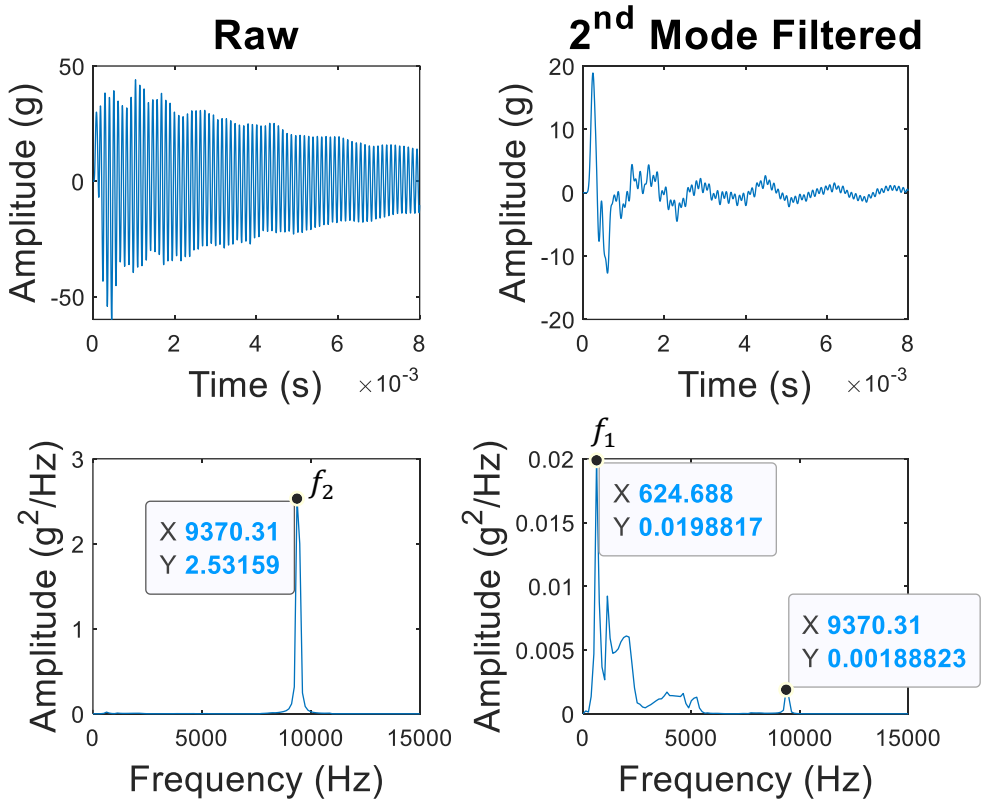

Figure 4-9. There appears to be a faint presence of the 1st mode in the response of the LOW interface condition that is completely masked off by the overwhelming presence of the f_2. A low pass filter can be used to attenuate f_2 and help in detecting the presence of f_1.

Table 4-3. Summary of the evaluated interface parameters for the INTERMEDIATE and HIGH experimental signals.

	INTERMEDIATE (Wax)		**HIGH (Superglue)**		$H_0: \eta_1 = \eta_2$
	η_1	IQR	η_2	IQR	p-value
k (N/m)	1.43×10^8	4.00×10^5	2.21×10^9	9.30×10^7	0.00794
f_1 (Hz)	3910	7.00	9530	103	0.00794
ζ_1 (%)	1.66	0.120	0.65	0.190	0.00794
f_2 (Hz)	9470	0	10600	50.0	0.00794
ζ_2 (%)	4.01	0.29	0.72	0.220	0.00794
Cosine Similarity (%)	97.7	1.40	99.9	0.100	—

4.5 Discussion

Cross validating the 1D FE formulation with the analytical and 3D FE solutions of a simplified uniform cylinder and obtaining nearly identical 1st and 2nd axial natural frequencies and mode shapes (Figure 4-5) indicated that the code is working properly in terms of generating the element-wise stiffness and mass matrices and assembling them. Theoretically, the mass and stiffness matrices are derived from the same governing PDE that generates the analytical solution (EQ 4-13) and thus for simple cases the solution of the 1D FE model should converge to the analytical solution with a sufficient number of elements [45], [59]. The next step of validation entailed modelling the actual geometry of the TFA system albeit without modelling the BII and the impactor and performing modal analysis using both the 1D FE and 3D FE models under a free-free boundary condition. The main purpose of this step is to investigate whether 1D bar elements have an acceptable approximation power to obtain the axial modes of interest accurately. Results indicated that the 1D model overestimated the 1st and 2nd modes by 1.17 and 2.02% respectively in comparison to the 3D FE simulations. This behavior is expected since 1D bar elements have fewer nodes than 3D full integration hexahedral elements; fewer degrees of freedom means that the

element is going to be less flexible [45], [59]. The slightly stiffer response of the 1D FE modal simulations could also be attributed to Poisson's effects which are modelled in the 3D simulation but are not accounted for in the governing PDE used in generating the 1D bar elements, Poisson's effects may be more prominent near the less uniform components of the system such as the distal screw-dual cone assembly (Figure 4-6). However, such a small systematic difference is not expected to yield significant alterations to estimating the BII condition and thus the current 1D mathematical representation was deemed representative of the implant system's geometric, stiffness and inertial properties. These results agree with our previous investigation with the bending behavior of the implant system and thus it can be deduced that 1D bar and beam elements have enough power to model the axial and bending behavior of the OPL implant system which may suggest considering them for other mathematical applications such as investigating the forces due to static load bearing or dynamic forces during ambulation instead of relying on computationally expensive 3D FE simulations [58].

The 1D model was extended to perform time domain analysis using modal superposition and was used to evaluate the stiffness for: 1) 3D FE signals under symmetric loading, 2) 3D FE signals under asymmetric loading and 3) Experimental signals. The results shown in Table 4-2 indicate that the developed 1D model was successful in distinguishing between the three extreme BII conditions. This was evident by the significant changes in the values obtained for the k and f_1 values. The relationship between the bone-implant system and the system's natural frequencies is well established in the literature for the fields of dentistry and hearing aids [4], [5], [10], [11]. The quality of osseointegration on implant stability can be viewed as the degree of interfacial micromotion, where stable implants experience limited degrees of micromotion [4]. Stiffness is defined as the resistance of the structure to applied forces and thus the BII stiffness (which is the k) in this model can be viewed as a direct measure of implant stability. Linear vibration theory predicts a direct (but not linear) relation between the stiffness and the natural frequencies of the structure [4], [5], [40]. Therefore, it is expected to observe an increase in the k and at least one of the natural frequencies (in this case it was f_1). Although, from this analysis it appears to be that both f_1 and the k are appropriate stability metrics, the k (being a direct measurement) of the BII conditions appears to be more sensitive to the interface condition. The change between the k of the LOW and HIGH condition was an increase in the order of $6.84\times10^4\%$ while the change in f_1 was $1.36\times10^3\%$ (Table 4-2). Similar findings were found for the ASIST for bone anchored hearing

aids where the ASC score (a non-dimensional score based on the k) was found to be more sensitive to changing the interface condition compared to the 1st and 2nd of the system [57]. Although different BII conditions should have different damping properties where higher damping is expected for the less stiff (softer) configurations, the BII condition in the 3D simulations was only controlled using a variable E and the damping properties were fixed by setting the second mode damping to $\zeta_2 = 1\%$ between the three interface conditions. Therefore, the 1D model should predict $\zeta_2 = 1\%$ for all the signals acquired from the 3D FE simulations. Table 4-2 showed that ζ_2 was overestimated by the 1D model from the specified value by 0.05-0.20% and 0.20-0.49% (absolute error) for the ideal and asymmetric striking conditions respectively. A possible interpretation is that modelling the rod as a particle misrepresents the kinetic energy transfer between the rod and the implant system which affects the amplitude of the response (modal contributions) and since the amplitude is also affected by the damping, the optimization routine can mistakenly attribute the lower amplitude for a higher damping value. Modelling the rod in the 1D FE model using bar elements should be considered in future work to better represent the inertia of the rod and the energy transfer between the impactor and the implant system. A skewed strike can trigger out of plane modes and thus takes energy from the axial modes of interest in the 3D FE simulation. However the 1D model can only account for the axial behavior and can see this reduction in the amplitude of the signal as higher damping and this could lead to overestimating ζ_2 by the 1D model. Therefore, it is important to consider the effect of striking asymmetry when designing the new impact rod for the system. Nevertheless, it seems that despite the larger error in estimating damping in asymmetric strikes, the error in estimating the k (the primary stability metric) is relatively minor (maximum error of 1.85% for the LOW condition) which suggests that the effects of asymmetry would be minimal in estimating the system's stability. Finally, the high cosine similarity scores indicate that the optimization routine managed to find the best fit between the input 3D FE signals and the 1D model's prediction with respect to the frequency domain objective function. Cosine similarity was chosen as the goodness of fit metric since it adds higher weight to the phase (frequency) compared to the amplitudes of the response since the frequency is a signal characteristic while the amplitude is sensitive to the striking conditions [40], [41].

The 1D model was able to evaluate the BII condition and the signal characteristics of the experimental INTERMEDIATE and HIGH conditions (Table 4-3). The significant change in k and f_1 further support the findings that argue that the 1D model is capable in detecting changes to the

BII condition. The IQR values for k and f_1 for a given interface condition are orders of magnitude smaller than the medians of the group between the two conditions which indicate that the test is highly repeatable. Unlike the 3D FE simulations damping cannot be fixed for the two materials, it is expected that the softer material would have higher damping characteristics. The 1D model was able to sense the differences in damping between the two interface conditions since it reported higher ζ_1 and ζ_2 values for the INTERMEDIATE condition compared to the HIGH condition. The IQR for the damping ratios is relatively (in comparison with the k, f_1 and f_2) higher, this is due to the influence of damping on the amplitude of the power spectrum. In linear vibration, the damping ratio is a system characteristic and is independent of the striking conditions (similar to the natural frequency) [40], [41]. However, since damping affects the amplitude of the response in the power spectrum, any source of experimental error that can influence the amplitude of the response (such as the striking conditions) could mistakenly be accounted for by damping in the optimisation process. This could increase the source of variability of the damping estimates in comparison to estimate the f and the k which are measured by the location of the peak in the power spectrum and are not as sensitive to the amplitude of the power spectrum [38], [39]. Despite the higher IQR values, there is still statistical significance to the difference between the two groups which suggests that the model can report damping as a stability metric albeit as a secondary one due to the higher variability. Although Shao et al. and Cairns et al. primarily investigated the bending behavior of the OPRA implant system, their findings support that the vibration response can be utilized to detect variations in the BII condition [17]–[20]. This investigation further supports this finding and extends it to the axial behavior of the OPL system using simulations and experimental findings. However, utilizing a model helps in determining the k which appears to be a more direct and sensitive measurement of the interface condition compared to relying on the natural frequencies. Furthermore, Cairns et al. (to have more confidence in their estimated frequencies) had to construct a FRF from averaging the measurements of 17 measurement and excitation locations distributed over the femur which is not clinically attainable [18]–[20]. Relying on a physically representative model of the bone-implant system can help in determining the signal characteristics, BII and even the mode shapes without the need for acquiring the signal from different measurement locations clinically.

The primary limitation of this investigation is the inability of the Periotest® to physically trigger the 1st axial mode sufficiently for the LOW stiffness case experimentally. Although, the

INTERMEDIATE and HIGH conditions had additional peaks (Figure 4-8) that represent potential noise in the system (that can be due to several factors such as the threaded connections or out of plane vibration due to the strike asymmetry), the 1st axial mode was the dominant frequency for both cases and thus the model was able to perform the analysis. On the other hand, the weak presence of the 1st axial mode can only be observed after attenuating the 2nd mode digitally using a filter. In experimental modal analysis, there are two main factors that come into play when selecting an impact hammer, the size of the hammer (or its mass) and the material (stiffness) of the impacting tip [41]. Those two parameters affect the input force profile and in turn affect the range of frequencies that the hammer can excite. Observing the mode shape of f_1 over a wide range of interface conditions shows that at very low interface conditions the mode shape is almost a rigid body mode where there is very little resistance at the interface to implant motion and the entire implant assembly is sliding with respect the BII. This suggests that the system (of almost 200g) would require a significant amount of inertia that the current Periotest® (9.4 g) is unable to impart on the system. Since this investigation is part of an ongoing project on extending the ASIST approach to the TFA OPL system, a parallel in-house project is experimentally investigating the effects of rods with different masses and tip material in triggering f_1 for the lower interface conditions.

The primary focus for future work is investigating different impact rod parameters in triggering f_1 experimentally and extending the current model to utilize the new rod. In addition to this, future work will test modelling the rod using bar elements instead of a particle to improve the damping estimation using the model. Finally, a sensitivity analysis is to be conducted to better understand the numerical errors due to the optimization routine and the matching between the input signal and the 1D FE model's prediction.

4.6 Conclusion

In this investigation, a 1D FE axial model for the OPL implant system was developed. The model is part of an ongoing project that aims at extending vibration methods for assessing the quality of the bone-implant interface non-invasively. Comparing the 1D mode shapes with the results of the 3D analysis showed that the 1D model accurately represents the implant system. The model was then incorporated in a simple MATLAB® based GUI that extracts the BII properties using an optimization routine that matches the response of the model to input signals. The input signals

were generated using 3D FE implicit simulations and an experimental benchtop setup. The model managed to extract the interface properties for all the 3D FE simulations and showed that the interface stiffness is highly sensitive to the interface condition and is a more direct and appropriate stability metric compared to the natural frequency. The 1D model also managed to extract the experimental interface properties for the INTERMEDIATE and HIGH conditions but the 1st axial mode was not triggered using the current impactor and thus the primary focus of future work entails redesigning the impactor to amplify the presence of the 1st axial mode for the lower interface configurations.

Chapter 5 Extending the Model to Evaluate the Interface Properties of the LOW Interface Condition

In the previous chapter, the 1D application successfully managed to evaluate the interface properties for all the 3D FE and the experimental INTERMEDIATE and HIGH conditions. It was noted that the modal contribution of the 1st mode (which is highly sensitive to the interface condition) is not observable enough for the experimental LOW conditions. In a separate (in-house project), the LOW interface setup was excited by different rod designs (masses and tips). Changing the rod parameters changed the modal contributions and made the presence of the 1st axial mode more observable for some of the striking conditions [61]. In this chapter, the 1D FE model is extended to evaluate the experimental LOW interface condition. Two changes are needed to extend the model, the first change is including the option to implement Rayleigh damping model and the second one is to model the impactor as a bar instead of a particle. Both changes will be further discussed in the coming subsections. The chapter concludes by summarizing the primary achievements and limitations of the investigations conducted on the TFA implant systems and the recommendation for future work.

5.1 Incorporating Rayleigh's Damping Model

In Chapter 4, stiffness proportional damping was used to model the dissipation of energy by the system (EQ 4-4 to EQ 4-6). In stiffness proportional damping, a single independent damping ratio is used to specify the remaining damping ratios as function of the natural frequencies of the system [40]. The simplicity of implementing stiffness proportional damping in modal superposition (since it preserves the orthogonality properties of the system's characteristic matrices) makes it a favorable technique for modelling damping for a number of vibration problems [40]. However, there are situations where the user may need to assign two independent damping ratios in the model. For example, the user, may need to increase the damping ratio of the 1st mode without increasing the damping ratio of the 2nd mode. In such a situation, it would be proper to incorporate mass proportional damping into the damping model. Rayleigh's proportional damping model incorporates both mass and stiffness damping and the energy dissipation behavior is now governed by two independent damping ratios instead of one (EQ 5-1 to EQ 5-3) [40]. The damping matrix $[C]$ is constructed from the mass $[M]$ and stiffness $[K]$ matrices (EQ 5-1). The α and β parameters can be computed from the system's natural frequencies ω and damping ratios ζ from any two

modes of interest (i, j) (EQ 5-2). Then the complete set of the system's damping ratios ζ_n can be computed for any mode n using the α and β parameters and the systems natural frequencies ω_n (EQ 5-3). Since the damping matrix is still constructed using the mass and stiffness matrices, the orthogonality property of the matrix is preserved and classical modal superposition can still be implemented in generating the time domain responses [40]. The primary limitation of relying on Rayleigh's damping model instead of the stiffness model is that the system of equations shown in EQ 5-2 can be ill-conditioned and this can lead to numerical inaccuracies in estimating α and β [40]. In Chapter 4, it was demonstrated that the interface stiffness varied by orders of magnitude for the LOW, INTERMEDIATE and HIGH conditions and since the optimization routine is iteratively searching for the best fit between the input signal and the model's prediction, it is possible that the system of equations becomes ill-conditioned for some of the optimization iterations and can give out negative α or β parameters which is physically unrealistic (negative damping adds energy to the system instead of dissipating it). In such cases, the damping model in the program was automatically overridden to stiffness proportional damping upon detection of a negative α or β using an "if condition" in the code. Another limitation of Rayleigh's damping is its physical interpretation, stiffness proportional damping can be viewed as material damping associated with the deformation of material throughout its dynamic response while mass proportional damping is associated with the resistance to inertial loads and can be viewed as air resistance [33]. For TFA systems, it would be expected that material damping as the primary mechanism of energy dissipation as compared to air resistance. However, incorporating Rayleigh's model can be a convenient way to better control the damping ratios. Therefore, it will be implemented in the program and tested in this section.

$$[C] = \alpha[M] + \beta[K] \tag{EQ 5-1}$$

$$\frac{1}{2}\begin{bmatrix} 1/\omega_i & \omega_i \\ 1/\omega_j & \omega_j \end{bmatrix}\begin{Bmatrix} \alpha \\ \beta \end{Bmatrix} = \begin{Bmatrix} \zeta_i \\ \zeta_j \end{Bmatrix} \tag{EQ 5-2}$$

$$\zeta_n = \frac{\alpha}{2\omega_n} + \frac{\beta\omega_n}{2} \tag{EQ 5-3}$$

The signals were generated using the same 3D FE implicit model previously discussed in Chapter 4. However, instead of only generating signals with ζ_2 at 1% an additional damping level was set

at $\zeta_2 = 4\%$ for the three BII conditions (LOW, INTERMEDIATE and HIGH). The main purpose of running this test is to check if the optimization routine would face uniqueness of solution issues with the introduction of Rayleigh's damping model. The 3D FE signals were generated using a single damping parameter (ζ_2) and ideally the 1D FE solver (that utilizes Rayleigh model and has the option to manipulate two damping ratios ζ_1 and ζ_2 during the optimization) would still be able to give out the same damping ratio predictions as the old 1D FE solver that used the stiffness damping model and only manipulated (ζ_2).

Table 5-1 shows a comparison between model's predictions and the input signals for different damping parameters. As it can be observed, the model's predictions of the damping estimates are very close with a maximum absolute difference of 0.037% and 0.06% for ζ_1 and ζ_2 respectively. This indicates that even though implementing Rayleigh's damping model complicates the optimization routine (since the routine solves for an additional unknown damping parameter instead of one), the optimization routine still managed to match the predictions reached by the simpler stiffness proportional model. Another side (but important) observation are the slight changes ($\approx$4%) in the interface stiffness (k) between the two damping levels for the HIGH condition (Table 5-1). The k and ζ are both system characteristics and are independent of each other and thus from a physical perspective the k should not change upon changing ζ_2, however from a numerical standpoint the damping decreases the number of observed cycles in a signal and the corresponding quality of the FFT (which can affect the performance of the optimization routine) and the predictions made by the model (Figure 5-1). Although, such a change in estimating the k is still orders of magnitude lower than the other two interface conditions, it will be importance to conduct a sensitivity analysis between the 1D model's outputs upon changing the interface stiffness and damping characteristics using the 3D FE model for a wide range of conditions.

Table 5-1 Comparison between Stiffness and Rayleigh damping models for 3D FE signals with different damping properties by ζ_2. Rayleigh damping model managed to predict similar damping values to the Stiffness proportional model.

3D FE Simulation with $\zeta_2 = 1\%$								
	Stiffness Proportional Damping				Rayleigh Proportional Damping			
Interface Condition	k (N/m)	ζ_1 (%)	ζ_2 (%)	Cosine Similarity (%)	k (N/m)	ζ_1 (%)	ζ_2 (%)	Cosine Similarity (%)
LOW ($E = 0.45$ MPa)	3.77×10^6	0.086	1.17	99.4	3.76×10^6	0.083	1.17	98.7
INTERMEDIATE ($E = 40$ MPa)	3.10×10^8	0.59	1.05	99.9	3.10×10^8	0.627	1.11	99.9
HIGH ($E = 1000$ MPa)	2.55×10^9	1.09	1.20	99.3	2.58×10^9	1.08	1.02	99.3
3D FE Simulation with $\zeta_2 = 4\%$								
	Stiffness Proportional Damping				Rayleigh Proportional Damping			
Interface Condition	k (N/m)	ζ_1 (%)	ζ_2 (%)	Cosine Similarity (%)	k (N/m)	ζ_1 (%)	ζ_2 (%)	Cosine Similarity (%)
LOW ($E = 0.45$ MPa)	3.74×10^6	0.264	3.72	99.9	3.74×10^6	0.264	3.72	98.7
INTERMEDIATE ($E = 40$ MPa)	3.10×10^8	2.13	3.75	99.9	3.11×10^8	2.13	3.75	99.8
HIGH ($E = 1000$ MPa)	2.69×10^9	4.13	4.54	99.9	2.68×10^9	4.13	4.55	99.2

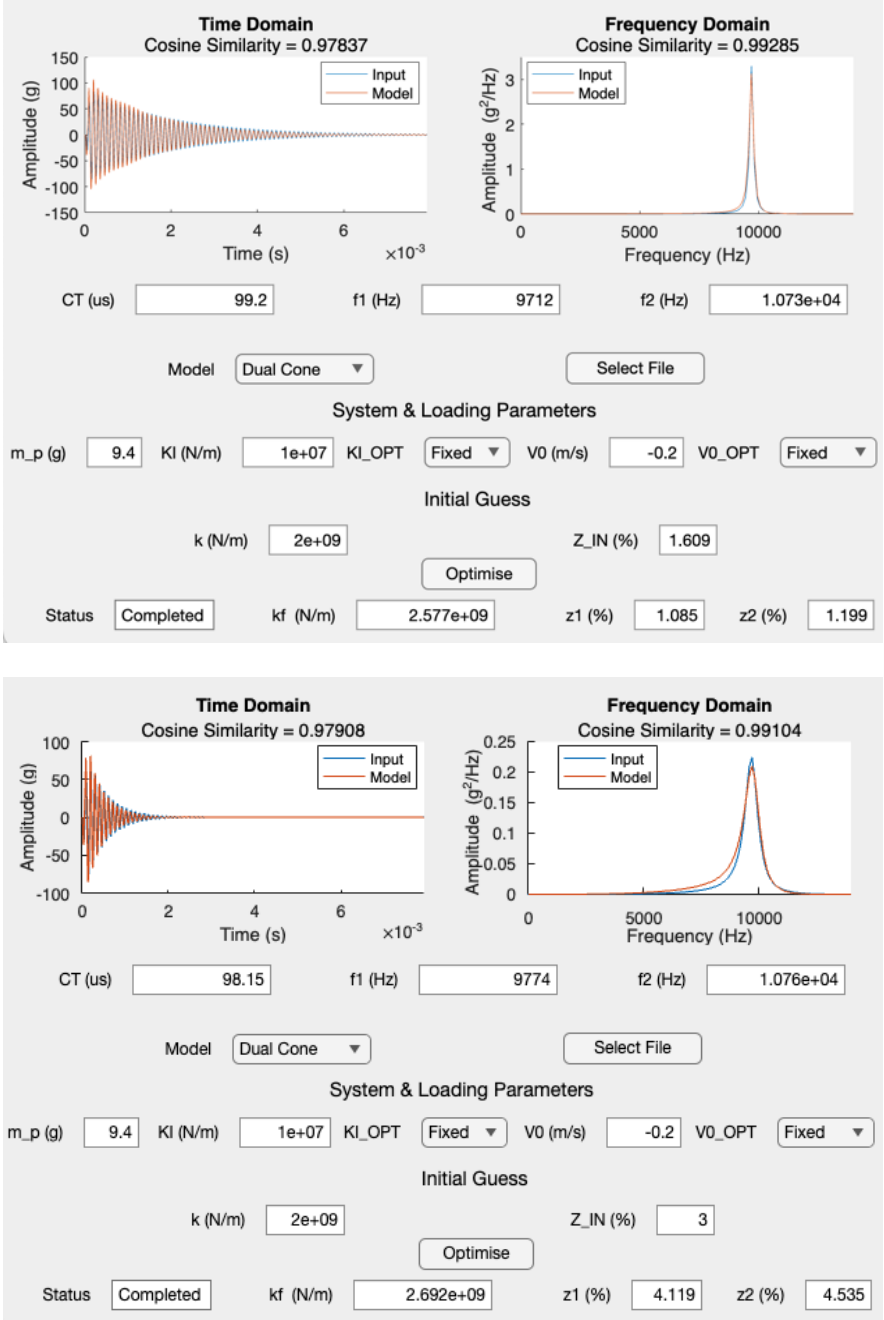

Figure 5-1 Increasing the damping level from $\zeta_2 = 1\%$ (Top) to $\zeta_2 = 4\%$ (Bottom) led to lowering the quality of the FFT and led to changes of around 4% in estimating k for the HIGH BII condition.

As it was mentioned earlier, Rayleigh's model has more flexibility in assigning the damping ratios compared to mass or stiffness proportional damping models. For the LOW interface condition, there are two observable modes in the signal and ζ_1 can be larger than ζ_2 and it is expected that Rayleigh's model would be able to account for this behavior while stiffness proportional damping would not. Therefore, an additional 3D FE simulation with $\zeta_1 = 3.0\%$ and $\zeta_2 = 0.50\%$ and both

damping models were used to extract the interface properties and estimate the damping ratios. Table 5-2 shows the model's output for both damping models. The stiffness proportional model was only able to predict ζ_2 accurately while ζ_1 was quite far from the value set in the 3D FE simulation. The stiffness proportional damping model also predicted ζ_1 to be lower than ζ_2. As for Rayleigh's model, the model was able to assign a higher damping value for ζ_1 compared to ζ_2 however the estimate for ζ_1 was lower by 1.27% (absolute difference) than the value set in the 3D FE simulation. While running the application, it seemed that beyond a certain damping threshold for ζ_1, the changes to the frequency spectrum were low due to the low modal contribution of the 1st mode of the response using the current impactor (Periotest®). A possible interpretation for this difference is that the objective function for the optimization routine (EQ 4-12) was defined using the L_4 norm which would assign higher weight to the dominant peak (which was chosen to assign higher weight to the dominant peak compared to potential noise in the experimental signals) and thus beyond a certain damping ratio changes to the frequency response may not be sufficiently large for the optimization routine and the routine may converge for a lower damping ratio. Another possible interpretation is the definition of the contact stiffness (K_I) between the 1D and 3D FE model. In the 1D model, K_I was modelled by a linear spring connecting the system with the impactor. In the 3D model, a linear pressure-overclosure curve was defined to model the relationship between the master-slave contact surfaces. A linear pressure-overclosure is defined by normalizing K_I (of the 1D model) with respect to the contact area in ABAQUS® and this approach worked well for all the 3D FE signals since there was no need to vary K_I in the optimization routine for all the previously discussed 3D FE signals. However, there can be differences between the contact modelling approaches between the 1D and the higher fidelity 3D FE simulation and the differences may be more prominent for some combinations of interface stiffnesses and damping ratios. Allowing K_I to vary between both models can be justifiable for these cases and Table 5-2 shows the 1D model's outputs when K_I is set as a variable in the optimization routine. For both stiffness and Rayleigh damping models, setting K_I as a variable improves the model prediction of ζ_2. ζ_1 is still quite far for the stiffness proportional model but is significantly improved using Rayleigh's model which got it closer to 3%. Changes to K_I should not physically change the estimates of k or ζ but K_I affects the modal contributions of the response and in turn can affect the numerical predictions made by the optimization routine. Therefore, it is important to also test the effect of changing K_I on the model's predictions by conducting sensitivity analysis.

Table 5-2 Comparison between Stiffness and Rayleigh damping models for a 3D FE signal for the LOW condition. Rayleigh damping model managed to predict that $\zeta_1 > \zeta_2$ while the stiffness damping model could not. Setting K_I as a variable significantly improved the damping predictions of Rayleigh damping model.

3D FE Simulation with $\zeta_1 = 3\%$ and $\zeta_2 = 0.5\%$							
Stiffness Proportional Damping				Rayleigh Proportional Damping			
k (N/m)	K_I (N/m)	ζ_1 (%)	ζ_2 (%)	k (N/m)	K_I (N/m)	ζ_1 (%)	ζ_2 (%)
3.95×10^6	1.00×10^7	0.0460	0.630	3.88×10^6	1.00×10^7	1.73	0.640
3.88×10^6	1.08×10^7	0.0353	0.488	3.85×10^6	9.15×10^6	2.55	0.570

5.2 Effect of the Impactor's Parameters on the Modal Contributions of the LOW Interface Condition

In chapter 4, it was concluded that the Periotest® is not capable in sufficiently exciting the 1st mode and that the 1D model is currently incapable of evaluating the interface properties for experimental LOW condition. The impact rod is currently being re-designed in a separate and parallel in-house project [61]. In this subsection however, a brief parametric study is conducted using the 1D FE model to better understand the potential impact of changing the rod's parameters on the presence of the 1st and 2nd mode in the signal for a LOW condition. From a design perspective, an impact excitation can be controlled by changing the mass of the impactor (m_p), the speed of impact (V_r) and the tip of the impactor which affects the contact stiffness (K_I). Those three parameters are varied using the 1D model as shown in Table 5-3 below and the amplitude of each mode is extracted from the power spectrum of the acceleration response.

Table 5-3 Parameters used in studying the effect of m_p, K_I and V_r on the presence of the 1st and 2nd modes for the LOW condition.

Parameter	**Symbol**	**Magnitude**	**Notes**
Mass of Impact Rod	m_p	{5-60} g	Default value of 9.4 g for K_I and V_r parametric studies
Contact Stiffness	K_I	{1-100}×10^6 N/m	Default value of 1×10^7 N/m for m_p and V_r parametric studies
Rod Velocity	V_r	{50-500} mm/s	Default value of 200 mm/s for m_p and K_r parametric studies
Interface Stiffness	k	3.80×10^6 N/m	This value is chosen to simulate a LOW interface condition
Damping Ratio	ζ_2	1%	Stiffness proportional damping with second mode set to 1%

Changing the velocity of the impact rod increases the presence of each mode linearly and the amplitude ratio is preserved as a result (Figure 5-2). The contact time is invariant to velocity changes. The contact time is measured from the acceleration response of the rod (Chapter 4) and is only a function of the inertial and stiffness parameters of the rod-bone-implant system and thus it is expected that changing the velocity should not change it. However, changing the velocity can be viewed as changing the initial condition from the model's perspective and in turn increases the amplitude of the response [40]. Increasing the velocity is a straightforward method of increasing the amplitude of the response, however there are practical considerations regarding the safety of the excitation level on the bone-implant system. Additionally, there are limitations imposed by the electromagnet and its ability to excite the impact rod to a specific velocity [61].

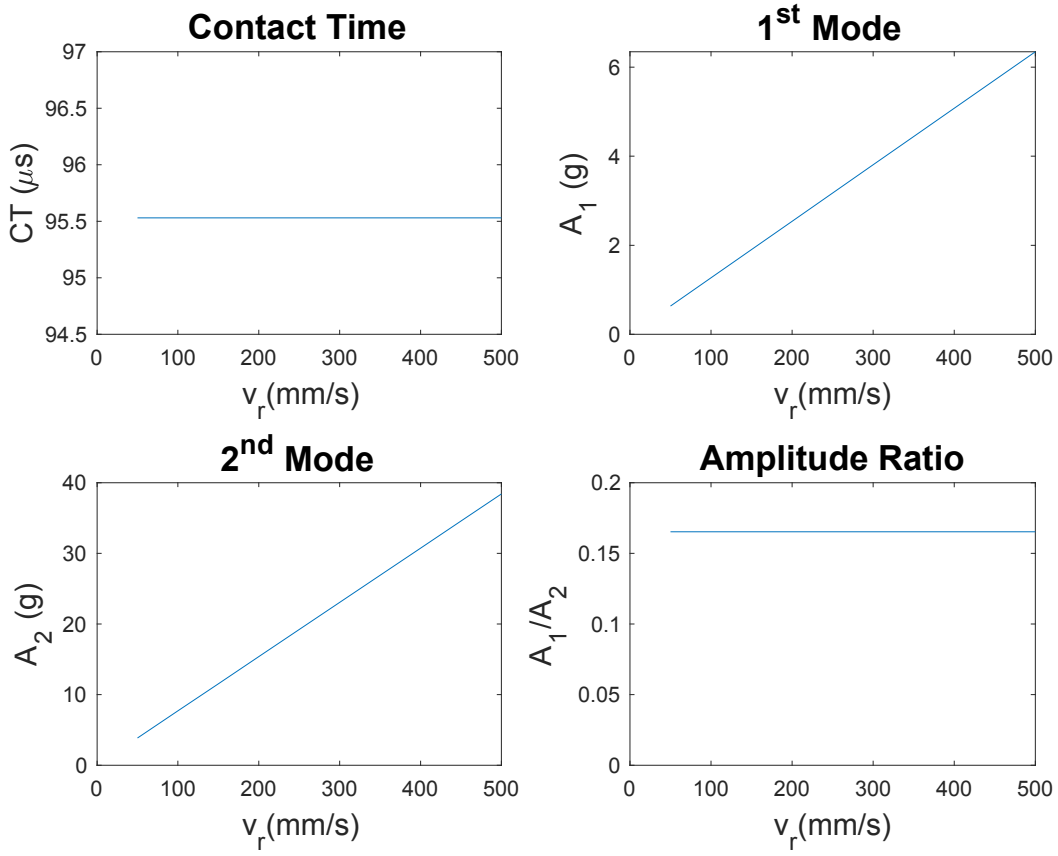

Figure 5-2 The presence of both modes of vibrations increases linearly upon increasing the velocity and the contact time and amplitude ratios are preserved.

The contact stiffness (K_I) is a function of the stiffness of the impactor and the impacted system. From a design perspective, only the impactor's stiffness can be controlled by the user and therefore commercial impact hammers can usually be fitted with various tips to manipulate the impactor's stiffness and in turn affect K_I [41]. Manipulating K_I affects the contact time of the input force (pulse) profile and in turn affects the range of excited frequency [41]. An ideal pulse is mathematically represented with a Delta-Dirac function and its Fourier transform would result in distributing the pulse energy equally over the entire frequency range [62]. However, practical input signals have a finite duration and this results in an uneven distribution of the pulse energy and the 3 dB point is normally taken as the threshold of the possible frequency excitation range of an impactor [41]. Although K_I is dependent on both the impactor and the impacted system stiffnesses, harder (stiffer) tips tend to have shorter pulse durations and in turn tend to have a wider frequency of excitation range compared to softer (less stiff) tips [41]. Changing K_I in the model while holding

the other parameters constant (Table 5-3), indicated that the contribution of the 1st mode is not affected by changing K_I (Figure 5-3). However, the contact time continuously decreases and the 2nd mode continuously increases up until 4×10^7 N/m and then plateaus. The behavior of the modes (upon changing the input pulse using K_I) predicted by the 1D model agrees with the trends mentioned in the literature [41]. Changing K_I has minimal effect on exciting the 1st mode, because the lowest K_I in the chosen K_I range already sufficiently excites the 1st mode of vibration and changing K_I becomes more influential at exciting the higher order modes. Therefore, the lower K_I values in range did not trigger the 2nd mode sufficiently and then more energy became available to this mode upon increasing K_I until reaching a phase of saturation. It should be noted that the chosen K_I range was centered around the estimated contact time values of the Periotest® and other impactors currently under investigation by Beaudry et al. [61] . Therefore, it appears that manipulating K_I will not amplify the presence of the 1st mode in the response, instead it will mainly affect the higher order modes.

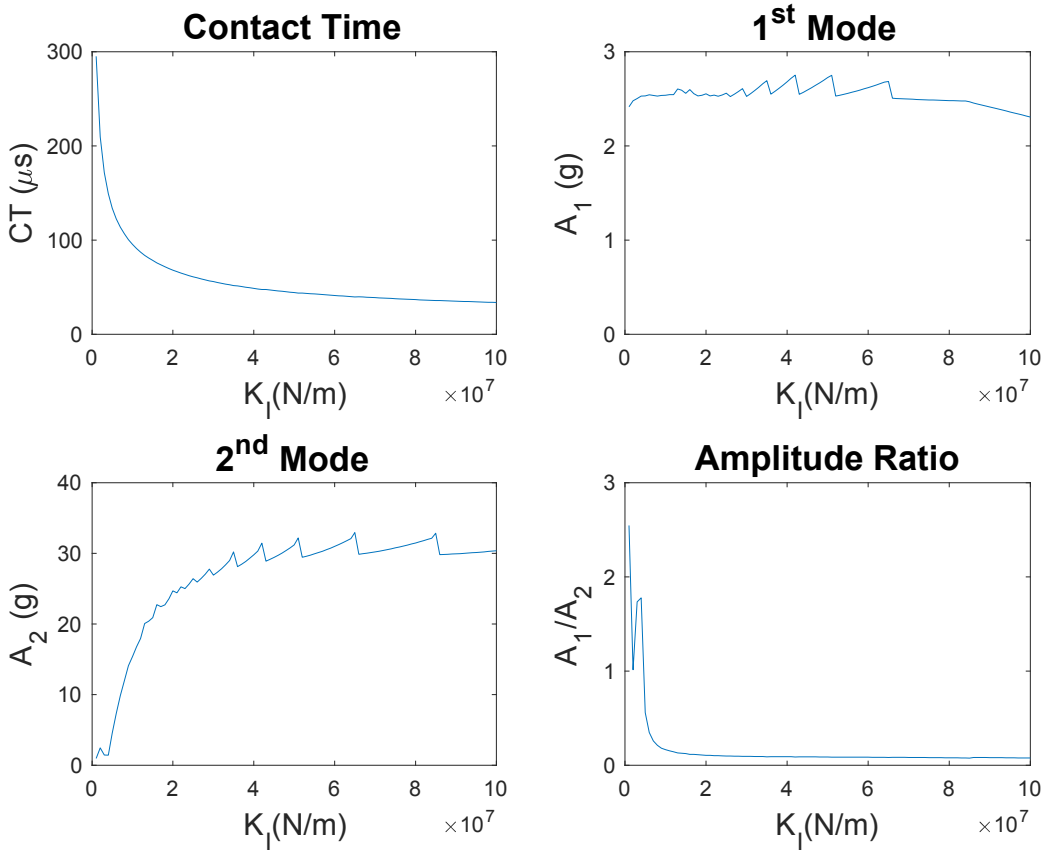

Figure 5-3 The contribution of the 1st mode is almost invariant to changes to the impact stiffness, however the contribution of the 2nd mode significantly rises until $4x10^7$ N/m and then plateaus. The contact time rapidly drops as K_I increases until $4x10^7$ N/m and then the rate of the drop decreases.

The last controllable rod parameter is the mass of the rod m_p. m_p is part of the mass matrix of the 1st problem (rod in contact with the system) and increasing it is expected to decrease the natural frequencies of the first problem in a similar manner to increasing the mass of single degree of freedom. The response of the rod and the contact profile are a function of the natural frequencies of the first problem and since the natural frequency is expected to decrease, the contact time is expected to increase upon on increasing the mass. This is clearly evident in Figure 5-4 where the contact time increases upon increasing m_p while holding everything else in the system constant. Increasing the contact time decreases the excitation range of an impactor [41], however the contact time is not the only variable influenced by changing m_p, the momentum of the rod also changes. The impulse (I) can be used to quantify the change in linear momentum of the rod upon changing m_p, the impulse can be calculated from the force profile $f(t)$ (Figure 5-5) of the rod for a given

m_p from the 1D FE model using EQ 5-4. Even though the contact time decreases and in turn the frequency range decreases upon increasing m_p, the impulse increases with m_p (Table 5-4). Therefore, there are two competing behaviors that occur upon changing m_p. For the 1st mode, increasing m_p (and the impulse) has a greater effect than potential losses due to the narrower excitation range of the rod. This is because the 1st mode is relatively very low (≈680 Hz) at this specific interface condition and any reduction in the rod's excitation range is still beyond this frequency. Therefore, for the current m_p range, it appears that the contribution of the 1st mode is continuously increasing (Figure 5-4). However, the behavior is more complex for the 2nd mode which is more sensitive to the exciting frequency range and the contact time of the input force due to its higher frequency magnitude (≈9380 Hz). As it can be observed, there are regions where the reduction in the excitation frequency range is more dominant than the increase in impulse and other regions where the increase in mass and impulse exceeds the losses from narrowing the frequency range (Figure 5-4). Varying K_I had a more predictable behavior than m_p for both modes of vibration, although the force profile also varies upon changing K_I (Figure 5-5) the impulse is almost preserved for a very wide range of K_I (Table 5-5). Therefore, more predictable patterns are observed upon changing K_I since the contact time is the main factor affecting the modal contributions and impulse plays no role in changing the presence of the modes. Similarly to changing V_I, there are practical considerations (safety and electromagnet specifications) that affect selecting a suitable rod mass. However, it appears that controlling the rod mass and velocity have a more important role for amplifying the presence of the 1st mode in the signal than the contact stiffness for the LOW interface condition.

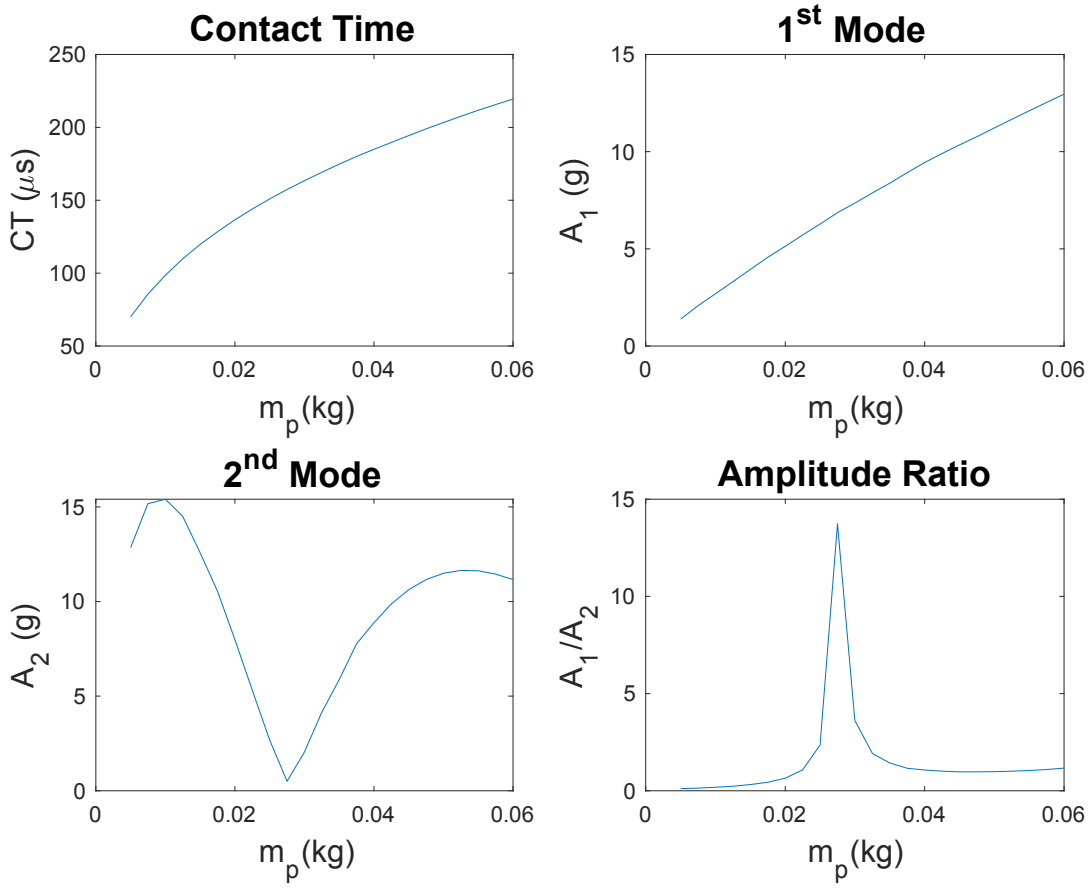

Figure 5-4. Increasing m_p increases the contact time of the rod's response. However, the contribution of each mode is the result of two competing behaviors that result from increasing m_p. Increasing m_p increases contact time and decreases the rod's ability to excite a wide frequency range but also increases the impulse to the system. The 1st mode appears to be increasing due to its lack of sensitivity to contact time and high sensitivity to impulse changes while the 2nd mode's behavior is complex since there are regions where the contact time reduction dominates and regions where the increase in impulse dominates.

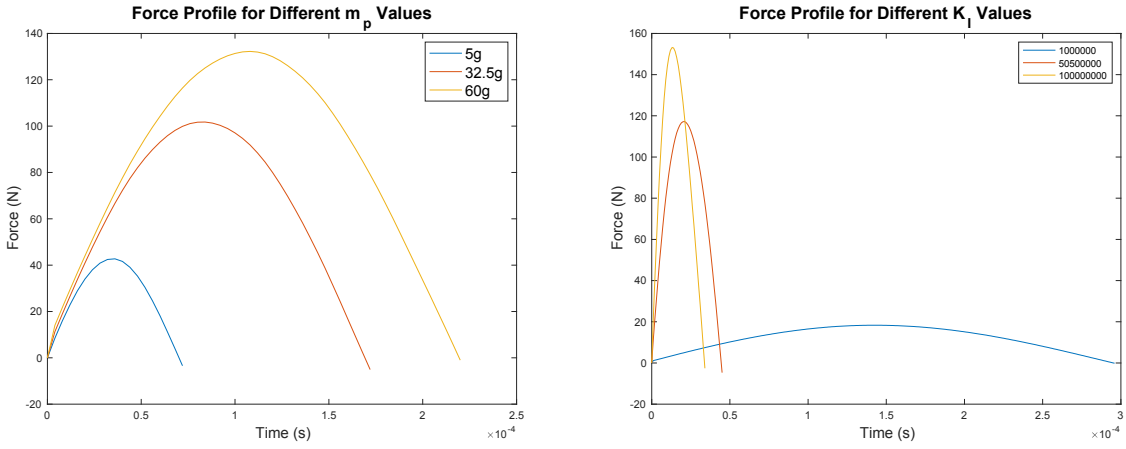

Figure 5-5 The force profile of the impact rod for three extreme m_p (Left) and K_I (Right) values.

$$I = \int_0^t F(t)\, dt \qquad \text{EQ (5-4)}$$

Table 5-4 Increasing m_p increases the impulse of the impact rod.

m_P (g)	I (Ns)
5	0.0019
32.5	0.0111
60	0.0186

Table 5-5 Changing K_I has almost no effect on the impulse.

K_I (N/m)	I (Ns)
1×10^6	0.00350
5.05×10^7	0.00340
1×10^8	0.00320

5.3 Modelling the Impactor Using Bar Elements

The impactor has been modelled as a particle in the 1D FE model and as a uniform cylinder with reduced length in the 3D FE simulations. However, the newer impactors that are currently under considerations have a wider range of masses [61] and it is important to test the particle assumption before incorporating it in the 1D FE model. Therefore, a 3D FE simulation is conducted for the LOW interface condition by modelling the impact rod as particle and the actual geometries of the impact rod (Figure 5-6). The 3D FE simulations are conducted for an impactor with a mass of 9.4 g and 30 g which represent the Periotest® and one of the new impact rods respectively.

Figure 5-6 Particle (Left), Periotest® (Middle) and the 30g rod (Right) geometries used in the 3D FE simulation. The particle's density is adjusted to end up with 9.4g and 30g. The sketches are not to scale.

The particle assumption appears to minimally affect the 1st mode of response for the 9.4 g and 30 g impactors (Table 5-6 and Figure 5-7), however there are more observable differences in the presence of the 2nd mode. A higher difference of 13.6% (EQ 5-5) is reported for the 2nd mode for the 30 g impactor compared to the 9.4 g impactor which had a difference of 5.94%. Thus, it appears that modelling the impact rod maybe more physically representative for the larger impactors.

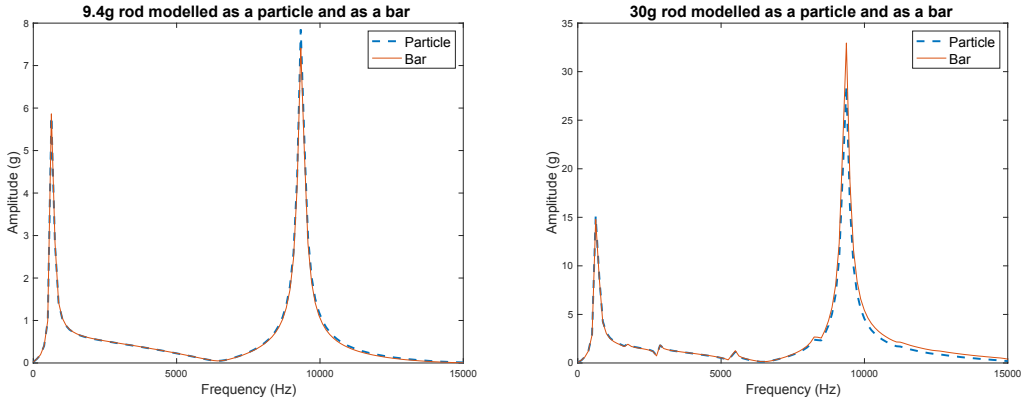

Figure 5-7 The particle assumption appears to be a reasonable approximation for the 9.4 g impactor (Left) however there are larger discrepancies in the amplitude of the signal (particularly for the 2nd mode) for an impactor with a 30 g (Right) mass between a particle and a bar model.

$$Difference = \frac{Bar - Particle}{Bar} \quad \text{(EQ 5-5)}$$

Table 5-6 Comparison of the changes on the 1st and 2nd modes contribution to the signal upon changing the impactor's modeling assumption from a particle to a bar.

	1st Mode Amplitude (g)			2nd Mode Amplitude (g)		
Mass (g)	Particle	Bar	Difference (%)	Particle	Bar	Difference (%)
9.4	5.80	5.86	1.02	7.85	7.41	-5.94
30	15.1	14.8	-2.03	28.5	33.0	13.6

5.4 Evaluating the Interface Properties of the LOW Interface Condition

The investigations done so far in this section aim at better understanding the behavior of the system at the LOW interface condition and implement the necessary changes in the 1D FE model. The first change was incorporating Rayleigh damping model in the 1D FE model and creating a second version of the application where the impactor is modelled using bar elements. The signal of the LOW interface condition using a 30 g rod was experimentally evaluated by Beaudry [61] and inserted to the 1D FE model for analysis after implementing the aforementioned changes.

Both the 1D FE particle and bar models were able to extract the interface properties for the LOW interface condition (Figure 5-8). The two models predicted close k and f_1 values and an identical f_2 and ζ_2 value (Table 5-7). Although there is a 6.50% difference in the estimated k values between both models, both models were able to predict a much lower (orders of magnitude lower) interface stiffness compared to the experimental INTERMEDIATE and HIGH interface conditions (Table 4-3). It appears that the two models are able to perform similarly in terms of extracting the features (f_1 and ζ_2) of the dominant peak (2nd) and that there are more differences in estimating the features (f_1 and ζ_1) of the 1st mode which resulted in those differences in k, f_1 and ζ_1. The peak of the 1st mode frequency does not appear to be well defined as there is an abrupt drop around this peak. Therefore, it is believed that the current estimate of ζ_1 is an underestimate using the particle and the bar model. It seems , however, that incorporating Rayleigh's model has a practical significance since in both cases the 1D FE model predicted that ζ_1 is higher than ζ_2 which is a behavior that could not be predicted using the stiffness proportional model.

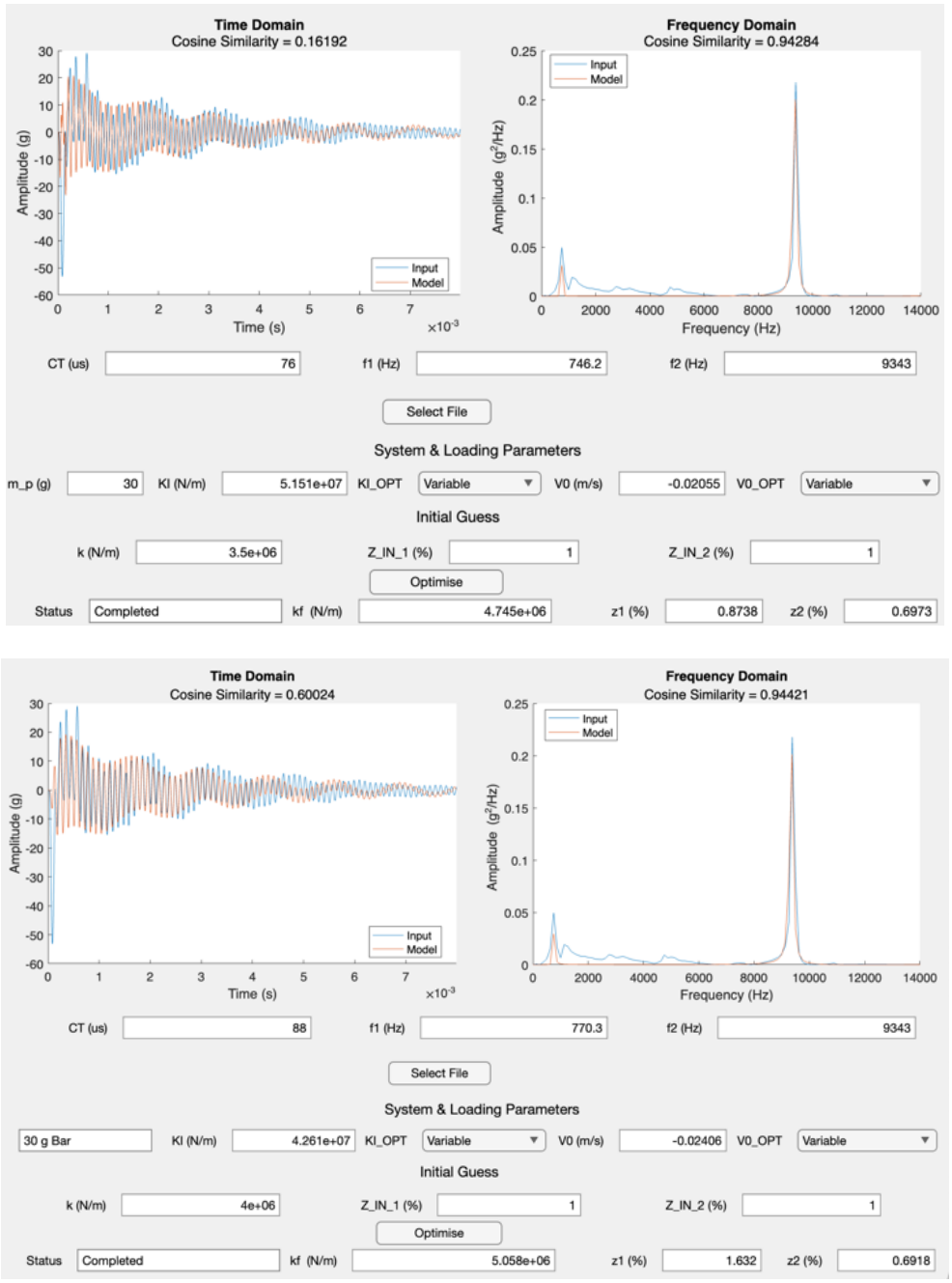

Figure 5-8 The 1D FE analysis of the experimental LOW signal using the version of the application that uses a particle model (Top) and a bar (Bottom) model.

In addition to the minor differences in estimating the k and f_1 and the more prominent difference in estimating ζ_1, the time domain similarity scores (sim_t) is higher for the bar model. Both models have lower time similarity scores compared to the experimental INTERMEDIATE and HIGH conditions (Figure 5-9). The time domain scores are generally much lower compared to the frequency domain similarity measure; this can be a result of the high sensitivity of the Cosine

similarity (cosine similarity of any two equal length vectors A and B can be defined using EQ 5-6) to the frequency of the signal. Even a difference of 5% to a simple sinusoid can result in significant drops to the time domain similarity score (Figure 5-10). The k appears to be highly sensitive to the location of the peaks in the frequency domain and therefore the frequency domain appears to be a more appropriate metric for evaluating the quality of the curve fit especially that the objective function is defined in terms of the power spectral density (which is in the frequency domain) of the response of the input signal and the model's prediction (EQ 4-12).

Table 5-7 The interface properties and system parameters extracted from the 1D FE particle and bar models.

Model	k (N/m)	K_I (N/m)	f_1 (%)	f_2 (Hz)	ζ_1 (%)	ζ_2 (%)	Sim_t (%)	Sim_f (%)
Particle	4.75×10^6	5.15×10^6	746	9343	0.874	0.697	16.2	94.3
Bar	5.06×10^6	4.26×10^6	770	9343	1.63	0.692	60	94.4

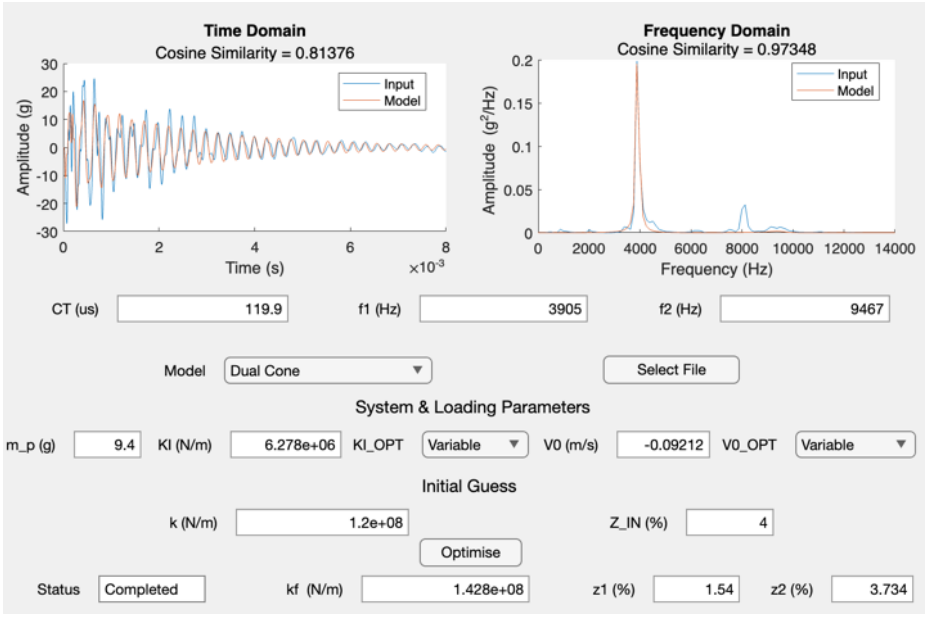

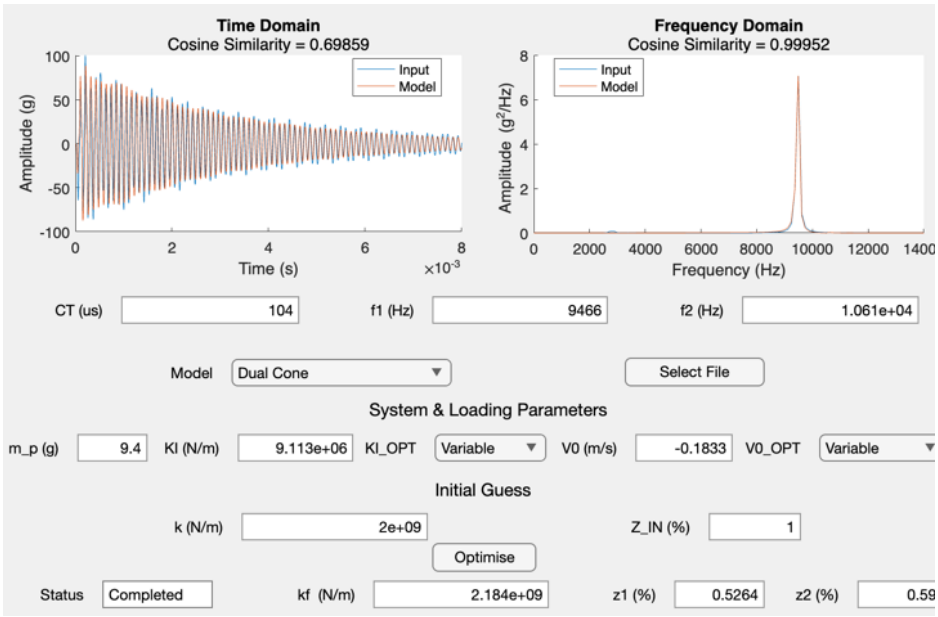

Figure 5-9 Analysis of the experimental INTERMEDIATE (Top) and HIGH (Bottom) conditions using the application. In both cases the time and frequency domain similarity scores are higher than the LOW similarity scores.

$$Cosine\ Similarity = \frac{A.B}{||A||||B||} \qquad \text{EQ (5-6)}$$

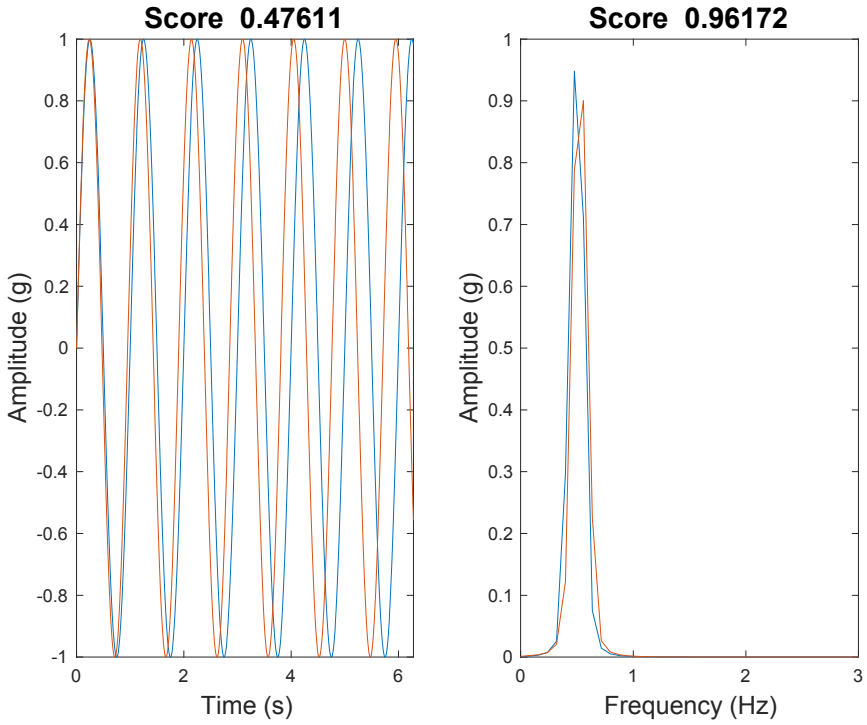

Figure 5-10 A minor difference of 5% in the frequency of a signal grows over time and leads to poor time domain similarity.

5.5 Summary and Concluding Remarks on the Dynamic Behavior of TFA Systems

Chapters 3, 4 and 5 were devoted to analyzing the dynamic behavior of the Osseointegrated OPL TFA bone implant system using mathematical and physical models. In chapter 3, preliminary 3D FE modal analysis and benchtop experimentation were used to survey the parameters that govern the system's response. It was concluded that focusing the development of the stability measurement system on the axial behavior has more potential (in terms of the measurement's sensitivity and specificity) than the bending behavior of the system. The weak presence of the 1st axial mode for the LOW interface condition posed the greatest challenge to relying on the axial behavior. To better understand the axial behavior of the system, an additional intermediate condition was imposed in Chapter 4 since the 3D FE simulations predicted a transition in the dominant behavior from the 2nd mode to the 1st mode once the LOW condition (with an elastic modulus of sub-megapascal range) is exceeded. Experimental measurements confirmed this

behavior by observing a dominant 1st axial mode ($f_u = 3910$ Hz) that is well separated from the 2nd axial mode ($f_\mu = 9310$ Hz) of the LOW condition and the 1st axial mode of the HIGH interface condition ($f_u = 9530$ Hz). Therefore, a 1D axial FE model was developed in Chapter 4 and was tested by evaluating the properties of signals generated from 3D FE simulations and experimental signals. The model was able to extract the interface stiffness and the damping properties for all the signals generated from the 3D FE model and the experimental INTERMEDIATE and HIGH conditions. Chapter 5 was primarily dedicated to incorporating Rayleigh damping model, better understanding the influence of the impacting parameters on the response and testing the impactor modelling assumption (particle/bar). The changes implemented in chapter 5 allowed for the evaluation of the interface stiffness for the experimental LOW signal obtained from the newer impact rods of Beaudry [61]. Thus, the 1D FE model is currently able to assess the interface stiffness of the three-interface condition (LOW, INTERMEDIATE and HIGH). The limitations and recommendations for future work are later discussed in the conclusion section. However, they can be summarized into: 1) conducting sensitivity analysis on the 1D FE model's output upon varying the system's parameters in the optimization over a wider range of stiffness and damping properties, 2) studying the effect of changing the assumption of the interface condition (such as its distribution/thickness and surrounding bone properties) and 3) lastly expanding the 1D FE model to incorporate different implant-adapter and GV connector configurations and conducting reliability analysis on the 1D FE predictions using 3D FE, benchtop experimental signals and clinical signals.

Chapter 6 Cross Validating the ASIST BAHA Analytical Model with Signals Generated from a 3D FE Model

In this chapter, the analytical model for analyzing the stability of the BAHA implants is cross validated with a 3D FE explicit model developed on ABAQUS®. Westover et al. developed the analytical model and tested it experimentally [14], [15]. Westover et al. also used the model to analyze clinical data [16]. However, testing the analytical model's ability in characterizing the interface condition of 3D FE signals provides an opportunity to better understand its limitations and capabilities since the 3D FE signals are more controlled than their in-vitro and in-vivo counterparts. This chapter was published in the Journal of Biomechanics (link to article) on the 19th of July 2021. It should be noted that this chapter was slightly modified from the original publication for inclusion in the thesis.

6.1 Abstract

The Advanced System for Implant Stability Testing (ASIST) was developed to evaluate the stability of osseointegrated implants. ASIST matches the physical response with an analytical model's prediction to determine the stiffness of the bone implant interface (BII) which is then used to calculate the ASIST stability coefficient (ASC). In this investigation, a 3D dynamic finite element (FE) model of the ASIST experimental impact technique for bone anchored hearing aids was created. The objectives were to evaluate the analytical model's ability to capture the behavior of the implant system and to assess its effectiveness in minimising the effects of the system's geometry on the ASC scores. The models were developed on ABAQUS®, they consisted of the implant, abutment, screw, base support and impact rod. The models relied on frictional contact definitions between the system's components. The simplified "three-part" model had the implant, abutment and screw merged as one part while the "five-part" model treated them as separate components. Different interface conditions were simulated (friction coefficient range: 0 – 0.9) for three abutment lengths (6, 9 and 12 mm). The simulation output was the average nodal acceleration response of the rod, which was imported to the custom ASIST program in Mathematica® to obtain the ASC scores. The overall quality of the curve fits indicate that the analytical model is capable of representing the system's behavior. Moreover, ASC scores provide a reliable assessment of implant stability as they are sensitive to interface conditions and are minimally influenced by the system's geometry.

6.2 Introduction

6.2.1 Background and Motivation

The use of bone anchored implants has been increasing in different applications such as dental implants, craniofacial prosthetics, finger joint replacement, and lower limb amputations [1]. The mechanical stability (denoted as osseointegration) of these systems is dependent on the formation of a layer between the implant and the surrounding biological tissues during the bone regeneration phase [4]. This layer is referred to as the bone implant interface (BII) and its mechanical and biomechanical properties govern the success of the implantation process [4]. Knowledge of the condition of the BII can help in predicting potential implant failure and in prescribing loads during the rehab process [4], [5], [10].

6.2.2 Development and Testing of the ASIST

Westover et al. introduced the Advanced System for Implant Stability Testing (ASIST) to assess the stability of the BII for bone anchored hearing aids [14]. ASIST uses an impact rod to excite the implant system using a free vibration test [14], [54]. The acceleration response is then recorded and imported to a custom Mathematica® code (Wolfram Mathematica, USA) that matches the response with the prediction of the analytical model [14]. The stiffness of the BII is an unknown parameter in the analytical model and is found numerically by the curve fitting process.

The model (Figure 6-1) consists of three inertial elements: a particle representing the impact rod, and two rigid bodies representing the abutment and implant. The model is a four degree of freedom (DOF) system; the impact rod can translate horizontally (x_1), the abutment tip can translate horizontally (x_2) and rotate about the vertical (θ_1) and the implant can rotate about the vertical (θ_2). There are three stiffness parameters in the model. K_I represents the spring element between the impact rod and the abutment. K_T is a torsional spring which is physically analogous to the locking screw connecting the abutment and the implant, the tightness level of the screw is controlled by a non-dimensional factor α. k is the distributed stiffness representing the BII. Viscous damping (not shown in the figure) is included at the BII and negligible elsewhere [14].

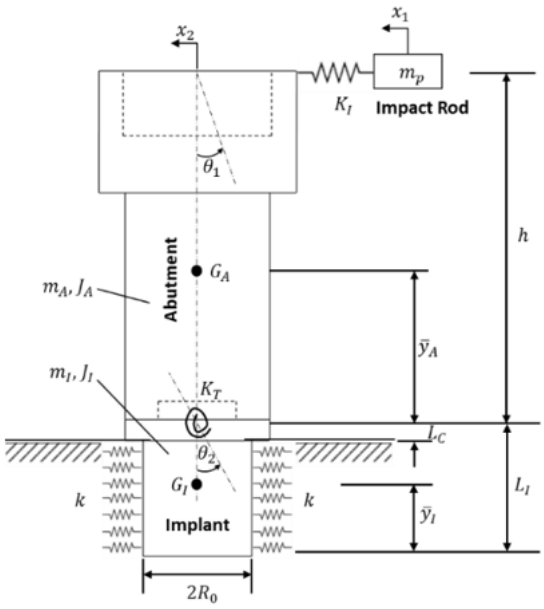

Figure 6-1 Analytical model of the BAHA system (Adapted from [14]).

Testing the ASIST experimentally using in-vitro models showed that the system was able to fit the analytical model's prediction to the recorded responses with high R^2 values (with reported averages of 0.97-0.98) [14]. It also revealed that the system is able to report close ASC scores for a given interface condition for different implant/abutment geometries [14]. This finding was supported further by comparing the ASC scores to the output of the Osstell™ ISQ system (Osstell AB, Sweden) which bases its scores on the system's natural frequency [11], [15]. It was reported that the ASIST was more reliable as it was more sensitive to interface changes and less influenced by the system's geometry compared to the Osstell™ ISQ [15].

6.2.3 Techniques of Implant Stability Assessment and Previous FE Models

Assessment of implant stability can be performed using X-ray based and reverse torque methods. Nevertheless, these methods have limited clinical applications due to their invasiveness, diffraction caused by metallic objects and, in most cases, lack of quantitative objective metrics [4], [5]. Alternatively, methods relying on vibration analysis, mechanical impedance and ultrasound were developed for non-invasive and quantitative assessment of implant stability [5], [10].

FE models have been extensively used in the development and validation of different methods for craniofacial implant stability testing [63]–[68]. This section, however, is dedicated to FE models that used vibration methods and studied the influence of the geometry on their results.

The effect of the geometry on the natural frequency has been reported by Pattijn et al. who used FE modal analysis to evaluate the frequencies for different implant geometries and implantation conditions [13]. It was concluded that systems that rely on the natural frequency, such as the Osstell^{TM}, are "not suited to compare implant stability in an absolute sense" because of the geometric effects [13]. Zhai et al. attempted to reduce effects of the geometry by replacing the Bending Resonant Frequency (BRF) with the Torsional Resonant Frequency (TRF) as the stability metric [69]. Using the TRF improved the assessment, as it increased the sensitivity towards interface changes and decreased the effects of other parameters (namely the effective implant length and the bone type) [69]. This improvement is still solely governed by the natural frequency of the system, another implant system with a different geometry or testing conditions might change the results. This point was raised by Zanetti et al. who investigated six different dental implant designs using FE modal analysis [12]. The interface conditions were varied along with the implant geometry and the mandibular bone length. The resonant frequencies (including the torsional mode) were extracted, and it was concluded that the frequencies can vary because of the boundary conditions and implant geometry [12].

6.2.4 Objectives and Scope of this Investigation

The objectives of this investigation are: (1) numerically evaluate the analytical model representation of the bone conduction hearing aid implant-abutment system by analysing the quality of the curve fit between the analytical acceleration response and the FE acceleration response, (2) evaluate the performance of the ASC as an implant stability metric capable of isolating the BII from the system geometry for three abutment lengths across a wide range of interface conditions, and (3) study the effect of changing the contact definitions of the systems components in the FE model.

6.3 Methods

6.3.1 System Idealization using the Three-Part FE Model

The FE model is based on the in-vitro model (Figure 6-2) of Westover et al. for the 4 mm long Oticon Ponto wide diameter implant with three abutment lengths (6, 9, and 12 mm) (Oticon Medical, Sweden) [14]. The abutment and the implant are assembled using a locking screw. The surrounding bone is represented by the base which is a circular disk (mimicking the in-vitro experiments). Components' geometries were measured using a digital Vernier caliper and then

reproduced as 3D CAD models on Solidworks® (Dassault Systèmes, USA). The threaded portion of the implant was modeled as a uniform cylinder with the same diameter as the hole in the supporting base. The implant threads were not individually modeled, the implant-base connection was simulated through frictional contact. Finally, the impact rod is represented as a uniform cylinder. The implant, abutment, and screw were merged into a single component. This model will thus be referred to as the "three-part" model (Figure 6-2). The effect of merging the parts will be further assessed by introducing the "five-part" model in Section 6.3.4.

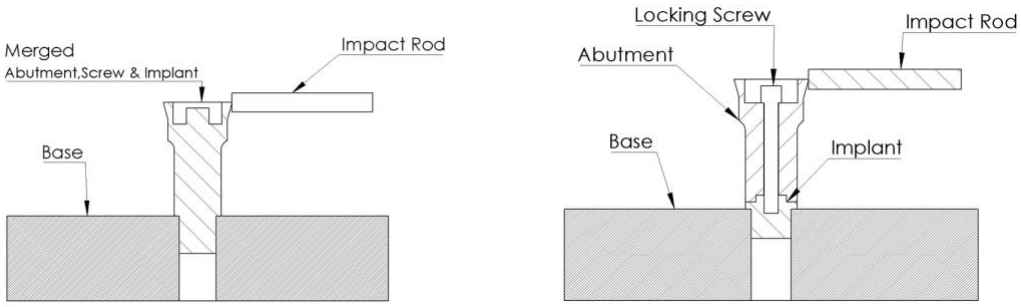

Figure 6-2 Idealization of the in-vitro experimental model used by Westover er al. as a three-part model (Left) and the five part model(Right).

6.3.2 Simulation Setup

The implant-abutment system, base, and impact rod geometric models were imported into ABAQUS® (Dassault Systèmes, France) for simulation. The linear, elastic, and isotropic material definition for the system components is shown in Table 6-1. The densities of the parts were defined to account for their inertial effects. The density of the base was 1.8 g/cm^3. For the rest of the components the density had to be altered from nominal ranges to ensure that the components end up with the actual mass measured with a mass balance (Table 6-1) [49]. The mass of the impact rod was 9.4 g and since it was idealised to a smaller cylinder to reduce computational time, the density had to be adjusted to a larger value. The densities of the remaining components were adjusted slightly to account for possible geometrical errors during measurement.

Table 6-1 Elastic Constants and mass properties of the system's components.

Elastic Constants for the System Components			
	Material	**Young's Modulus (GPa)**	**Poisson's Ratio**
Base	FRB 20	5.70	0.300
Impact Rod	Stainless Steel	200	0.265
Abutment-Implant-Screw	Titanium	105	0.310
Mass and Density of the System Components			
	Mass (g)	**Nominal Density (g/cm^3)**	**Simulation Density (g/cm^3)**
Stainless Steel	9.4	7.48-8	200
6 mm Implant Abutment System	0.782	4.5	4.06
9 mm Implant Abutment System	0.942	4.5	3.93
12 mm Implant Abutment System	1.192	4.5	3.997

General contact was used to define normal and frictional behavior between the implant and the base and between the abutment tip and the impact rod. The friction coefficients, F, were 0.7 (a variable that will control the interface condition in section 6.3.3) and 0.2 respectively [70]. The explicit scheme was chosen as the time stepping method. The stable time increment was based on the more conservative "element by element estimation" criterion. The choice for the contact formulation and the time integration scheme are based on the software's documentation recommendations for short contact problems [71]. The contact time was known beforehand to be approximately 0.003-0.007 ms [14]. The boundary and initial conditions (Figure 6-3) were set to mimic the experiment. The base was fully fixed from its sides. The impact rod was constrained to translate horizontally and had an initial velocity of 200 mm/s.

Second order tetrahedral elements were used to generate the meshes for the system's components (Figure 6-3). A mesh independence study was carried out for the three abutment models, the total number of elements ranged from 20000 to 90000. The study was carried out for an interface with $F = 0.7$ since initial simulations showed it to be a relatively stiff configuration. A stiffer configuration, with larger acceleration amplitudes and shorter contact time, would generally require higher spatial and temporal resolution than less stiff configurations. The convergence criterion is the ASC score which is based on the average nodal acceleration of the impact rod.

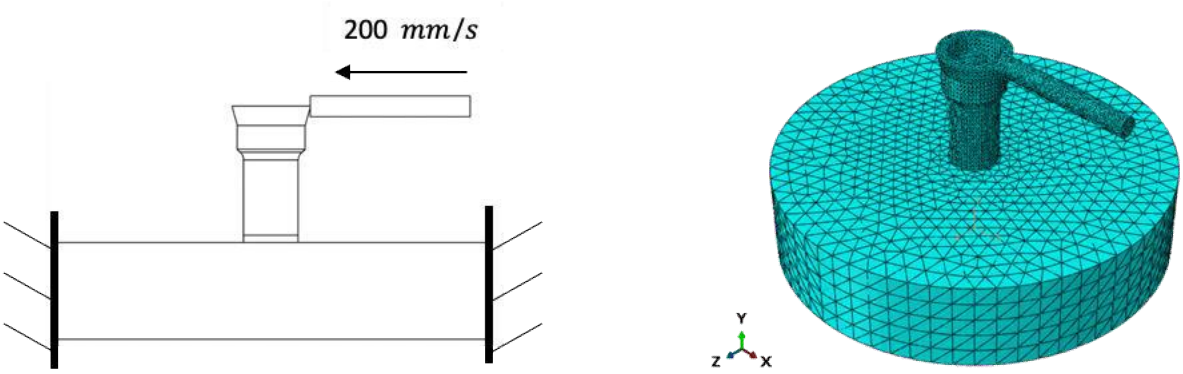

Figure 6-3 Boundary and initial conditions (Left) and the mesh (Right) used in the FE simulation.

6.3.3 Simulating Different Interface Conditions and Extracting the ASC Scores

The main parameter used in controlling the interface stiffness is the friction coefficient (F) defined between the base and the implant. Simulations for the three abutment models were carried out over an F range from 0 to 0.9. Afterwards, the average nodal acceleration response of the rod was obtained from ABAQUS®, converted to Volts and then imported to the ASIST utility on Mathematica®.

The utility requires specifying the number of unknowns in the system which can be any combination of k, K_I and α. The interface stiffness k is an unknown while K_I and α were previously determined by Westover et al. experimentally to be 2.90×10^6 N/m and 0.26 respectively [14]. In this investigation α was set to 1 since the screw was merged to the abutment and the implant (rigid connection) and K_I was set to 2.35×10^6 N/m based on an average from the different simulations. The interface stiffness is calculated through an optimization routine by minimizing the difference between the acceleration response of the impact rod and the analytical model [11]. The ASC value is then calculated directly from the effective interface stiffness over

the implant length and normalized to a non-dimensional value. Furthermore, the utility reports the R^2 value to evaluate the quality of the fit.

6.3.4 Five-part model

The system was also modelled as a five-part model where the implant, abutment, and locking screw were treated as separate components. The 12 mm abutment was used for this model. The model would require the definition of additional contact surfaces (Figure 6-4). Contact regions 1 (impact region) and 2 (interface region) in Figure 6-4 are common with the three-part model. Region 3 is defined between the screw and the abutment, region 4 is the surface connecting the abutment and the screw and region 5 defines the surface between the implant and the screw. The five-part model was used to perform four simulations that involved different conditions (loose $F = 0.2$, intermediate $F = 0.7$ and fully tied).

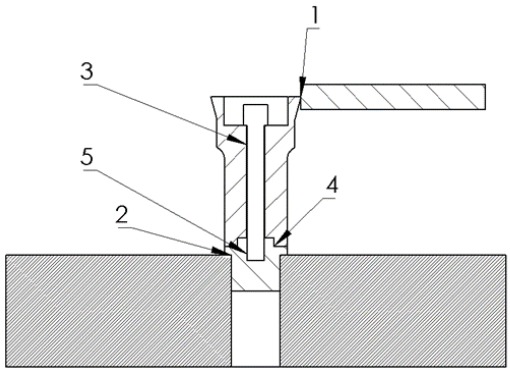

Simulation	Friction Condition for each Region				
	1	2	3	4	5
1	0.2	Tied			
2	0.2	Tied	0.2	0.2	0.2
3	0.2	0.7	Tied		
4	0.2	0.7	0.2	0.2	0.2

Figure 6-4 Contact regions for the five-part model

6.4 Results

6.4.1 Mesh Independence

The total number of elements is plotted against the ASC scores (Figure 6-5) for the three abutment geometries. The 6 and 12 mm models achieved convergence when the total number of elements exceeded 60000 while the 9 mm model converged after exceeding 70000 elements. The results presented in the next sections are based on the minimum number of elements required to achieve convergence for each abutment model.

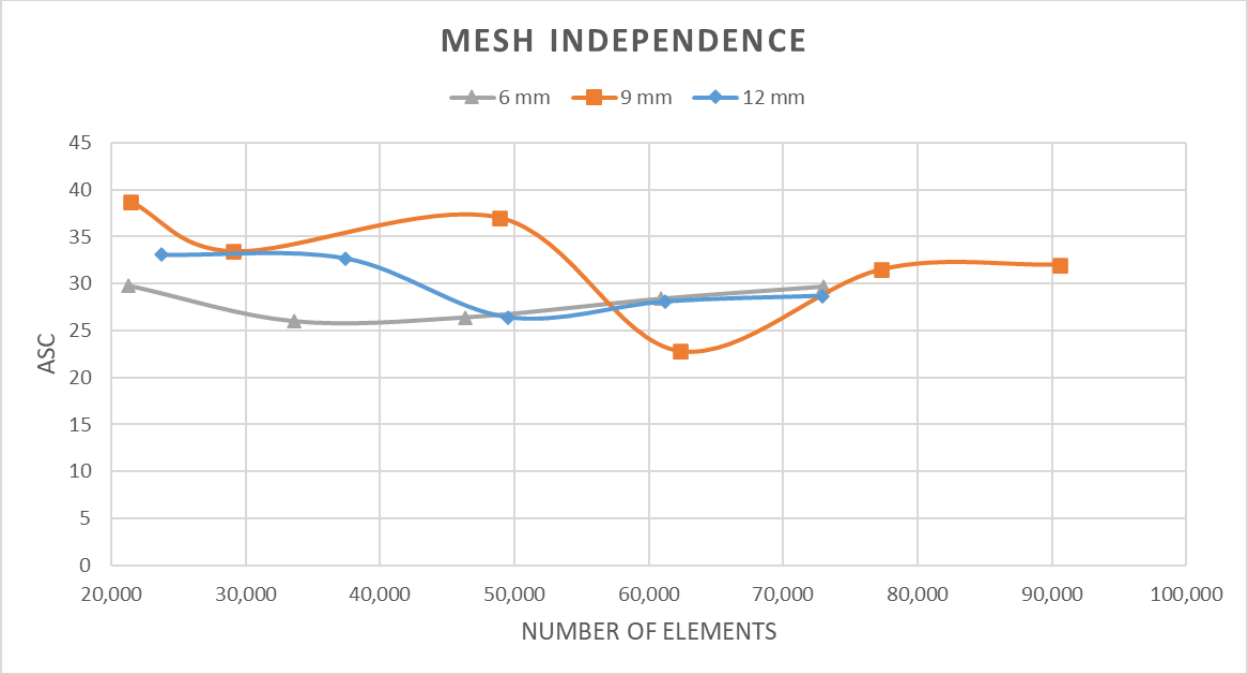

Figure 6-5 Mesh independence for the three abutment models.

6.4.2 Curve fitting the FE model's Response using the Analytical Model

Figure 6-6 shows representative examples of the FE simulation output (grey curves) with the analytical model response (black curves). The R^2 values were high (ranging from 0.983 to 0.995) for the models that had $F = 0.7$ while they were lower (0.850 to 0.931) when F was 0.1. The lowest R^2 values, of 0.850-0.900, were recorded for the lower F simulations (ranging from 0 to 0.2). Setting K_I as an additional unknown in the optimization routine, along with k, improved the quality of the curve fit to range from 0.920 to 0.961 for $F = 0.1$ (Figure 6). Since the ASC scores were minimally affected by this change it was justified to set K_I as an unknown for the lower F models (0 to 0.2). Therefore, the overall quality of the curve fits ranged from 0.870 to 0.995 with an average of 0.967.

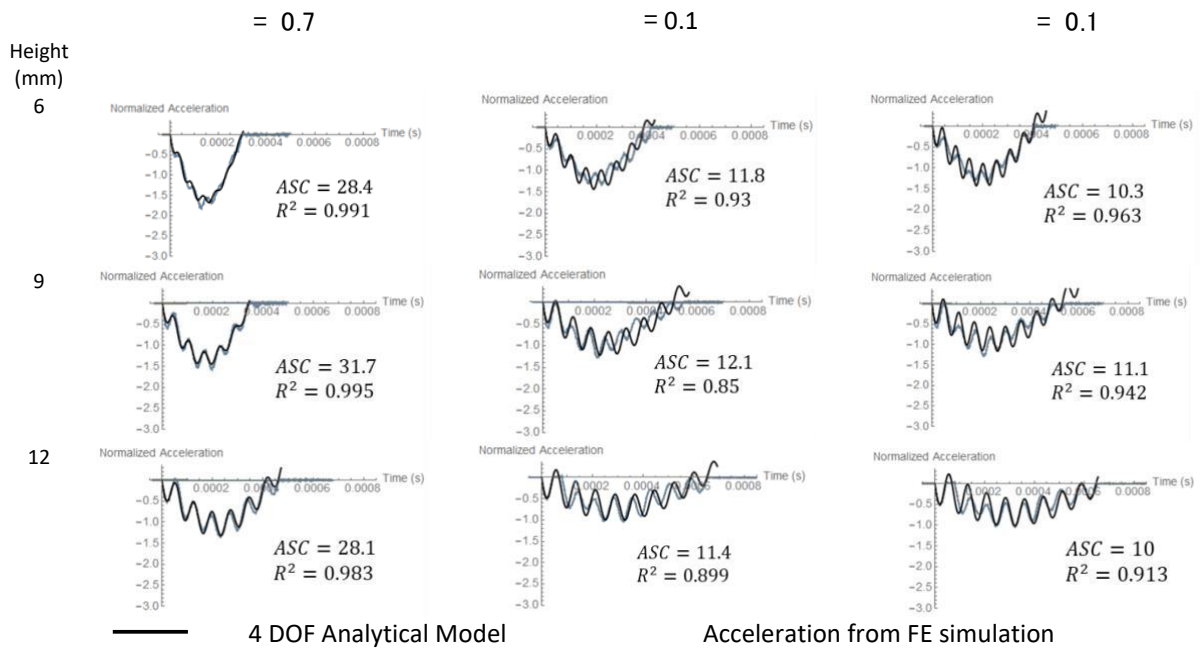

Figure 6-6 Quality of Curve fits (Grey curves: Acceleration response from FE Simulation Black curve: 4 DOF analytical model prediction): an example of a good fit when F = 0.7 (Left), an example of a poor fit when F = 0.1 (Middle), improving the poor fit by setting KI as an unknown (Right)

6.4.3 ASC Scores for Different Interface Conditions

The ASC scores for different friction coefficients are shown in Figure 6-7, demonstrating an overall direct relationship between the ASC value and F. Additionally, for a given interface condition there is minimal difference between the ASC scores for the three abutment models (Figure 6-7). If the 9 mm model is used as the baseline for the ASC scores, the average absolute difference would be 6.56% and 10.9% for the 6 and 12 mm models respectively.

The relationship between the interface friction coefficient and the first and second mode frequencies are plotted in Figure 6-8. The first mode frequency is more sensitive to the interface condition and is therefore a more appropriate stability metric. However, it is clear that the natural frequencies are affected by the abutment length with the longer systems having lower natural frequencies (Figure 6-8). If the average absolute difference is to be calculated for the first mode frequencies, the difference would be 27% and 23% for the 6 and 12 mm models respectively.

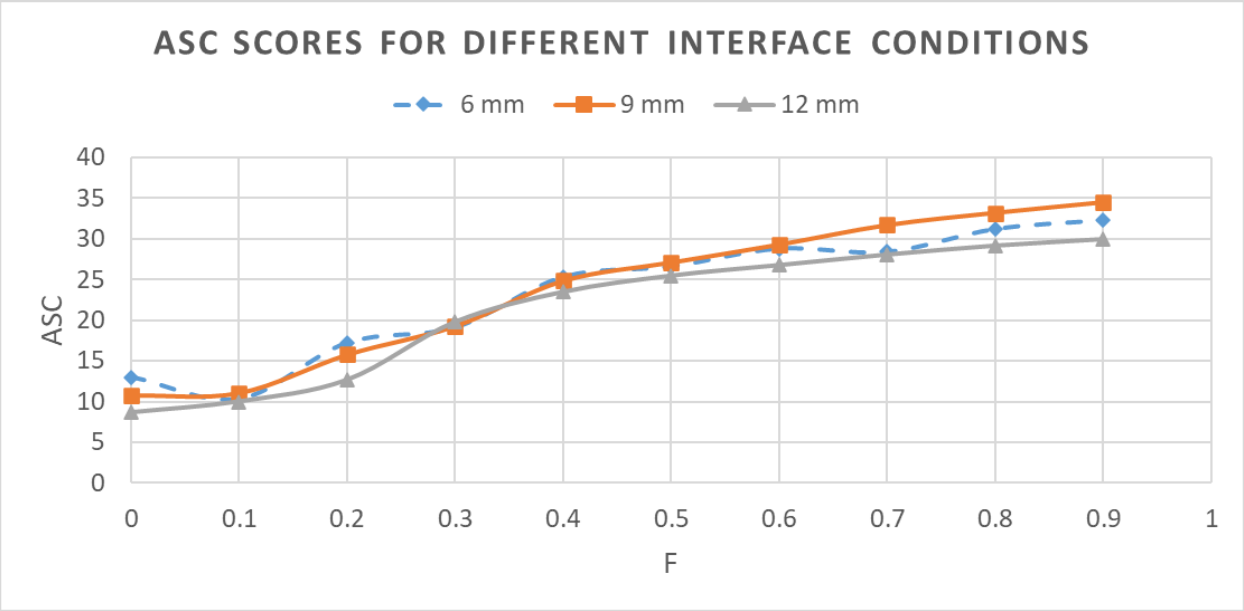

Figure 6-7 ASC values for various interface conditions for the three models.

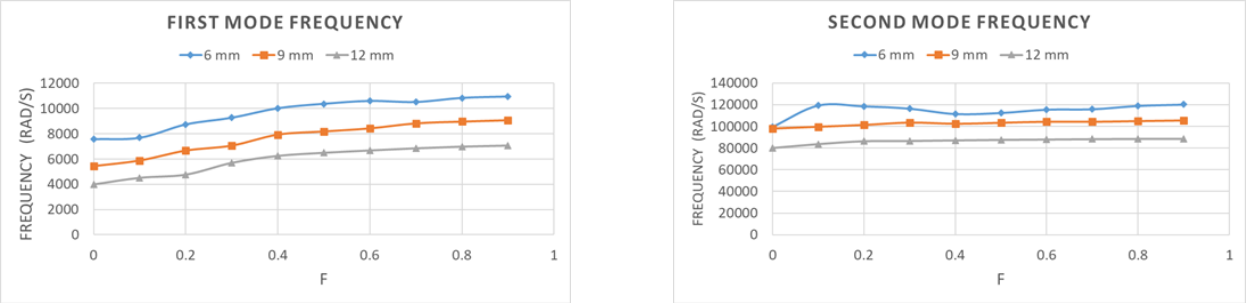

Figure 6-8 First (Left) and Second mode (Right) frequencies for different interface conditions.

6.4.4 Effect of Changing the Contact Definition using the Five Part Model

Figure 6-9 shows the differences in the acceleration response of the impact rod between the three-part model and the four simulations of the five-part model (Figure 6-4). Simulation 1 involved tying the implant, abutment, screw together and tying the implant to the base which increased the stiffness of the model significantly compared to the three-part model (Figure 6-9A). In Simulation 2, the implant and the base were tied (an indication of good osseointegration) while the rest of the components were allowed to relatively slide (an indication of a loose screw). Since the friction coefficient of the locking screw was relatively low (0.2) the fundamental frequency is significantly lower than the three-part model (Figure 6-9B). Simulation 3 allows for relative motion between the base and the implant ($F = 0.7$) and inhibits motion elsewhere by tying the abutment, screw

and implant surfaces. This is essentially the three-part model; thus, the responses are similar (Figure 6-9C). Simulation 4 allows for relative sliding on every connected surface. This has the effect of substantially decreasing fundamental frequency of the response (Figure 6-9D).

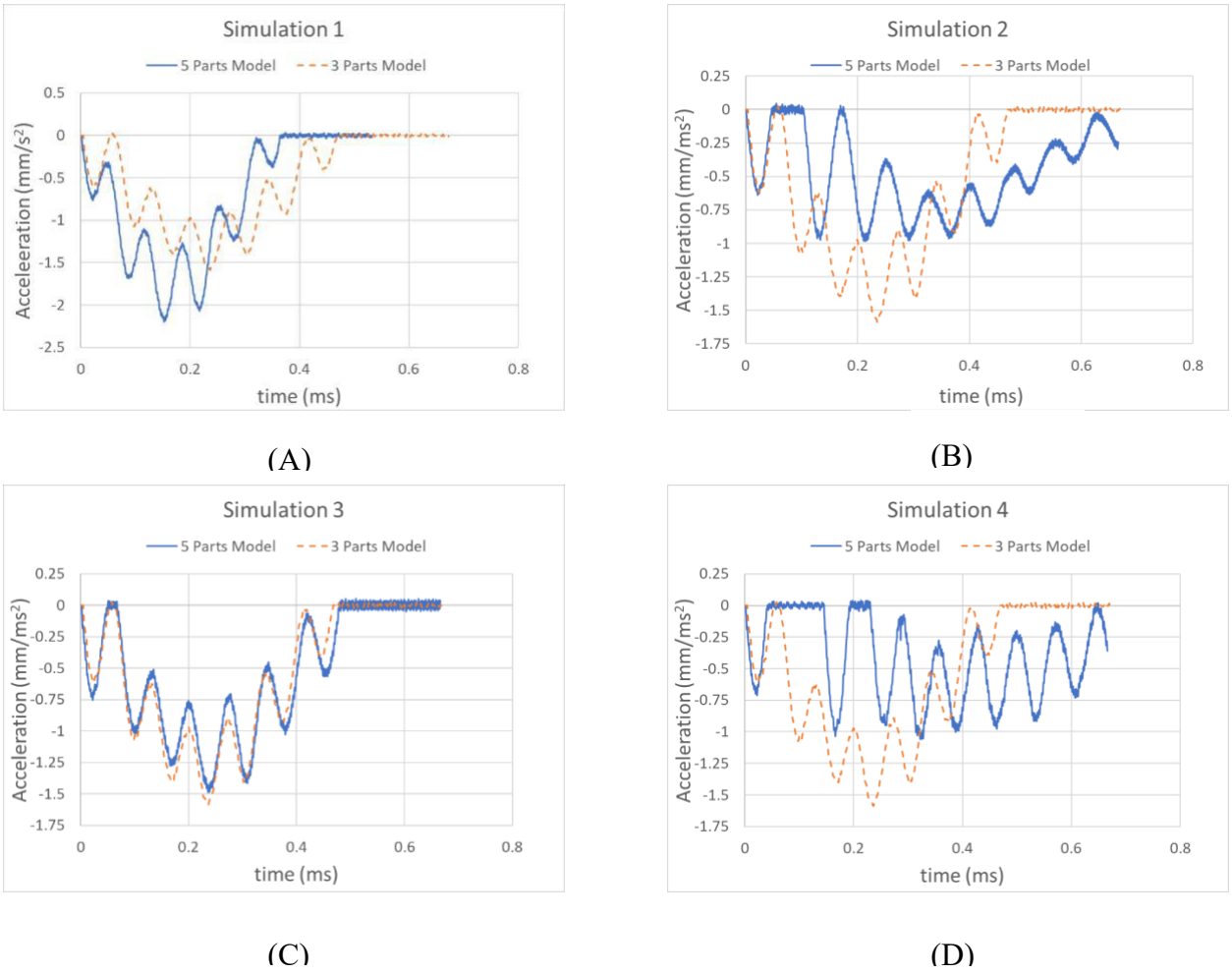

Figure 6-9 Comparison between Simulations 1,2,3 and 4 with the three parts model.

6.5 Discussion

6.5.1 Quality of the Curve Fits

The average R^2 value of 0.967 across different interface conditions and abutment lengths is close to the average R^2 range of 0.970-0.980 previously reported by [14]. For most of the simulations ($F = 0.3$ to 0.9) setting k as the system's only unknown was sufficient to get a good curve fit, with the few exceptions of lower friction simulations ($F = 0$ to 0.1) where both k and K_I were set as unknown values. K_I is the stiffness parameter governing the deformation of the impact rod and the

abutment tip. Physically, though, the stiffness is not a lumped parameter, it is distributed over the abutment and impact rod lengths. The value of K_I in the analytical model can thus be viewed as an estimate of this stiffness and using a constant value for the implant-abutment system provides a good representation for most of the FE simulations. In the lower interface stiffness conditions (i.e., $F = 0$ to 0.2), the stiffness of the abutment and impact rod may have a larger effect on the system response, in particular on the second mode frequency. Therefore, it is physically justifiable to set K_I as unknown parameter in the analytical model for those simulations to improve the curve fit. Furthermore, setting K_I as an unknown parameter primarily affected the second mode frequency of the response, which influenced the quality of the curve fit but had a minimal effect on the reported ASC scores.

6.5.2 ASC as a Metric for Implant Stability Assessment

There is a direct correlation between a higher friction coefficient and the ASC scores (Figure 6-7) indicating that the ASC is sensitive to interface changes which is important for clinical applicability. A higher F is an indication of less relative motion between the implant and the bone and hence a more stable configuration. The sensitivity and range of ASC scores (7-35) is in agreement with the experimental and clinical results of [15], [16]. Therefore, it can be deduced that ASC is a suitable stability metric.

Furthermore, for a given F the ASC scores between the different abutment models were close, indicating that the ASC can isolate the interface properties from the rest of the system. The difference between the ASC scores with different abutments reported by Westover et al. was 8% which is close to the values found here. Figure 6-8 showed that the first mode frequency is more sensitive to interface changes than the second mode frequency. The correlation between the interface condition and the natural frequencies of the system is firmly established in the literature [5], [10]. However, the main limitation of this approach is the influence of the geometry on the natural frequencies [12]–[15]. The systematic difference between the natural frequencies of the three abutment models is evident in Figure 6-8. This is analogous to cantilever beams which have an inverse relationship between their length and their stiffness. Moreover, the percent differences between the frequency values of different abutment lengths are more than double the corresponding difference reported by the ASC. Finally, the ASC scores had wider changes with respect to interface changes than the fundamental frequency. For the 9 mm model the change in

ASC range (10 to 35) was around 220% while the change in fundamental frequency (5423-9086 Hz) was around 67%. This indicates that the ASC is a more reliable stability metric than the natural frequencies of the system, as it is more sensitive to interface changes, and is independent of abutment length (eliminates the systematic difference).

6.5.3 Effect of changing the contact Definitions and Potential Applications of the Five-part model

Fully tying the system (i.e., Simulation 1) does not allow for any relative motion between the implant and the base (bone) and increases the stiffness of the model. This could have an implication on FE models that rely on modal analysis since in modal analysis nonlinear effects (such as contact) are ignored and the interacting surfaces have to be tied. Zhuang et al. reported higher natural frequencies from their numerical results in comparison with their experiments and mentioned that lack of contact definition is a possible reason for the overestimated values [72]. Therefore, using frictional contact definitions might be more physically representative.

Simulation 2 represents a situation where the implant is well osseointegrated into the bone, yet the locking screw is loose. The contact time significantly increases which indicates that the loose screw is dominating the response. In the analytical model K_T can be adjusted for different screw tightness levels by changing the factor α [14]. Accordingly, a potential application of the model used in simulation 2 is to solve for K_T for known interface stiffness conditions and for different screw tightness levels. This relationship will be useful in extending the applicability of the analytical model to account for different tightness levels and still being able to measure the interface condition.

Simulation 3 should ideally be identical to the three parts model; however, there are minor differences in the amplitude due to the minor geometrical differences between the two models which hindered the exact replication of the meshing process. Simulation 4 is a case where both the implant is unstable, and the locking screw is loose. This model, along with simulation 2, can be used in investigating whether the ASIST can be adjusted to detect both behaviors simultaneously.

6.5.4 Implications and Recommendations for Future Work

Although the analytical model was previously tested experimentally [14], the FE analysis allowed for simulating a wider range of interface conditions. The previous clinical study cannot be labelled

as a validation technique as well, since the interface condition is unknown [16]. Therefore, the FE model served as a validation technique of the simplified analytical model (convenient clinically due to its efficiency) with a more realistic representation under ideal testing conditions. The FE analysis showed that the analytical model is representative of the system and that the ASC scores are sensitive and directly related to the interface condition without being influenced by the abutment length. This is consistent with the previous work and strengthens the confidence in using the ASIST for clinical applications. The model also has future potential applications such as improving the current understanding of the physical interpretation of some of the analytical parameters.

Future work using the current FE model could incorporate more realistic implant and bone geometries. The BII can be modelled as a separate layer which can be used to simulate more interface conditions and osseointegration stages such as non-homogenous distributions and effective implantation length.

Chapter 7 Analyzing the Dynamic Behavior of BAHA using 3D FE Models

In chapter 6, the analytical model of the ASIST of BAHA implants was used to determine the interface condition of various signals generated from a 3D FE simulation of BAHA implants. In this chapter, the 3D FE model is first validated with experimental and clinical signals and then used to better understand the dynamic behavior of BAHA implants. The chapter was published in Medical & Biological and Engineering & Computing (link to article) on the 20th of July 2022. It should be noted that this chapter was slightly modified from the original publication for inclusion in the thesis.

7.1 Abstract

The dynamic behavior of osseointegrated implants can be used for the non-invasive evaluation of the bone-implant-interface (BII) condition. The Advanced System for Implant Stability Testing (ASIST) is a vibration measurement system that relies on an impact technique and an analytical model to compute the interface stiffness and the ASIST stability coefficient (ASC). The objective of this work is to develop a finite element (FE) model capable of capturing the dynamic behavior of the bone anchored hearing aid under the ASIST loading condition. The model was validated with previously collected in-vitro and in-vivo data which were compared to the model's acceleration responses and ASC scores. Similar acceleration responses were obtained and the maximum absolute difference in ASC scores between the FE model and the in-vitro and in-vivo data were 1.15% and 5.48% respectively. The model was then used to show the existence of a relationship between the rod's acceleration response and the BII stress field. Finally, the model was used to interpret the factors that affect the stiffness parameters of the ASIST analytical model. The interface stiffness and the system's dynamic properties were more influenced ($p < 0.05$) by the BII material and friction coefficient compared to the implant geometry.

7.2 Introduction

The term osseointegration describes the anchorage of implants to the surrounding bone tissues [1]. The success of an osseointegrated implant (OI) is governed by its stability which can be classified into primary stability, achieved during surgery, and secondary stability which is associated with the quality of the bone-implant interface (BII) [4], [5], [73].

A stable implant experiences limited degree of micromotion at the BII which is dependent on the BII stiffness [4], [5], [73]. Imaging techniques (such as MRI, CT, or X-ray) provide insight on the bone-implant morphology [4], [5], [73]. However, they have a number of limitations including: (1) exposure risks, (2) metal artefacts noise, (3) lack of quantitative metrics, and (4) limited sensitivity [4], [5], [73]. Alternatively, reverse torque and vibrations analysis are two common stability measurement methods. In reverse torque, the OI is tested against a prescribed load. However, there are associated risks of damaging the bone/BII [5]. In vibration methods the dynamic properties (namely the natural frequencies) of the OI are determined [4], [5], [73]. The main limitation of relying on the natural frequency is its dependency on several factors besides the BII, such as the system's geometry, and therefore cannot be used as an absolute stability metric [12]–[15], [57].

The Advanced System for Implant Stability Testing (ASIST) is a vibration measurement system that overcomes the aforementioned limitation of frequency based methods by solving for the interface stiffness (k) directly [14]. This is achieved by mathematically representing the bone-implant and impact rod system as a set of rigid bodies connected to each other using linear springs, the governing equation of this system can be analytically obtained using the Newton's second law of motion [14]. k, which controls the magnitude of the linear springs that connect the bone and the implant, is the primary unknown in the mathematical model and is estimated by: (1) exciting the bone-implant system using the impact rod on the abutment and recording the rod's acceleration response, (2) the collected response is uploaded to the ASIST program (developed on Mathematica®, Wolfram alpha, USA) and is iteratively matched with the mathematical model's predication of the rod's acceleration using an optimization algorithm until a good fit (measured by the coefficient of determination or R^2) is achieved and (3) finally the k is normalised to obtain the dimensionless ASIST stability coefficient denoted as the ASC [14].

Finite element (FE) analysis has contributed to various OI applications such as optimising implant designs and improving their performance and investigating failure scenarios [65]–[67]. FE analysis can also be coupled with advanced imaging techniques (such as high resolution micro CT scans) as a proposed technique to assess implant stability [74]. Furthermore, FE analysis has been extensively used to test new stability assessment concepts (such as ultrasound) and to evaluate the performance of existing ones [12], [13], [66], [67], [69], [75].

In our previous investigation, an FE model was developed to test the reliability of the ASIST for bone anchored hearing aid implants using a simplified system geometry [57]. The ASC score was evaluated for three implant/abutment configurations over a wide range of interface conditions. It was demonstrated that the ASIST was able to quantify the interface condition with higher sensitivity and was less influenced by the system's geometry compared to solely relying on the natural frequencies [57].

In the present study, an improved FE model that better represents the physical system geometry of the bone anchored hearing aid implant system will be developed. The objectives involve: (1) validating the developed model with previously collected experimental and clinical results of Westover et al. [14], [16] and then using the model to: (2) study the relationship between the impact rod acceleration and the mechanical response of the system during and after the impact event and (3) formulate a better understanding of the analytical model's stiffness parameters.

Having a validated dynamic FE model of the system has several benefits. First, it can be used to study the ASIST's excitation mechanism as it offers the full field response. Additionally, FE analysis is capable of offering a better representation of the system's parameters. The interface stiffness, for example, is modelled analytically with linear spring elements, however in the FE model it can be modelled using the material, surface, and geometric properties of the BII.

7.3 Methods

7.3.1 Development of the Finite Element Model

The high fidelity FE model developed in this study closely resembles the five part model previously developed by Mohamed et al. for the Oticon Ponto bone anchored hearing aid implant system [46]. The modeled system is composed of the: (1) implant, (2) locking screw, (3) abutment, (4) base (representing the bone) and (5) impact rod. In the present model, however, the CAD geometry of the implant, abutment, and screw (implant-abutment system) were obtained from the manufacturer (Oticon Medical, Sweden) and hence are more accurately represented compared to the simplified parts of the previous investigation which improves the model's representation of its geometric and mass parameters (such as mass moment of inertia) and affects the dynamic response. Two implant models (Oticon Ponto 4 mm/wide and 4 mm/narrow with implant diameters of 4.5 and 3.75 mm respectively) along with the 9 mm abutment were used to construct two implant-

abutment configurations. The three parts were imported to Geomagic Design X (3D Systems, USA) and were modified to a simpler geometry for ease of meshing. The modifications involve: removing the threads (modelled using frictional contact), straightening the implant's taper, and smoothening any sharp and abrupt changes in the geometry. Those modifications were meant to reduce the complexity of the meshing process and improve the simulation time without making major changes to the dynamic response of the system. The three parts were imported to Solidworks (Dassault Systèmes, France) for assembly. The CAD models of the impact rod and the base were modelled as a uniform a cylindrical rod (with a reduced length of 1.5 cm and diameter of 2 mm) and a uniform circular disk (with a diameter of 40.7 mm and thickness of 9.05 mm which is similar to the in-vitro experiments) respectively.

Three models were developed in ABAQUS® explicit (Dassault Systèmes, France): (1) Oticon 4 mm/wide installed in a photo elastic (fiber reinforced plastic) FRB material base, (2) Oticon 4 mm/wide installed in a polylactic acid (PLA) material base and (3) Oticon 4 mm/narrow installed in an FRB base (which models the temporal bone) [14]. The first two models emulate the in-vitro investigations carried out by Westover et al. [14] while the third represents the in-vivo clinical tests [16]. The material properties of the system components are summarised in Table 7-1 [49], [57]. The linear elastic isotropic material model was used for all components. Although the human temporal bone is orthotropic, however the isotropic model can be an acceptable approximation for small deformations [76]. Investigations on the elastic modulus of the temporal bone have reported a wide range (2-18 GPa) that depends on a number of factors such as age, sex, sample storage/preparation/thickness, bone density and mineral density [77], [78]. In this investigation the same material properties used for the FRB material were used for modelling the temporal bone since FRB plastics fall within this range [54].

Table 7-1 Material properties of the different components of the model.

Components	Material	Elastic Modulus (GPa)	Poisson's Ratio	Density (g/cm^3)
Impact Rod	Stainless Steel	190	0.265	200
Implant, Abutment and Screw	Titanium	105	0.310	4.40
Base	FRB-20/Bone	5.70	0.360	1.90
Base	PLA	1.50	0.350	1.50

General contact and tied interactions were used to define the behavior between the different parts (Figure 1). Tying two connected surfaces inhibits any relative motion between them [79] and this constraint was imposed on the connected regions of the implant, abutment, and screw. The general contact algorithm was used to define the contact interaction for two regions: (1) the abutment tip and rod and (2) the implant and the base. Hard contact was used to model the normal contact behavior and the frictional penalty method was used to define the tangential behavior. The friction of the interface between the implant and the bone/base was used to model different BII conditions. As for the boundary and initial conditions, the base was fully fixed from its sides and the impact rod was assigned an initial velocity of 200 mm/s in the horizontal direction to simulate the experimental setup [58]. The solver used in this model is ABAQUS® explicit with a local time increment estimator which is based on satisfying Courant's requirement for the smallest element in the mesh [79].

Linear tetrahedral elements (C3D4) were used to generate the mesh (Figure 7-1). Special attention was paid to increasing the mesh density at the softer (slave) surfaces relative to the harder (master) surfaces for all of the contact pairs. H-refinement was performed to ensure that the solution has converged. The main output of interest is the average nodal acceleration of the impact rod in the horizonal direction and therefore it was used to study the convergence of the solution. Three meshes were used to with a total number of elements of 135,199, 221,059 and 311,674. The

solution converged using the second mesh (Appendix A[1]) and thus it was used for all of the subsequent simulations.

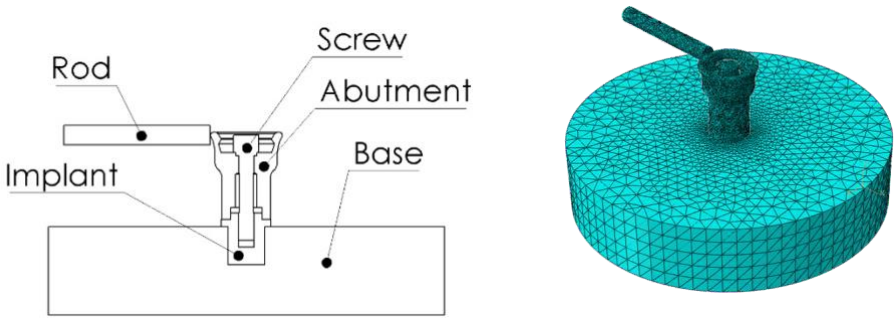

Figure 7-1 Section view of the system: Contact pairs defined between: (1) Abutment tip/Rod and (2) Implant/Base and Tied constraint applied between implant, abutment and screw (Left). The mesh used for the simulation generated using C3D4 elements (Right).

7.3.2 Objective 1: Validation of the FE model with the Experimental and Clinical Data

The previously developed experiments involved simulating different BII conditions by installing several implant/abutment configurations into uniform circular disks made from different materials (FRB and PLA) [14]. A thin layer of adhesives was applied to ensure a uniform BII [14]. The main sources of uncontrolled experimental variability were the installation torque, adhesive application, and implant installation angulation [14]. For each experimental setup the disk was fully fixed from its outer sides and then the handpiece was used to strike the abutment's tip and collect the corresponding horizontal acceleration response which was then analyzed using a custom Mathematica® (Wolfram, USA) program (ASIST Utility) to determine the ASC scores [14]. In a subsequent study, clinical data was collected for 39 patients with different implant/abutment configurations (Oticon Ponto system) over a 1-year longitudinal investigation and the ASC scores for the patients were computed on the ASIST utility [16].

Due to the previously mentioned sources of experimental noise the interface condition cannot be solely controlled with the base material's elastic modulus. An additional parameter is needed to control the connection between the implant and the base and to match the response between the

[1] This appendix refers to an appendix that was included in the original manuscript and is not part of this document.

FE model and the corresponding experimental and clinical case. The interface friction coefficient (F) between the implant and the base was used for this purpose. F was varied between 0 and 1.2 with an increment of 0.4 for each of the three models. The average acceleration of the rod was obtained for each F and then the response was imported to Mathematica® and processed using the ASIST Utility to extract the ASC score [14]. An ASC and F relationship was computed using least square regression curve fitting with a second order polynomial performed on MATLAB®'s curve fitting toolbox (MathWorks, USA). Since the experiment/clinical data have a predetermined ASC score, the regression model can be used to find the F value that should be equivalent to each clinical and experimental case. The equivalent F values were used to run additional FE simulations where the average horizontal nodal acceleration response of the impact rod was evaluated and compared to their respective experimental/clinical counterparts. This approach was used to validate the FE model for two extreme in-vitro interface conditions (Experiment 1: FRB Oticon 4 mm/wide and Experiment 2: PLA Oticon 4 mm/wide) and two randomly selected patient data (Clinical 1: FRB Oticon 4 mm/narrow and Clinical 2: FRB Oticon 4 mm/wide).

7.3.3 Objective 2: Relationship between the Impact Rod Acceleration and the Mechanical Response of the Bone Implant System

The first application of the validated FE model is to study the development of the stress field throughout the bone implant system and its connection to the impact rod acceleration. This type of analysis can be used to understand how the current impact technique excites the bone implant system and its possible limitations. In this work, the spatially averaged Von Mises stress field is extracted over the BII length and plotted as a function of time and then compared with the acceleration of the impact rod for two extreme interface conditions (F= 0 and $F = 0.8$) using the Oticon 4 mm/wide FRB model. The stress contours of five selected time points were extracted for both interface conditions to qualitatively compare between the effect of the interface condition on the stress and acceleration responses upon impact.

7.3.4 Objective 3: Formulating a Better Understanding of the Stiffness Parameters in the Analytical Model

There are three main analytical parameters of interest: (1) the interface stiffness (k), (2) the impact stiffness (K_I) and the (3) torsional stiffness (K_T) [14]. k is expected to be a function of several mechanical and geometric parameters in the bone-implant system such as the BII elastic properties

and its spatial distribution [4]. In the previous investigation by Mohamed et al., the effect of changing F on the first two natural frequencies (f_1 and f_2) and the ASC scores (which is a normalised non-dimensional score based on the k) was documented [46]. In this work, a 2^3 un-replicated ANOVA balanced design is used to study the effect of the base material, m, (PLA and FRB), interface friction coefficient, F, (0 and 1.2) and implant width, i, (Wide = 4.5 mm and Narrow = 3.75 mm) on three main response parameters f_1, f_2 and ASC. For each response parameter, the main effects and interaction effects were calculated based on the contrasts and then Pareto analysis was conducted to extract the parameters that contribute the most (with cumulative contribution $\leq 90\%$) to the response. ANOVA analysis was conducted on the significant factors and the error was estimated based on the excluded effects. The full analysis is included in Appendix B[2].

The impact stiffness (represented as K_I in the ASIST analytical model) physically governs the local deformation between the abutment and the rod upon impact, which can be viewed as the contact stiffness [14]. There are existing analytical solutions to some contact problems such as the Hertzian contact models, however more complex problems are modelled experimentally [80]. The simplest analytical Hertzian model predicts the normal elastic frictionless contact stiffness for a cylindrical surface in contact with an infinite half plane and it predicts that the contact stiffness is a function of the elastic properties of the materials in contact [80]. The Hertzian model does not exactly represent the abutment/rod interaction, nevertheless by analogy it can be used to predict that K_I is influenced by the elastic modulus and Poisson's ratio of the impact rod and the abutment. When designing a vibration measurement system, there is limited control on the material properties of the abutment. Therefore, the elastic modulus (E) of the rod in the FE model was varied from 20 to 400 GPa to study the effect of potential changes to the rod's material on the dynamic response. The torsional stiffness between the implant and the abutment (represented as K_T in the ASIST analytical model) has an analogous role to the tightening level of the locking screw [14]. In order to model this parameter, the tied constraints between the locking screw and the implant/abutment were replaced by frictional contact pairs. Frictional contact allows relative

[2] This refers to an appendix that was part of the original manuscript and was not included in this document.

motion between the parts and the degree of this motion was controlled by the friction coefficient between those surfaces (F_S). F_S was varied from 0 to 5 to study its effect on the system response. It should be noted that relatively high values of the friction coefficient were used since pretension was not introduced to the screw in the model. Simulations involving changes to E and F_s were performed using the FRB Oticon 4 mm/wide model. For each case the average nodal acceleration response of the rod in the horizontal direction was extracted and then imported to MATLAB®, where Fast Fourier transform (FFT) analysis was carried out to extract f_1 and f_2. A typical acceleration response collected by the ASIST impact rod consists of the first half cycle of the response (where the rod is in contact with the system), nevertheless the analytical model predicts that the response is periodic if there are hypothetical means of permanently attaching the rod to the system (Figure 7-2). To improve the estimation of the 1st and 2nd modes using FFT, the rod's response of the FE model is replicated and the largest two peaks in the frequency domain are taken as the 1st and 2nd mode (Figure 7-2).

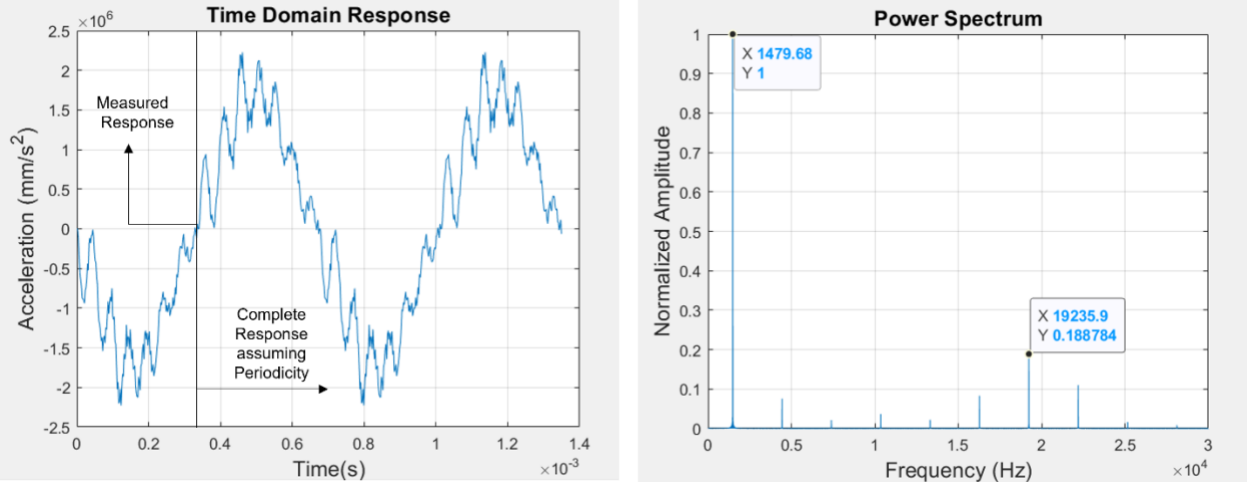

Figure 7-2 A typical time domain signal collected by the impact rod consists of the first half cycle of the response when the rod is in contact with the system (first intersection with x-axis); however, the analytical model predicts that the response is periodic if there are hypothetical means of attaching the rod to the system Left). The periodicity can be used to improve the prediction of the frequencies in the frequency domain where the 1st and 2nd modes are the largest two peaks in the power spectrum (Right). Smaller peaks can exist due to noise (local element dilations) from the mesh. 1st mode frequency is associated with the half of the contact time period (intersections with x-axis), and the 2nd mode is associated with the secondary peaks evolving between those intersections.

7.4 Results

7.4.1 Objective 1: Validating the FE model with Experimental and Clinical data

The relationships between the friction of the interface and the ASC value are shown in Figure 7-3 for the three models. The coefficient of determination (R^2) is almost unity for the three cases indicating that the 2nd order polynomial model is an appropriate choice in representing the ASC and F relationship. The trend is similar for the three models; the ASC value experiences sharp changes at the low interface condition and then reaches a plateau at the higher interface condition.

The FE models were first compared to the experimental results of Westover et al. for two extreme interface conditions with ASC scores of 35.3 and 8.5 representing Experiment 1 (FRB Oticon 4 mm/wide) and Experiment 2 (PLA Oticon 4 mm/wide) respectively. Using the appropriate ASC and F relationship (Figure 7-3), the corresponding F values were found to be 0.66 and 0.44 respectively. Those values were assigned to their respective FE models and were used to run additional simulations to extract the acceleration response of the rod. A comparison between the acceleration responses of the FE models and the experimental results are shown in Figure 7-4. The FE curves closely resemble their experimental counterparts with minor differences in the amplitude, the first mode frequency, and the damping. The first mode frequency seems to be slightly higher (shorter contact time) than the experimental results while damping is shown to be more evident in the FE models. To quantitatively compare between the FE and experimental models, the acceleration responses were further analysed on the ASIST Utility on Mathematica® where the ASC scores were evaluated (Table 7-2). The ASC score is a dimensionless metric of implant stability, and it is directly computed from the interface stiffness (k). The coefficient of determination (R^2) evaluates the goodness of fit between the hypothesized analytical model and the acceleration response generated by the FE simulation and is used to measure our confidence in the ASC value generated from the ASIST utility after the numerical matching. The ASC score of the FE model were very close to the experimental results with the largest reported absolute difference in the order of 0.1 (1.15%) which indicates that dynamic behavior of the FE model is highly consistent with the physical in-vitro models.

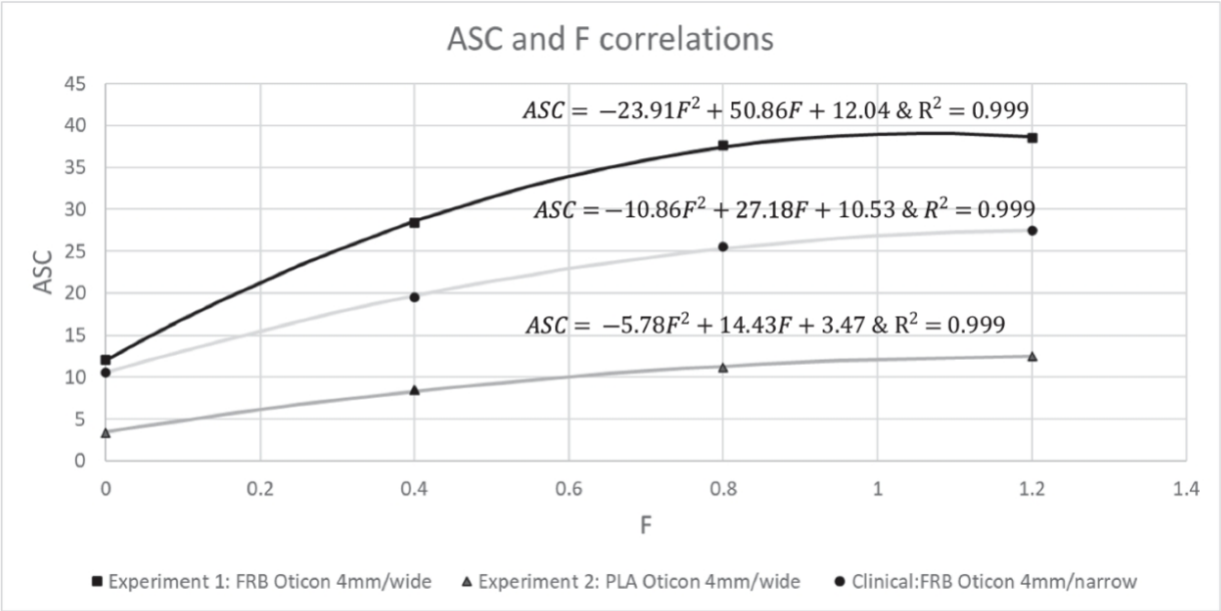

Figure 7-3 ASC and F relationship for the three FE models.

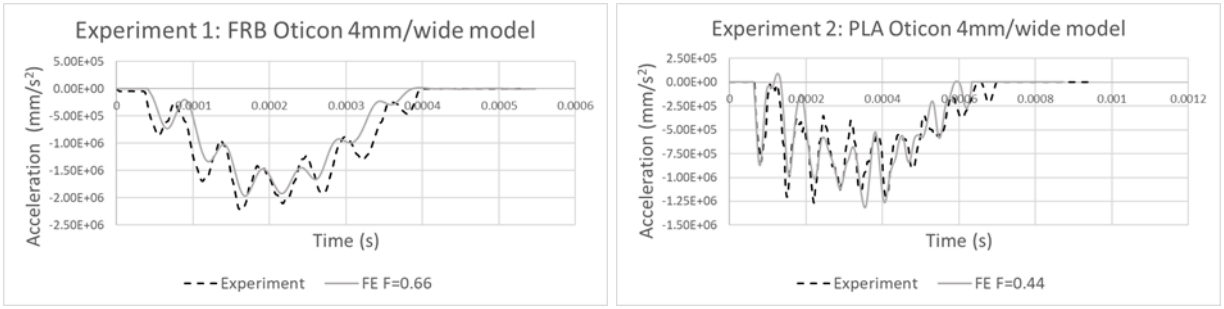

Figure 7-4 Comparison between the acceleration response of Experiment 1: FRB Oticon 4mm/wide (Left) and Experiment 2: PLA Oticon 4mm/wide (Right) with the FE models.

Similarly, the F values corresponding to two clinical cases (Clinical 1 and Clinical 2 with ASC scores of 17.2 and 22.4 respectively) were found to be 0.566 and 0.274 respectively. The resulting acceleration responses (Figure 7-5 also demonstrate similarity between the FE model and the clinical results. However, there are still minor differences in the amplitude, first mode frequency, and damping. Moreover, there are more noticeable differences in the second mode frequencies compared to the experimental/FE results. This is demonstrated by the misalignment of some of the peaks of the responses. The slightly larger differences in the response are also reflected in the ASC scores (Table 7-2) with a maximum ASC difference of 1.23 (5.48%). The difference, however, is not large enough to cause difficulty in distinguishing between the different interface conditions of both patients.

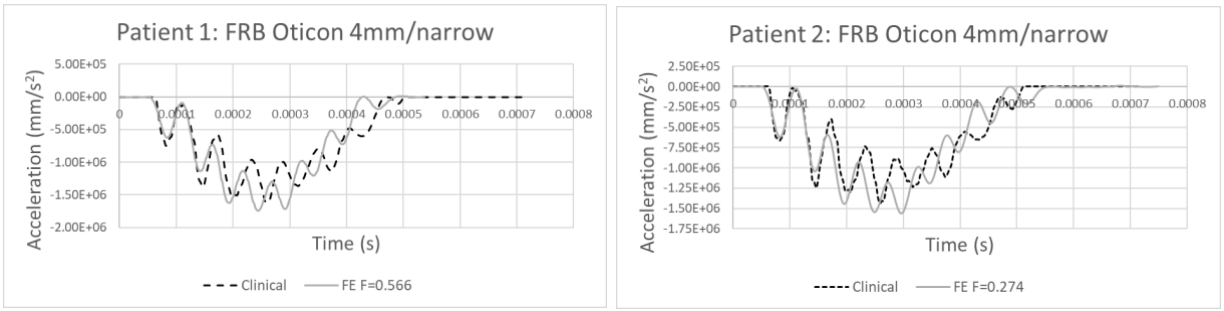

Figure 7-5 Comparison between the acceleration response of Clinical 1: FRB Oticon 4 mm/narrow (Left) and Clinical 2: FRB Oticon 4 mm/wide (Right) with the FE models.

Table 7-2 Comparison between the ASC scores of the Experimental/Clinical results and the FE simulations.

Model	Experimental/Clinical		FE		Absolute Difference in ASC Scores
	ASC	R^2	ASC	R^2	(%)
Experiment 1: FRB Oticon 4mm/wide	35.3	0.99	35.3	0.99	0.140%
Experiment 2: PLA Oticon 4mm/wide	8.70	0.95	8.60	0.95	1.15%
Clinical 1: FRB Oticon 4mm/narrow	22.4	0.98	23.7	0.94	5.48%
Clinical 2: FRB Oticon 4mm/wide	17.2	0.98	16.4	0.90	4.48%

7.4.2 Objective 2: Relationship between the Stress Development and the Impact Rod Acceleration

The response of the impact rod and the Von Mises Stress (effective stress) of the BII (spatially averaged over the integration points of the elements) are displayed in Figure 7-6. There is an apparent relationship between the stress field at the interface and the response detected by the impact rod. The contour plots of the stress field at five time points of interest are extracted to help

with explaining this relationship. At the first point, Pt 1, (immediately after impact) a stress concentration is generated at the point of impact (Figure 7-7A). Shortly afterwards (Pt 2), the stress wave starts propagating away from the impact location (Figure 7-7B) nevertheless, the stress field is still locally confined to the abutment and therefore the first peak of the acceleration and stress responses are identical for both interface conditions. At Pt 3 (Figure 7-7C), the stress wave had enough time to reach the BII and differences in the response between the two interface conditions start appearing from this point onwards. For example, at Pt 4 (Figure 7-7D), the stress field is quite different for the two interface conditions and in turn both the acceleration and stress responses are also different. At Pt 5 (Figure 7-7E), the rod of the higher interface condition is no longer in contact with the abutment, and this is reflected in the interface stress field which, unlike the less stiff case, is dying out.

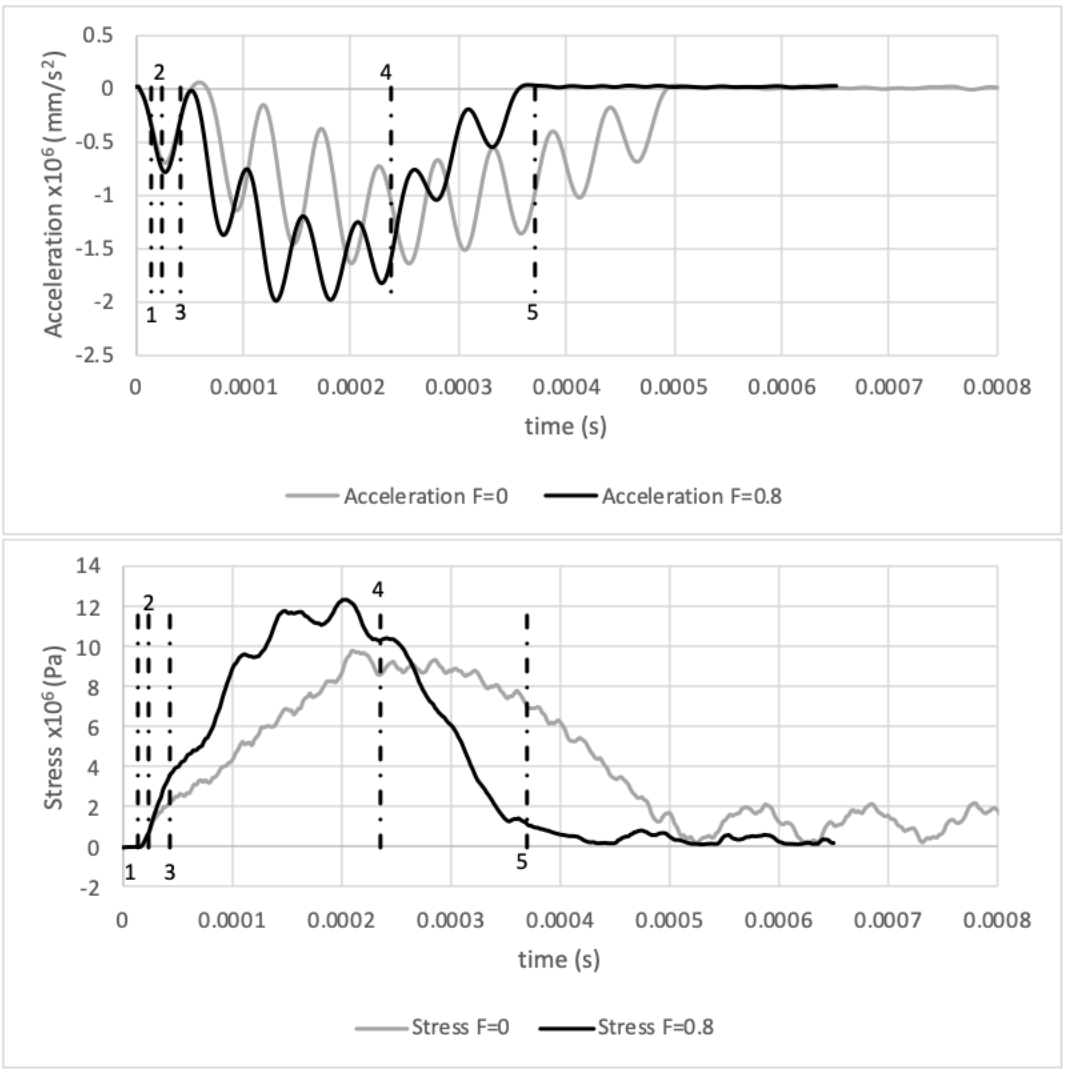

Figure 7-6 Acceleration responses of the Impact rod and the average Von Mises stress of the bone implant interface for two interface conditions: F = 0 and F = 0.8 and the five points of interest.

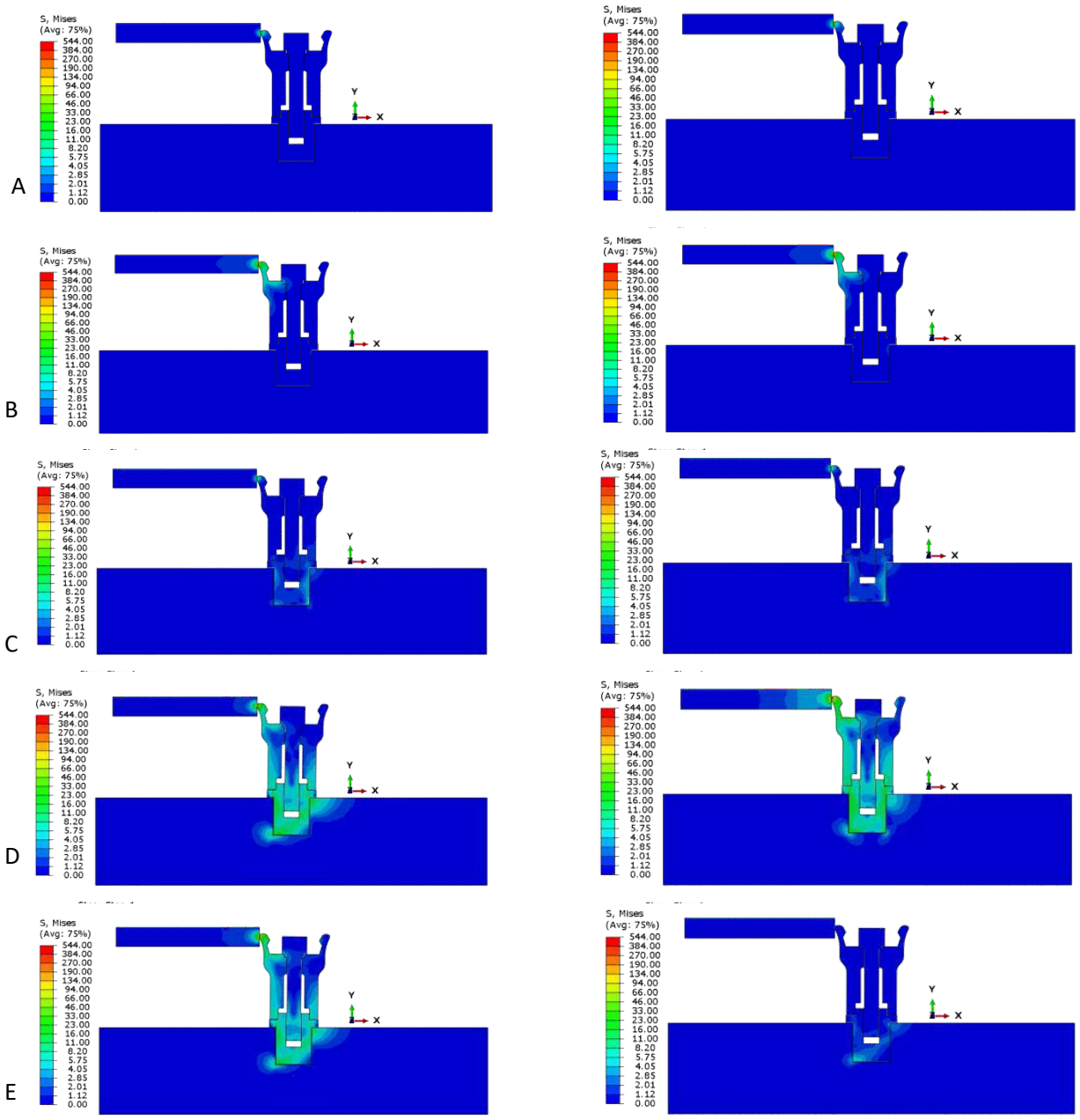

Figure 7-7 Section views of the system showing the stress fields for F = 0 (Left) and F=0.8 (Right). A: Pt 1 (t = 1.49E-5s), a stress concentration is generated at the abutment tip due to impact. B: Pt 2 (t = 2.37E-5s), the stress wave starts to propagate across the abutment however, the stress field is still locally confined to the abutment and thus the acceleration response is similar for both interface conditions. C: Pt 3 (t = 4.25E-5s), The stress wave reaches the bone implant interface and differences in the stress fields, and, in turn, acceleration responses emerge. D: Pt 4 (t = 2.36E-4s), different stress fields emerge at the interface. E: Pt 5 (t = 3.7E-4) The stress field is still prominent in F=0 and the rod, in turn, still vibrating, while the stress field is dying out for F = 0.8 since the rod is no longer in contact with the abutment.

7.4.3 Objective 3. Formulating a Better Understanding of the Model's Stiffness Parameters

Pareto Analysis (Appendix B[3]) indicated that the cumulative effect of the factors m (base material), f (friction coefficient) and their interaction mf accounts for approximately 89% of the total effect on the first mode frequency f_1 and thus ANOVA analysis was conducted using those factors as shown in Table 7-3 with a significance level set to $\alpha = 0.05$. The analysis has demonstrated that f and the m are statistically significant parameters ($p \leq 0.001$) that affect the response parameter f_1. Similar analysis approaches were used for the second mode frequency f_2 and the ASC score indicated that the material of the base (m) is the only significant parameter for f_2 ($p \leq 0.03$) while the ASC score was mainly influenced by both f and m . It should be noted that i (implant diameter) was not a statistically significant parameter for the three response variables. It should also be noted that all of the considered factors had a positive effect (with the exception of imf on f_2) on the response variables.

[3] This appendix refers to an appendix that was included in the original manuscript and is not part of this document.

Table 7-3 ANOVA analysis indicates that f and m are statistically significant ($p < 0.05$) parameters for f_1 and ASC while m is the only statistically significant parameter for f_2.

ANOVA Analysis for f_1 (Hz)								
Factor	Effect	Cumulative Effect	DOF	SS	MSE	F ratio	p-value	
f	474	42 %	1	448000	448500	164	<0.001	
m	449	82 %	1	403000	403000	148	<0.001	
mf	75.1	89 %	1	11300	11300	4.13	0.110	
Error			4	10920	2730			
Total			7					
ANOVA Analysis for f_2 (Hz)								
Factor	Effect	Cumulative Effect	DOF	SS	MSE	F ratio	p-value	
m	5580	42 %	1	3890000	3890000	29.7	0.03	
f	2990	64 %	1	1120000	1120000	8.56	0.10	
i	1873	78 %	1	439000	439000	3.35	0.21	
im	419	81 %	1	21900	21900	0.17	0.72	
imf	-564	85 %	1	39700	39700	0.30	0.64	
Error			2	262000	131000			
Total			7					
ANOVA Analysis for ASC								
Factor	Effect	Cumulative Effect	DOF	SS	MSE	F ratio	p-value	
m	15.0	31 %	1	452	452	36.8	0.001	
f	14.8	62 %	1	430	430	35.0	0.001	
mf	6.99	77 %	1	97.9	97.8	7.97	0.067	
i	3.96	85 %	1	31.3	31.3	2.55	0.21	
Error			3	36.8	12.3			
Total			7					

Figure 7-8 shows the effect of changing the elastic modulus of the impact rod (which should have an analogous role to changing the impact stiffness K_I in the analytical model) on the first and second mode frequencies of the response. Increasing the elastic modulus of the impact rod from 20 GPa to 400 GPa (an increase of 1900%) only led to an increase of 100 and 1726 Hz (an increase of 7.12% and 9.65%) of the first and second mode frequencies, respectively. The torsional stiffness of the analytical model (K_T) was indirectly controlled by F_s (friction coefficient of the surfaces in contact with the locking screw). Figure 7-9 shows an initially steep rise (130%) in the first mode frequency between the lowest and highest F_S value, while the changes in the frequency flatten afterwards. The increase in the first mode frequency between $F_S = 1$ and $F_S = 5$ was a mere 14%, which is an indication that the curve is reaching a plateau. The second mode frequency appears to be insensitive to changes to F_S, the second mode frequencies fluctuated between 18.4 and 19.2 kHz for the entire range with a maximum change of 4% and average change of 0.7%.

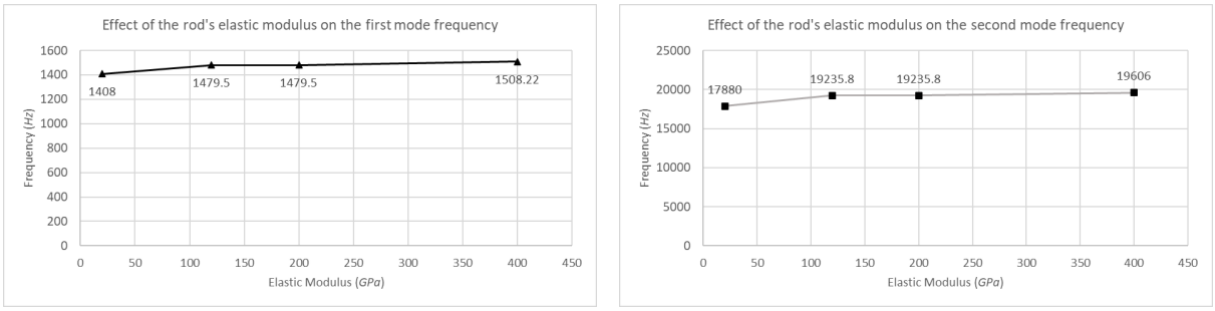

Figure 7-8 The effect of the rod's elastic modulus on the first (Left) and second (Right) mode frequencies.

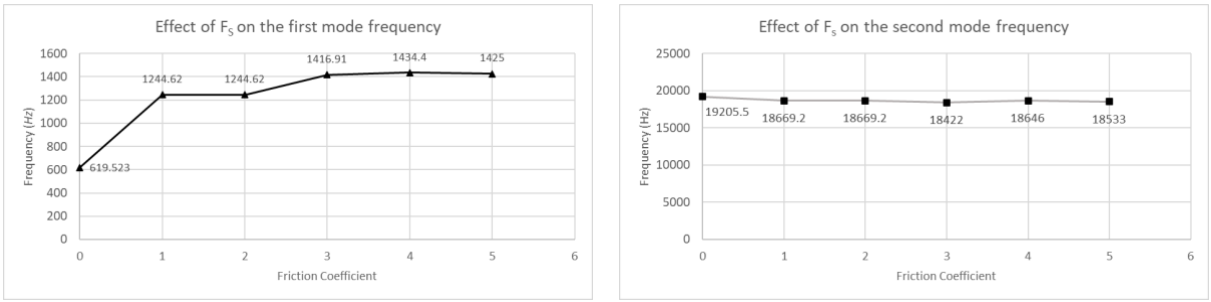

Figure 7-9 The effect of the friction coefficient between the abutment, screw and implant on the first (Left) and second (Right) mode frequencies.

7.5 Discussion

The first part of this investigation involved validating the FE model with the previously collected experimental and clinical data [14], [16]. The relationship between the ASC score and the interface

condition (F) showed initial sharp changes in the ASC scores followed by a plateau (Figure 7-3). At low F values, the implant was able to move more freely but as the F value increased the motion of the implant became more constrained until reaching a limit where no slipping occurs (no relative sliding between implant and base) and therefore the change in ASC scores decrease as F increases (assuming that the other interface parameters such as the E are held constant). The analytical model of Westover et al. predicted similar trends when the stiffness of the interface was varied for different implant/abutment configurations and the ASC was more sensitive to changes in the BII at lower stiffness values [81]. Furthermore, other in-vitro investigations using the Osstell^{TM} (ISQ) have shown the same behavior between the curing time of a resin and the ISQ value [16]. Additionally, FE modal simulations carried out by Zanetti et al. on dental implants showed similar frequency (output of interest) and osseointegration level (interface condition) trends [12]. Although the previous investigations studied different implant systems and implemented different controls for the interface condition (such as the elastic modulus of the interface), the trend can be used to understand the general dynamic behavior of osseointegrated implants as the interface condition changes, Changes in low interface conditions result in significant changes to the observed outcome of interest (such as ASC score or natural frequency) while changes in high interface conditions generate less prominent changes in the observed outcome since the implant starts to be fully embedded with the surrounding bone.

There were minor differences in the amplitude, first mode frequency (characterised by the contact time) and damping between the experimental and the FE simulations (Figure 7-4). The minor differences in amplitude can be attributed to the initial velocity. In the simulation the velocity was set 200 mm/s which is a nominal value of the Periotest®. The ASIST user does not have direct control of the rod's speed under the current ASIST interface, instead the user can slightly change the rod's speed by changing the supply voltage to the electromagnetic solenoid that drives the rod and this is sometimes done to improve the quality of the collected signal. Additionally, the experimental and clinical readings are more susceptible to noise from handling the rod by hand and this can also result in slight deviations from the nominal 200 mm/s initial condition imposed on the implant system. The amplitude of the response is governed primarily by the initial conditions according to the classical theory of vibrations [40]. As for the first mode frequency, the mesh was constructed using linear tetrahedral elements which are generally stiffer than other higher order elements [82]. However, analysing the response of the rod in the FE simulation

quantitatively using the ASIST utility shows very close values between the experiment and the FE simulation (ASC score = 8.7/8.6 and 35.3/35.3 for experiment/FE) and this indicates that the model is a good representation of the in-vitro situation (Table 7-2). Comparing the FE simulations with clinical results revealed similar differences in the first mode frequency and amplitude, however larger discrepancies were observed in the second mode frequency (Figure 7-5). As it was shown in the ANOVA analysis (Table 7-3), the second mode frequency is mainly influenced by the material of the base. The exact material properties of the patients' temporal bone are an unknown and FRB was only used as an approximation since it lies within the reported range of elastic properties for temporal bone [54], [77], [78], [83]. Therefore, it is plausible that the larger reported differences in the ASC scores between the clinical and FE simulations are due to the lack of knowledge of the exact material of the bones.

The first application of the validated FE model was to formulate a better understanding of how the rod excites the system. We found strong evidence suggesting that the acceleration response detected by the impact rod is governed by two events: (1) local deformation between the rod and the abutment upon impact and (2) the response (which was shown in terms of the Von Mises stress field) at the bone implant interface (Figure 7-6 and Figure 7-7). The former is independent of the interface condition and is thus redundant from a design perspective. Therefore, understanding this relationship and using the FE model can be used to change the rod's parameters (such as its geometrical features and material properties) to minimize the effect of the local rod-abutment impact event and maximize the effect of the interface condition with respect to the rod's total measurement. Similar analysis can be used by a designer to see if the impact technique is safe on the surrounding bone tissues by coupling this analysis with an appropriate failure criterion. The model, however, has two limitations: (1) it assumes that the BII is uniformly distributed (spatially) and (2) it models the threads using frictional contact. Even though, it can be deduced that on "average" the stress field is a good approximation (since the acceleration field is close to the experimental/clinical results), an accurate representation of the threads and the distribution of the BII is needed to get a more representative stress distribution at the interface [68]. The objective of this study was to evaluate the overall dynamic response of the system rather than finding the exact stress distribution at the BII and therefore the simplified (and computationally efficient) model was appropriate for meeting this objective. The ANOVA analysis has demonstrated that the dynamic response parameters (ASC, f_1 and f_2) are mainly affected by the material of the interface

and the interface friction coefficient while the implant diameter had no statistically significant effect (Table 7-3). The relationship between the quality of the bone surrounding the implant and the stability of the implant (measured by the natural frequency and interface stiffness) is well established in the literature and supports the findings of this study [4], [12], [13]. The significance of the implant diameter to implant stability has been controversial in the literature [84]–[86]. Clinical investigations carried on the bone anchored hearing aid with the same implant diameters of 3.75 and 4.50 mm argued that the 4.50 mm is more stable in terms of ISQ scores [84], [86]. However, these investigations only considered the diameter as the factor, a more encompassing clinical study on dental implant designs with comparable diameters (3.75-4.20 mm) indicated that the diameter is not a statistically significant compared to the implant's anatomical region and bone healing stage (which was investigated by comparing primary and secondary stability) [85]. Both implant anatomical region and healing stages can be viewed as variations in the surrounding bone properties, and this indicates that the quality of the bone is more important to implant stability compared to the implant diameter.

The ANOVA analysis also showed that the response parameters (ASC, f_1 and f_2) behave differently to m and f. f_2 (For example) was highly sensitive to the base material m ($p \leq 0.03$) and not sensitive to the friction at the interface ($p \leq 0.1$). The ASIST user is provided with the ASC score and the natural frequencies. Currently, ASIST users estimate the interface stiffness from the non-dimensional ASC score [14]. Interface stiffness is a general way of quantifying the implant's resistance to micromotion, however the interface condition is a function of several complex attributes of the BII (such as the bone's density, elastic modulus and bone implant contact ratio) [4]. This study showed that the outputs of the ASIST (ASC, f_1 and f_2) have varying sensitivities to some of these interface properties, and this can be exploited to better quantify the interface condition (such as in terms of the bone density and elastic properties) by using the FE model to establish mathematical relationships between the ASIST outputs and the explicit parameters of the FE model.

The effect of the rod's elastic properties on the response in terms of the first and second mode frequencies is similar to the trends previously reported in the analytical model findings of Westover et al. [81]. Westover et al. used the analytical model to study the effect of the contact stiffness on the 1st and 2nd mode of vibrations and they found that doubling the impact stiffness

resulted in relatively minor changes in the 1st and 2nd mode frequencies of 6 and 9% respectively [81]. In this study, the impact stiffness was controlled by the elastic modulus of the rod and significant changes in the elastic modulus gave rise to changes of approximately 7.12% and 9.65% for the 1st and 2nd modes respectively. This indicates that changing the material of the impact rod within the working range of normal metals has a minor effect on the response. K_T and F_S however, significantly affect the first mode frequency for low K_T values. This information can potentially be used clinically to identify the condition of the locking screw, if sharp and sudden and unexplained changes were noticed in the first mode frequency while no observable changes are reported in the second mode frequency. The effect of K_T also justifies the use of the tied constraint for running the other simulations in this study. The frequency components of the response are not affected by K_T, which indicates that beyond a certain threshold the three parts (implant, abutment, and locking screw) behave as a rigid body.

Future work with this FE model will aim to explore more efficient excitation mechanisms. The FE model has indicated that a good portion of the measured acceleration response is dedicated to the impact event rather than the interface condition. Therefore, the model can be used to explore the required changes to the rod's design and can be used to maximise the sensitivity of the rod's response to the interface condition. Additionally, the model can be expanded to incorporate a more realistic geometry of the threads and the BII to compute the stress distribution at the BII and evaluate the safety of the excitation method on the response. The FE model can also be used to explore further the effect of varying the interface mechanical and surface properties and its geometric properties (such as interface thickness and spatial distribution) to determine the influencing parameters on the ASIST's outputs. The simulations can be used to construct regression models that can correlate the outputs of the ASIST (dynamic properties and ASC score) to more clinically relevant parameters.

7.6 Conclusion

In this work, an FE model was developed for the bone anchored hearing aid bone implant system. The model was first validated with two extreme experimental settings and two randomly selected clinical data samples. The largest reported differences in the ASC scores (dimensionless interface stiffness measure) between the FE model and the experimental and clinical data were 1.15 % and 5.48% respectively. The validated model was then used to show that there is a relationship between

the rod's acceleration and the stress wave generated in the bone implant system. This relationship showed that the earlier phases of the response were primarily dominated by the local impact event between the rod and the abutment but as time passes the influence of the BII properties start to take over. The model was also used to show that the analytical model outputs (such as the natural frequencies and the ASC scores) are a function of several interface parameters such as the material of the interface and the friction coefficient between the implant and the supporting base. This indicates that the analytical model, despite being good clinical stability metrics, simplify the interface condition and a future application of similar FE models can be used to correlate those analytical model outputs to clinically relevant parameters such as the bone properties or distribution of the BII.

Chapter 8 1D FE Model of BAHA Systems

The 3D FE models of the BAHA system of the previous two chapters showed the models' ability in predicting the dynamic behavior of the system. Similar to the work done for the TFA system using the 1D FE representation, it is of interest to model the BAHA system using a 1D FE model. The analytical model of Westover et al. relied on modelling the implant and the abutment as rigid bodies and the impactor as a particle with a total of 4 DOF [14]. The 1D FE representation is expected to add more modelling power to the mathematical representation without substantially increasing the computational cost for evaluating the interface properties. The 1D modelling process is similar to the one adopted for TFA system, however there are two main differences: 1) instead of relying on axial formulation for representing the system, the Timoshenko beam formulation is used to model the bending behavior of the system and 2) the analysis only involves the portion of the problem where the impact rod is in contact with the system. The chapter commences by briefly introducing the Timoshenko Beam formulation and then tests its ability in obtaining the natural frequency of the implant abutment system. Finally, the chapter concludes by integrating the 1D FE model in a MATLAB® application that uses modal superposition and optimization to evaluate the interface properties. The application is tested by analyzing the 3D FE signals generated in chapter 6 and comparing the results of the 1D FE model with the results of the 4 DOF model of the current ASIST utility.

8.1 Timoshenko Beam Formulation for BAHA Systems

A beam is a solid structure that experiences transverse deflection along its longitudinal axis. Euler Bernoulli, Rayleigh, and Timoshenko beam models can all be used to describe the dynamic behavior of beams [45]. The Euler Bernoulli model is the simplest beam model since it ignores rotary inertia and shear deflection, Rayleigh's model accounts for rotary inertia and Timoshenko beam accounts for both rotary inertia and shear deflection [45]. It was concluded from the investigation conducted on the bending behavior of TFA systems under different 1D FE beam models (Appendix A) that the Timoshenko beam model was the most appropriate choice since the shearing effects were prominent for the higher order modes of the implant system with complex mode shapes. The BAHA implant-abutment system is not as slender as the TFA system, the length to diameter ratio is in the order of 14 and 2 for the TFA and BAHA systems respectively. Therefore, it is expected that the Euler Bernoulli and Rayleigh models would not be able to predict the

frequencies accurately and Timoshenko beam theory would be the more appropriate choice for modelling the system. EQ 8-1 is the governing equation for a Timoshenko beam experiencing free vibration, $y(x,t)$ is the dependent variable and describes the transverse deflection with respect to the longitudinal position x and time t [45]. To fully define the model, the tensile and shear moduli, E and G, the mass density, ρ, second moment of area, I, cross-sectional area, A, and the shear factor, κ, must be obtained. The element-wise stiffness and mass matrices can be derived from EQ 8-1 using a Bubnov-Galerkin formulation in a similar manner to the axial vibration of bars (Appendix A) [59]. The derivation of the stiffness and mass matrices is well established in the literature and the matrices are presented in Appendix A [45], [59], [87].

$$EI\frac{\partial^4 y}{\partial x^4} + \rho A\frac{\partial^2 y}{\partial t^2} - \rho I\ \frac{\partial^4 y}{\partial x^2 \partial t^2} - \rho I\ \frac{E}{\kappa G}\frac{\partial^4 y}{\partial x^2 \partial t^2} + \frac{\rho^2 I}{\kappa G}\frac{\partial^4 y}{\partial t^4} = 0 \qquad \text{EQ (8-1)}$$

8.2 Modal Analysis of BAHA Implant-Abutment System

As a starting point, the fundamental bending frequency of the BAHA implant-abutment under a free-free boundary condition is evaluated using the 1D Timoshenko beam formulation and then compared to the 3D FE modal solution generated from ABAQUS®. The purpose of performing this comparison is to test the ability of 1D Timoshenko beam elements in properly representing the stiffness and inertial properties of implant-abutment system. Figure 8-1 shows a schematic of the implant-abutment system and Table 8-1 summarises the model's parameters. The 1D model is developed on MATLAB® in similar manner to the axial TFA model. Timoshenko beam elements were used to generate the element-wise stiffness and mass matrices and then they were assembled into the global mass and stiffness matrices. The fundamental bending mode was computed using the built-in MATLAB® eigenvalue function (eig). As for the 3D FE model, the geometry of the implant-abutment model used in chapter 6 was imported to ABAQUS® and the fundamental bending mode was computed using the Lanczos eigenvalue solver. The 3D model computed the fundamental bending mode for two boundary conditions; Case 1: the implant-abutment system was free in all directions and Case 2: the implant-abutment system was free to move within one plane and out of plane motion was inhibited. For both models (the 1D and 3D) h-refinement was carried out until convergence (frequency changes do not exceed 1%) was achieved.

Table 8-1 Summary of the 1D model parameters for the BAHA systems.

Parameter	**Value/Formula**	**Notes**
E	105 GPa	_
μ	0.31	Poisson's Ratio
G	$\frac{E}{2(1+\mu)}$	Shear Modulus is computed from E & μ
ρ	4.4 g/cm^3	_
A	$\frac{\pi}{4}(d_o^2 - d_i^2)$ m^4	d_o: External Diameter d_i: Internal Diameter which is 0 for some sections
I	$\frac{\pi}{64}(d_o^4 - d_i^4)\ m^4$	
κ	$\frac{6(1+\mu)}{7+6\mu}$	For a uniform circular section
	$\frac{6(1+\mu)(1+M^2)^2}{(7+6\mu)(1+M^2)^2 + (20+12\mu)M^2}$	For a hollow Circular Section $M = \frac{d_i}{d_o}$

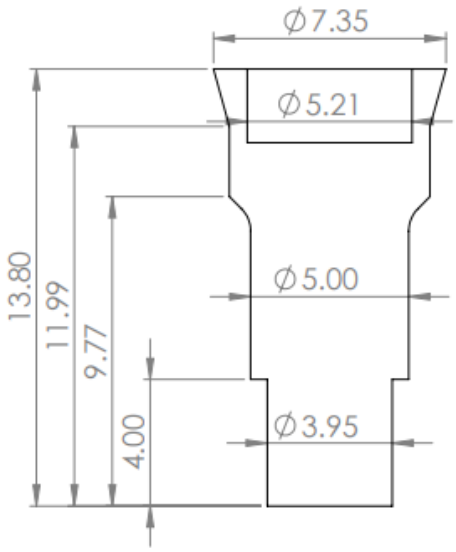

Figure 8-1 Section view of the BAHA Implant-Abutment system.

Table 8-2 shows a comparison between the 1D FE model prediction of the fundamental bending mode and the 3D FE simulations for Case 1 and 2. As it can be observed, there is a larger percentage difference (4.09%) between the 1D model and Case 1 compared to the 0.54% difference between the 1D model and Case 2. This difference can be attributed to the out of plane effects for Case 1 (Figure 8-2), there is a torsional component to the dynamic behavior of the system at this mode of vibration. Inhibiting any out of plane deformation and only allowing the system to deform within the $y - z$ plane (Figure 8-2) brings the 1D model's prediction closer to the 3D FE simulation. This is because the Timoshenko model cannot account for out of plane effects such as torsion and this increases the apparent stiffness of the structure since the structure is only allowed to experience planar deformation while in reality it is more flexible than this and can deform out of its plane. It should be noted however, that unlike the TFA system where the rod mass (9.4 g) is much smaller in comparison to the system (200 g) , the rod mass has a significant effect (since the implant-abutment mass is in the order 2 g) on the natural frequencies while the rod is in contact with the implant-abutment system. This means that the natural frequencies of the rod-implant-abutment system is going to be significantly lower and if the Timoshenko model is able to predict the high frequency value of the implant-abutment system (without the rod) with a fair amount of accuracy, it is expected that the Timoshenko model would predict the natural frequencies of the rod-abutment-implant system with an even higher accuracy.

Table 8-2 Summary of the modal analysis results for the BAHA Implant-Abutment system.

	1D FE	**3D FE Case 1**	**3D FE Case 2**
$f\ (Hz)$	92800	89200	92300
$Difference\ (\%)$	_	4.09	0.54

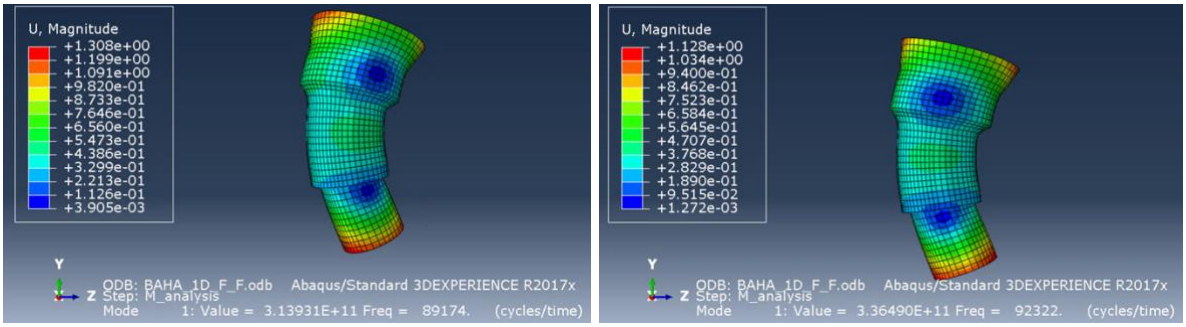

Figure 8-2 The bending mode shapes of the implant-abutment system for Case 1 (Left) and Case 2 (Right). Allowing the system to deform freely in all directions indicates that the bending behavior of the system has out of plane components.

8.3 Evaluation of the Interface Condition using the 1D FE model

The 1D Timoshenko model of the system is incorporated in a MATLAB® based GUI interface. Similarly to the 1D FE TFA model, the application relies on computing the time domain response using modal superposition and uses stiffness proportional damping for energy dissipation. The interface stiffness is modelled as a series of linear springs introduced over the implant diameter in a similar manner to the 4 DOF model of Westover et al. [14]. The application asks the user for the initial guess of the interface stiffness (k_s) and 2nd mode damping ratio (z) and then applies a least square minimization routine based on minimizing the Euclidean norm between the time domain acceleration responses of the input signal and the 1D model's prediction using the unconstrained minimization routine "fminsearch" (Figure 8-3). The ASC score is computed by normalizing the effective interface stiffness (k_{eff}) with respect to 4×10^6 N/m [11].To test the 1D FE the signals generated from the 3D FE model of chapter 6 were used as input signals and the interface properties (ASC scores) were evaluated and compared to the results presented in chapter 6.

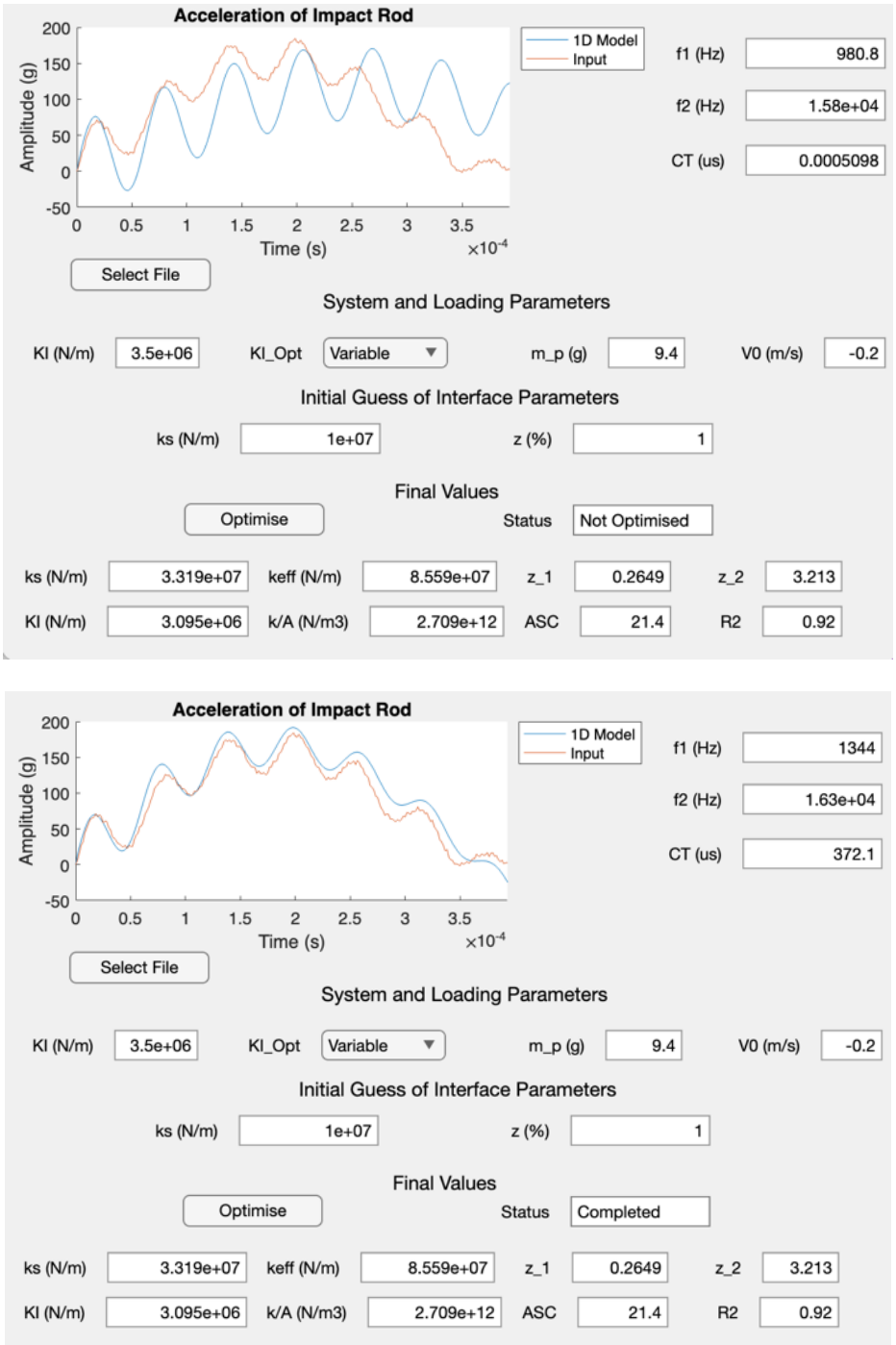

Figure 8-3. The 1D FE model application prompts the user to set the initial guesses for the interface parameters (Top), the application then computes the interface properties and the ASC score in a similar manner to the ASIST utility (Bottom).

The signals generated using the 3D FE model of chapter 6 relied on varying the interface condition by changing the friction coefficient (F) between the implant and the base. Figure 8-4 summarizes the ASC scores, first and second mode frequencies (f_1 and f_2) for the 4 DOF and the 1D FE models.

The 1D FE application outputs are presented in Appendix B for the five interface conditions. Both models were able to detect changes to the interface condition and associated higher ASC scores, f_1 and f_2 to higher F coefficients. It appears that the ASC scores and f_2 values are consistently lower for the 1D FE model while the differences in f_1 do not follow a certain trend (Table 8-3). The lower values of f_2 can be attributed to the higher power (represented with the significantly higher DOF) of the 1D FE model in comparison to the 4 DOF in estimating a higher order mode. Since the ASC score is influenced by both f_1 and f_2, estimating a lower f_2 consistently led to lower ASC scores for the 1D FE model. The differences in f_1 (apart from F =0) appear to be minor between the two models and virtually zero in some cases. The higher correlation coefficient for the 4 DOF can be due to the ASIST's utility initial estimates of the amplitude of the input acceleration signal and adjusts the rod's initial velocity. In the current 1D FE application, the amplitude is not adjusted and set to the same initial velocity used in the simulation. This could lead to deviations between the model's prediction and the input signal. Allowing the velocity to be a varying parameter in the optimization routine could potentially improve the R^2 values for the 1D FE model. Despite of these limitations, it appears that the 1D FE modelling approach of BAHA systems has potential in predicting the interface properties. Similarly to the current ASIST utility, it is well suited for clinical application due to the simplicity of the GUI and its computational efficiency in comparison to 3D FE modelling. However, it has the added benefit of having a significantly higher number of DOF which has potential in increasing its accuracy and helps in better visualization of the response since the 1D model can be used to estimate the dynamic stress and strain fields if it is coupled with a constitutive relationship. It is also easier to apply more complex boundary conditions (such as non-uniform interface stiffness) in comparison to the currently adopted 4 DOF model.

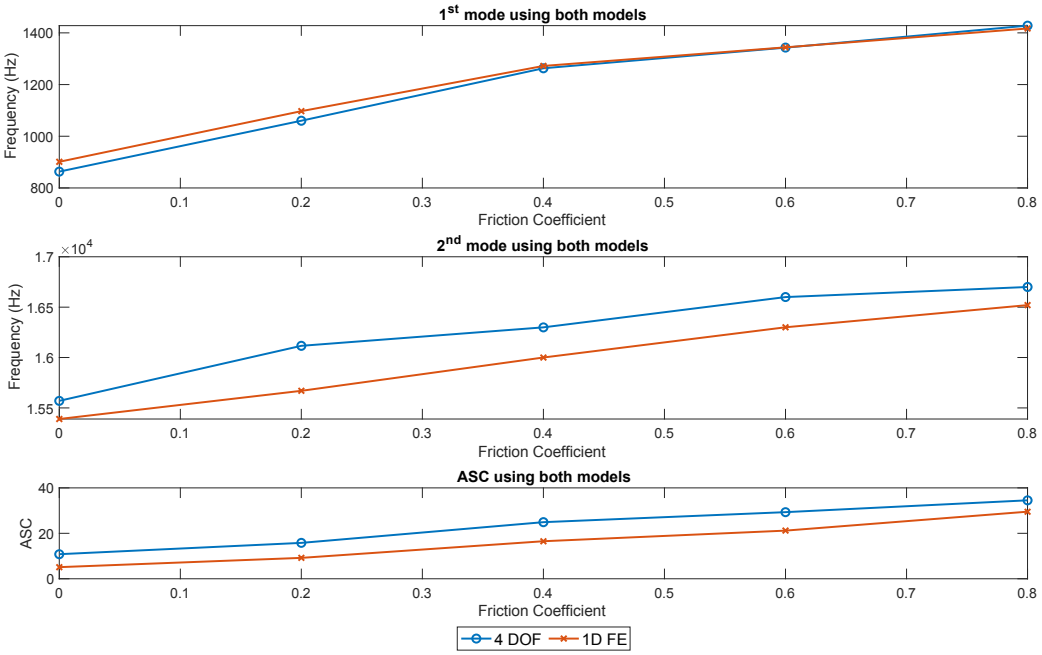

Figure 8-4 Comparison between the 4 DOF and 1D FE model in computing the interface stiffness. Both models computed similar f_1 values except for $F = 0$ (Top), f_2 was consistently lower for the 1D FE model (Middle) and thus the ASC score (Bottom) is consistently lower for the 1D FE model.

Table 8-3 The difference in predictions between the 4 DOF and the 1D FE model.

Difference between the 4 DOF and 1D FE Models						
F	ASC		f_1		f_2	
	Difference	Difference (%)	Difference (Hz)	Difference (%)	Difference (Hz)	Difference (%)
0	-5.70	-52.7	38	4.4	-180	-1.16
0.2	-6.60	-41.8	37	3.5	-446	-2.76
0.4	-8.40	-33.7	9	0.71	-299	-1.83
0.6	-8.10	-27.6	1	0.07	-300	-1.84
0.8	-5.00	-14.5	-11	-0.77	-180	-1.07

Chapter 9 Conclusions, Limitations and Recommendations for Future Work

9.1 Summary and Conclusions

Vibration analysis is an appealing choice for assessing for the stability of osseointegrated implants due to its non-invasive and quantitative nature. Vibration methods rely on exciting the implant system and analyzing the signal for some characteristics (such as the natural frequencies and damping ratios) that can be indicative of the quality of the bone implant interface (BII). Nevertheless, vibration of structures is a complex dynamic phenomenon and requires the use of mathematical analysis and benchtop experimentation to ensure that the conclusions inferred from it are physically relevant and indicative of the BII condition. In this work, extensive mathematical analysis was conducted to formulate a comprehensive understanding of the dynamic behavior of the osseointegrated transfemoral implant system (TFA) and bone conduction hearing aids (BAHA). The objective was to develop representative mathematical models of both implant systems and use the models to measure the BII stiffness using vibration-based measurement approaches.

The first phase of the analysis for TFA systems commenced with surveying its dynamic response under two extreme interface conditions that mimicked LOW (fibrous tissue) and HIGH (healthy bone) under different loading conditions, femoral boundary conditions, adapter/connector geometries and accelerometer mounting techniques. The analysis was conducted mathematically (3D FE modal analysis) and experimentally. It was concluded that testing the system under an axial excitation condition has more potential in characterizing the response due to its higher immunity to the femoral boundary condition and its generation of more characterizable signals upon attaching the GV connector compared to the transverse loading modes. Therefore, the second phase involved developing a 1D FE model of the TFA system and cross validating its axial modes of vibrations with the 3D FE solution. The excellent agreement between both models in terms of the predicted natural frequencies (maximum difference of 2.02 %) and mode shapes indicates that the 1D FE model is physically representative of the TFA implant geometry. The 1D FE model was then extended to perform modal superposition to evaluate the time domain response under an impact condition. Afterwards, the model was incorporated in a simple MATLAB® based GUI interface that matches between an input signal and the model's prediction using an optimization

routine. The developed application was tested using 3D FE implicit and experimental signals. The analysis indicated that the measurement and analysis approach is highly sensitive to the interface stiffness. The analysis of the experimental signals using the model revealed an interface stiffness of 4.75×10^6 N/m, 1.43×10^8 N/m and 2.21×10^9 N/m for the LOW, INTERMEDIATE and HIGH interface conditions respectively. The 1D FE model was also able to extract the damping properties accurately for the 3D FE signals where damping can be specified to known values. Thus, it can be concluded that the current mathematical representation of the TFA system using the 1D FE model is highly representative of the physical models and has the potential to quantitatively estimate the BII characteristics. To the authors best knowledge, this is the first investigation to comprehensively study the Osseointegrated Prosthetic limb (OPL) TFA system and propose a stability measurement system for it through the use of mathematical and physical models.

The previous work done for BAHA primarily focused on analyzing the system's behavior using physical models and mathematically using a 4 degree of freedom (DOF) analytical model. This investigation built upon the previous work and modelled the system using 1D and 3D FE models. The 3D FE model allowed for testing the implant system under a wide range of interface conditions that could not be replicated easily using benchtop setups. The first BAHA investigation involved varying the friction coefficient between the implant surface and the surrounding bone. The signals generated from the 3D FE simulations were analyzed using the ASIST utility which matches between the 4 DOF prediction and input signals. The analysis revealed that the ASIST Stability Coefficients (ASC), which are directly related to the interface stiffness, are more sensitive to the interface condition and less sensitive to implant-abutment geometry compared to the system's natural frequencies. The 3D FE model was also validated using benchtop and experimental signals and useful information on the excitation mechanism and the influencing parameters on implant stability were deduced from it. Finally, the BAHA system was also (like the TFA system) modelled using a 1D FE formulation. The 1D BAHA model utilized Timoshenko beam elements and managed to evaluate the interface properties in a similar manner to the previously developed 4 DOF system. The higher fidelity of the 1D BAHA model, offers higher potential: 1) in estimating the system's natural frequency (particular the higher order 2^{nd} mode), 2) in offering the user more flexibility in imposing the implant's boundary condition and 3) improving the results post-processing owing to the presence of a larger number of DOF which can be used to obtain the stress/stress distributions at the interface or reaction forces directly from the 1D FE model.

9.2 Limitations and Recommendations for Future Work

For the proposed measurement and analysis system for TFA systems, the first limitation of this work is that it focussed on the mathematical and in-vitro experimentation of the TFA system. It is critical to expand the 1D FE model to include the GV connector and different implant and dual cone adapter sizes (since they vary in nominal length and diameter) to start analysing the clinical signals. Once a statistically significant group of patients are analysed with the proposed measurement system, the analysis outcomes (such as the BII stiffness and/or the system's damping ratios) can be assessed for their correlation with other clinical outcomes (such as radiographic assessment or failure rates) to clinically validate the approach. In addition to clinical validation, the BII stiffness extracted from the 1D model can be experimentally cross-validated with another mechanical test such as a pull-out test or animal studies.

Another limitation of this work is the numerical errors in estimating the interface properties that can occur due to the optimization process. It was observed that increasing the damping ratios led to reducing the number of cycles and this affected the quality of the Fast Fourier transform and led to some numerical differences in estimating the interface stiffness. It was also observed that varying the impact stiffness can numerically affect the estimates of the interface stiffness and the damping ratios. From a physical standpoint, the impact stiffness only affects the natural frequencies and the damping behavior of the 1^{st} problem (where the rod is in contact with the implant system which is a minor portion of the signal) and should not influence the natural frequencies or damping behavior of the second problem (implant system's vibration which is the major portion of the signal). The differences result from the fact that the impact stiffness can influence the modal contributions of the signal and the optimization routine can account for them by adjusting the damping which can result in numerically inaccuracies. The nature of the impact stiffness is complex, in the 1D FE model it is treated as a linear spring but physically it can be much more complex than this representation since it is defined by both the impactor and the impacted system, and the impacted system has a variable interface stiffness. Unless there is a consistent way to empirically define the impact stiffness based on physical measurements (such as the contact time), the impact stiffness is probably going to be set as a variable in the optimization routine. Accordingly, conducting sensitivity analysis is important to quantify the magnitude of the numerical errors that can result from setting the impact stiffness as an additional optimization variable besides the interface stiffness. It is recommended that the sensitivity analysis follows an

un-replicated factorial design where the signals are generated using the 3D FE model for a wide range of interface stiffness and damping parameters and system parameters (mass of impactor and impact stiffness). Afterwards, the signals generated from the 3D FE analysis can be analysed using the 1D FE model under different settings such as fixed/variable impact stiffness, different definitions of the objective function and different impactor models (particle/bar). This will help in quantifying the error and come up with the best combination of settings in the 1D FE model that minimises the error for a wide range of conditions.

Another limitation of this work is the modelling assumption of the BII. The BII was modelled as a uniform cylinder connecting the implant to a healthy cortical bone and the quality of the interface was controlled by changing the material of this layer. The quality of the interface is the by-product of a complex interaction of several parameters such as the distribution of the interface, its material properties (stiffness and inertial) and quality of the surrounding bone. Therefore, it is recommended that future investigations to consider experimentally and numerically modelling these parameters and studying their effect on the signal and the possible modification required to the 1D FE model. Furthermore, it is important to test the 1D FE model's ability to extract the interface properties for different implant geometries and dual cone configurations and different impact rods. Ideally, the model's predictions of the interface stiffness should be invariant to these geometric changes and excitation conditions in a similar manner to the ASIST measurements for BAHA systems. Finally, the 3D FE models developed in this work can be extended and used to analyse the safety of the new impactors on the BII and the surrounding bones and ensure that the generated stress waves are within an acceptable level that is safe for clinical operation.

As for the BAHA systems, the 3D FE models could benefit from modelling the threads which would provide a more accurate representation of the implant's interaction with the surrounding bone. Furthermore, similarly to the TFA optimization analysis, conducting a sensitivity analysis on the 1D FE model's predictions using signals generated (with a wide range of interface and system parameters) from the 3D FE model can help in quantifying the error bounds of the 1D models prediction and help in choosing the best optimization settings.

References

[1] R. Brånemark, P. I. Brånemark, B. Rydevik, and R. R. Myers, "Osseointegration in skeletal reconstruction and rehabilitation: A review," *J Rehabil Res Dev*, vol. 38, no. 2, pp. 175–181, 2001.

[2] M. Ramakrishna, S. Arunachalam, Y. Ramesh Babu, L. Srivalli, T. Srikanth, and S. Soni, "A brief history of osseointegration: A review," *IP Annals of Prosthodontics and Restorative Dentistry*, vol. 7, no. 1, pp. 29–36, Feb. 2021, doi: 10.18231/j.aprd.2021.006.

[3] B. M. Isaacson and S. Jeyapalina, "Osseointegration: A review of the fundamentals for assuring cementless skeletal fixation," *Orthop Res Rev*, vol. 6, pp. 55–65, 2014, doi: 10.2147/ORR.S59274.

[4] X. Gao, M. Fraulob, and G. Haïat, "Biomechanical behaviours of the bone – implant interface : a review," *J.R.Soc.Interface*, vol. 16, pp. 1–20, 2019, doi: 20190259.

[5] E. M. Zanetti, G. Pascoletti, M. Cali, C. Bignardi, and G. Franceschini, "Clinical Assessment of Dental Implant Stability During Follow-Up : What Is Actually Measured , and Perspectives," *Biosensors (Basel)*, vol. 8, no. 68, pp. 1–18, 2018, doi: 10.3390/bios8030068.

[6] A. Maryniak, B. Laschowski, and J. Andrysek, "Technical Overview of Osseointegrated Transfemoral Prostheses : Orthopedic Surgery and Implant Design Centered," vol. 1, no. May, pp. 1–7, 2018, doi: 10.1115/1.4039105.

[7] K. Hagberg and R. Brånemark, "One hundred patients treated with osseointegrated transfemoral amputation prostheses - Rehabilitation perspective," *J Rehabil Res Dev*, vol. 46, no. 3, pp. 331–344, 2009, doi: 10.1682/JRRD.2008.06.0080.

[8] M. Al Muderis *et al.*, "The osseointegration group of Australia accelerated protocol (ogaap-1) for two-stage osseointegrated reconstruction of amputated limbs," *Bone and Joint Journal*, vol. 98B, no. 7, pp. 952–960, 2016, doi: 10.1302/0301-620X.98B7.37547.

[9] M. Al Muderis, W. Lu, K. Tetsworth, B. Bosley, and J. J. Li, "Single-stage osseointegrated reconstruction and rehabilitation of lower limb amputees: The Osseointegration Group of

Australia Accelerated Protocol-2 (OGAAP-2) for a prospective cohort study," *BMJ Open*, vol. 7, no. 3, pp. 1–4, 2017, doi: 10.1136/bmjopen-2016-013508.

[10] N. Meredith, "A Review of Nondestructive Test Methods and Their Application to Measure the Stability and Osseointegration of Bone Anchored Endosseous Implants," *Crit Rev Biomed Eng*, vol. 26, no. 4, pp. 275–291, 1998.

[11] L. Sennerby and N. Meredith, "Implant stability measurements using resonance frequency analysis: Biological and biomechanical aspects and clinical implications," *Periodontol 2000*, vol. 47, no. 1, pp. 51–66, 2008, doi: 10.1111/j.1600-0757.2008.00267.x.

[12] E. M. Zanetti *et al.*, "Modal analysis for implant stability assessment : Sensitivity of this methodology for different implant designs," *Dental Materials*, vol. 34, no. 8, pp. 1235–1245, 2018, doi: 10.1016/j.dental.2018.05.016.

[13] V. Pattijn, C. Van Lierde, G. Van Der Perre, I. Naert, and J. Vander Sloten, "The resonance frequencies and mode shapes of dental implants: Rigid body behaviour versus bending behaviour. A numerical approach," *J Biomech*, vol. 39, no. 5, pp. 939–947, 2006, doi: 10.1016/j.jbiomech.2005.01.035.

[14] L. Westover, G. Faulkner, W. Hodgetts, and D. Raboud, "Advanced System for Implant Stability Testing (ASIST)," *J Biomech*, vol. 49, pp. 3651–3659, 2016, doi: 10.1016/j.jbiomech.2016.09.043.

[15] L. Westover, G. Faulkner, W. Hodgetts, and D. Raboud, "Comparison of implant stability measurement devices for bone-anchored hearing aid systems," *J Prosthet Dent*, vol. 119, no. 1, pp. 178–184, 2018, doi: 10.1016/j.prosdent.2017.02.021.

[16] L. Westover, G. Faulkner, W. Hodgetts, F. Kamal, E. Lou, and D. Raboud, "Longitudinal Evaluation of Bone-Anchored Hearing Aid Implant Stability Using the Advanced System for Implant Stability Testing (ASIST)," *Otology & Neurotology*, vol. 39, pp. e489–e495, 2018, doi: 10.1097/MAO.0000000000001815.

[17] F. Shao, W. Xu, A. Crocombe, and D. Ewins, "Natural frequency analysis of osseointegration for trans-femoral implant," *Ann Biomed Eng*, vol. 35, no. 5, pp. 817–824, 2007, doi: 10.1007/s10439-007-9276-z.

[18] N. J. Cairns, C. J. Adam, M. J. Pearcy, and J. Smeathers, “Evaluation of modal analysis techniques using physical models to detect osseointegration of implants in transfemoral amputees,” *Proceedings of the Annual International Conference of the IEEE Engineering in Medicine and Biology Society, EMBS*, no. January 2014, pp. 1600–1603, 2011, doi: 10.1109/IEMBS.2011.6090463.

[19] N. J. Cairns, M. J. Pearcy, J. Smeathers, and C. J. Adam, “Simulating the bone-titanium interfacial changes around transfemoral osseointegrated implants using physical models and modal analysis,” in *1st International Workshop on Innovative Simulation for Health Care, IWISH 2012, Held at the International Multidisciplinary Modeling and Simulation Multiconference, I3M 2012*, 2012, pp. 1–9.

[20] N. J. Cairns, M. J. Pearcy, J. Smeathers, and C. J. Adam, “Ability of modal analysis to detect osseointegration of implants in transfemoral amputees: A physical model study,” *Med Biol Eng Comput*, vol. 51, no. 1–2, pp. 39–47, 2013, doi: 10.1007/s11517-012-0962-0.

[21] Grand View Research, “Dental Implants Market Size, Share & Trends Analysis Report By Implant Type (Zirconium, Titanium), By Region (North America, Europe, Asia Pacific, Latin America, MEA), And Segment Forecasts, 2023 - 2030,” San Francisco, 2018.

[22] S. E. Ellsperman, E. M. Nairn, and E. Z. Stucken, “Review of Bone Conduction Hearing Devices,” *Audiol Res*, vol. 11, no. 2, pp. 207–219, May 2021, doi: 10.3390/audiolres11020019.

[23] J. S. Hoellwarth, K. Tetsworth, S. R. Rozbruch, M. B. Handal, A. Coughlan, and M. Al Muderis, “Osseointegration for Amputees,” *JBJS Rev*, vol. 8, no. 3, pp. 1–10, 2020, doi: 10.2106/jbjs.rvw.19.00043.

[24] R. M. Grzeskowiak, J. Schumacher, M. S. Dhar, D. P. Harper, P. Y. Mulon, and D. E. Anderson, “Bone and Cartilage Interfaces With Orthopedic Implants: A Literature Review,” *Frontiers in Surgery*, vol. 7. Frontiers Media S.A., Dec. 21, 2020. doi: 10.3389/fsurg.2020.601244.

[25] B. Imam, “Incidence and Rehabilitation of Lower Limb Amputation in Canada and Feasibility of a Novel Training Program,” The University of British Columbia, Vancouver, 2017.

[26] J. S. Hebert, M. Rehani, and R. Stiegelmar, “Osseointegration for lower-limb amputation: A systematic review of clinical outcomes,” *JBJS Reviews*, vol. 5, no. 10. Journal of Bone and Joint Surgery Inc., 2017. doi: 10.2106/JBJS.RVW.17.00037.

[27] J. P. M. Frölke, R. A. Leijendekkers, and H. Van de Meent, “Osseointegrated prosthesis for patients with an amputation Multidisciplinary team approach in the,” *Unfallchirurg*, vol. 120, pp. 293–299, 2017, doi: 10.1007/s00113-016-0302-1.

[28] P. Stenlund, M. Trobos, J. Lausmaa, R. Brånemark, P. Thomsen, and A. Palmquist, “Effect of load on the bone around bone-anchored amputation prostheses,” *Journal of Orthopaedic Research*, vol. 35, no. 5, pp. 1113–1122, May 2017, doi: 10.1002/jor.23352.

[29] J. S. Hoellwarth, A. Oomatia, K. Tetsworth, E. Vrazas, and M. Al Muderis, “Bone density changes after five or more years of unilateral lower extremity osseointegration: Observational cohort study,” *Bone Rep*, vol. 18, Jun. 2023, doi: 10.1016/j.bonr.2023.101682.

[30] R. Atallah, R. A. Leijendekkers, T. J. Hoogeboom, and J. P. Frölke, “Complications of bone-anchored prostheses for individuals with an extremity amputation: A systematic review,” *PLoS One*, vol. 13, no. 8, p. e0201821, Aug. 2018, doi: 10.1371/journal.pone.0201821.

[31] S. N. Ghossaini and P. C. Roehm, “Osseointegrated Auditory Devices: Bone-Anchored Hearing Aid and PONTO,” *Otolaryngol Clin North Am*, vol. 52, no. 2, pp. 243–251, 2019, doi: 10.1016/j.otc.2018.11.005.

[32] J. C. Hobson, A. J. Roper, R. Andrew, M. P. Rothera, P. Hill, and K. M. Green, “Complications of bone-anchored hearing aid implantation,” *Journal of Laryngology and Otology*, vol. 124, no. 2, pp. 132–136, Feb. 2010, doi: 10.1017/S0022215109991708.

[33] O. Medical, “How bone conduction systems work.” Accessed: Jun. 15, 2020. [Online]. Available: https://www.oticonmedical.com/ca/bone-conduction/new-to-bone-conduction/what-is-bone-conduction/how-bone-conduction-systems-work

[34] The Ear Center of Greensboro, “Ear Center: Ponto Hearing Implant by Oticon.” Accessed: Sep. 29, 2023. [Online]. Available: http://www.earcentergreensboro.com/hearing-implants/ponto_device.php

[35] V. Swami, V. Vijayaraghavan, and V. Swami, “Current trends to measure implant stability,” *Journal of Indian Prosthodontist Society*, vol. 16, no. 2. Medknow Publications, pp. 124–130, Apr. 01, 2016. doi: 10.4103/0972-4052.176539.

[36] A. Nebergall, C. Bragdon, A. Antonellis, J. Kärrholm, R. Brånemark, and H. Malchau, “Stable fixation of an osseointegated implant system for above-the-knee amputees: Titel RSA and radiographic evaluation of migration and bone remodeling in 55 cases,” *Acta Orthop*, vol. 83, no. 2, pp. 121–128, 2012, doi: 10.3109/17453674.2012.678799.

[37] R. L. Hansen, B. L. Langdahl, P. H. Jørgensen, K. K. Petersen, K. Søballe, and M. Stilling, “Does migration of osseointegrated implants for transfemoral amputees predict later revision? A prospective 2-year radiostereometric analysis with 5-years clinical follow-up,” *Orthopaedics and Traumatology: Surgery and Research*, vol. 105, no. 5, pp. 1013–1020, 2019, doi: 10.1016/j.otsr.2019.05.010.

[38] F. Bottner, E. Su, B. Nestor, B. Azzis, T. P. Sculco, and M. Bostrom, “Radiostereometric Analysis: The Hip,” *HSS Journal*, vol. 1, no. 1, pp. 94–99, 2005, doi: 10.1007/s11420-005-0114-2.

[39] R. Vayron, E. Soffer, F. Anagnostou, and G. Haïat, “Ultrasonic evaluation of dental implant osseointegration,” *J Biomech*, vol. 47, no. 14, pp. 3562–3568, 2014, doi: 10.1016/j.jbiomech.2014.07.011.

[40] A. K.Chopra, *Dynamics of Structures Theory and Applications to Earthquake Engineering*, Fourth. Prentice Hall, 2012.

[41] P. Avitable, *Modal Testing: A Practitioner’s Guide* . Hoboken: John Wiley & Sons Ltd, 2018.

[42] J.-S. Shim, M.-Y. Kim, S.-J. An, E.-S. Kang, and Y.-S. Choi, “Evaluation of implant stability measurements according to implant placement site and duration in elderly patients: A prospective multi-center clinical study,” 2023, doi: 10.20944/preprints202305.0593.v1.

[43] S. Al-Jetaily and A. A. F. Al-dosari, “Assessment of Osstell™ and Periotest® systems in measuring dental implant stability (in vitro study),” *Saudi Dental Journal*, vol. 23, no. 1, pp. 17–21, 2011, doi: 10.1016/j.sdentj.2010.09.003.

[44] L. Westover, “Evaluation of the Interface Mechanical Properties of Craniofacial Implants and Natural Teeth,” Edmonton, Jun. 2014.

[45] S. Rao, *Vibration of Continous Systems*, Second Edi. New Jersey: Wiley, 2019.

[46] R. Huiskes, "ON THE MODELLING OF LONG BONES IN STRUCTURAL ANALYSES*," *Journal of Biomechanics* , vol. 15, no. 1, pp. 65–69, 1982, doi: https://doi.org/10.1016/0021-9290(82)90036-7.

[47] SAWBONES, "Biomechanical Materials for Precise, Repeatable Testing." Accessed: Jan. 20, 2022. [Online]. Available: https://www.sawbones.com/biomechanical-product-info

[48] MatWeb, "Overview of materials for Cyanoacrylate Adhesives," https://www.matweb.com/search/datasheet.aspx?matguid=d0d7dbec7666421caf8aa08724b634c5&ckck=1.

[49] Engineering Toolbox, "Metals and Alloys-Densities." [Online]. Available: https://www.engineeringtoolbox.com/metal-alloys-densities-d_50.html

[50] V. Waide, L. Cristofolini, J. Stolk, N. Verdonschot, G. J. Boogaard, and A. Toni, "Modelling the fibrous tissue layer in cemented hip replacements: Experimental and finite element methods," *J Biomech*, vol. 37, no. 1, pp. 13–26, 2004, doi: 10.1016/S0021-9290(03)00258-6.

[51] Henkel, "Super Glue Ultra GEL Control," Mississauga, 2015.

[52] ANALOG DEVICES, "ADXL 1004 Technical Datasheet," Norwood MA, 2018.

[53] J. O. Smith, *Spectral Audio Signal Processing*. W3K Publishing, 2011.

[54] R. Swain, "Development and Modelling of an Impact Test to Determine the Bone Implant Interface Properties of Osseointegrated Implants," University of Alberta, 2006.

[55] R. Swain, G. Faulkner, D. Raboud, and J. Wolfaardt, "A Dynamic Analytical Model for Impact Evaluation of Percutaneous Implants," vol. 130, no. October, pp. 1–13, 2008, doi: 10.1115/1.2970061.

[56] J. Tillander, K. Hagberg, Ö. Berlin, L. Hagberg, and R. Brånemark, "Osteomyelitis Risk in Patients With Transfemoral Amputations Treated With Osseointegration Prostheses," *Clin Orthop Relat Res*, vol. 475, no. 12, pp. 3100–3108, Dec. 2017, doi: 10.1007/s11999-017-5507-2.

[57] M. Mohamed, H. Pisavadia, and L. Westover, “A finite element model for evaluating the effectiveness of the Advanced System for Implant Stability Testing (ASIST),” *J Biomech*, vol. 124, 2021, doi: https://doi.org/10.1016/j.jbiomech.2021.110570.

[58] M. Mohamed, D. Raboud, J. S. Hebert, and L. Westover, “Stabillity Assessment of Osseointegrated Transfemoral Bone-Implant Systems using Finite Element Modal Analysis,” in *Progress in Canadian Mechanical Engineering* , Edmonton, 2022. doi: http://dx.doi.org/10.7939/r3-s23c-as14.

[59] J. N. Reddy, *Introduction to the Finite Element Method*, 4th Editio. McGraw Hill, 2019.

[60] M. E. Hossain, C. Ketata, and M. R. Islam, “EXPERIMENTAL STUDY OF PHYSICAL AND MECHANICAL PROPERTIES OF NATURAL AND SYNTHETIC WAXES USING UNIAXIAL COMPRESSIVE STRENGTH TEST,” in *Proceedings of the Third International Conference on Modeling, Simulation and Applied Optimization*, Sharjah, Jan. 2009.

[61] E. Beaudry, “Development and Benchtop validation of an impactor for transfemoral osseointegrated implant Stability Assessment ,” University of Alberta, Edmonton, 2023.

[62] SIEMENS, “What Modal Impact Hammer Tip should I use ?,” SIEMENS. Accessed: Jul. 13, 2023. [Online]. Available: https://community.sw.siemens.com/s/article/what-modal-impact-hammer-tip-should-i-use

[63] K. R. Williams and A. D. C. Williams, “Impulse response of a dental implant in bone by numerical analysis,” *Biomaterials*, vol. 18, no. 10, pp. 715–719, 1997.

[64] H.-M. Huang, S. Lee, C. Yeh, and C. Lin, “Resonance frequency assessment of dental implant stability with various bone qualities : a numerical approach,” *Clin. Oral Impl.Res*, vol. 13, pp. 65–74, 2002.

[65] M.-C. Pan, Z.-W. Chen, H.-B. Zhuang, and S.-Y. Lee, “Technique and Device of Irregular Osseointegration Detection for Dental Implant,” in *Proceedings of BioMed2008 3rd Frontiers in Biomedical Devices Conference*, 2008, pp. 5–6.

[66] E. Lamalfa and P. Rizzo, “Modeling the electromechanical impedance technique for the assessment of dental implant stability,” *J Biomech*, vol. 48, no. 10, pp. 1713–1720, 2015, doi: 10.1016/j.jbiomech.2015.05.020.

[67] R. Vayron, V. H. Nguyen, R. Bosc, S. Naili, and G. Haïat, “Finite element simulation of ultrasonic wave propagation in a dental implant for biomechanical stability assessment,” *Biomech Model Mechanobiol*, vol. 14, no. 5, pp. 1021–1032, 2015, doi: 10.1007/s10237-015-0651-7.

[68] D. Pammer, “Evaluation of postoperative dental implant primary stability using 3D finite element analysis,” *Comput Methods Biomech Biomed Engin*, vol. 22, no. 3, pp. 280–287, 2019, doi: 10.1080/10255842.2018.1552682.

[69] M. Zhai, B. Li, and D. Li, “Effects on the torsional vibration behavior in the investigation of dental implant osseointegration using resonance frequency analysis : a numerical approach,” *Med Biol Eng Comput*, vol. 55, no. 9, pp. 1649–1658, 2017, doi: 10.1007/s11517-017-1612-3.

[70] H. D. Espinosa, A. J. Patanella, and M. Fischer, “Dynamic Friction Measurements at Sliding Velocities Representative of High-Speed Machining Processes,” *Transactions of the ASME*, vol. 122, no. October, pp. 834–848, 2000.

[71] Dassaullt Systemes Simulia Corp, *Simulia User Assistance 2017*. Providence,RI: Dassault Systemes, 2016.

[72] H. Zhuang *et al.*, “Non-contact Vibro-acoustic Detection Technique for Dental Osseointegration Examination,” *J Med Biol Eng*, vol. 33, no. 1, pp. 35–44, 2012, doi: 10.5405/jmbe.993.

[73] V. Mathieu *et al.*, “Biomechanical determinants of the stability of dental implants: Influence of the bone-implant interface properties,” *J Biomech*, vol. 47, no. 1, pp. 3–13, 2014, doi: 10.1016/j.jbiomech.2013.09.021.

[74] M. A. L. Hernandez-Rodriguez, G. R. Contreras-Hernandez, A. Juarez-Hernandez, B. Beltran-Ramirez, and E. Garcia-Sanchez, “Failure analysis in a dental implant,” *Eng Fail Anal*, vol. 57, pp. 236–242, 2015, doi: 10.1016/j.engfailanal.2015.07.035.

[75] H. B. Zhuang, M. C. H. Pan, J. Z. Chen, J. W. Wu, and C. S. Chen, “A noncontact detection technique for interfacial bone defects and osseointegration assessment surrounding dental implants,” *Measurement (Lond)*, vol. 55, pp. 335–342, 2014, doi: 10.1016/j.measurement.2014.05.039.

[76] J. Rahmoun, A. Auperrin, R. Delille, H. Naceur, and P. Drazetic, “Characterization and micromechanical modeling of the human cranial bone elastic properties,” *Mech Res Commun*, vol. 60, pp. 7–14, 2014, doi: 10.1016/j.mechrescom.2014.04.001.

[77] J. Peterson and P. C. Dechow, “Material properties of the human cranial vault and zygoma,” *Anatomical Record - Part A Discoveries in Molecular, Cellular, and Evolutionary Biology*, vol. 274, no. 1, pp. 785–797, 2003, doi: 10.1002/ar.a.10096.

[78] R. Delille, D. Lesueur, P. Potier, P. Drazetic, and E. Markiewicz, “Experimental study of the bone behaviour of the human skull bone for the development of a physical head model,” *International Journal of Crashworthiness*, vol. 12, no. 2, pp. 101–108, 2007, doi: 10.1080/13588260701433081.

[79] M. Smith, *ABAQUS/Standard User’s Manual, Version 6.9*. United States: Dassault Systemes Simulia Corp, 2009.

[80] A. A. Polycarpou, “Measurement and Modeling of Normal Contact Stiffness and Contact Damping at the Meso,” vol. 127, no. February, pp. 52–60, 2005, doi: 10.1115/1.1857920.

[81] L. Westover, “Evaluating of the Interface Mechanical properties of Craniofacial Implants and Natural Teeth Through Development of the Advanced System for Implant Stability Testing (ASIST),” University of Alberta, 2016. doi: 10.1088/1751-8113/44/8/085201.

[82] S. Adeeb, *Introduction to Solid Mechanics & Finite Element Analysis*. 2021. [Online]. Available: http://sameradeeb.srv.ualberta.ca

[83] J. H. C. Lee *et al.*, “An Investigation on the Correlation between the Mechanical Properties of Human Skull Bone, Its Geometry, Microarchitectural Properties, and Water Content,” *J Healthc Eng*, vol. 2019, 2019, doi: 10.1155/2019/6515797.

[84] S. Foghsgaard and P. Caye-Thomasen, “A new wide-diameter bone-anchored hearing implantvprospective 1-year data on complications, implant stability, and survival,” *Otology and Neurotology*, vol. 35, no. 7, pp. 1238–1241, 2014, doi: 10.1097/MAO.0000000000000345.

[85] A. Moreira, J. Rosa, F. Freitas, H. Francisco, H. Luís, and J. Caramês, “Influence of implant design, length, diameter, and anatomic region on implant stability: a randomized clinical

trial," *Revista Portuguesa de Estomatologia, Medicina Dentária e Cirurgia Maxilofacial*, vol. 61, no. 1, 2021, doi: 10.24873/j.rpemd.2021.01.816.

[86] R. C. Nelissen, C. A. den Besten, E. A. M. Mylanus, and M. K. S. Hol, "Stability, survival, and tolerability of a 4.5-mm-wide bone-anchored hearing implant: 6-month data from a randomized controlled clinical trial," *European Archives of Oto-Rhino-Laryngology*, vol. 273, no. 1, pp. 105–111, 2016, doi: 10.1007/s00405-015-3593-x.

[87] B. S. Gan, *An Isogeometric Approach to Beam Structures*. Springer, 2018.

[88] R. G. Robertson, "Multiple Impulse Method of Tooth Mobility Assessment," 1995.

Appendix

Appendix A: Mass and Stiffness Matrices of Bar, Beam Elements and Transverse Modelling of TFA System

Derivation of Axial Bar Elements

In this appendix, the derivation of the element-wise stiffness and mass matrices is presented. The derivation relies on the harmonic nature of the response and uses separation of variables to reduce the dimensionality of the governing differential equation by limiting its dependence on the space coordinate, x, instead of depending on both space and time (EQ A-1 to EQ A-6). EQ A-1 is the governing equation (or equation of motion) of a linear elastic isotropic and homogenous bar undergoing axial vibration: the axial displacement, $u(x,t)$, is the dependent variable and is a function of the space coordinate (x) and time coordinate (t). ρ, A and E represent the mass density, cross sectional area and elastic modulus of the bar respectively and can either be constants or functions of x. f is the axial force per unit length acting on the bar and can be a function of x and t. u can be expressed as the product of U and T using the principle of separation of variables, where U and T are single variable functions of x and t respectively (EQ A-2). The periodic nature of eigenvalue problems allows for expressing T as a harmonic function (EQ A-3). i is the imaginary number $\sqrt{-1} = 1$ and ω_n is the natural frequency of the system (EQ A-3). The terms of EQ A-1 can be rewritten in terms of the assumed solution forms of EQ A-2 and EQ A-3. Substituting the expressions found in EQ A-4 and dropping the f term on the RHS (since this is a free vibration problem) yields EQ A-5. It should be noted that $e^{-i\omega_n t}$ cannot be zero so this term can be removed from the equation. Separation of variables allowed for reducing the number of independent variables and resulted in a differential equation that is only dependent on x (EQ A-6).

$$\rho A \frac{\partial^2 u}{\partial t^2} - \frac{\partial}{\partial x}\left(EA\frac{\partial u}{\partial x}\right) = f \qquad \text{(EQ A-1)}$$

$$u(x,t) = U(x)T(t) \qquad \text{(EQ A-2)}$$

$$T(t) = e^{-i\omega_n t} \qquad \text{(EQ A-3)}$$

$$\frac{\partial^2 u}{\partial t^2} = -\omega_n^2 U e^{-i\omega_n t} \text{ and } \frac{\partial}{\partial x}\left(EA\frac{\partial u}{\partial x}\right) = \frac{d}{dx}\left(EAe^{-i\omega_n t}\frac{dU}{dx}\right) \qquad \text{(EQ A-4)}$$

$$\rho A\left(\omega_n^2\, e^{-i\omega_n t}\right)U - \frac{d}{dx}\left(EAe^{-i\omega_n t}\frac{dU}{dx}\right) = 0 \text{ and } e^{-i\omega_n t} \neq 0 \quad \text{(EQ A-5)}$$

$$(\rho A\omega_n^2)U - \frac{d}{dx}\left(EA\frac{dU}{dx}\right) = 0 \quad \text{(EQ A-6)}$$

The solution can be approximated by introducing a linear bar element with two nodes (Figure A-1) using an approximate function $U(x)$ and linear interpolation functions $\theta(x)$ (EQ A-7 and EQ A-8). The approximate solution (along with the test function $v(x)$) can be substituted into the integral form of the differential equation and then the weak form can be obtained by applying integration by parts (EQ A-9 to EQ A-13). The stiffness and mass matrices can be directly inferred from the weak-form by re-arranging the terms and comparing it to a standard eigenvalue form (EQ A-14 to EQ A-15). Finally, the expressions for the stiffness and mass matrices can be found by evaluating those integrals over the element's length (EQ A-16. To EQ A-21). This derivation follows the process used by J.N. Reddy in Introduction to the Finite Element Method (chapter 7) [59], it utilizes a Bubnov-Galerkin formulation however variational methods would be equally valid and would yield similar results.

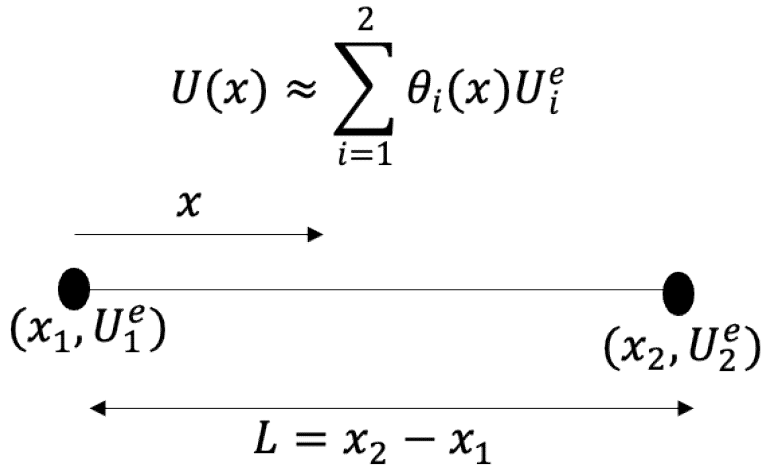

Figure A-1 A linear bar element with two nodes located at its extreme ends x_1 and x_2 can be used to approximate the solution (U). The solution can be specified at each node as U_1^e and U_2^e respectively and at any location on the element using linear interpolation. L is the difference between x_2 and x_1 and physically represents the length of the element.

$$U \approx \sum_{i=1}^{2} \theta_i U_i^e \quad \text{(EQ A-7)}$$

$$\theta_1 = \frac{x_2 - x}{L} \quad \text{and } \theta_2 = \frac{x - x_1}{L} \tag{EQ A-8}$$

$$\int_{x_1}^{x_2} (\rho A \omega_n^2) v U \, dx + \int_{x_1}^{x_2} v \frac{d}{dx}\left(EA \frac{dU}{dx}\right) dx = 0 \tag{EQ A-9}$$

$$\text{Where } \int_{x_1}^{x_2} v \frac{d}{dx}\left(EA \frac{dU}{dx}\right) dx = \left(EAv \frac{dU}{dx}\right]_{x_1}^{x_2} - \int_{x_1}^{x_2} EA \frac{dv}{dx}\frac{dU}{dx} \, dx \tag{EQ A-10}$$

$$(\rho A \omega_n^2) v U - \int_{x_1}^{x_2} EA \frac{dv}{dx}\frac{dU}{dx} \, dx \tag{EQ A-11}$$

$$v = \sum_{j=1}^{2} \theta_j v_j \tag{EQ A-12}$$

$$\omega_n^2 \int_{x_1}^{x_2} (\rho A) \theta_i \theta_j U_i^e v_j \, dx - \int_{x_1}^{x_2} EA \frac{d\theta_i}{dx}\frac{d\theta_j}{dx} U_i^e v_j \, dx = 0 \text{ and } v_j \neq 0 \tag{EQ A-13}$$

$$\int_{x_1}^{x_2} EA \frac{d\theta_i}{dx}\frac{d\theta_j}{dx} \, dx \, U_i^e - \omega_n^2 \int_{x_1}^{x_2} (\rho A) \theta_i \theta_j dx \, U_i^e = 0 \tag{EQ A-14}$$

$$([K] - \omega_n^2 [M])\{U^e\} = 0 \tag{EQ A-15}$$

$$K = \int_{x_1}^{x_2} EA \frac{d\theta_i}{dx}\frac{d\theta_j}{dx} \, dx \text{ and } M = \int_{x_1}^{x_2} (\rho A) \theta_i \theta_j dx \tag{EQ A-16}$$

$$K_{11} = EA \int_{x_1}^{x_2} \frac{d\theta_1}{dx}\frac{d\theta_1}{dx} \, dx = \frac{EA}{L} \text{ and } K_{12} = EA \int_{x_1}^{x_2} \frac{d\theta_1}{dx}\frac{d\theta_2}{dx} \, dx = -\frac{EA}{L} \tag{EQ A-17}$$

$$K_{21} = EA \int_{x_1}^{x_2} \frac{d\theta_2}{dx}\frac{d\theta_1}{dx} \, dx = -\frac{EA}{L} \text{ and } K_{22} = EA \int_{x_1}^{x_2} \frac{d\theta_2}{dx}\frac{d\theta_2}{dx} \, dx = \frac{EA}{L} \tag{EQ A-18}$$

$$K = \frac{EA}{L}\begin{bmatrix} 1 & -1 \\ -1 & 1 \end{bmatrix} \tag{EQ A-19}$$

$$M_{11} = \rho A \int_{x_1}^{x_2} \theta_1 \theta_1 dx = \frac{\rho AL}{3} \text{ and } M_{12} = \rho A \int_{x_1}^{x_2} \theta_1 \theta_2 dx = \frac{\rho AL}{6} \tag{EQ A-19}$$

$$M_{12} = \rho A \int_{x_1}^{x_2} \theta_2 \theta_1 dx = \frac{\rho AL}{6} \text{ and } M_{22} = \rho A \int_{x_1}^{x_2} \theta_2 \theta_2 dx = \frac{\rho AL}{3} \tag{EQ A-20}$$

$$M = \frac{\rho AL}{3}\begin{bmatrix} 2 & 1 \\ 1 & 2 \end{bmatrix} \quad \text{(EQ A-21)}$$

Timoshenko Beam Elements

A 1D beam element consists of two nodes, each node is allowed to translate in the transverse, y, direction and rotate, θ, as shown in Figure A-2. The stiffness and mass matrices (EQ A-22 to EQ A-25) were obtained from the literature [87]. However, the matrices can be derived from the weak-form of the governing equation using the Bubnov-Galerkin formulation in a similar manner to axial bar elements. EQ A-17 defines C and ϕ in terms of the element's geometric and material properties: Tensile Modulus (E), Shear modulus (G), Second moment of Area (I), bar length (L), shape factor (κ) and cross-sectional area (A). EQ A-18 and EQ A-19 are used to define the element-wise stiffness and mass matrices respectively.

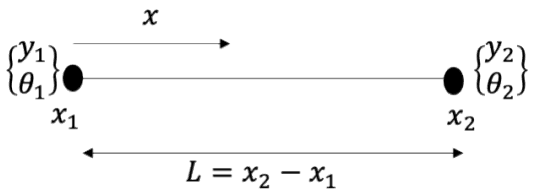

Figure A-2 A 1D Beam element has two nodes and each node has 2 DOF: 1) translation (y) and 2) rotation (θ).

$$C = \frac{EI}{(1+\phi)L^3} \quad and \quad \phi = \frac{12(EI)}{L^2 \kappa GA} \quad \text{(EQ A-22)}$$

$$K = C\begin{bmatrix} \frac{A}{I}(1+\phi) & 0 & 0 & -\frac{A}{I}(1+\phi) & 0 & 0 \\ 0 & 12 & 6L & 0 & -12 & 6L \\ 0 & 6L & (4+\phi)L^2 & 0 & -6L & (2-\phi)L^2 \\ -\frac{A}{I}(1+\phi) & 0 & 0 & \frac{A}{I}(1+\phi) & 0 & 0 \\ 0 & -12 & -6L & 0 & 12 & -6L \\ 0 & 6L & (2-\phi)L^2 & 0 & -6L & (4+\phi)L^2 \end{bmatrix} \quad \text{(EQ A-23)}$$

$$M_{\rho A} = \frac{\rho AL}{210(1+\phi)^2}\begin{bmatrix} 70(1+\phi^2) & 0 & 0 \\ 0 & (70\phi^2+147\phi+78) & (35\phi^2+77\phi+44)\frac{L}{4} \\ 0 & (35\phi^2+77\phi+44)\frac{L}{4} & (7\phi^2+14\phi+8)\frac{L^2}{4} \\ 35(1+\phi)^2 & 0 & 0 \\ 0 & (35\phi^2+63\phi+27) & (35\phi^2+63\phi+26)\frac{L}{4} \\ 0 & (-35\phi^2+63\phi+26)\frac{L}{4} & -(7\phi^2+14\phi+6)\frac{L^2}{4} \end{bmatrix}$$

(EQ A-24)

$$\begin{bmatrix} 35(1+\phi)^2 & 0 & 0 \\ 0 & (35\phi^2+63\phi+26) & (-35\phi^2+63\phi+26)\frac{L}{4} \\ 0 & (35\phi^2+63\phi+26)\frac{L}{4} & -(7\phi^2+14\phi+6)\frac{L^2}{4} \\ 70(1+\phi^2 & 0 & 0 \\ 0 & (70\phi^2+147\phi+78) & (-35\phi^2+63\phi+26)\frac{L}{4} \\ 0 & (-35\phi^2+63\phi+26)\frac{L}{4} & (7\phi^2+14\phi+8)\frac{L^2}{4} \end{bmatrix}$$

$M_{\rho I}$

$$= \frac{\rho I}{30(1+\phi)^2}\begin{bmatrix} 0 & 0 & 0 & 0 & 0 & 0 \\ 0 & 36 & -(15\phi-3)L & 0 & -36 & -(15\phi-3)L \\ 0 & -15(\phi-3)L & (10\phi^2+5\phi+4)L^2 & 0 & (15\phi-3)L & (5\phi^2-5\phi-1)L^2 \\ 0 & 0 & 0 & 0 & 0 & 0 \\ 0 & -36 & (15\phi-3)L & 0 & 36 & (15\phi-3)L \\ 0 & -(15\phi-3)L & (5\phi^2-5\phi-1)L^2 & 0 & (15\phi-3)L & (10\phi^2+5\phi+4)L^2 \end{bmatrix}$$

(EQ A-24)

$$M = M_{\rho A} + M_{\rho I}$$

(EQ A-25)

1D DE Transverse modelling of TFA Systems

This main body of this thesis focuses on the axial response of the TFA system based on the conclusions of chapter 3. However, if the femoral boundary condition is clinically closer to the free-end case and if the GV connector can installed and removed frequently, there would be merit in considering the transverse vibration modes. The bending behavior of the TFA system was investigated in a conference paper published in the Canadian Society of Mechanical Engineering International Congress (link to publication). This appendix serves as a summary of the main findings of this investigation.

The natural frequencies of a simply supported uniform beam with a length to diameter ratio of 14.3 (similar to a TFA system) were analyzed using Euler-Bernoulli, Rayleigh and Timoshenko beam formulations and the results were compared with the analytical solutions and 3D FE simulation (Figure A-3). All the formulations converged to their respective analytical solution. The three beam models also behaved similarly for the first three modes and served as a good approximation to the 3D FE solution, however Timoshenko beam model managed to better capture the higher order modes since it accounts for both rotary inertia and shear deflection.

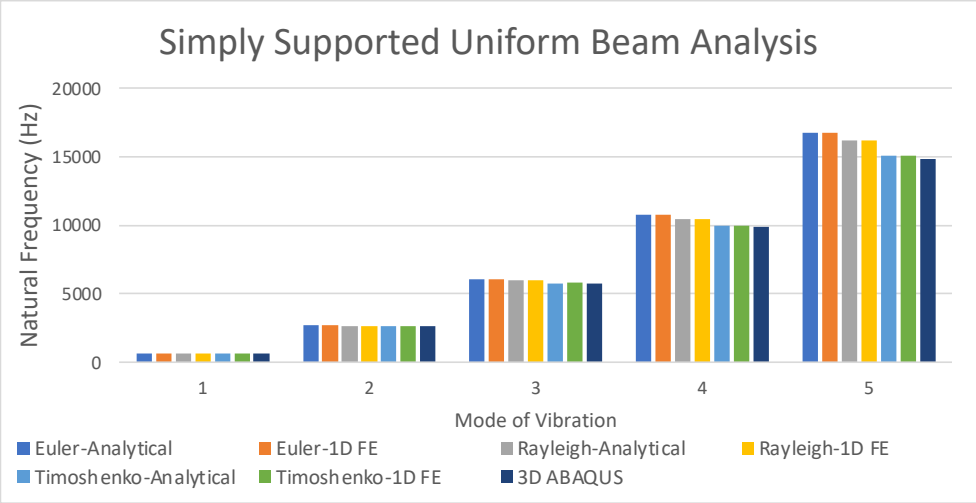

Figure A-3 Natural Frequency of a simply supported uniform beam using the three FE beam models, analytical solutions, and 3D ABAQUS® model.

An actual TFA system was then modelled using Timoshenko beam elements under a simply supported boundary condition and the first five mode shapes were compared to 3D FE simulation (Table A-1). The 1D FE model captured the modes of interest with a high degree of accuracy and is thus viewed as an appropriate mathematical representation of the TFA system.

Table A-1 Natural frequency of a fimply fupported TFA system.

	1D FE Model	3D ABAQUS Model	Difference
Mode	f_n (Hz)	f_n (Hz)	(%)
1	623	621	0.37%
2	2710	2650	2.45%
3	6130	6030	1.71%
4	9830	9640	1.95%
5	15163	14710	3.08%

The BII is then introduced to the 1D FE model as linear spring and the natural frequencies of the system were compared with a 3D FE model for a LOW (E =0.5 MPa) and HIGH (E =9600 MPa) interface conditions. The matching was performed manually by changing the BII stiffness (k) of the 1D model until the 1st mode is within $\pm$0.5% of the 3D model and then comparing the remaining modes. Using the k (found using the first mode of vibration) yields highly accurate results for the LOW interface situation (Figure A-4). The results (except for the third mode) are also accurate for the high interface situation (Figure A-4). In terms of the mode shapes, the 1D FE model captured highly similar deformation patterns (mode shapes) for all the modes of vibration. Figure A-5 and Figure A-6 are selected excerpts of the first and fourth mode of vibration (the BII and bone were suppressed for visualization) for the LOW stiffness case. Even the relatively complex bending behavior of the fourth mode was captured appropriately using the 1D model. The third mode of the HIGH stiffness had the highest difference of 9.2% is shown in Figure A-7. The 3D ABAQUS® model reveals that the behavior for this mode is not strictly bending (with significant axial and out of plane effects) and this is a plausible explanation for the higher difference between the 1D and 3D models. However, the initial conditions are not expected to trigger this mode, since the loading is transverse and so the effect of this mode is not expected to be significant on the time domain response. Additionally, this mode is mostly contained within the tip most part of the implant where the BII does not develop and is believed to have little effect on the structural stability of the OPL bone-implant system.

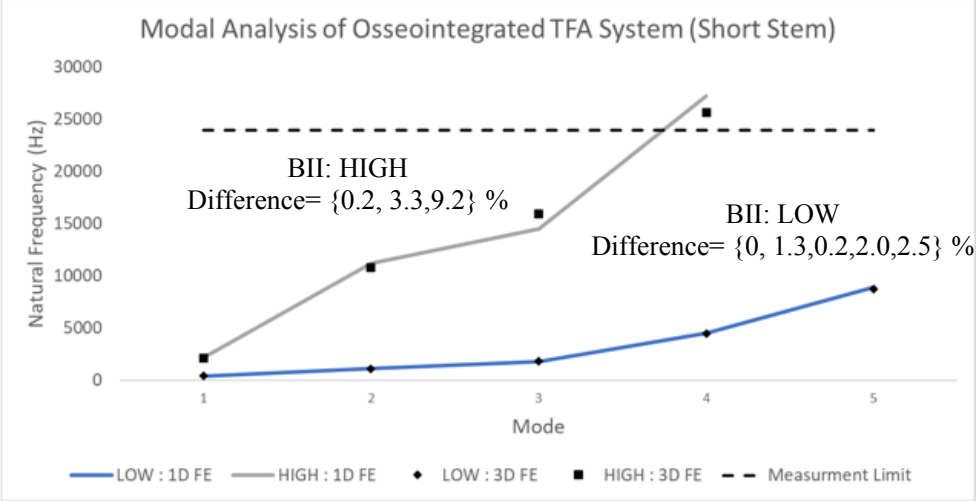

Figure A-4 Frequencies of the short TFA stem for LOW (E = 0.5 MPa & k = 8.2×10^{10} N/m^3) and HIGH BII conditions (E=9600 MPa & k = 5.5×10^{14} N/m^3)

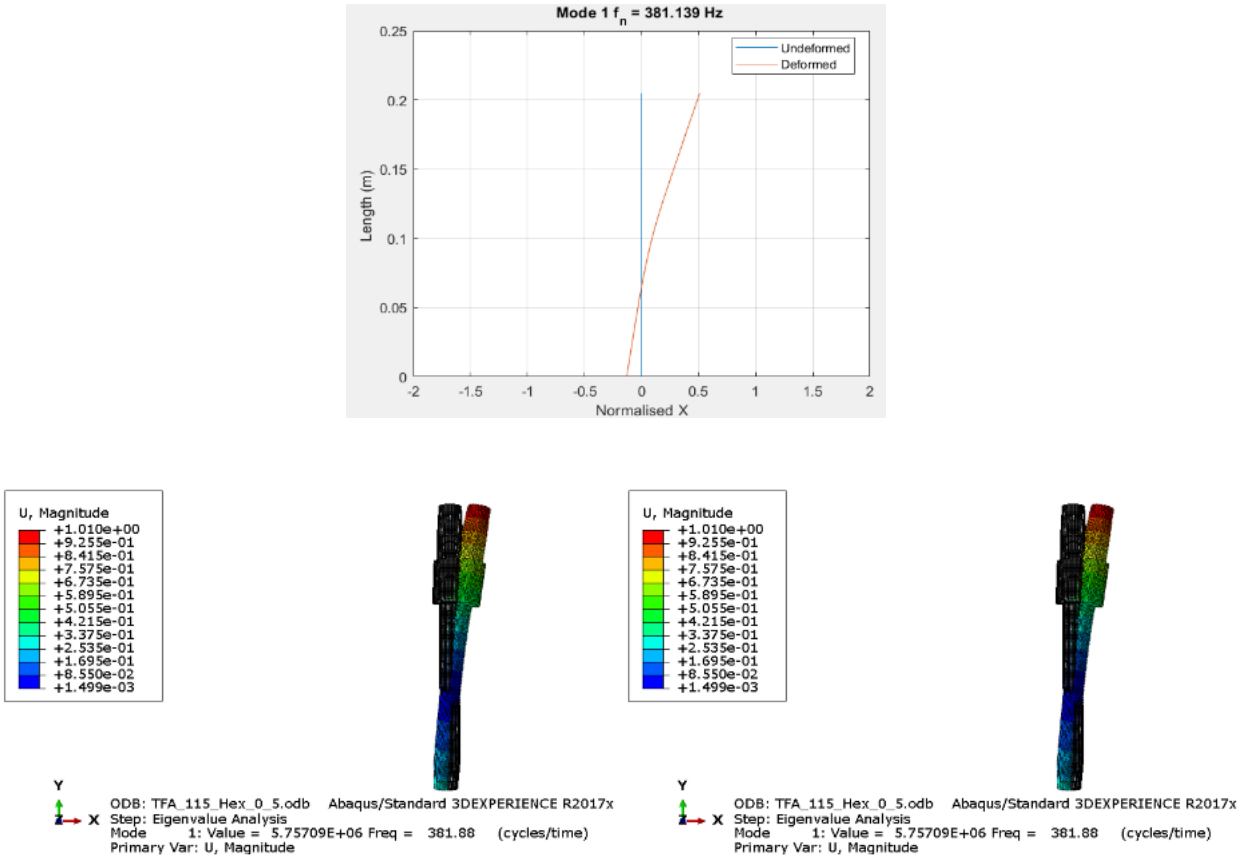

Figure A-5 First mode of a short stem for LOW (E = 0.5 MPa & k = 8.2×10^{10} N/m^3) condition using the 1D (Top) and 3D (Bottom) FE models

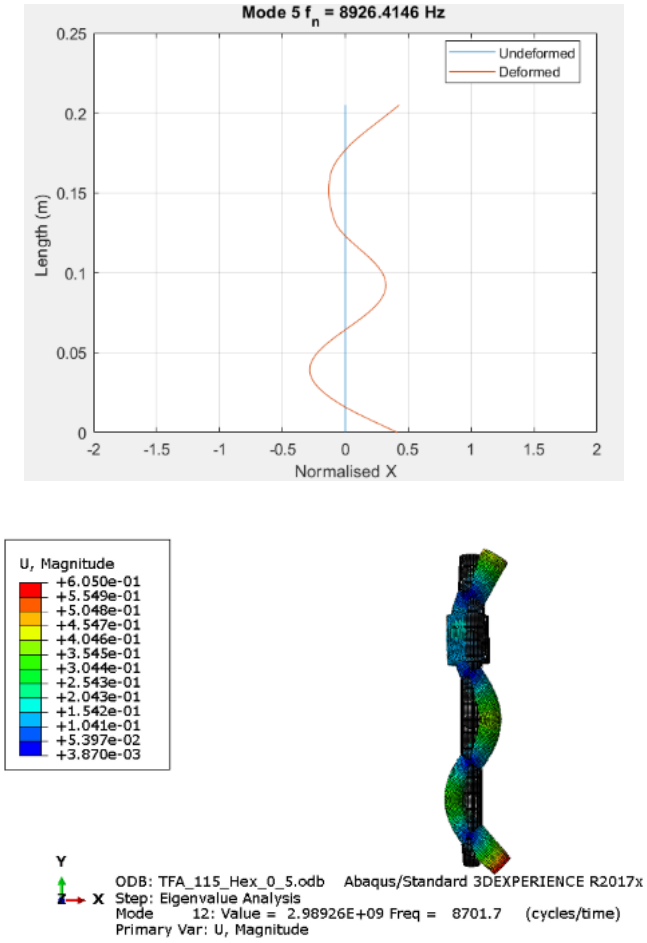

Figure A-6 Fourth mode of a short stem for LOW (E = 0.5 MPa & k = 8.2×10^{10} N/m^3) BII condition using the 1D (Top) and 3D (Bottom) FE models

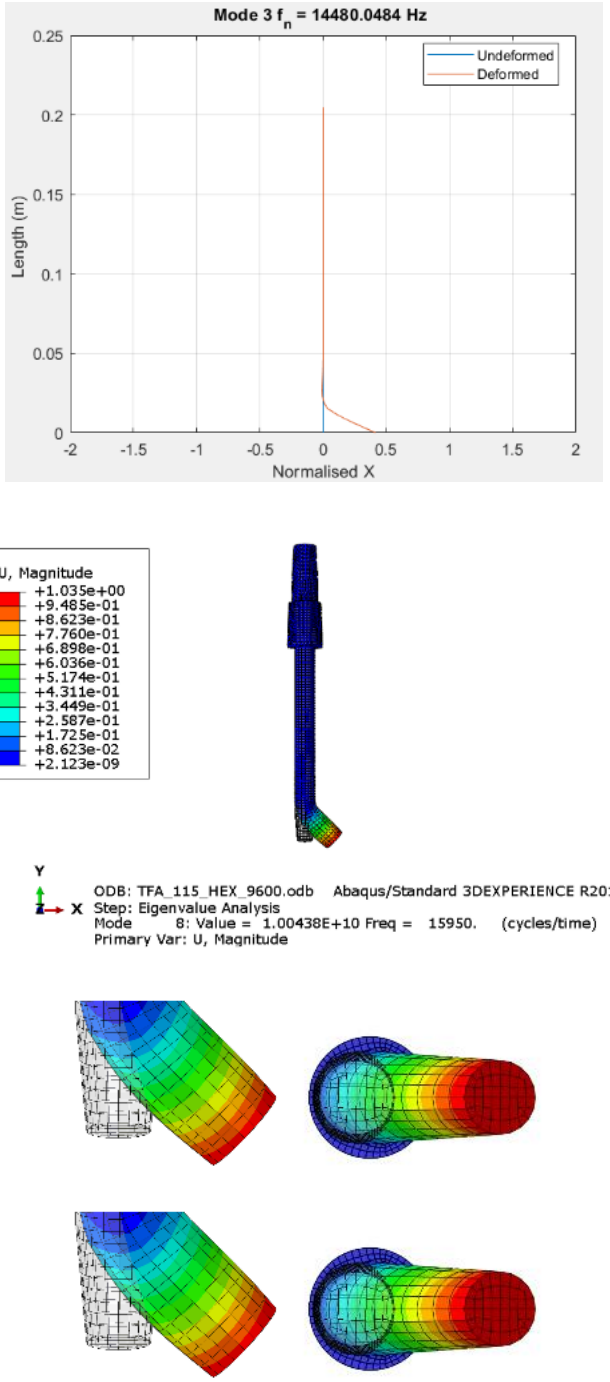

Figure A-7 Third mode of a short stem for HIGH (E = 9600 MPa & k = 5.5 ×10^{14} N/m^3) BII condition using the 1D (Top) and 3D (Bottom) FE models.

Using the same values of k k found for the short stem, the 1D FE model was used to extract the natural frequencies and mode shapes for the long stem and the results were compared to the 3D

ABAQUS® model. The results are shown in Figure A-8 for both interface conditions. There is excellent agreement between the 1D and 3D FE models with an average and maximum difference of 1.3% and 2.5% respectively for the LOW interface condition. While the higher BII condition had an average and maximum difference of 3.9% and 7.6% (excluding the fourth mode as it exceeds 24 kHz) respectively.

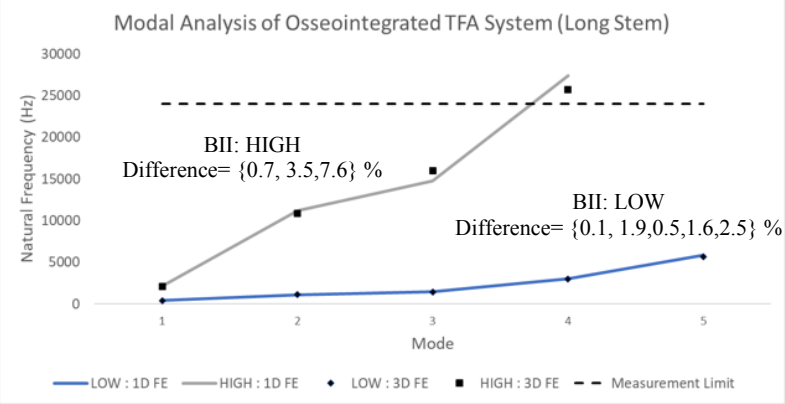

Figure A-8 Natural Frequencies of the long TFA stem for LOW (E = 0.5 MPa & k=8.2×10^{10} N/m^3) and HIGH BII conditions (E = 9600 MPa & k = 5.5×10^{14} N/m^3)

Appendix B: 1D FE Model Outputs

1D FE Axial Model Outputs for TFA System

3D FE Ideal Signals with $\zeta_1 = 1\%$

Condition	Model Output
LOW	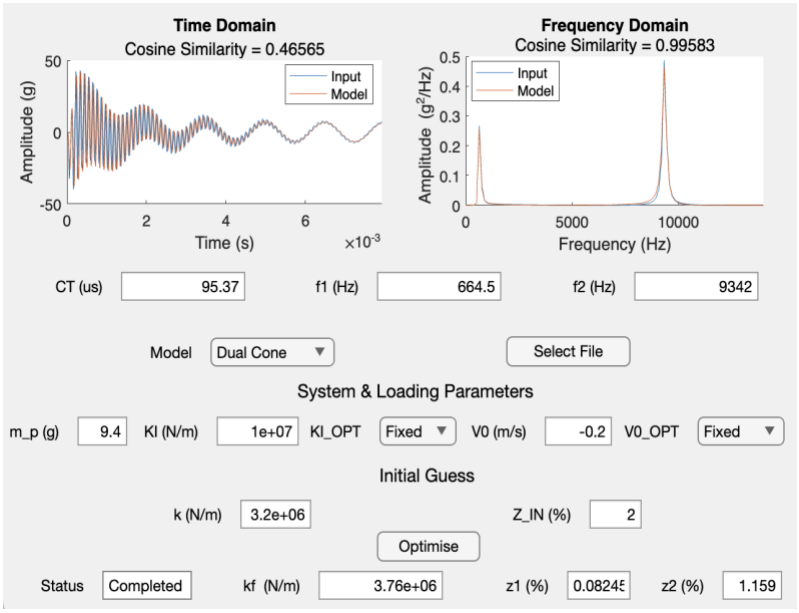
INTERMEDIATE	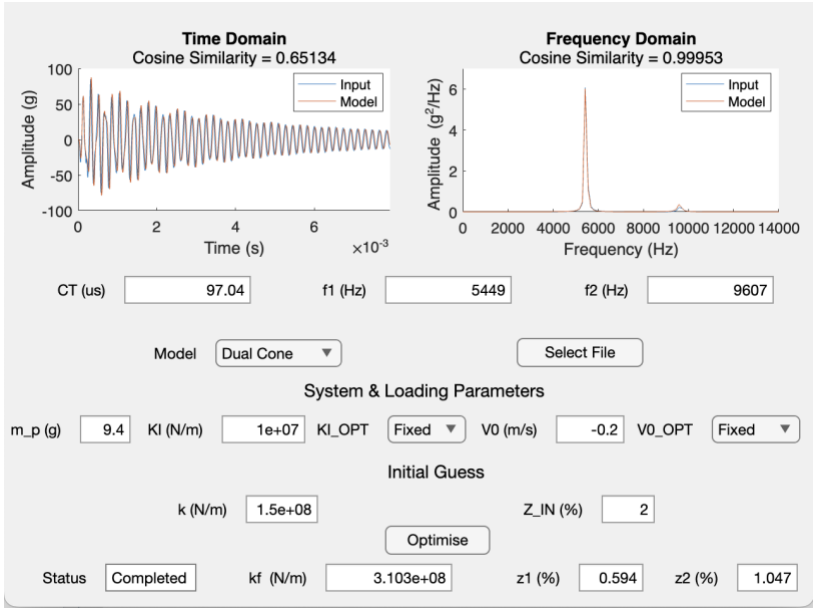

HIGH

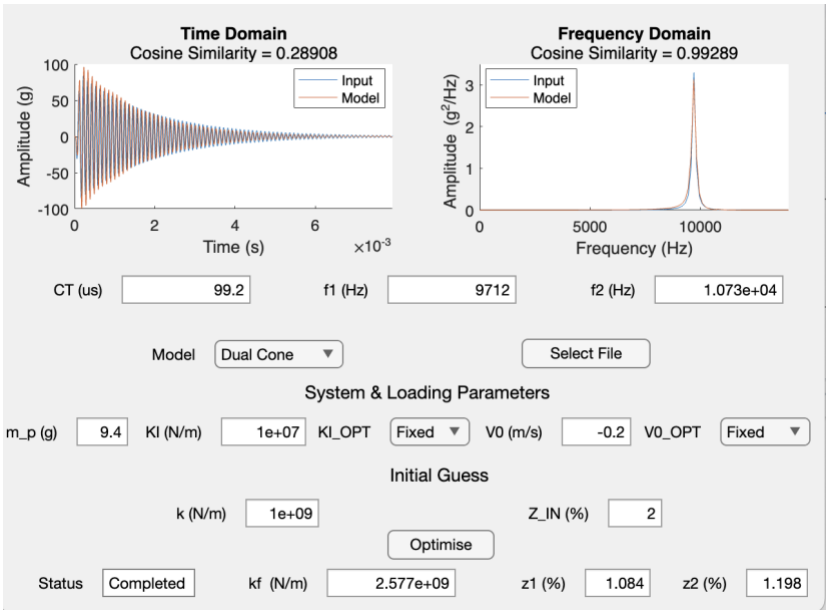

3D FE Ideal Signals with $\zeta_1 = 4\%$

Condition

Model Output

LOW

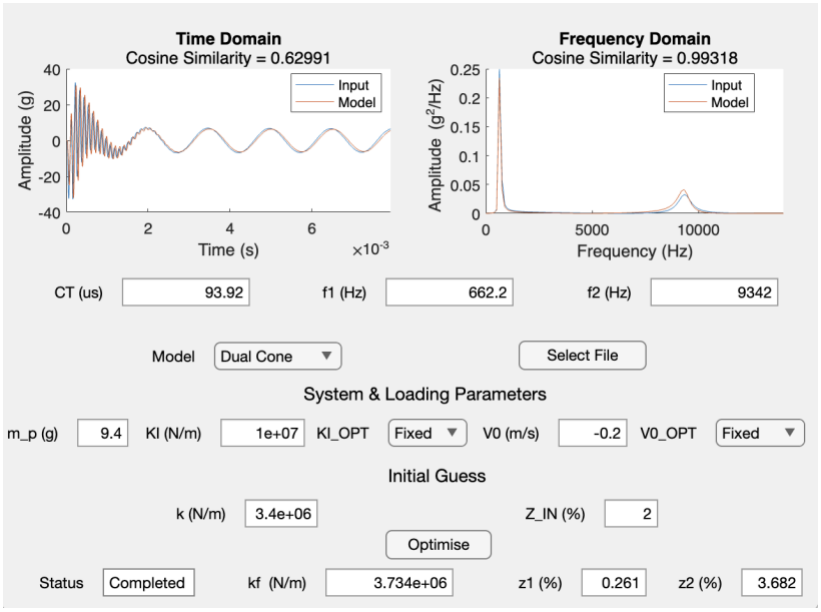

INTERMEDIATE

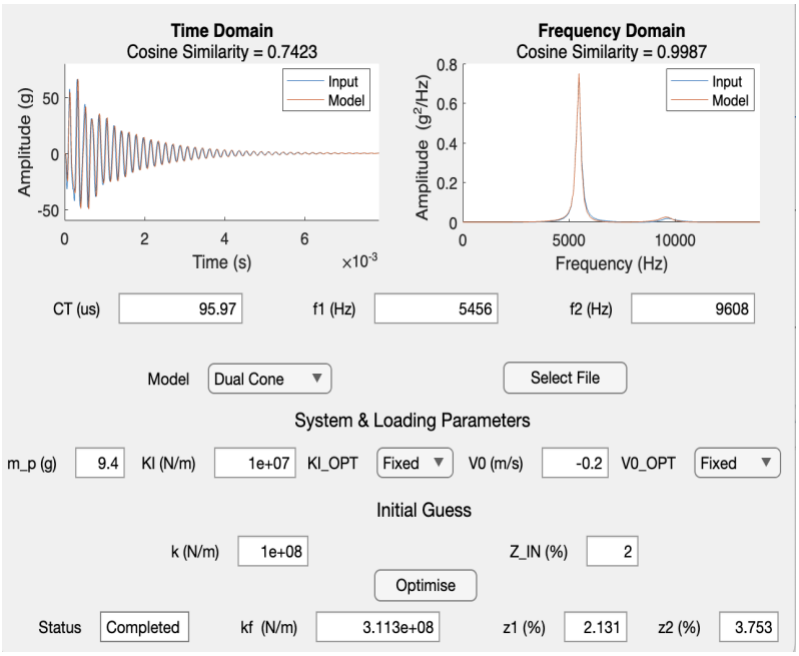

HIGH

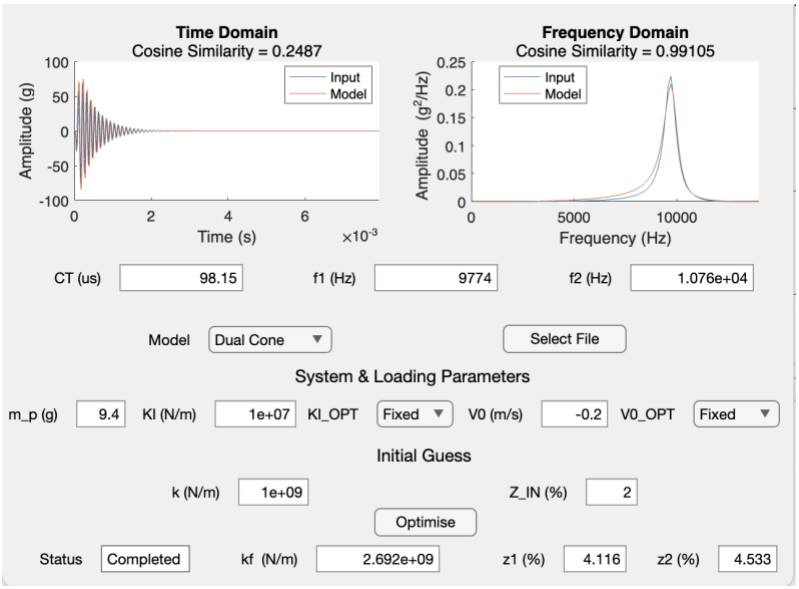

3D FE Asymmetric Signals with $\zeta_1 = 1\%$

Condition	Model Output
LOW	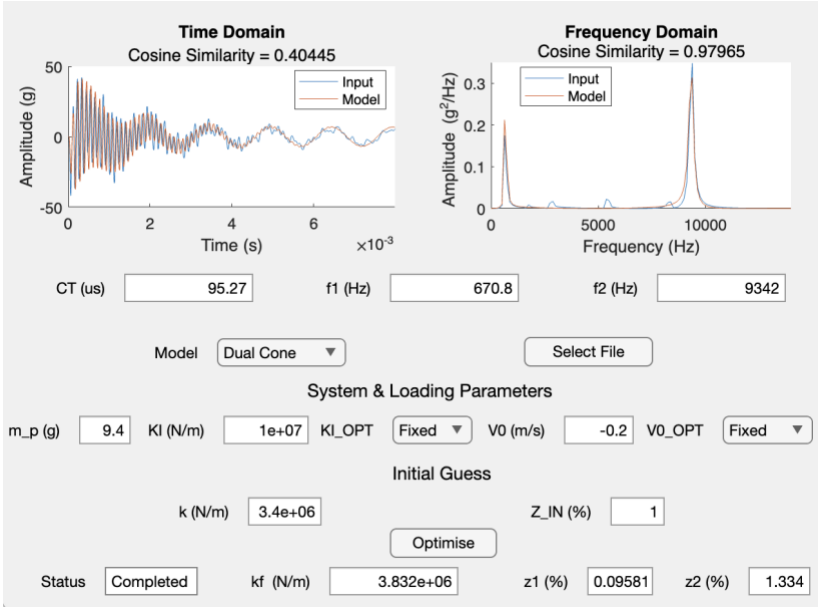
INTERMEDIATE	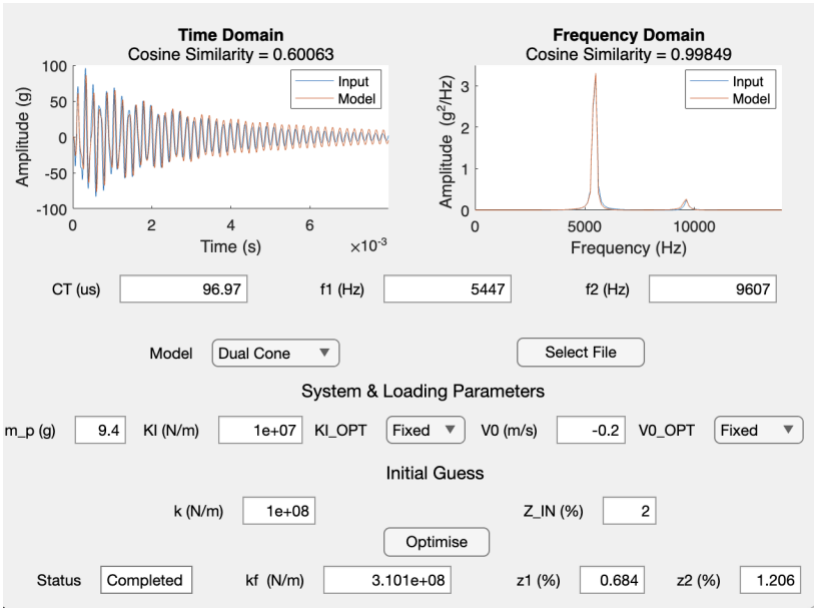

HIGH

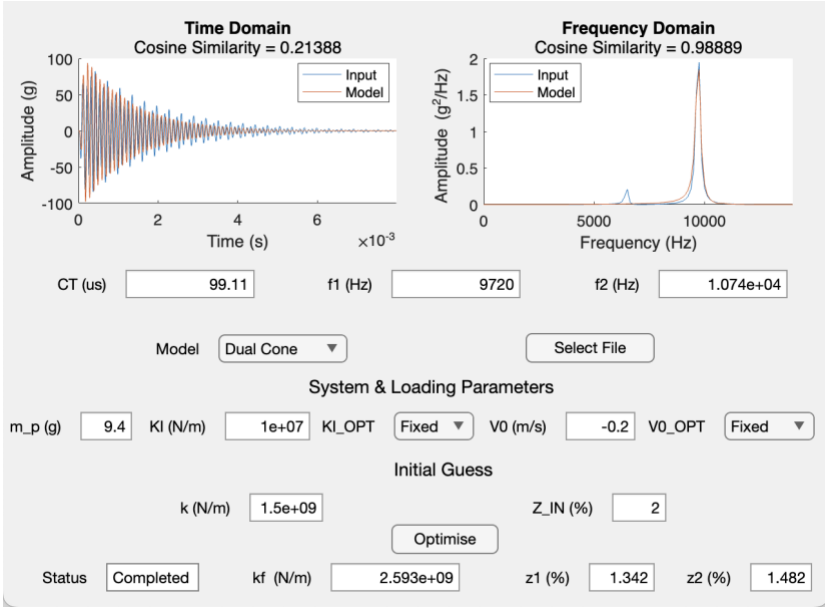

3D FE Ideal Signals with $\zeta_1 = 3\%$ & $\zeta_2 = 0.5\%$

Condition

Model Output

LOW with Fixed K_I with Rayleigh Damping

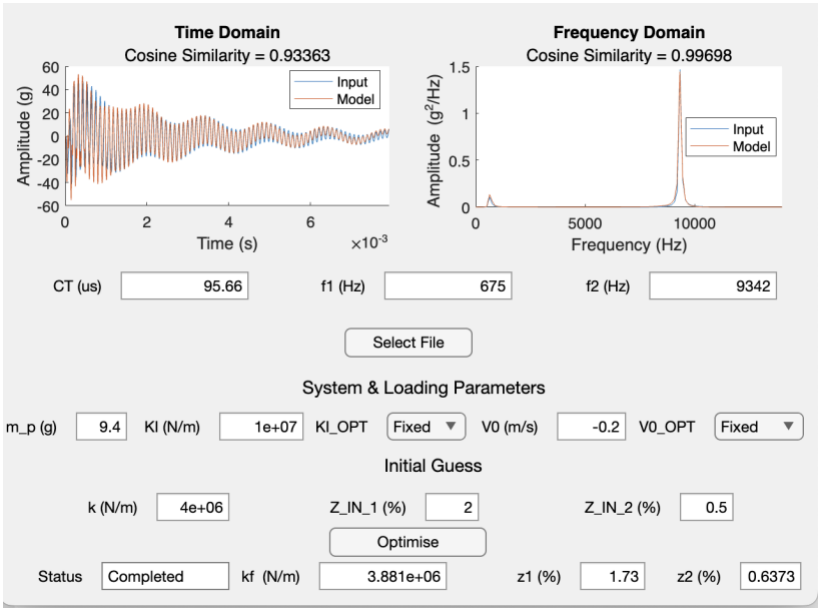

LOW with Variable K_I with Rayleigh Damping

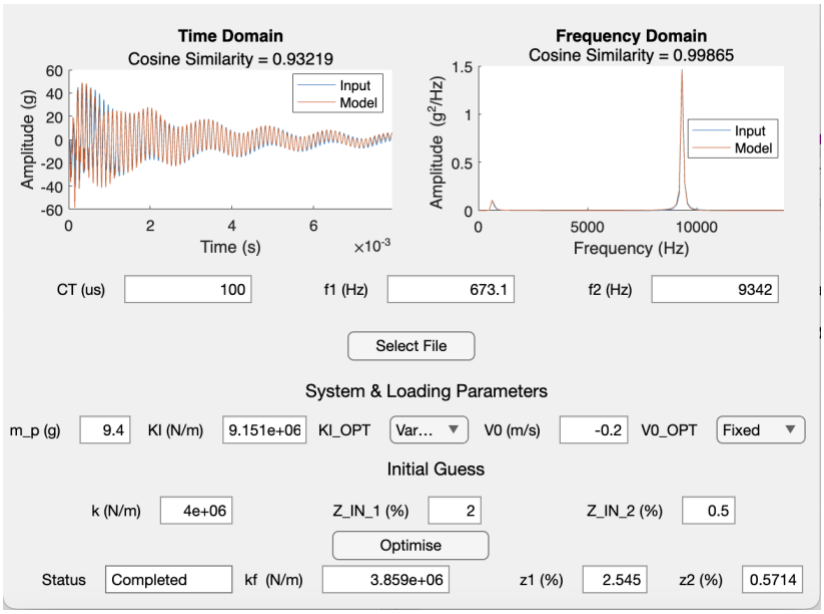

Experimental Signals

Discussed in Chapter 4 and Chapter 5

Condition	Model Output
LOW with Particle Impactor Model	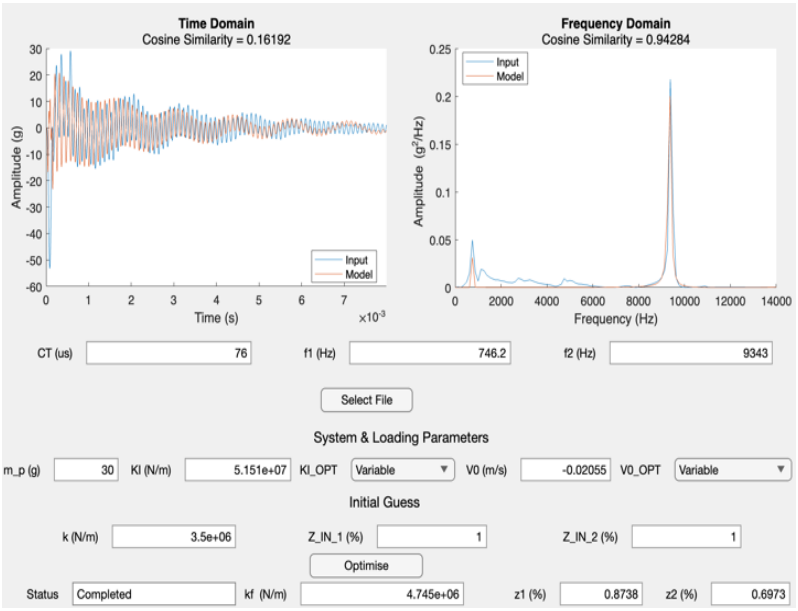

LOW with Bar Impactor Model

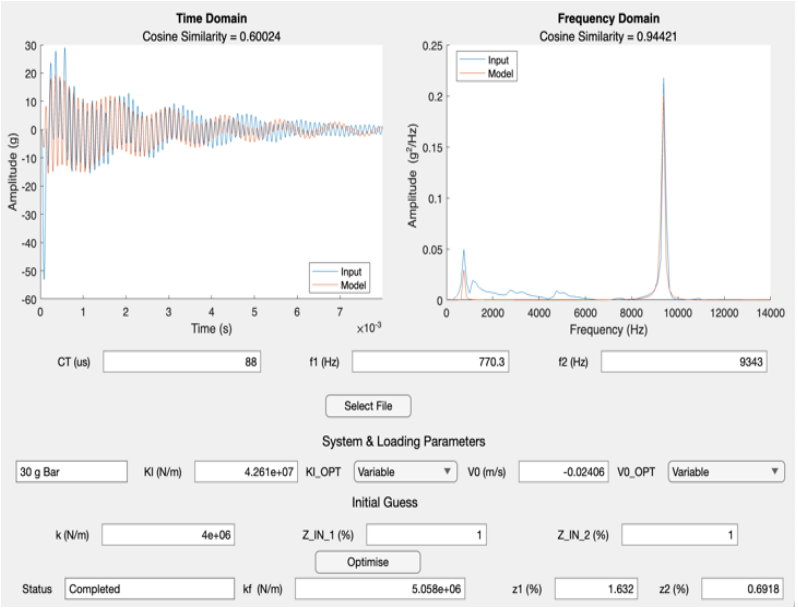

INTERMEDIATE

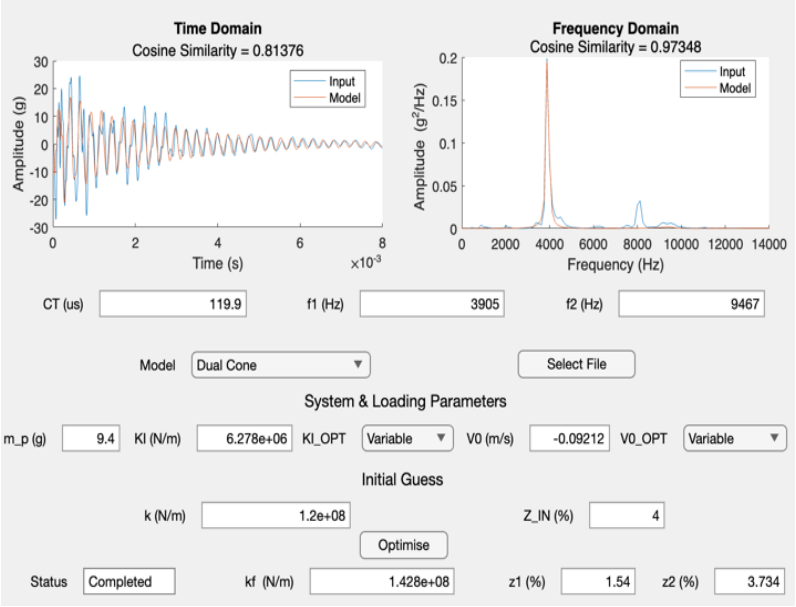

HIGH

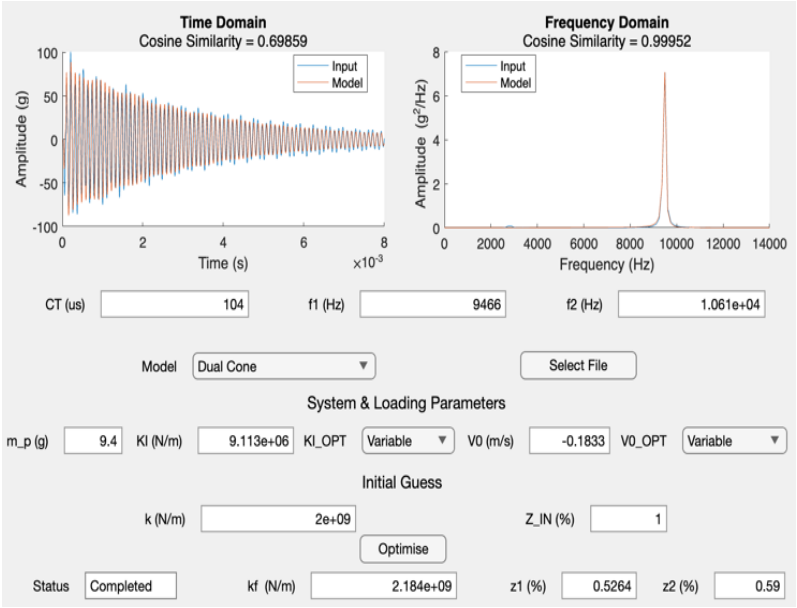

1D FE Transverse Model Outputs for BAHA System

This appendix includes screenshots of the 1D FE model outputs of the BAHA system presented earlier in chapter 8.

$F = 0$

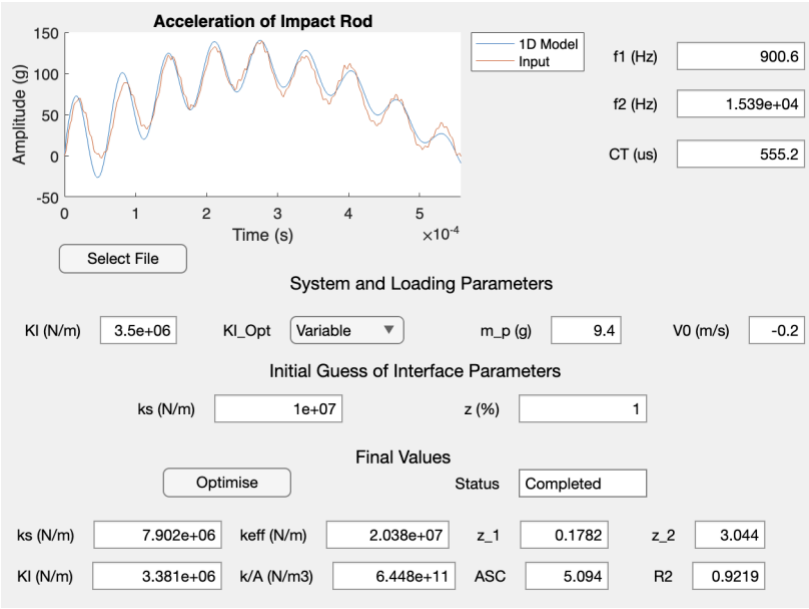

$F = 0.2$

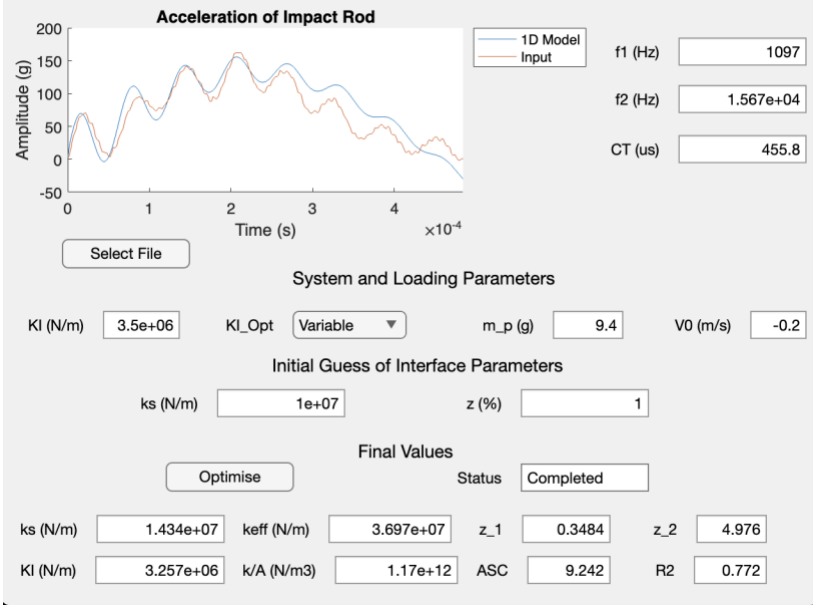
Acceleration of Impact Rod
Amplitude (g)
Time (s)
×10^-4
1D Model
Input
f1 (Hz) 1097
f2 (Hz) 1.567e+04
CT (us) 455.8
Select File
System and Loading Parameters
KI (N/m) 3.5e+06
KI_Opt Variable
m_p (g) 9.4
V0 (m/s) -0.2
Initial Guess of Interface Parameters
ks (N/m) 1e+07
z (%) 1
Final Values
Optimise
Status Completed
ks (N/m) 1.434e+07
keff (N/m) 3.697e+07
z_1 0.3484
z_2 4.976
KI (N/m) 3.257e+06
k/A (N/m3) 1.17e+12
ASC 9.242
R2 0.772

$F = 0.4$

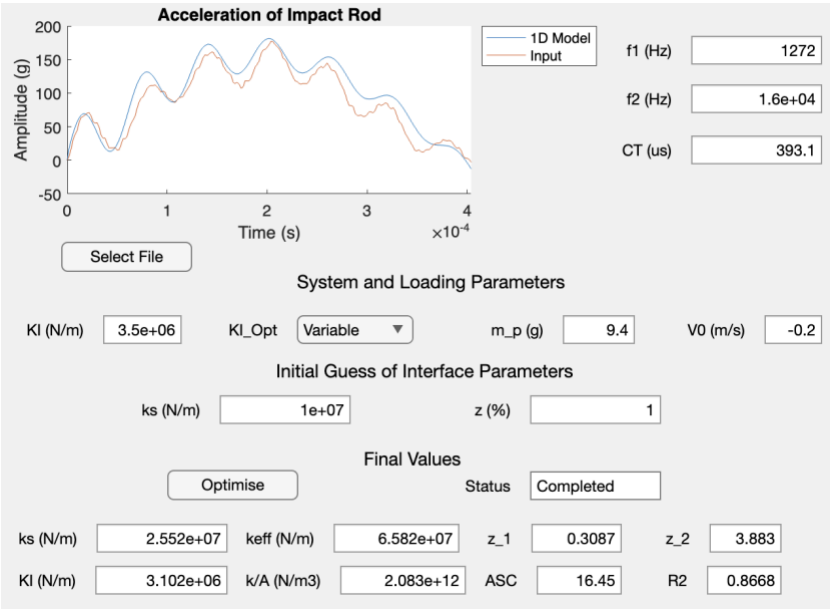
Acceleration of Impact Rod
Amplitude (g)
Time (s)
×10^-4
1D Model
Input
f1 (Hz) 1272
f2 (Hz) 1.6e+04
CT (us) 393.1
Select File
System and Loading Parameters
KI (N/m) 3.5e+06
KI_Opt Variable
m_p (g) 9.4
V0 (m/s) -0.2
Initial Guess of Interface Parameters
ks (N/m) 1e+07
z (%) 1
Final Values
Optimise
Status Completed
ks (N/m) 2.552e+07
keff (N/m) 6.582e+07
z_1 0.3087
z_2 3.883
KI (N/m) 3.102e+06
k/A (N/m3) 2.083e+12
ASC 16.45
R2 0.8668

$F = 0.6$

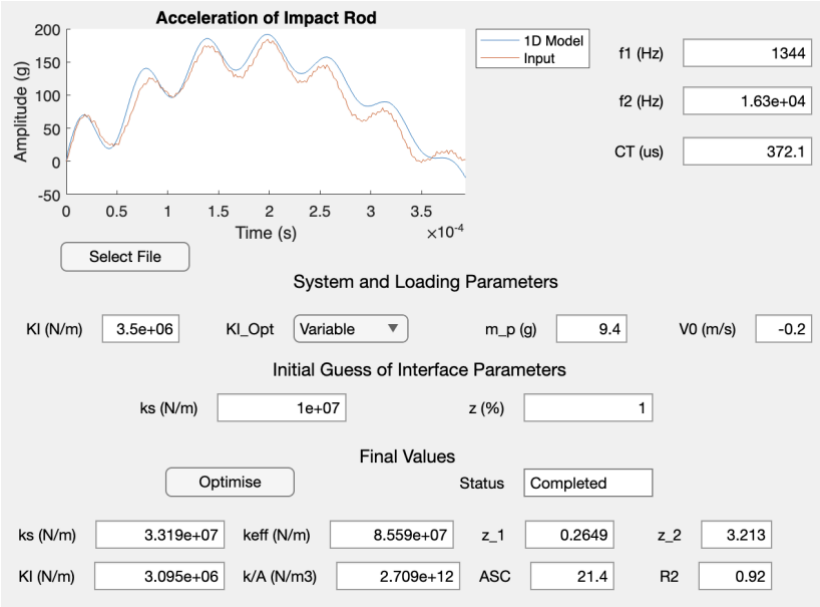
Acceleration of Impact Rod
Amplitude (g)
Time (s)
×10^-4
1D Model
Input
f1 (Hz) 1344
f2 (Hz) 1.63e+04
CT (us) 372.1
Select File
System and Loading Parameters
KI (N/m) 3.5e+06
KI_Opt Variable
m_p (g) 9.4
V0 (m/s) -0.2
Initial Guess of Interface Parameters
ks (N/m) 1e+07
z (%) 1
Final Values
Optimise
Status Completed
ks (N/m) 3.319e+07
keff (N/m) 8.559e+07
z_1 0.2649
z_2 3.213
KI (N/m) 3.095e+06
k/A (N/m3) 2.709e+12
ASC 21.4
R2 0.92

$F = 0.8$

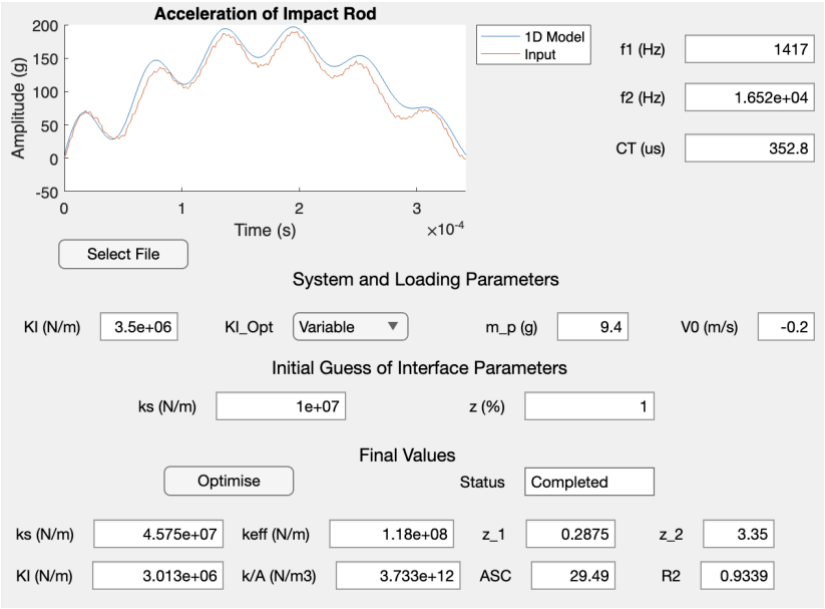
Acceleration of Impact Rod
Amplitude (g)
Time (s)
×10^-4
1D Model
Input
f1 (Hz) 1417
f2 (Hz) 1.652e+04
CT (us) 352.8
Select File
System and Loading Parameters
KI (N/m) 3.5e+06
KI_Opt Variable
m_p (g) 9.4
V0 (m/s) -0.2
Initial Guess of Interface Parameters
ks (N/m) 1e+07
z (%) 1
Final Values
Optimise
Status Completed
ks (N/m) 4.575e+07
keff (N/m) 1.18e+08
z_1 0.2875
z_2 3.35
KI (N/m) 3.013e+06
k/A (N/m3) 3.733e+12
ASC 29.49
R2 0.9339

Appendix C: Periotest® Displacement Profiles

The initial velocity of the impact rod is one of the input parameters of the model. In the current versions of the application, the user can choose to fix the initial velocity to a specific value or allow it to vary in the optimization routine. Although the primary outputs of the optimization process (natural frequencies, damping ratios and interface stiffness) are system characteristics and do not dependent on the excitation conditions, those parameters can influence the modal contributions (amplitude) in the frequency spectrum of the response and can lead to numerical inaccuracies due to the optimization process. The optimization routine can mistakenly attribute higher damping ratios to lower amplitudes and achieve a better fit between the input signal and the model's prediction by changing damping while the main influencing parameter could be the initial velocity. Therefore, having a better understanding of the impactor's initial velocity is important for better quantifying the interface parameters. Furthermore, it is important to understand the excitation conditions in order to compare the performance of different impactors (which is a separate parallel project) in exciting the system. In this section, the displacement profile of the modified Periotest® (which is the Periotest® handpiece connected to ASIST board V3) is determined using high speed imaging and documented. It should be noted that in this section, the rod's motion is analyzed before striking any object. The current setup does not have enough temporal resolution to capture the rod's behavior while it is in contact with the system. Therefore, this section is primarily dedicated to showing the rod's behavior before impact and better understanding the initial conditions.

Figure C-1 shows the setup used in determining the displacement profile of the handpiece. The Fastec© IL5 (Fastec Imaging, USA) is used to capture the position of the impact rod throughout time. The original Periotest® manufacturer specifies that its average speed is 200 mm/s over an approximate distance of 2 mm [88]. Since the exact knowledge of the velocity is unknown the frame rate was set to 10000 frames per second to ensure that there is enough spatiotemporal resolution for capturing the motion accurately. The propulsion speed of the rod can be controlled by the hammer extension time in the ASIST® GUI. The extension time (Ex) was varied between 13-20 ms and for each extension time 3 strikes were recorded. The frames were recorded and analyzed on MATLAB®, the code relied on the RGB color scale (255, 255, 255 which corresponds to white) to track a single point along the rod. The user must manually specify this point in the first frame and the code will rely on finding the location of this boundary point (first point to have RGB scale of 255 on the specified vertical position) in the subsequent frames automatically based on its

color (Figure C-2). The position can then be converted to displacement by taking the difference between those frames and converting the scale from pixels to mm using a calibration block. The rod's forward motion (before impact) is the primary interest of this investigation and therefore the motion is analyzed up to the lowest point (which corresponds to maximum position of the rod before moving backwards) on the curve (t_f). The raw displacement data are then curve fitted with a 2nd order polynomial which can describe the rod's motion throughout time. The fitted expression can be differentiated to find the velocity as a function of space and time. The analysis process is summarized in Figure C-3 below.

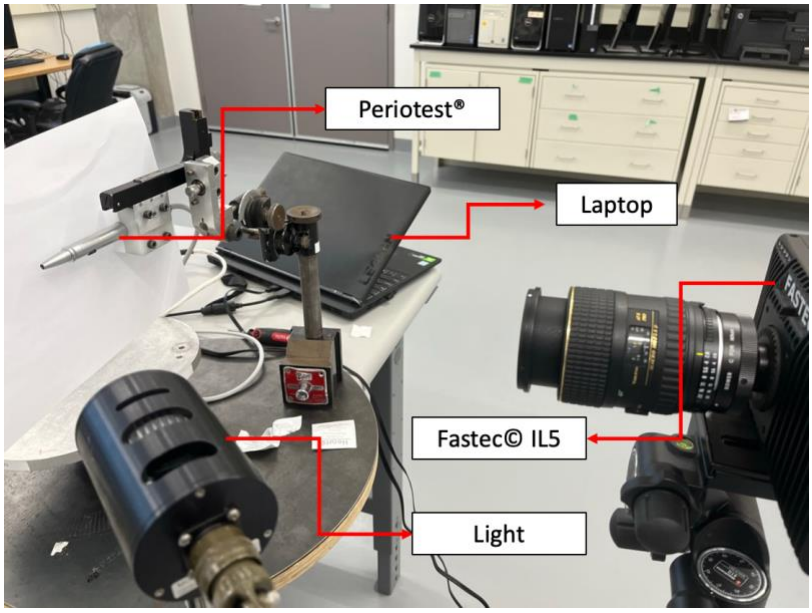

Figure C-1 Experimental setup for determining the ASIST handpiece displacement profile.

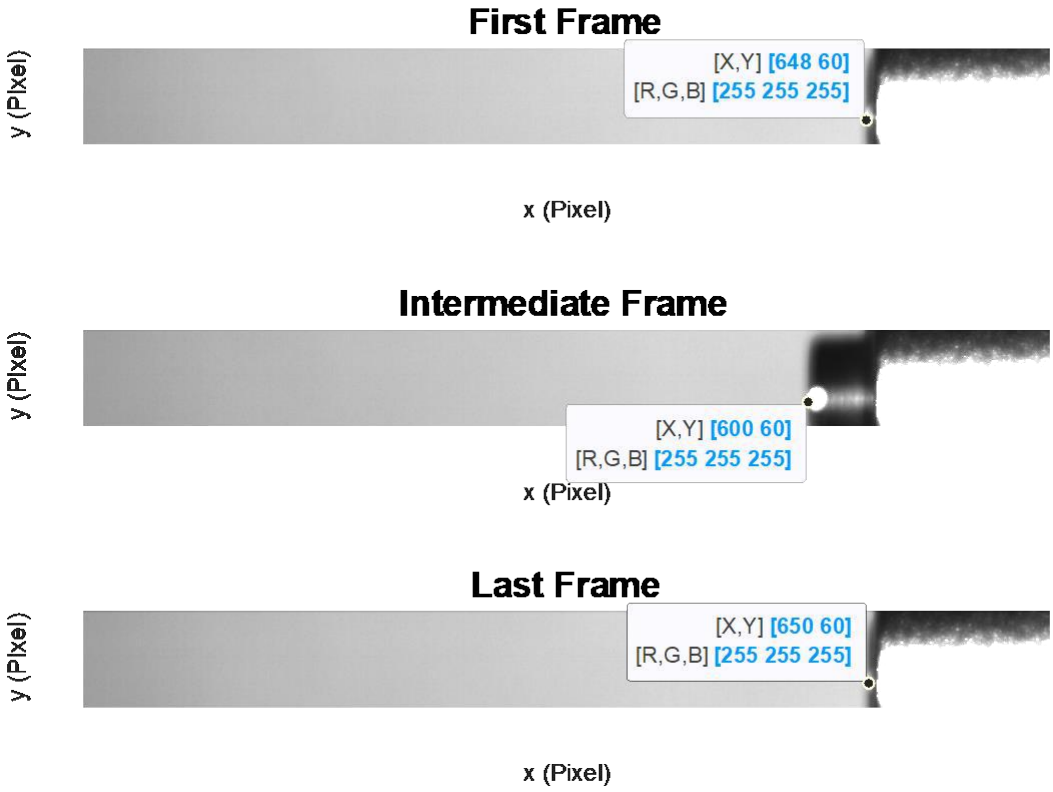

Figure C-2 The code tracks a single point along the rod throughout different frames. The user manually chooses the 1st and last frames of interest and selects the point that will be tracked.

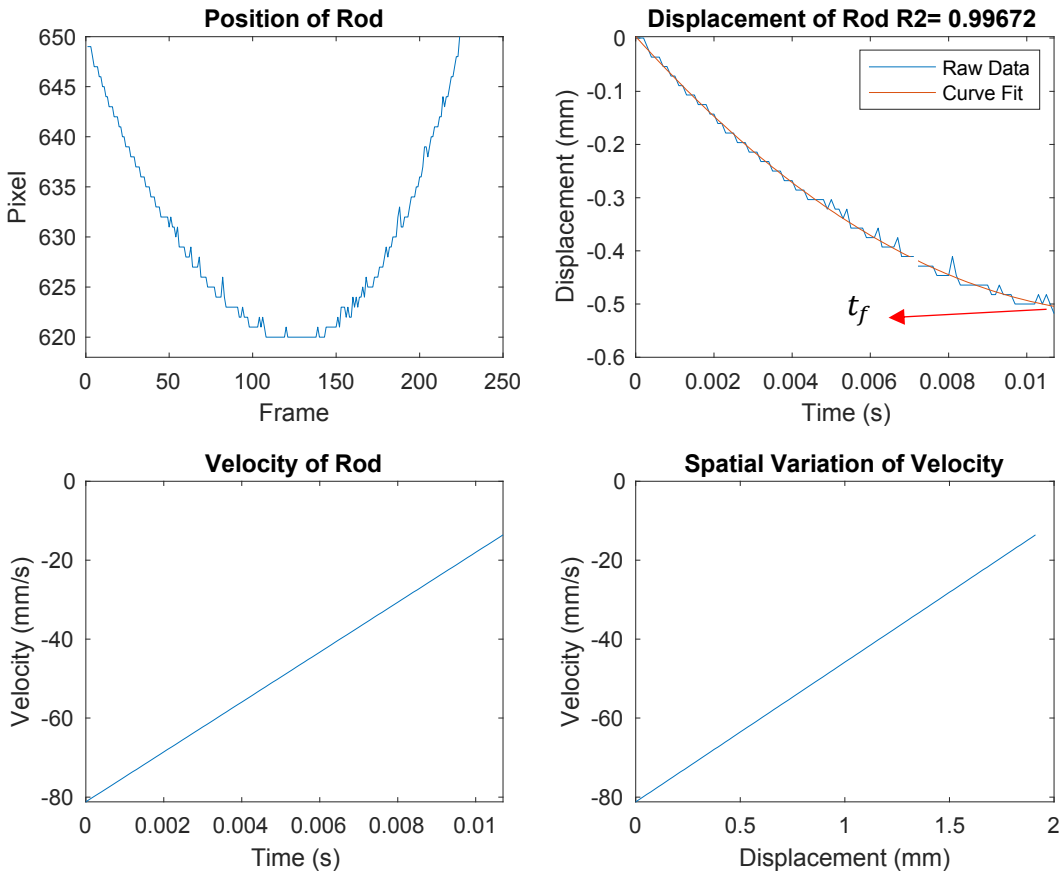

Figure C-3 The position of the point is tracked throughout the different frames. The lowest point on the curve corresponds to maximum position of the rod beyond which the rod starts moving backwards. The forward motion of the rod is analyzed by converting the position to displacement in mm and then a polynomial fit is used to mathematically describe the displacement as a function of time. The expression can be differentiated to obtain the velocity as a function of space or time.

The results showed an interesting behavior of the rod's motion. Although it was always perceived that the rod attains a constant velocity profile throughout its motion, it was found that the displacement profile of the rod is parabolic and in turn the velocity profile is linear and not constant. This parabolic displacement profiles were highly noticeable for the extension times of 13-17 ms, from 18-20 ms the rod's displacement profile can be approximated with a linear profile and a constant velocity profile (Figure C-4). Table C-1 and Table C-2 summarize the mathematical expressions that can be used to describe the behavior of the rods and the acceptable time domain that they can be applied in. From this analysis, it can be inferred that with the Periotest as an impactor the striking distance can be an influencing parameter on the response' amplitude and that

the new measurement system should either have more controls over the velocity profile or incorporate a tool for measuring the velocity (or distance) before the strike.

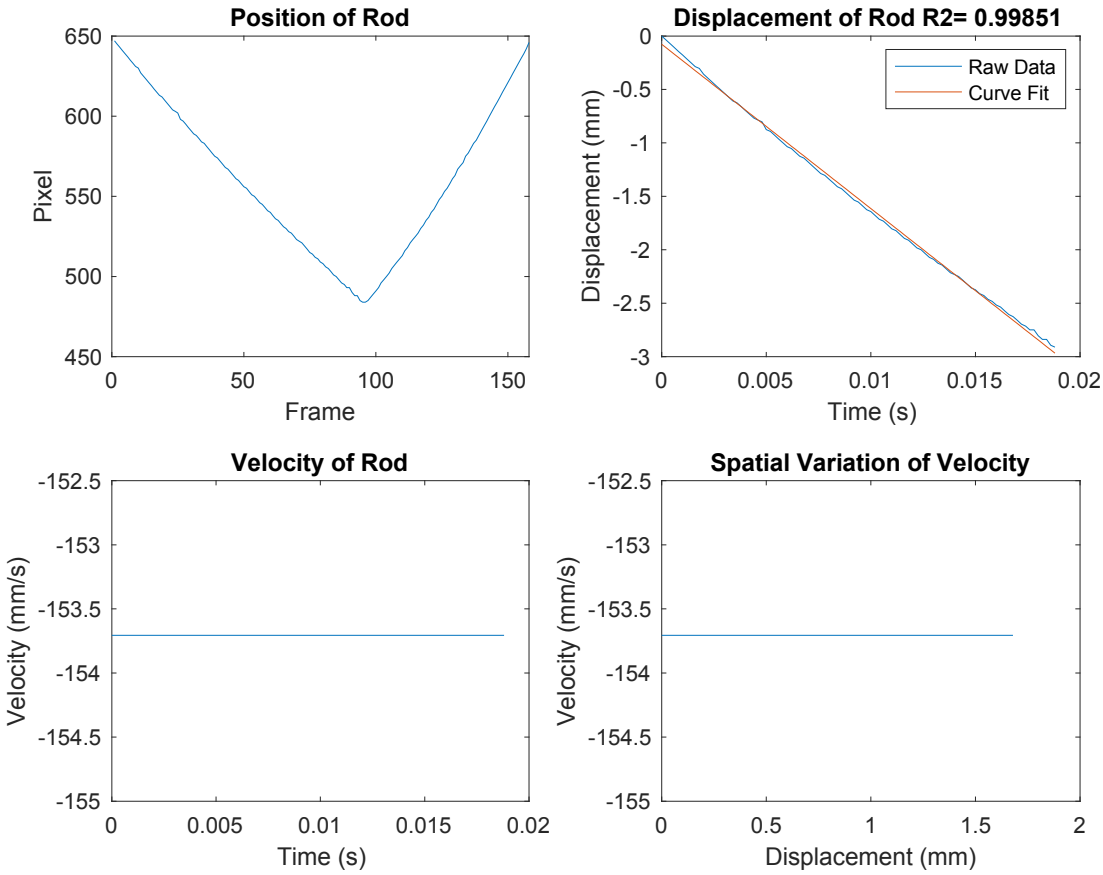

Figure C-4 For higher extension times (18-20 ms), the rod's displacement can be approximated with a linear profile and a constant velocity profile.

Table C-1 Summary of the mathematical expression for the displacement's profiles for each extension time.

	Ex = 13 ms		**Ex = 14 ms**		**Ex = 15 ms**		**Ex = 16 ms**	
i	$u(t)$ mm	R^2	$u(t)$ mm	R^2	$u(t)$ mm	R^2	$u(t)$ mm	R^2
1	$3160t^2 - 81.2t$	99.9	$4836.8t^2 - 168t$	99.9	$4144t^2 - 199t$	1	$1058t^2 - 125t$	1
2	$3123t^2 - 86.0t$	99.9	$5154.7t^2 - 168t$	99.9	$4094t^2 - 203t$	1	$1097t^2 - 125t$	1
3	$3453.2t^2 - 71.38t$	99.6	$5077t^2 - 167t$	99.9	$4158t^2 - 199t$	1	$1123t^2 - 126t$	1
	Ex = 17 ms		**Ex = 18 ms**		**Ex = 19 ms**		**Ex = 20 ms**	
i	$u(t)$ mm	R^2	$u(t)$ mm	R^2	$u(t)$ mm	R^2	$u(t)$ mm	R^2
1	$1164t^2 - 152t$	1	$1170t^2 - 175.7t$	1	$1101t^2 - 193.2t$	1	$3215t^2 - 309t$	1
2	$1044t^2 - 157t$	1	$1181t^2 - 180.2t$	1	$819t^2 - 185t$	1	$3296t^2 - 306t$	1
3	$1044t^2 - 157t$	1	$1117t^2 - 176.2t$	1	$1108t^2 - 193t$	1	$3052t^2 - 306t$	1

Table C-2 The acceptable domain for applying the expressions of Table C-1

	Ex = 13 ms	**Ex = 14 ms**	**Ex = 15 ms**	**Ex = 16 ms**
i	$0 < t \leq t_f$ (ms)	$0 < t \leq t_f$ (ms)	$0 < t \leq t_f$ (ms)	$0 < t \leq t_f$ (ms)
1	8.4	18.1	25	30
2	12.6	16	25.2	31
3	10.7	16.7	24.2	30
	Ex = 17 ms	**Ex = 18 ms**	**Ex=19 ms**	**Ex = 20 ms**
i	$0 < t \leq t_f$ (ms)	$0 < t \leq t_f$ (ms)	$0 < t \leq t_f$ (ms)	$0 < t \leq t_f$ (ms)
1	23	18.8	16.6	10.8
2	21.2	18.2	17.0	11
2	21.2	18.6	16.8	10.8

Appendix D: Extending the TFA Model to Clinical Data (Preliminary Analysis)

This investigation is part of larger ongoing project that aims at extending the ASIST methodology to the OPL TFA system, the project encompasses the modelling of the bone-implant system and the redesign of the ASIST handpiece. This investigation primarily focused on the modelling aspect of the project and the developed 1D FE model was tested with signals generated from the 3D FE and in-vitro experimental models. However, this project also entails collecting the longitudinal clinical measurements of patients within the Alberta Limb Osseointegration Program. The 1D FE model can be extended to the clinical measurements by incorporating the geometry of the GV connector to the model. In this appendix, the 1D FE model is tested with randomly selected data from one of the patients who has the same implant and dual cone adapter geometries of the developed models. The purpose of this preliminary analysis is to observe the 1D model's ability in evaluating the BII properties of the clinical signals. The clinical signals were acquired in a similar manner to the benchtop experimental signals using the ASIST handpiece and the same accelerometer and data acquisition system discussed earlier in chapters 3 and 4.

Figure D-1 shows the results of analyzing the clinical signals with the model, the model managed to find a good fit for both cases (>97%) in the frequency domain. This indicates that the model can potentially predict the dynamic behavior of the clinical signals. In addition to this, the clinical response appears to be in-line with the 3D FE and the benchtop experimental signals where the response was primarily dominated by a single frequency (1st axial mode) for the INTERMEDIATE and HIGH interface condition which is the expected interface conditions for the patients who are not experiencing loosening. The values of the 1st mode frequency and the interface stiffness appear to be close to the HIGH values observed using the benchtop experimental signals, however the damping prediction appears to be higher than the experimental predictions which is expected due to the presence of muscles and soft tissues clinically. As it can be observed the model managed to find differences in the 1st axial mode and the BII stiffness between both days. However, statistical analysis should be conducted to make strong conclusions on the longitudinal evaluation of the BII properties for the patients. Furthermore, the 1D FE model with the GV connector should undergo a series of validation steps (in a similar manner to the dual cone model) that involve comparing the 1D and 3D mode shapes for a free-free TFA system and testing the model with 3D FE and experimental signals (Figure D-2) before fully utilizing it for clinical. However, it appears that the model can be readily extended to analyze clinical signals.

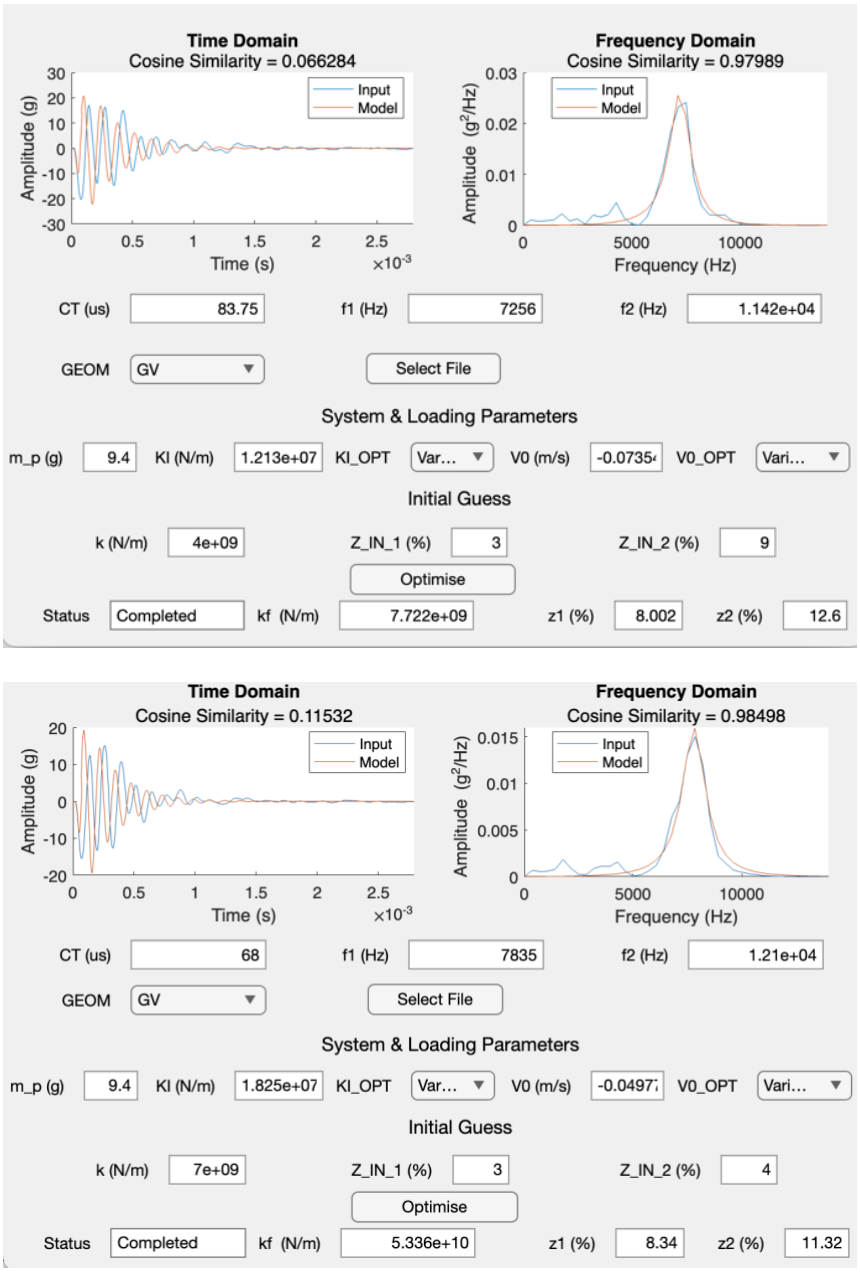

Figure D-1 Analyzing randomly selected clinical data for the same patient on different days (286 days post-operation Top) and (353 days post-operation Bottom)

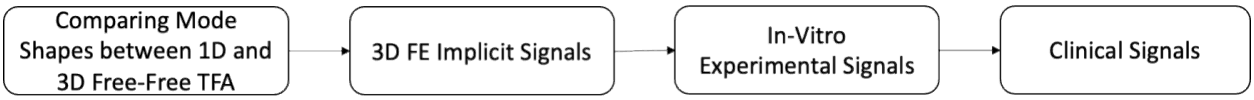

Figure D-2 The 1D FE model with the GV connector should undergo the same validation steps before fully utilizing it for clinical application.